ProQuest LLC.
789 East Eisenhower Parkway
P.O. Box 1346
Ann Arbor, MI 48106 – 1346

The Ultrasonic Machining of Silicon Carbide / Alumina Composites.

Garth Martyn John Nicholson, B.Eng (HONS)

A thesis submitted in partial fulfilment of the requirements of
Sheffield Hallam University
for the degree of
Doctor of Philosophy.

February 1998

Collaborating Organisation :

Extrude - Hone Limited, Milton Keynes.

PREFACE

This thesis refers to research completed during the period from October 1994 to November 1997 within the School of Engineering at Sheffield Hallam University.

As part of this research programme, an M.Sc. module "Fracture & Fatigue" was studied at Sheffield Hallam University. Instruction was given in the use of the "Talysurf" surface roughness machine, and also in the use of the scanning electron microscope at the University Materials Research Institute.

Samples of the material under investigation were provided by Rolls-Royce Aerospace Group, Bristol.

Abrasive media used during the experimentation was provided by Extrude-Hone Ltd., Milton Keynes.

I confirm that this work has not been presented for any other award.

G. M. J. Nicholson.

December 1997.

ABSTRACT

Silicon carbide fibre reinforced alumina is a ceramic composite which was developed in conjunction with the Rolls-Royce Aerospace Group. The material is intended for use in the latest generation of jet engines, specifically for high temperature applications such as flame holders, combustor barrel segments and turbine blade tip seals. The material in question has properties which have been engineered by optimizing fibre volume fractions, weaves and fibre interface materials to meet the following main requirements : high thermal resistance, high thermal shock resistance and low density.

Components intended for manufacture using this material will use the "direct metal oxidation" (DIMOX) method. This process involves manufacturing a near net shape component from the woven fibre matting, and infiltrating the matting with the alumina matrix material. Some of the components outlined require high tolerance features to be included in their design. The combustor barrel segments for example require slots to be formed within them for sealing purposes. the dimensions of these features preclude their formation using DIMOX, and therefore require a secondary process to be performed. Conventional machining techniques such as drilling, turning and milling cannot be used because of the brittle nature of the material. Electrodischarge machining (E.D.M.) cannot be used since the material is an insulator. Electrochemical machining (E.C.M.) cannot be used since the material is chemically inert. One machining method which could be used is ultrasonic machining (U.S.M.).

The research programme investigated the feasibility of using ultrasonic machining as a manufacturing method for this new fibre reinforced composite. Two variations of ultrasonic machining were used : ultrasonic drilling and ultrasonic milling. Factors such as dimensional accuracy, surface roughness and delamination effects were examined. Previously performed ultrasonic machining experimental programmes were reviewed, as well as process models which have been developed. The process models were found to contain empirical constants which usually require specific material data for their calculation.

Since a limited amount of the composite was available, and ultrasonic machining has many process variables, a Taguchi factorial experiment was conducted in order to ascertain the most relevant factors in machining. A full factorial experiment was then performed using the relevant factors. Techniques used in the research included both optical and scanning electron microscopy, surface roughness analysis, x-ray analysis and finite element stress analysis. A full set of machining data was obtained including relationships between the factors examined and both material removal rates, and surface roughness values. An attempt was made to explain these findings by examining established brittle fracture mechanisms. These established mechanisms did not seem to apply entirely to this material, an alternative method of material removal is therefore proposed. It is hoped that the data obtained from this research programme may contribute to the development of a more realistic mathematical model.

ACKNOWLEDGEMENTS

I would like to thank the following people, who have all contributed a great deal to the completion of this project :

My parents, for their encouragement and support throughout my academic career.

Prof. A. J. Fletcher for his supervision, advice and support throughout this project.

Dr. D. Gillibrand, for his support throughout this project.

Dr. A. Fioravanti for his advice in the initial phase of the research.

Dr. J. Callender for his help and advice.

The technical staff of both the Engineering Department of Sheffield Hallam University, and at the Materials Research Institute, for their co-operation and assistance in the last three years.

Mr. J. Mackie and Dr. S. Trengove of Extrude-Hone Limited for their support, and for supplying the abrasive materials used throughout the project.

Mr. C. McIntyre, Mr. D. Jones and Mr. G. Merrill of the Rolls-Royce Aerospace Group, for providing the sample materials used in the project, offering guidance and giving technical information.

My friends and colleagues at Sheffield Hallam University for their valuable support throughout the past three years.

I also appreciate very much the co-operation and understanding of Mr. A. Wood, and my colleagues in the design department of River Don Castings Limited, for allowing me enough time to complete the project.

CONTENTS

1. INTRODUCTION

Silicon carbide fibre reinforced alumina (SiC/Al_2O_3) is a recently developed ceramic composite intended for use in the aerospace industry. There are many variations in the way this composite is manufactured, each giving slightly different characteristics. The variant under investigation was developed by the Dupont corporation, specifically for the Rolls-Royce Aerospace Group. The main benefits of the material are its excellent thermal properties (stability at elevated temperatures and thermal shock resistance), coupled with low density. These properties make the material an ideal candidate for use in the high temperature sections of jet engines. Flame holders, combustor barrels and turbine blade tip seals have all been made as prototypes using this material as discussed by Schmid [1].

The material has the following specification : The fibres (of diameters between 12 and 16 microns) are formed into tows, each tow contains around 500 fibres. The tows are woven into sheets using an 8 tow repeat weave which gives low fibre crimp and improved fabric drape. Components to be manufactured from this material will primarily use the DIMOX (Direct Metal Oxidation) process, in which the near net shape of the component is produced in one operation. The fabric is laid up over a pattern or within a mould, creating a 'preform'. The silicon carbide fibres (Nicalon®) within the preform are then given a boron nitride coating by the process of chemical vapour infiltration (C.V.I.), this forms the interface material of the composite. The alumina matrix is then deposited within the voids of the preform using DIMOX. Detail features of a component such as high tolerance holes or slots must be produced by a secondary process. Since the material is brittle, conventional milling and drilling is impossible. Electrical discharge

machining (E.D.M.) cannot be used due to the material being non-conductive. Electrochemical machining (E.C.M.) cannot be used since the material is chemically inert. Laser drilling could be used for holes, but not for slots. Similarly, grinding or abrasive jet machining could be used for hole drilling and slicing, but not for blind slots, or slots with complex geometries. Since the material is brittle, ultrasonic machining (U.S.M.) can be used for both hole drilling and slot milling, and is the most versatile post manufacturing process for this material.

Ultrasonic machining utilizes an ultrasonically vibrating tool to impart energy to particles contained in an abrasive slurry. The slurry is placed between the tool and workpiece, and material is removed as abrasive particles are impelled against the surface of the workpiece, abrading a reverse image of the tool upon it. Abrasives commonly used include silicon carbide, aluminium oxide and boron carbide. Tool materials are usually mild steel, brass or tool steel. If the tool is traversed during the process, slots may readily be produced. A variation of conventional ultrasonic machining is rotary ultrasonic machining (R.U.M.), in which the tool is rotated to facilitate improved abrasive flow around the tool.

1.1 PROJECT AIMS

The aims of this project (as discussed and agreed with the industrial partners) were as follows :

- To analyse the mechanisms by which ultrasonic vibration removes material from the surface of silicon carbide fibre reinforced alumina composites during ultrasonic machining.

- To use the information obtained to identify the key parameters that affect this machining process.

- To optimize the conditions under which the ultrasonic machining of silicon carbide fibre reinforced alumina composites can be most readily carried out.

1.2 PROGRAMME OF RESEARCH

The project aims will be achieved with the following programme of research :

- To obtain material removal rates and surface roughness changes introduced by the machining of the composite when certain process parameters are varied within clearly defined limits. These variables include amplitude of tool vibration, average grit diameter, concentration of abrasive slurry, static load on tool, rotation speed of tool, tool diameter and traverse speed of tool.

- To use the finite element technique to determine the distribution of stress in the workpiece under the conditions specified above.

- To identify the state of stress and the point at which fracture occurs, in the light of the accepted mechanism for the removal of brittle material, and the known mechanical properties of the material.

- To develop a mathematical model of the process by which material is removed in the ceramic composite under consideration, in the light of the relationship between process parameters, stress distribution in the composite and incidence of fracture.

In order to facilitate the direct observation of fracture surfaces within the machined material, a combination of scanning electron microscopy and optical microscopy will be used.

2. LITERATURE REVIEW

2.1 INTRODUCTION

This literature survey contains reviews of papers and standard works which relate to six main areas of interest which apply when investigating the ultrasonic machining of a fibre reinforced ceramic composite. These subject areas are as follows :

1) The suitability of the process for the material under investigation (section 2.2).
2) Previously conducted experimental investigations into ultrasonic machining (section 2.3).
3) Previously suggested ultrasonic machining process models (section 2.4).
4) Ceramics and composites (section 2.5).
5) Brittle fracture mechanisms (section 2.6).
6) Finite element analysis (section 2.7).

2.2 PROCESS SUITABILITY.

There have been many descriptions of the basic mechanisms and applications of ultrasonic machining in journals and standard manufacturing textbooks such as those by Khols [2], Moore [3], Moreland [4], Chapman [5], Kaczmarek [6] and Davidson [7], as well as general investigations into the ultrasonic machining process capabilities such as that of Kamoun [8]. The process is generally accepted to be as follows : grains in an abrasive slurry are periodically impacted into the workpiece by an ultrasonically vibrating

tool (the frequency range being from 18 KHz to 22 KHz), which causes the production by erosion of a mirror image of the tool on the surface of the workpiece. Basic process capabilities are commonly stated as follows : holes between 0.076mm and 80mm in diameter and maximum depths of around 100mm with dimensional accuracy's of +/- 0.005mm. The actual figures in a specific case depend greatly on the capabilities of the machine and operator. The references quoted establish the basic capabilities of the process such as the ability to drill through and blind holes, mill through and blind slots, sinking and piercing dies, blanking and forging. The characteristics of suitable workpiece materials have also been well established : Brittle materials which do not necessarily have to be good electrical or thermal conductors and which may be chemically inert are all candidates. Standard texts written specifically on the ultrasonic machining process include those by Markov [9] and Rozenberg [10], in which the suitability of the process for homogeneous, brittle materials such as glass or ceramics is investigated in more depth.

Literature regarding applications which are more relevant to the study of specific material types is also available. Komanduri [11] discussed the problems faced when attempting to machine fibre reinforced materials (including ceramics) by conventional methods such as milling or turning : alternate contact of the tool with fibre and matrix materials (whose response to machining can differ greatly) is cited as the greatest problem. An example of an aramid fibre-epoxy matrix composite is given in which the tool encounters the soft epoxy matrix, and the brittle aramid fibres simultaneously. In theory, the most effective method of cutting the aramid fibres is to preload them in tension before shearing them (which is almost impossible when they are surrounded by

an epoxy matrix), but the softer epoxy matrix responds better to a conventional cutting tool 'slicing' action. Ideally therefore, two quite different methods of cutting would have to operate simultaneously for both the fibres and matrix to be cut effectively. This is not possible when using conventional machining techniques. Rapid tool wear and de-lamination effects may also present problems. This example highlights the advantages of a non-contact machining method. Laser-cutting, abrasive water-jet cutting and electro-discharge machining are all suggested alternatives, with ultrasonic machining proposed as a suitable machining method for hard, brittle materials, and for applications in which intricate shapes of high accuracy and surface finish are required.

In a general overview of machining methods for use in composite materials, Abrate & Walton [12] also discussed laser-cutting, abrasive water-jet cutting, electro-discharge machining, electro-chemical spark machining and ultrasonic machining. The investigation concluded that laser cutting and abrasive water-jet cutting had gained widespread use in industry, but that the other methods (including ultrasonic machining) required further investigation before widespread use would became common.

Sheppard [13] also recognised that the properties which made advanced ceramics attractive to engineers (high hardness, high thermal resistance, chemical inertness and low thermal and electrical conductivity), also made them extremely difficult to machine conventionally. Since many ceramic components are intended for high tolerance applications, net-shape manufacturing is often impossible, and therefore a certain amount of finish machining is required. Sheppard states that "Since conventional machining can be costly - up to 80% of the total manufacturing cost - the ceramics

industry is developing novel methods that may be more economical." The relative performance and limitations of grinding, water-jet machining and laser machining are discussed, but ultrasonic machining is said to have advantages over conventional grinding systems, with ultrasonic machines capable of yielding high machining efficiency for a low energy input.

Kremer & Mackie [14] discussed the machining methods available specifically for ceramics, and stated that ultrasonic machining was ". . . the only process able to machine two or three dimensional shapes in ceramics, with fine details or sharp angles." They also stated that "U.S.M. is a process which has minimum effect on surface integrity. There is no corrosion or thermally affected zone". The conclusion of the report was that although ultrasonic machining was developed several decades ago, it is only now that advanced ceramics are gaining widespread use in industry, that the ultrasonic machining process is being used to it's full potential in a manufacturing capacity.

Watkins [15] also concluded that ultrasonic machining was one of the most suitable machining method for the latest generation of hard engineering ceramics such as silicon carbide and silicon nitride compounds.

Diverse applications of ultrasonic machining have also been discussed : Black [16] described how ultrasonic machining may be used to form and redress electrodes for electro-discharge machining. Trendler [17] discussed how ultrasonic machining could be

used to form and finish dies, and Walpington *et al* [18] described how ultrasonic drills could be used in dentistry for creating filling cavities.

New methods for the machining of modern ceramics were proposed by Suzuki *et al* [19] and Li [20]. Based on ultrasonic machining, these processes used a biaxially vibrated, non rotational tool, which was said to produce more accurate shapes than conventional single axis vibration ultrasonic machining. The proposed processes did not use an abrasive slurry, relying on a diamond encrusted tool tip. Although these types of machining differ slightly from machining with slurry based abrasives, the proposal of new methods of machining hard materials highlights the perceived importance of the need to manufacture efficiently high tolerance components from advanced composites.

2.3 EXPERIMENTAL INVESTIGATIONS INTO ULTRASONIC MACHINING

In order to design a suitable experimental programme for the project, the experimental details of other recent investigations were studied carefully.

An early study by Kazantsev & Rosenberg [21] set out to establish the mechanism of ultrasonic cutting. The technique used was high speed photography of the ultrasonic cutting of glass. The basic mechanism involved was as follows : As the tool moved down toward the workpiece, it impinged upon the largest abrasive grains. Since these grains were harder than the workpiece material, they were pressed into the workpiece, generating stresses which eventually lead to fracture. Since the grains were also harder

than the tool material, they became embedded in the tool. As the tool moved down further, smaller grains came into contact with the workpiece, causing stresses of lower magnitudes. Under these conditions, the tool would only cease to move downwards when all it's kinetic energy had been reduced to zero by the reaction forces of the particles. It was therefore established that material was removed by direct impact of the abrasive grains on the workpiece surface. Each impact caused stresses to be generated in the workpiece which led to failure by cracking. The high speed film clearly showed radial cracks propagating from underneath an abrasive grain. It was further established that the amount of fracturing depended on the magnitude of the force applied to each particle.

Soundararajan & Radhakrishnan [22], also set out to determine the main mechanisms involved in ultrasonic machining. The theoretical mechanisms were well known i.e. direct hammering, indirect hammering, projection impacts, rolling impacts and cavitation erosion, but the relative contribution of each parameter was more difficult to establish. The experiment in this study involved the use of a relocation fixture for the workpieces. This allowed the cumulative effect of differing parameters to be analysed. For example, for a set grit size and concentration, the height of the tool above the work was progressively lowered and the amount of material removed was checked. The workpieces used in the experiment were plate glass, high speed steel and tungsten carbide. The tool material was mild steel, and the abrasive boron carbide. The conclusions drawn from the study were that as long as the working gap between the tool and the work surface was more than the mean size of the abrasive particles used, no

significant machining took place. This implied that the main mechanism involved in material removal was direct impact.

A similar study was conducted specifically on monolithic ceramic materials by König & Hilleke [23]. In this experiment, the sample was mounted obliquely below the tool, resulting in a tapered working gap. The effect of the differing mechanisms could then be observed on one material sample. The predominant mechanism was found to be direct impact, followed by projection and indirect impacts. It was also concluded that the amplitude of vibration must correspond to half the mean grain size. Values of amplitude higher than this resulted in incomplete grit replenishment, whereas lower amplitude values resulted in inefficient energy transfer. Static load was found to be important, but specific to workpiece material. Tool material was also considered. It was found that harder tool materials are inefficient due to grain fracture (as opposed to workpiece fracture). Softer tool materials such as mild steel did not cause as much grain fracture, and were therefore considered more efficient. Again this was largely dependent on the relative properties of the tool and workpiece material.

Experimental studies by Komaraiah [24] investigated material removal rates as a function of depth of penetration, and examined methods of increasing abrasive flow to the tool tip. The conclusions drawn from this experiment were as follows. In conventional ultrasonic machining, material removal rates fell to zero at about 10mm depth. This was due to inefficient abrasive replenishment. Special tool design (stepped, fluted, hollow and helical types) combined with repeated tool withdrawal increased the machining rates by 20% - 40%. Increasing the amplitude of vibration also increased

machining rates. The concentration of the abrasive slurry was found to have an optimum value : too low a concentration, and too few grains appeared in the working gap, too high a concentration, and the grains began to "pile up" and pulverise each other rather than the workpiece. Likewise, static load was found to have an optimum value. This is due to the maximum working gap size becoming too small for abrasive replenishment. None of the previously mentioned parameters had any noticeable effect on maximum penetration depth. The main thrust of the paper involved rotating the workpiece in an attempt to improve abrasive circulation, which was found to be successful. This study was incomplete, since no reference was made to the rotation of the tool, as opposed to the workpiece.

An investigation by Komaraiah & Reddy [25] concentrated on tool materials in ultrasonic machining. Experiments were conducted using conventional ultrasonic machining and rotary ultrasonic machining (workpiece rotation). As established earlier, the rotary ultrasonic machining yielded higher material removal rates in all cases. The experiment involved using seven tool materials, which were, in order of ascending hardness : mild steel, titanium, stainless steel, maraging steel, silver steel, Nimonic - 80A and thoriated tungsten. Each tool was then used to drill four consecutive holes each of 6mm depth, giving a cumulative machined depth for each tool of 24mm. The machining rate was then calculated for each tool and each consecutive hole. As expected, the harder the tool material, the higher the material removal rate, and the less tool wear resulted (both longitudinal and diametrical wear). The surface finish of the workpiece was also found to be less rough with high hardness tools. It was concluded that the best overall tool material for ultrasonic machining was Nimonic 80A. It was noted that the findings

of this experimental programme were not in complete agreement with the conclusions drawn by König & Hilleke [23], i.e. that hard tool materials reduce material removal rates due to grain fracture.

A further investigation by Komaraiah & Reddy [26], studied the influence of workpiece properties on ultrasonic machining. Again, conventional and rotary ultrasonic machining were considered. It was concluded that the fracture toughness and the hardness of the workpiece were very important when attempts were made to calculate the material removal rate. The material removal rate was found to be inversely proportional to both hardness and fracture toughness. It was shown that crack lengths within the workpiece are proportional to the fracture toughness and hardness of the workpiece material.

The relevance of abrasive properties in ultrasonic machining of ceramics was ascertained by Koval'chenko *et al* [27]. It was found that increasing the average mesh size of the abrasive proportionally increased the material removal rate from the workpiece. Furthermore, the relative wear (ratio of penetration depth to linear tool wear) of the tool tip decreased with increasing mesh size. It was concluded that this was due to an increase in the level of stress required to fracture the workpiece. It was also noted that boron carbide was superior to silicon carbide in terms of material removal rate. This was attributed to the superior mechanical properties of boron nitride (in terms of hardness and fracture toughness). The recommendations for the abrasive properties for the ultrasonic machining of ceramics were as follows : silicon carbide 80μm - 100μm, and

boron nitride 60μm - 100μm. These grit sizes should give the optimum material removal rates and the greatest dimensional accuracy.

Nandy *et al* [28] investigated tool wear in the ultrasonic machining of glass ceramics. The materials under investigation (plate glass, opal glass and slag ceramics) were said to give high tool wear rate, which warranted further investigation. The causes of tool wear were stated as follows : abrasive type, size and concentration, static load, tool configuration and the behaviour of the abrasive in the cutting zone. It should be noted that tool material properties were not mentioned, an omission which makes the investigation somewhat incomplete. Silicon carbide and aluminium oxide abrasives of mesh size #400 (23 microns) were used, mixed to a concentration of 1 : 10^5 (abrasive : water) by volume. Six tools (of unspecified material type) of working area 7.2mm^2 were used, two on each type of workpiece material - one for each slurry type. The experiment was conducted as follows : Machining was conducted for 10 minutes, after which the tool wear was measured in terms of reduction in mass with a spring balance. Workpiece material removal was also measured. This process was repeated up to a total of 40 minutes for each tool. Lateral and frontal wear of each tool was photographed through a microscope. It was found that tool wear decreased with cutting time, and that material removal rate also decreased with cutting time. The latter was attributed to three previously established factors :

1) Abrasive circulation restriction around the tool tip.

2) Blunting of abrasives.

3) Blunting of the tool tip reducing the effective area of the tool face.

Unsurprisingly, hard workpiece materials were found to give higher tool wear rates, as confirmed by the study by Komaraiah & Reddy [25]. Relative tool wear (tool wear as a percentage of material removal rate) was found to be a function of workpiece hardness, structural properties of the workpiece, density of the workpiece, abrasive material used and the duration of cutting. Although the experiments verified several assumptions - such as that tool wear would be proportional to workpiece hardness and machining time - the omission of data on the material properties of the tool made this study somewhat incomplete.

A study of productivity, surface quality and tolerances in the ultrasonic machining of ceramics was made by Dam *et al* [29]. The materials investigated were as follows : plate glass, Al_2O_3, TiB_2, HPSN (hot pressed silicon nitride), $TZ_{12}Ce$ (tetragonal zirconiumoxide stabilised with cerium) and TZ_3YB (tetragonal zirconiumoxide stabilised with yttrium). The tools used were tubular in section 10mm o.d. and 8mm i.d. Tool material was steel (ST37). Trials were carried out under maximum material removal conditions, with a tool rotation speed of 400 r.p.m. Boron carbide abrasive grit of #280 mesh size was used in conjunction with vacuum extraction from the centre of the tool to improve abrasive flow and therefore machining rates. The following results were obtained :

i) Productivity and tool wear : It was found that a high material removal rate corresponded to low tool wear and *vice versa*. When the workpiece materials were graduated according to their machining rates, it was found that the materials were also in exact order of fracture toughness, an observation which confirmed fracture toughness as

the most important factor in the determination of the material removal rate in ultrasonic machining. Work by Haas [30] and Grathwohl *et al* [31] was quoted as confirmation of this statement. The fracture toughness theory was then explained in terms of energy as follows : "The toughness of a material is a measure of the energy required to make a crack grow. Therefore when energy is kept at a constant rate (as in these experiments) the only way to put more energy into the machining process is to increase the machining time. In this context, it is also worth mentioning that the hardness of the materials seem to have very little influence on productivity and tool wear". The assertion that hardness of the workpiece does not influence material removal rate is not generally accepted, and investigators who reached similar conclusions regarding the importance of workpiece fracture toughness do not seem to share similar opinions about the relative irrelevance of workpiece hardness, notably Komaraiah & Reddy [26], and Nandy *et al* [28], who all found workpiece hardness to be highly significant.

ii) Precision : Materials which yielded the highest material removal rates (i.e. those with a low fracture toughness and which gave low tool wear figures) also produced the most accurate holes. Furthermore, materials with high fracture toughness and correspondingly high tool wear rates gave the least accurate holes. This was explained by the observation that as the tool wears mostly at it's edges, the effective diameter of the tool is reduced, leading to a deterioration in the accuracy of the holes.

iii) Surface characteristics : It was concluded that the surface roughness of a material cannot be related directly to a specific material property, although as a general trend, the

most productive material (highest material removal rates) give the highest roughness figures.

The experimental study by Dam *et al* [29], resulted in the following conclusions :

1) The tougher the materials, the greater is the tool wear, and the smaller are the machining rates, and the lower the dimensional accuracy's of the holes become.

2) A smaller machining rate tends to give a lesser roughness parameter.

3) The more brittle the materials are, the greater is the tendency for the removal of debris by fracture.

4) The tougher the materials are, the greater is the tendency for material removal based on fatigue mechanisms.

A similar study (of surface roughness and accuracy in ultrasonic machining) was performed by Komaraiah *et al* [32]. In this case, the workpiece materials under investigation were glass, porcelain, ferrite and alumina. Tool materials were stainless steel, Nimonic 80A and titanium. Silicon carbide of mesh size #220 at a concentration of 28.5% by weight of water was used as the slurry. The results of the investigations indicated the following :

i) Surface roughness : Surface roughness increased with material removal rate, while the harder the workpiece, the higher were the material removal rates. Surface roughness was found to decrease with increasing tool hardness, with Nimonic 80A giving the lowest Ra values, and titanium the highest.

ii) Accuracy : When using rotary ultrasonic machining, roundness fluctuations were found to be around one third of the values obtained from conventional ultrasonic machining. The accuracy of the holes drilled could be improved by both decreasing abrasive grain size and increasing static load.

This study confirmed the findings of Dam *et al* [29] , for all corresponding parameters, but in addition, the study emphasises the possible increase in efficiency gained by using rotary ultrasonic machining.

Zhixin & Xing [33] recognised that since there were a large number of variables involved in the ultrasonic machining process, any experimental investigation would be complicated. Their investigations therefore attempted to isolate each machining factor individually, establish how accurately each factor could be controlled and therefore quantify the effect of each parameter on the process. For this investigation, the machining process was split into four groups, *viz* :

i) Parameters of the acoustic system : It was found that material removal rates increased with increasing amplitude, but tool wear could affect the resonance of the system resulting in a reduction in effective amplitude. Static load was also found to be

important, and that an optimum value of static load should be reached at which material removal rate was highest. Various static load systems were discussed, such as counterweights, pneumatic/hydraulic and servo motors, but all were found to deviate somewhat from the preset load values due to system inertia and creep feeding.

ii) Characteristics of the abrasive slurry : assuming that parameters such as static load and vibration amplitude were set accurately, it was found that larger grit particles gave higher material removal rates. However, 'dulling' of grit particles as the process proceeded caused a reduction in the material removal rate, a characteristic which, it was suggested, could be minimised by using a large volume of slurry. It was also suggested that abrasives should be of high hardness in relation to the workpiece, and the higher the concentration of the slurry, the higher material removal rates should become - up to concentrations of around 40% by volume, after which 'piling up' of abrasive particles becomes a problem (also noted by Komaraiah [24]). It was also suggested that a large volume of slurry would help to keep a constant concentration of abrasive circulating around the tool tip.

iii) Parameters relating to the workpiece material. : It was found that workpiece hardness and fracture toughness are both inversely proportional to material removal rates, hence highly brittle materials are machined more quickly than tough materials.

iv) Characteristics of the hole geometry : As tool penetration depth increased, so it was found that machining rates decreased, an observation attributed by Xhixin & Xing [33] as is the case with most investigators, to the increasing inaccessibility of the tool tip to the slurry at high penetration depths. This is attributed to the very narrow gap between

the tool flank and the workpiece when the penetration depth becomes great. It was suggested that small diameter holes were associated with more efficient machining, due to the smaller area under the tool which needed to be covered with abrasive.

The work of Xhixin & Xing [33] is a very useful contribution since it attempted to provide means of reducing process parameter variations during a machining operation, thereby increasing the validity of the results obtained. It should be noted that all the trends and observations described were in agreement with the results of most other investigators cited.

An experimental study by Ghosal *et al* [34], was concerned specifically with the ultrasonic machining of glass. It was stated that "experimental results do not tally with theoretically predicted values", and that material removal rates increase after a certain amount of time has elapsed from the start of machining. An attempt was then made to explain this phenomenon. It was suggested that since glass cannot be considered either a truly brittle or truly ductile material, then a 'visco-elastic' failure mode would predominate. A visco-elastic failure mode was described as follows : Initially, the surface of the material (under indenter loading) is deformed elastically, then plastically. Failure at the surface may occur through a fatigue mechanism initially, but subsequent elastic deformations will induce a strain hardening effect in the material, allowing true brittle fracture to occur. This two stage fracture mechanism is proposed to explain the perceived inaccuracies of the theoretically predicted values, since most theoretical models use only brittle fracture as a basis for material removal calculations. Although the

proposed explanations are interesting, no other investigator cited appears to note a significant change in initial material removal rates during the ultrasonic machining of glass. Most investigators attribute the *lowering* of material removal rates (as opposed to the increasing material removal rates found in this study), to reducing slurry supply to the tool tip as the tool feeds into the workpiece.

Continuing with studies of the ultrasonic machining of specific materials, Hocheng and Hsu [35] performed a preliminary study of the ultrasonic drilling of fibre reinforced plastics. The abrasives used were SiC of mesh sizes #150, #220, #400, #400, and B_4C of mesh size #220. Abrasive concentrations were 13.4% and 18.6% by volume with water for SiC, and 14.7%, 18.7%, 22.8% and 25.6% by volume with water for B_4C. The tool used was mild steel of tubular section, 10mm o.d. and 5.8mm i.d. The workpiece materials under investigation were : carbon fibre reinforced epoxy (cured at three temperature and pressure combinations), and carbon fibre reinforced PEEK (poly ether ether ketone), again cured at three temperature and pressure combinations. The Taguchi method was successfully used to reduce the number of experimental runs needed to obtain a suitable number of results with a limited amount of material. The authors findings concurred with most other experimental studies, for example, surface roughness increased with increasing grit size, abrasive concentration and vibration amplitude. The most significant finding with respect to the current research was that no de-lamination effects were found at the edges of the holes drilled. De-lamination was potentially the most serious problem to be encountered when machining fibre reinforced composites, and the lack of any evidence of de-lamination in this study was encouraging.

An investigation into the erosion by projectile particles of silicon carbide fibre reinforced alumina composites was performed by Sykes *et al* [36]. Although ultrasonic machining and projectile erosion are quite different material removal processes, there are parallels which may be drawn, primarily the removal of material by projectile impacts. This mechanism is similar to the "projection" mechanism identified by most investigators into ultrasonic machining. The major difference in the erosion process is that the abrasive particles project through air, whereas in ultrasonic machining, the particles project through a liquid medium. It was found that the addition of silicon carbide reinforcing fibres to the alumina matrix provided significant improvements in abrasion resistance. A silicon carbide fibre addition of around 5% by mass to the alumina matrix was found to be a significant figure. In samples containing less than this percentage of fibres, the erosion rate was found to rise significantly, whereas samples containing more than this 5% value gave considerably lower erosion rates. This critical value of 5% was assumed to be the point at which cracking within the composite changed from being dependent mainly on the fracture toughness of the alumina matrix, to being dependent mainly on the combined fibre-matrix fracture toughness. In addition, at values of fibre content between 5% by mass and up to the maximum content measured of 25% by mass, erosion rates were found to stabilise. Erosion rates were found to increase with the increasing erodant particle diameter, furthermore, it was found that there was no optimum particle size for material removal. The diameter of the silicon carbide fibres was stated to be 1μm, and since the smallest erodant particle diameter used was of 37 μm, therefore there could be no assessment of the possible effect of particles which were similar in diameter to the fibres on erosion rates. Despite this, the investigation provided an insight into the properties of silicon carbide fibre reinforced alumina composites when subjected to projectile impacts, especially in terms of the effects of fibre content on erosion rates.

2.4 ULTRASONIC MACHINING PROCESS MODELS

Ultrasonic Machining is a well developed method of machining brittle materials such as glass and ceramics. A considerable amount of work has aimed to determine the mechanism by which machining is effected, and a correspondingly large number of models of the process have been produced. There have also been many attempts to model the material removal mechanisms involved in ultrasonic machining. However, all these models have met with limited success, and all incorporate undesirable empirical factors that have been introduced to validate the model in the light of available experimental data.

Miller [37], discussed the rate of cutting in ultrasonic machining in a semi-quantitative way. It was assumed that the material removal rate was related to the level of work hardening and the amount of plastic deformation of the workpiece, so that the results of this model could be applied primarily to ductile materials. However, most materials used for ultrasonic machining undergo brittle fracture. Miller [37] also assumed that the abrasive grains were cubes, and that all cubes were of the same size, and that all the cubes take part in the cutting process. This is obviously a major assumption, since in reality, abrasive grains are complex polyhedra, and approximate spheres only after a

period of machining (the actual time being dependant on machining and material parameters). These considerations limit the value of the proposed model.

In the model proposed by Shaw [38], it was assumed that the main material removal mechanism involved direct impact, with projection of only minor significance. He assumed that the volume of material removed was proportional to the volume v of material removed per grain impact, the number of grains N making an impact during one cycle, and the number of cycles (frequency f). The model assumed that each grain was spherical, and that all grains were of the same diameter d.

$$v \propto [dh]^{3/2} Nf$$

Where h is the depth of penetration. The depth of penetration h was found by equating the mean static force with the mean force of impact of the tool on the grains. It was assumed that the number of particles in the working gap was inversely proportional to the square of the mean diameter of the grains, giving the following expression for h :

$$h = \left[\frac{8 F_s y_o d}{\pi K H C (1+q)} \right]^{\frac{1}{2}}$$

Where,

F_S = Static Force.

y_O = Amplitude of tool vibration.

H = Hardness of the tool.

q = The ratio of workpiece : tool hardness.

C = The concentration of the abrasive slurry.

K = A constant of proportionality.

Shaw's model [38] of the main machining process (direct impact) has been checked experimentally using high speed cinematography, but the theoretical analysis did not agree quantitatively with the experimental data. This may be due to over-simplification of the model (in terms of grain size and distribution). Also, the constant of proportionality K can only be defined experimentally, which reduces the value of the proposed model.

The model developed by Kainth *et al* [39], considered only direct grain impact, assumed that all grit particles were spherical (whereas in reality they are complex polyhedra) and also assumed that the volume of material removed from each impact was hemispherical. The varying size of grit particles was considered, and incorporated into the model by the use of the statistical distribution given by Rozenberg [10]. The theoretical results obtained from the model did not entirely match the results obtained by experimentation. The analysis of the model predicted a continuous increase in machining rate with increasing static load. In practice this is not the case, as an optimum level is reached after which the machining rate falls. The theoretical values of material removal rates for a given amplitude agreed qualitatively with experimental data, but were of an order of magnitude higher than the practical value of around 32mm^3/min. The theoretical results obtained for varying abrasive size also showed a continuous linear increase, and again, in

practice there is an optimum abrasive size for a set amplitude. These anomalies could be due to the following factors :

- It was assumed that the amplitude of vibration remained constant even under maximum static load conditions. In practice this was not the case, since the amplitude of vibration decreased at higher static loads due to the tool being restricted by grains in the working gap.

- Although the model considered a statistical distribution of grain sizes under the tool, the model did not consider grain fracture, or stress relief in the workpiece due to the elastic / plastic behaviour of the abrasive material.

- The grains were not actually spherical, but a combination of spherical and point indenters. This has a direct influence on the amount of material removed per grain.

- The assumption that each grain removed a hemispherical volume of workpiece material was incorrect. Studies of brittle fracture by Evans & Wilshaw [40], Lawn & Swain [41], Lawn & Wilshaw [42] and Cook & Pharr [43] show that there are several mechanisms by which cracks in brittle solids propagate underneath indenters. The predominant mechanism depends on the predominant type of indenter geometry (spherical or pointed).

- Subsequent to the initial surface breaking of the tool, the abrasive particles impinged on a rough, pitted surface, as opposed to a flat sheet of material. This made prediction of crack initiation and propagation very difficult.

The model proposed by Nair & Ghosh [44] also assumed that the abrasive particles were removed by direct impact only. Material removal by projection, indirect impact and cavitation were not considered. Furthermore, the abrasive grains were considered spherical, and no statistical distribution of the particles under the tool tip was considered.

In addition to material removal process models, Dharmadhikari & Sharma [45], proposed a mathematical model which predicted the life of the abrasive materials used in ultrasonic machining. In comparison with the previous material removal models, this investigation is one of the few studies of the economics of the ultrasonic machining process. The study was conducted by deriving the quantitative variation of material removal rate with the time for which the abrasive had been used. In this way, the optimum abrasive life with respect to the objective functions of maximum production rate was obtained for a range of production scenarios.

2.5 CERAMIC COMPOSITES

Composites in general have been discussed widely by many authors including Partridge [46], Ashbee [47], Hull [48], Davidge [49] and Newey & Weaver [50]. Many ceramic materials have desirable properties for industrial use. High hardness, chemical resistance and the ability to withstand high temperatures are some of these characteristics. Some of these properties also make ceramics difficult to machine, since their hardness and brittle nature can make conventional material removal techniques such as turning or milling either impossible or highly inefficient, processes discussed by Frei & Grathwohl [51] and Evans [52]. For these reasons, ceramics have not found widespread use in industry, other than for applications which do not require a large amount of manufacturing resources, such as refactory linings for molten metal ladles. Recently, progress in ceramic materials technology has resulted in the manufacture of advanced ceramics and ceramic composites, as discussed by Wynne & Price [53] and Yajima *et al* [54] and [55]. Ceramic composites offer the advantages of homogeneous ceramics, but, depending on the type of reinforcement used, may have increased toughness values, higher tensile strengths and lower densities than a homogeneous ceramic. Several authors have discussed the properties of ceramic composites, Davidge [49], Stull & Parvizi-Majidi [56] and Sarin & Ruhle [57] have all made comparative studies of various ceramics and ceramic composites, and noted their superior properties. The use of ceramic composites in advanced gas turbine engines was investigated in detail by Schmid [1], who concluded that before the widespread use of these materials can become common, substantial progress in the design, manufacture and inspection of components must be made. Hunt

[58], discussed the potential of ceramic composites in industry, and charted the move from their use mainly in aerospace and defence applications to more consumer orientated applications such as electronics, automotive components and industrial machinery.

Matrix materials commonly used in ceramic composites include silicon carbide (SiC), silicon nitride (Si_3N_4) and alumina (Al_2O_3).

Silicon carbide is a common material for use in reinforcement, and may be used in continuous fibre, discontinuous fibre (whisker) or particle form.

One of the most critical factors in the performance of a composite, ceramic or otherwise, is the specification of the interface material. The interface material is a coating on the fibres, which can be used to engineer the way in which cracks are deflected around fibres, or the way in which fibres pull out of the matrix under tensile loading. A study of the influence of the interface material on the mechanical properties of fibre re-enforced alumina was performed by Barron-Antolin *et al* [59]. This investigation revealed that un-coated fibres did not improve the strength or toughness of alumina matrix composites, whereas coated fibres showed significant improvements.

Alternative manufacturing methods, specifically developed for ceramic composites, are available, making the manufacturing of ceramic composite materials more efficient. The "DIMOX" direct metal oxidation process which was used to produce the composite under investigation in this programme, is one such manufacturing technique, in which the near net shape of the component is produced in one operation. The DIMOX process is discussed extensively by Urquhart [60]. Detail features of a component such as high

tolerance holes or slots must be produced by a secondary process. This secondary machining process can cause problems in the case of ceramic composites. Komanduri [11] discussed these problems, and identified de-lamination, flaking and extreme tool wear as some of the effects which can make machining difficult or impossible using conventional cutting techniques such as turning or milling. Ultrasonic machining was proposed as a suitable machining method for ceramic composites, and in some cases such as die sinking, is the only machining method available.

The advantages of ceramic composites have been well documented, and there seems to be a consensus of opinion by most investigators that many more practical studies of the design, manufacture and testing of these materials must be carried out before their use in everyday engineering situations becomes widely accepted.

2.6 BRITTLE FRACTURE INVESTIGATIONS

Since ultrasonic machining is used primarily on brittle materials, an essential component of any analysis of the process involves the established theories on brittle fracture. Many books have been written on this subject, two of the most quoted references being the works of Lawn & Wilshaw [61] and Lawn [62]. Several observational experiments and many theories have been presented to explain the various phenomena encountered, including those by Lawn *et al* [63], Hagan & Swain [64] and Tabor [65].

One of the foremost investigations of brittle fracture was undertaken by Evans & Wilshaw [40], who studied fracture by plastic indentation in a wide range of brittle materials. Stress analysis indicated the importance of plastic penetration and interface friction in fracture development, and crack extension was found to depend primarily on impression radius and the ratio of hardness to fracture toughness. The experiments were conducted as follows : For each material, the critical indenter radius for plastic penetration was determined, which is characterised by the transition from circumferential to radial fracture. All experiments were then performed with an indenter radius below this critical value. On initial loading, the first cracks to form were shallow radial cracks emanating from the periphery of the indention crater, but with increasing load these cracks extended. Subsurface circular cracks parallel to the load axis (median vents) then began to form, and extended until, under coplanar conditions, they merged with the radial cracks. Finally, under further loading, cracks parallel to the surface (lateral vents), formed. On unloading, all cracks extended, and sometimes new cracks formed. The main material removal mechanism involved the lateral cracks propagating to the surface. It was also noted that for each material, there was a critical indenter separation distance, below which lateral cracks (and under certain conditions, radial cracks) would merge.

Lawn & Swain [41] presented theories to explain the micro fracture patterns around point indentations in brittle solids, and proposed that the findings could be used as a basis for predicting material removal rates in abrasion / erosion processes.

A comprehensive experimental study of indentation cracking in glasses and ceramics was recently performed by Cook & Pharr [43]. They concluded that there could be up to five main crack types present in indentation. These were :

Cone cracks : Generated by the elastic loading of spherical or flat punch indenters. These cracks initiated at the contact circumference of the indenter, and spread away from the surface of the material at a characteristic angle to the load axis.

Radial cracks : When loading produced an area of plastic deformation, radial cracks emanated from the edge of the surface plastic zone, and propagated parallel to the load axis. Radial cracks usually formed at an indention corner, and remained close to the surface.

Median cracks : Were also produced parallel to the load axis, and initiated below the plastic region. Median cracks (or vents), were circular in appearance, sometimes truncated by the plastic zone or material surface.

Half-penny cracks : Fractography of indentation fracture suggested that median vents sometimes had a semi - circular appearance although it was unclear as to whether these were formed by coalescence of median and radial cracks.

Lateral vents : Were formed below the plastic zone, ran parallel to the surface, and were circular in shape.

There appeared to be two variations on these crack types. The first of these, the secondary radial crack, emanated from the edge of the contact impression adjacent to rather than at an indentation corner. Propagation into the surrounding material was at an angle to the load axis. The second variation was the shallow lateral crack. These were also observed to form at the indentation edge, and propagated almost parallel to the surface of the material.

All experimentation was performed with a Vickers type diamond type indenter, and load - displacement apparatus (loads up to a maximum of 40N). Optically transparent materials were used exclusively : soda - lime silica glass, aluminosilicate glass, fused silica, borosilicate glass, sapphire and MgO.

In contrast to the findings of Evans and Wilshaw [40], Cook & Pharr [43] did not observe a general cracking sequence. The types of crack formed depended on a number of factors such as material properties, indenter geometry, peak and contact load. All crystalline materials showed radial crack formation extremely early in the loading cycle (possibly instantly), whereas glasses exhibited either no radial cracks on loading, or cracks at loadings near to the maximum applied. None of the materials showed any sign of median vent formation. Half penny cracks were observed forming from the coalescence of radial cracks. It was also noted that the accepted material removal mechanism of deep lateral vents propagating from the base of the plastic zone to the surface of the material was inaccurate. Removal by this process would have left crater like impressions on the material surface - removing the indenter impression in the process. In all cases, the indenter impressions were left substantially intact, and were easily observed after the indenter and fractured material were removed. The actual

material removal mechanism suggested was the propagation of the shallow lateral cracks to the surface, combined with secondary radial cracks propagating vertically from the material surface before arcing round and breaking the surface. This left "scallop shell" lateral impressions. It was also observed that direct reloading of the material greatly exacerbated removal rates. The authors suggested that it was this phenomenon that accounted for the failure of single impact wear models to predict accurately the wear rates for multiple impact processes (such as ultrasonic machining).

The effects noted by these investigations (Evans & Wilshaw [40], Lawn & Swain [41], Cook & Pharr [43], Lawn & Wilshaw [61] and Lawn [62]) i.e. median / radial crack systems, their origins and derivatives have been verified by many other investigators for a wide range of brittle materials. Homogeneous ceramics were specifically investigated by Lawn *et al* [66], who proposed fracture models using coefficients from optical investigations of soda-lime glass. A further study by Lawn *et al* [63], investigated indentation cracks in soda-lime glass. Hagan & Swain [64], also investigated fracture in soda-lime glass, specifically the origin of median and lateral cracks around plastic indents.

2.7 FINITE ELEMENT ANALYSIS

The finite element method is now well established as a means of stress analysis, due largely to the widespread availability of powerful computers. The problem of stress analysis of indentation processes (such as ultrasonic machining) is fundamentally a "contact" problem, because in this situation, the indenter (which could represent a grit particle) is in contact with the work surface. As the indenter is pressed into the work surface, so the indenter and work surface deform, the relative extent of which depends on the material properties of the two components.

A comparison of a 3-dimensional finite element numerical analysis of Vickers indentation, with an experimentally observed indentation load-depth (P-h) relation on soda-lime glass was performed by Zeng *et al* [67]. The P-h relationship of the finite element analysis proved to be accurate when compared with the experimentally observed relationship. In addition, the finite element numerical calculation was thoroughly compared with the experimental measurement of residual stress on the surface of the glass during Vickers indentation. Both Von Mises stress and hydrostatic stress showed a very good agreement with the experimentally measured Von Mises and hydrostatic stresses. This experiment did not consider the effect of crack formation within the workpiece, and although the formation of cracks leads to the modification of the stress field (especially immediately in front of the crack tip), a very good agreement with the experimentally obtained Von Mises stresses was still obtained. A deviation from the experimental results for the hydrostatic stress indicated that the cracks have a greater

effect on this parameter than on the Von Mises stresses. The authors concluded that the results supported the idea that the finite element numerical calculations and the experiments performed are useful tools to help understand better the mechanics of Vickers indentation brittle materials such as glass and ceramics.

The modelling of crack growth within the workpiece complicates finite element analyses considerably, but, notwithstanding the apparent levels of accuracy achieved by Zeng *et al* [67], crack growth must be included in any finite element model which is to be considered realistic. One such model was proposed by Lyons [68], who predicted failure mechanisms of short fibre-reinforced ceramic matrix composites. In order for these mechanisms to be investigated, the fibre-matrix interface had to be included in the model, as well as the orientation of the fibres within the matrix. A two dimensional model was constructed, in which fibre orientation, residual stress state and interface bond strength were varied. This permitted the isolation of the effects of these individual features to be investigated, as well as the prediction of crack paths in and around individual fibres at discrete locations within the matrix. Further studies on crack growth were made by Ming-Chang Jeng *et al* [69], who presented a finite element based methodology for the prediction of remaining crack growth life. This parameter matched experimentally obtained figures very closely, thereby validating the finite element method for this particular study.

Although extremely time consuming, it is possible to write finite element codes specifically for a particular problem. One example of this is the finite element programme for the analysis of damage and brittle fracture of an orthotropic material, proposed by Hamlili *et al* [70]. A more straightforward approach would be to use an existing finite

element software programme, which has the capability to perform contact and crack growth problems. The ABAQUS finite element code is one such programme, and provides the user with example programming routines including "The Hertz contact problem" [71], and "Conical cracks in a half space with and without sub-modelling" [72]. Variations and combinations of these two routines were used in this investigation, and are described in section 3.8 .

2.8 LITERATURE REVIEW SUMMARY

Although ultrasonic machining has been the subject of several investigations, most previous work appears to have been conducted on glass or monolithic ceramics, there appears to have been no experimental work conducted specifically on the ultrasonic machining of silicon carbide fibre reinforced alumina.

In addition, all previous ultrasonic machining process models require empirically obtained constants for validation, and therefore cannot be used in the absence of data which is specific to the workpiece material.

3. PROCEDURE

3.1 OVERVIEW

The experimental programme essentially consisted of two parts, viz., a Taguchi analysis to determine the significant variables (or factors), and a full factorial experiment using the significant factors identified by the Taguchi analysis.

Since only a limited amount of material was available, it was decided to use the Taguchi technique to establish which of the experimental variables had a significant effect on material removal rate. The Taguchi method allowed many variables to be evaluated for significance while using the absolute minimum of material. Before any experimental work began, there were several modifications which were made to the ultrasonic machine in order to make certain parameters available (such as amplitude measurement, and x-axis semi-automatic traversing). A more detailed account of this procedure is outlined in the following paragraphs.

3.2 INITIAL MACHINE DEVELOPMENT

3.2.1 STANDARD ULTRASONIC MACHINE DESCRIPTION

The basis of the machine used for the project was a McLean "Sonimill", a diagram of which is shown in Figure 1. This machine utilised a 150 watt transducer of the magnetostrictive type, and incorporated a variable speed 1/8 hp. D.C. electric motor for rotary machining operations. The motor spindle could be locked to enable conventional machining to be performed. Static tool load was controlled by a buoyancy system in which the machining head was counterbalanced by a mass contained within a cylinder. This cylinder could be filled with oil by an electric pump, thereby altering the buoyancy of the counterbalance, and so altering the tool load. The flow of oil into the cylinder (and therefore the static load) was controlled by a gate valve. The penetration depth of the tool was obtained from a standard dial gauge mounted beside the sonotrode. The machine had a standard manually controlled 2 axis milling bed. The tool tips supplied with the machine were diamond coated, and therefore did not require an abrasive slurry to be used. A single cooling fluid jet was fitted. The machine was operated from a separate console, which had controls for the power setting (amplitude), rotation speed, hydraulic pump and coolant pump. A small meter indicating amplitude was also provided. Three power settings were provided, marked "STAND-BY", "LOW", "MEDIUM" and "HIGH". Once the appropriate setting had been selected, the frequency could be fine tuned by means of a rotary switch which had nine increments. This was set to give the highest peak to peak amplitude on the meter.

3.2.2 MODIFICATIONS MADE TO STANDARD MACHINE

In order to carry out the initial experimental programme, several modifications to the standard machine were required. A diagram of the modified machine is shown in Figure 2. Details of the specific modifications are outlined in the following paragraphs.

A replacement sonotrode was required, as the original brass item was matched to the standard diamond tipped tools. The geometry of the new sonotrode was designed in accordance with the equations given by Markov [9], and turned from aluminium alloy, as shown in Figure 3. This optimised sonotrode incorporated a female thread in the tip, so that tools of different diameter could be quickly changed. A selection of tool tips of various diameters was also designed and manufactured from mild steel, as shown in Figure 3.

Since no provision was made for the use of abrasive slurry during machining, an entire system was designed, manufactured and fitted. The main component in this system was a stainless-steel hopper constructed around a raised machining surface, as shown in Figure 4. This fabrication was bolted to the existing machining bed, to form a collector for used slurry, and a sump from which the slurry would be recirculated. A propeller type stirrer was used to agitate the slurry in the sump, thereby ensuring thorough mixing and a more consistent abrasive : water concentration.

The abrasive slurry was recirculated by a peristaltic pump, which had its inlet tube positioned in the sump of the hopper. The slurry was then passed up a delivery tube and through a copper nozzle. The nozzle was mounted in an adjustable clamp to allow accurate positioning relative to the tool.

The gate valve which controls the oil flow into the buoyancy cylinder did not allow accurate enough adjustment for experimental purposes, and was supplemented by a smaller, indexed valve, mounted in parallel with the original valve. This allowed pre-set levels of flow rate, and therefore static load, to be selected with a higher degree of repeatability. The new valve was calibrated by placing a "Kistler" load washer underneath the tool, and noting the applied forces for different valve settings. In this way, a calibration chart was drawn, and is shown in Figure 5.

The amplitude gauge on the control console was found to be inaccurate, so was supplemented by fitting a "Kaman" amplitude transducer fitted at the top end of the new sonotrode, and used in conjunction with an oscilloscope. After calibration by feeler gauges, the transducer was left in place to enable "in process" amplitude to be measured. The calibration chart used is shown in Figure 6. The settings on the standard machine were found to correspond to the following tool amplitudes :

LOW : 13.6 microns

MEDIUM : 18.2 microns

HIGH : 22.7 microns

Since the industrial partners were interested in the milling of the material, it was decided to retro-fit the x-axis lead screw of the machining bed with an electro-mechanical drive. This involved the design of mountings and couplings for a D.C. motor. The motor was connected to a variable speed controller and adjustable limit switches. The variable speed control was then calibrated in mm/min., and the position of the limit switches fixed to

give the appropriate slot length defined in "Experimental Procedure". The calibration chart for the traverse speed controller is shown in Figure 7.

It was also necessary to draw a calibration chart for the tool rotation speed function, since the controller was not graduated in revolutions per minute. A mechanical tachometer was used to determine the actual rotation speed of the tool at different settings, and the calibration chart is shown in Figure 8.

Once the modifications to the machine had been made, several test runs were made on plate glass to verify the systems. Two preliminary runs (one milling, one drilling) were then made on the sample material in order to establish whether the process would, in practice, be suitable for this specific material. With these initial tests successfully performed, the full experimental programme could begin.

3.4 EXPERIMENT DESIGN

3.4.1 INDUSTRIAL AND ACADEMIC REQUIREMENTS

Ultrasonic machining is a process with many variable parameters, each of which can have a significant effect on either the material removal rate and/or surface finish and integrity of the material being machined.

Since the project involved using a new advanced material which had never before been the subject of an ultrasonic machining study of any kind, it was decided to conduct a full experimental programme in order to establish the suitability of the material for the process.

Certain process details were defined by the industrial collaborators: The abrasive slurry was to be an aqueous solution. This was due to the fact that it had been established in development that the material in question was unaffected by water, and that water would not therefore contribute in any way to the erosion of the material by chemical reaction. Silicon carbide was also recommended as the abrasive due to it's chemical neutrality and availability.

Previously conducted studies of ultrasonic machining on common homogeneous materials such as glass (Kazantsev & Rozenberg [21], Soundararajan & Radharkrishnan [22], Komaraiah *et al* [32], Ghosal *et al* [34]), had used conventional ultrasonic drilling

as a basis for material removal rate models and experiments. However, the industrial collaborators in this project were primarily concerned with the ultrasonic *milling* of the material. It was therefore decided to conduct two initial experimental programmes, one for drilling, the other for milling.

3.4.2 EXPERIMENTAL PARAMETERS

On the basis of previous experimental studies of ultrasonic machining by Kazantsev & Rozenberg [21], Soundararajan & Radharkrishnan [22], König & Hilleke [23], Komaraiah [24], Komaraiah & Reddy [26], Koval'chenko *et al* [27], Nandy *et al* [28], Dam *et al* [29], Komaraiah *et al* [32], Zhixin & Zing [33], Ghosal *et al* [34] and Hocheng & Hsu [35], the following process variables were considered :

- Power Setting (Amplitude μ, microns).
- Abrasive size (Average mesh size, microns).
- Abrasive Concentration. (% v/v).
- Tool Tip Ø (mm).
- Static Load (kg.).
- Rotation Speed (r.p.m.).
- Traverse Speed (mm/min.).

3.4.3 EXPERIMENTAL CONSIDERATIONS

It is evident that if all these factors were to be taken into consideration in a full experimental grid, the initial programme would be very large. Even using the minimum of two levels for each factor, with no repeats, there would be 64 experimental runs for the hole drilling operation, and 128 runs for the slot milling operation. This gave a total of 192 runs. An experimental programme of this size would have taken a considerable amount of time to complete, would have provided unverifiable results, and would have required a much larger amount of material than was available.

It was therefore decided to use a factorial type experiment which would significantly reduce the total number of runs required, and reveal which of the variables were significant and which were insignificant to the material removal rate of the process. The significant factors yielded would then form the basis of a full experimental programme the results of which could be used to construct an empirical mathematical model for the specific material removal rate of the process.

3.5 THE TAGUCHI METHOD

Since the Taguchi method was a well established procedure for quality control in industrial engineering and can be applied readily to large experiments of this type, it was decided to use this method as a starting point for the programme (the experimental programme conducted by Hocheng & Hsu [35] used this method). The Taguchi method is described in detail by Ross [73].

3.5.1 PROCESS VARIABLES

The first stage in the Taguchi process involved identifying the variables (or factors) to be studied. In the case of ultrasonic drilling these factors were :

- Power Setting (Amplitude μ, microns).
- Abrasive size (Average mesh size, microns).
- Abrasive Concentration. (% v/v).
- Tool Tip Ø (mm).
- Static Load (kg.).
- Rotation Speed (r.p.m.).

And for ultrasonic milling, the factors were :

- Traverse Speed (mm/min.).
- Power Setting (Amplitude μ, microns).
- Abrasive size (Average mesh size, microns).
- Abrasive Concentration. (% v/v).
- Tool Tip Ø (mm).
- Static Load (kg.).
- Rotation Speed (r.p.m.).

3.5.2 EXPERIMENTAL FACTORS AND LEVELS

The next stage involved the determination of the number of required levels to represent each factor. For initial experiments such as this, it was common practice to use the highest and lowest practically usable or available extremities of each factor. This was the best method of obtaining the greatest magnitude of difference between levels, since it made differentiation of significant factors more definite. The relevant factors and levels are shown in Table 1. Each factor was also assigned an identification letter at this stage.

Factor A - Power setting. The Power Settings were assigned 'high' and 'low' since the machine control dial was only calibrated in terms of HIGH, MEDIUM and LOW power settings. The corresponding amplitudes are given in Section 3.2.2

Factor B - Abrasive size. The abrasive sizes of #320 and #120 represent the common size limits of silicon carbide abrasive used in ultrasonic machining. #120 (equivalent to

142 microns) is commonly used for roughing, and #320 (equivalent to 32 microns) for finishing. A summary of abrasive mesh sizes is shown in Table 2.

Factor C - Abrasive concentration. The abrasive concentrations were selected on a more practical basis. A concentration of anything greater than 40% v/v became too viscous to pump effectively, and with anything less than 20% v/v, it became difficult to maintain a consistent mixture of abrasive and water due to the settling out of the abrasive - especially with large grit sizes.

Factor D - Tool diameter. Tool Tip diameters were settled by consideration of the minimum diameter which could be turned in the machine shop without requiring special techniques, and by considering the dimensions of the slots which were to be machined in industry. This minimum diameter was settled at 1mm. The maximum diameter was governed by the end dimensions of the optimised sonotrode. After considering allowances for machining spanner flats on the interchangeable tips, the maximum diameter was set at 6mm.

Factor E - Tool rotation speed. Rotation speeds were simpler to define. A zero value was obviously the lower limit, and a value of 300 r.p.m. was set as the higher limit.

Factor F - Static tool load. The maximum static load was similarly defined by the machine's capabilities. The minimum static load was again zero, but very little machining would take place at this load; certainly not enough to provide the necessary data for any meaningful analysis. It was therefore decided to use 1kg as the lower limit. The upper limit was set at 5kg, since this was the limit of the machine's capability.

Factor G - Traverse speed. An upper limit of 1000 mm/min. was chosen, since this would allow sufficient time between switching traverse direction. Although the minimum traverse speed is zero, this would not be milling, but drilling. An arbitrary lower limit of 150 mm/min. was therefore chosen.

3.5.3 ORTHOGONAL ARRAYS

Once the factors and levels had been defined, they were placed in an "Orthogonal Array" (condensed versions of full factorial grids, having only a fraction of the total number of cells of a full factorial grid). The type of orthogonal array used depended on three parameters : The number of factors, the number of levels each factor was to be represented at, and whether or not any of the factors were anticipated to interact with each other.

Since there were no anticipated interactions for either drilling or milling, both experiments could be performed using an "L8" orthogonal array. This means that eight experimental runs must be performed for drilling and eight for milling, in order to obtain the necessary data for the Taguchi analysis. An L8 array is shown in Table 3.

3.5.4 TAGUCHI EXPERIMENT RUNS

An experiment run was then performed in the following way : Trial 6 (Table 3) for example : Factors B, E & G were set at level one, and factors A, C, D & F were set at level two (refer to Table 1 for the actual values). Once the timed trial was complete, the machined area could be measured and the material removal rate calculated.

3.5.5 SATURATION OF ORTHOGONAL ARRAYS

It is clear that for the slot milling operation, there were seven factors available in the grid, and seven factors to be evaluated. In this case, the L8 orthogonal array is said to be "Fully Saturated".

For the hole drilling operation, again there were seven factors available, but only six factors to be evaluated. In this case, the redundant factor was assigned as "noise", which could be used during the data analysis stage for verification purposes (this is discussed in more detail in Section 4).

3.6 TAGUCHI EXPERIMENT PROCEDURE

3.6.1 MACHINE FAMILIARISATION

In order to reduce the amount of experimental error to a minimum and to conserve the test material sample, it was considered important to become familiar with the operation of the systems of the machine. With this in mind, several runs were performed on glass and homogeneous ceramics before using the composite material.

3.6.2 HOLE DRILLING TRIALS

Each trial was conducted for hole drilling as follows : The material sample was clamped to the machine bed, and positioned underneath the tool by means of the hand crank and motor. The hopper was filled with one litre of abrasive slurry, pre-mixed to the appropriate concentration. The slurry agitator and pump were then started. The slurry nozzle was positioned beside the tool tip, and the ultrasonic transducer switched on and set to the appropriate power setting. The buoyancy valves were turned to their pre-set positions allowing the tool to move downwards. When the tool tip impinged on the workpiece, the stopwatch was started. As soon as a depth of > 1mm was reached (as read from the dial gauge), the buoyancy valves were opened, raising the tool. The stopwatch was stopped simultaneously and the time recorded.

3.6.3 SLOT MILLING TRIALS

For slot milling, the procedure was very similar, with the addition of setting the traverse speed and starting the motor just before the tool tip impinged on the workpiece. When the pre-set limit switches were tripped, the motor direction was reversed.

3.6.4 PARAMETER RANDOMISATION

On the basis established experimental techniques outlined by Ross [73], it was decided to randomise completely the order in which the trials were performed. In many cases, this required the setting, changing and subsequent re-setting of machine controls.

3.6.5 TRIAL REPETITION

Each trial was repeated three times, again not necessarily consecutively. This ensured that each individual run had the minimum chance of being affected by any unforeseen external influence.

3.6.6 SYSTEMS CHECKING

Machining parameters such as static load, rotation speed, traverse speed and amplitude were checked several times during the experiment to ensure consistency.

3.7 FULL FACTORIAL EXPERIMENT DESIGN

3.7.1 ADDITIONAL MODIFICATIONS FOR FULL FACTORIAL EXPERIMENT

After successfully completing the Taguchi experiment and therefore establishing which of the parameters were of significance, there were several modifications which were made to the machine in order to increase the accuracy and ease of operation of the systems. These are illustrated in Figure 2.

The main modification was the fitment of a large load cell between the bed of the machine and the slurry hopper / machining table fabrication. This allowed accurate in-process static load data to be observed.

A more sturdy clamping system for the material samples was also used, this was basically two steel strips, drilled at each end. Bolts were then passed through the holes and screwed into four corresponding threaded holes in the machining bed, thus enabling the samples to be clamped firmly against the machining bed in any horizontal orientation.

3.7.2 FACTORS USED IN THE FULL FACTORIAL EXPERIMENTAL PROGRAMME

The main difference between the Taguchi analysis and the full experimental programme was the variation of each factor. In the Taguchi analysis, each factor was represented with just two levels, a "high" setting and a "low" setting. For example, abrasive size was represented by #120 grit and #320 grit. For the full factorial experiment, a wider range of grit sizes was used i.e. #120, #220, #320 and #600. This enabled a more comprehensive analysis of the effect of grit size. A summary of the full experimental programme is shown in Table 4 (for hole drilling) and Table 5 (for slot milling).

3.7.3 NOMINAL PARAMETER SETTINGS

The "nominal parameter settings" are the settings which were used as a datum from which the main parameters were varied. A summary of these settings is shown in Table 6 (for hole drilling) and Table 7 (for slot milling).

3.7.4 ADDITIONAL CONSIDERATIONS FOR THE FULL FACTORIAL EXPERIMENTAL PROGRAMME

Further reading between completing the Taguchi analysis and beginning the final experimentation revealed the possibility that tool material may also be an important factor in ultrasonic machining. With this in mind, three different tool materials were

chosen : mild steel, stainless steel and Nimonic 80A. Three identical tools were produced from each material (to the same dimensions as shown in Figure 3), and each factor was repeated with the different tool materials.

3.7.5 FULL FACTORIAL EXPERIMENTAL PROGRAMME : SAMPLE MATERIAL CONSIDERATIONS

It was decided to repeat each run twice, in order to give some degree of confidence in each result. Repeats of three or more runs are common in many experimental programmes (each run was repeated three times in the Taguchi procedure for example), but it was impossible to do this due to the limited amount of material available. For the same reason slot lengths also had to be limited. A nominal traverse length of 20 mm was proposed since this would conserve workpiece space while still allowing a significant "free" traverse length between the end stops.

3.7.6 INCLUSION OF PLATE GLASS IN THE FULL FACTORIAL EXPERIMENTAL PROGRAMME

A further addition to the experimental programme was the inclusion of plate glass samples for both hole drilling and slot milling. The reason for this was to enable a direct comparison of the machining characteristics of a homogeneous material of known mechanical properties and machinability (glass) with a composite material of unknown machinability. Even with only two repeats, the total number of runs performed was 540.

3.7.7 MACHINE CALIBRATION

Before beginning the programme, the ultrasonic machine systems were fully checked and calibrated.

3.7.8 ABRASIVE CONCENTRATION TEST

In order to check that the abrasive concentration at the tool output nozzle would be similar to the concentration in the sump, the following procedure was followed:

1) A slurry was mixed using #220 grit to a known concentration of 65% by volume.

2) The slurry was placed in the hopper and agitated for 5 minutes with the pump switched on.

3) Samples of slurry were taken from the delivery tube at two minute intervals.

4) After 2 hours of settling time, the concentration of the samples was ascertained.

Results of the concentration test are shown in the Table 8. These results indicated that the slurry concentration remained constant for all practical purposes, with a grit concentration range of 1.73 % by volume over a time period of 6 minutes. A grit size of #220 was chosen since this represented the "mid range" of the parameter, slightly biased towards the larger, heavier particle sizes which were more difficult to keep in suspension.

The relatively high concentration of 65% was chosen since this would be more prone to settling out than the actual experimental value of 20%.

3.7.9 LOAD CELL CALIBRATION

The replacement load cell apparatus was calibrated and checked by placing standard masses on the machining bed. The load cell proved accurate with respect to the calibration previously obtained from the load washer (Section 3.2.2).

3.7.10 AMPLITUDE TRANSDUCER CHECKING

The amplitude transducer was checked by using feeler gauges, and the figures obtained were found to concur with those in Figure 6

3.7.11 EXPERIMENTAL PROCEDURE

A typical hole drilling procedure is outlined below. Additional actions required for slot milling are shown in square brackets [].

(1) The appropriate tool tip was screwed into the sonotrode tip using Loctite 241. This was necessary in order to prevent vibrations loosening the tool due to the low fixing torque required by the aluminium sonotrode.

(2) The sample was placed on the bed of the machine.

(3) The tool tip was lowered onto the surface of the sample and the dial test indicator zeroed.

(4) An abrasive slurry of the appropriate concentration for the run was prepared and placed in the hopper.

(5) The load cell was zeroed.

(6) The appropriate load was applied to the sample by adjusting the "fine tune" oil valve.

(7) With the set load still applied, the tool head was raised manually, and secured with a wedge.

(8) The agitator and pump were started.

(9) The ultrasonic transducer was switched on (having been preset to the appropriate amplitude).

(10) The wedge was removed from the tool head, allowing the latter to fall gently onto the surface of the sample, which produced contact between the loaded tool tip and the surface to be machined.

[10a] Once the tool was in contact with the surface, the y-axis traverse motor was started. When the tool reached the automatic end stop, the tool motion was reversed.

(11) When the dial test indicator registered approximately 1mm, the tool was raised manually, and wedged in position out of contact with the specimen surface.

[11a] The y-axis traverse motor was stopped.

(12) The machine bed was moved to the next marked area, and the same process repeated from step (9) with identical machine settings. Or, when experimental factors required changing, the machine bed was moved to the next marked area, and the process was repeated from step (1) onwards .

All drilling and milling operations were stopped at a nominal machined depth of approximately 1 mm. This ensured that any depth related factors (such as abrasive slurry circulation around the tool tip or tool vibration damping effects) were kept constant as much as possible.

3.8 FINITE ELEMENT MODEL

3.8.1 STATIC MODELLING

In order to establish the stress fields below the grit particles during machining, a finite element stress model was employed. It was hoped that knowledge of the stresses produced within the model would enable the onset of fracture and crack propagation to be predicted. From this, the volume of material removed for each impact might be estimated, leading to the prediction of the relationships between theoretical material removal rates and the various experimental parameters. All finite element analysis work performed utilised "ABAQUS" software.

The basis of the models constructed was a single grit particle impinging upon a workpiece of homogeneous material as described by Bhattacharya & Nix [74]. Each grit particle was represented by a sphere, since it would be impossible to construct a realistic complex polyhedral particle model in the time available. In practice, grit particles attain spheroidal dimensions after a short time in use, since the sharp protrusions are quickly blunted by the forces involved in machining. Hence the use of spheres in the model, which appeared to be a realistic compromise.

The construction of a representation of the workpiece fibre lay-up and topology would also require a significant amount of modeling time, and subsequent analysis time. The practical experimental programme results revealed that the conventional crack stopping/diverting properties present in a conventional composite under stress did not

apply to this ceramic composite under impact loading (these observations are examined in detail in the discussion chapter). Also, in view of the relative sizes of grit and fibre diameters (i.e. the fibres are much smaller than the particles), it was decided to model the workpiece material as a homogeneous material, and input the material's bulk properties.

These two initial assumptions served the purpose of simplifying the model, allowing faster processing times and simplified editing.

The meshes were constructed using a combination of 8-noded plain-strain axi-symmetric elements and rigid surface elements. Elements which came into contact with each other during movement were linked by 8 noded interface elements. These elements allowed an accurate analysis of the deformation of the grit and workpiece surfaces, as well as a more accurate analysis of the stress distribution in the machined material.

Several modeling techniques were used in order to ascertain the most efficient method of modeling (in terms of time for geometry construction and post-processing). Some models represented the grit/workpiece model sliced through the vertical axis of symmetry i.e. through the mid-plane of the grit particle and the point of contact. In this case the elements were fully restrained along the base of the workpiece, and restrained in the x-direction along the axis of symmetry. The top node of the top grit element was then subjected to a pre-determined force of 0.05 N (to represent the static load, obtained by dividing the static tool load by the average number of abrasive particles present underneath the tool), and simultaneously displaced downwards by 20 microns (representing the amplitude of vibration). These boundary conditions then represented

the loads and conditions applicable to a single abrasive particle under maximum load conditions.

However, the models which were chosen for the investigation represented the lower half of a grit particle impinging on the workpiece. In this case, the grit was modeled as a "rigid surface", and was loaded by moving the central node (represented by a centre mark) downwards. This method produced stresses and deformations in the workpiece only. The "rigid surface" method of modeling was much quicker than a complete meshing of the grit, in terms of both geometry input time and processing time, but was less accurate, as the stress distribution in the particle and the effect of this on the stress distribution in the workpiece could not be analysed.

3.8.2 CRACK PROPAGATION MODELLING

These models were produced in collaboration with Woon [75] as part fulfillment of the degree of Master of Science.

As with the static modeling, ABAQUS software was used for these models. The geometry was constructed in three dimensions, using a one quarter model of the sphere and workpiece, using symmetry about the x-y and y-z planes. Up to a distance of around 10 times the crack length away from the crack, reduced integration elements (C3D20R and CAX8R) were used. Beyond this distance, infinite elements (CIN3D12R and CINAX5R) were used. Elements surrounding the crack tip (parallel to the y-axis consisted of 16 elements arranged in 8 rings. In order to obtain the strain singularity, all

nodes in each crack front node set were tied together using multi-point constraints, and on element edges radial to the crack front, the mid-side nodes were moved to the 1/4 point position. This improved the modeling of the strain field near the crack tip, resulting in more accurate J-integral values. There were three areas of degenerate elements; at the crack tip, collapsed elements were used to provide the desired singularity. The elements at the crack opening and the elements along the y-axis were also collapsed to simplify the meshing.

3.9 MICROSCOPY

Microscopy was used extensively to analyse the effect of ultrasonic machining on the following :

- The ceramic composite under investigation
- The abrasive grit used in the machining slurry.
- The tools which were used in the process.

A combination of optical, and scanning electron microscopy was used, depending on the nature and scale of observation required.

3.9.1 OPTICAL MICROSCOPY

Optical microscopy was used exclusively for the examination of tools after processing, for the initial examination of machined regions of the composite and of used grit particles. Magnifications used were of the order of 100x. Areas identified as being of interest were then subjected to more the powerful analytical techniques available when using a scanning electron microscope.

3.9.2 SCANNING ELECTRON MICROSCOPY

The scanning electron microscope (S.E.M.) was used to examine machined areas of composite, and the debris left within the grit slurry after machining up to magnifications of around 3100x. In order to determine the composition of selected particles in the grit slurry debris, any suitable particle targeted was subjected to X-ray composition analysis. This technique proved invaluable in ascertaining the nature of material removal during ultrasonic machining.

3.10 POST EXPERIMENT PROCESSING

3.10.1 MEASUREMENT OF MACHINED HOLE AND SLOT DIMENSIONS

For material removal rate calculations, the exact depth of each hole and slot was determined by using a digital dial test indicator in the metrology department under laboratory conditions. Depths were measured by placing the dial test indicator on the sample immediately adjacent to the hole or slot, and zeroed. The sample was then moved and the dial test indicator placed in the cavity. In this way, an accurate indication of depth was gained, since any errors of form of the sample (i.e. waviness) were minimised.

Hole depths were measured in one place, and slot depths were measured in two places, and the average taken.

Hole diameters and slot lengths were measured with an optical toolmakers microscope (as for the Taguchi experiment).

3.10.2 SURFACE ROUGHNESS MEASUREMENT OF SLOTS

Measurements of surface roughness were taken from the base of each slot, and compared with readings from the unmachined surface of the sample. The surface roughness parameters used were as follows :

Traverse length : 10mm

Evaluation length : 7.5mm

Sample length : 3 x 2.5mm

Filter : Gaussian

Analysis method : Least squares line

The machine used was a Rank Taylor-Hobson Talysurf.

4. RESULTS

4.1 INTRODUCTION

This chapter outlines the results obtained from the procedures performed during this investigation.

4.1.1 EXPERIMENTAL RESULTS

The experimental results were broken into two groups; firstly, those from the Taguchi experiments (Section 4.2), and secondly, those from the full factorial experiments (Section 4.3). The results from the full factorial experiments included data regarding both material removal rates and, in addition for slot milling, surface roughness values. Data from the use of differing tool materials was also gathered.

4.1.2 MICROGRAPHIC RESULTS

Micrographs were obtained of the structural features of the holes and slots in the composite both pre and post machining. In addition, an examination was made of samples of post machining debris, and various tool tips after their use for the machining of the composite. The micrographs are described in Section 4.4 .

4.1.3 FINITE ELEMENT ANALYSIS RESULTS

Plots and data files from the finite element analysis programme were obtained, in order to ascertain the likely stress concentration areas and probable crack paths in the composite adjacent to a grit particle (Section 4.5)

4.2 TAGUCHI EXPERIMENT RESULTS

4.2.1 RAW DATA OBTAINED FROM THE TAGUCHI EXPERIMENT

After performing the Taguchi analysis as outlined in "Preliminary Experimental Procedure", tables containing raw data were drawn. Table 9 shows the hole diameter, hole depth and volume of material removed during the trials for the Taguchi hole drilling experiment. Since each trial for the Taguchi experiment was repeated three times, and there were eight separate trials in the orthogonal array used (see Section 3.5.3 and Table 3). There were 24 runs in total. With reference to Table 9 , holes 1 - 3 represent trial 1, holes 4 - 6 represent trial 2, holes 7 - 9 represent trial 3 etc. The average of the three hole volumes was then taken. A similar approach was taken when dealing with data from the slot milling trials : Table 10 shows the slot width, slot length, slot depth and volume of material removed during trials for the Taguchi slot milling experiment.

4.2.2 ORTHOGONAL ARRAY AND DATA FOR HOLE DRILLING

Table 11 shows the completed L8 orthogonal array. Table 11 is basically a combination of Table 3 ("the L8 orthogonal array") and Table 9 ("Raw data obtained from the Taguchi hole drilling experiment"). The material removal rate was calculated for each trial by dividing the volume of material removed by the time taken for removal. The

average material removal rate was then obtained. The factors A - G are discussed in detail in Section 3.5.2, and summarised in Table 1 "Factors and levels used for the Taguchi analysis".

4.2.3 APPLICATION OF THE TAGUCHI METHOD

After calculating the average material removal rate of each experimental run, the Taguchi method could be applied. This basically involved averaging all the material removal rates set at level one, and all at level two, for each factor. Since the orthogonal array is constructed so that all other factors become irrelevant, the difference between these averages is the "Significance Rating" of the chosen factor. The significance rating of each chosen factor is given in Table 12. Since the factor "G" was not used in this experiment, the data obtained could be assumed to be the significance rating of experimental "noise". The "F-Ratio" (introduced in Table 12) was then the ratio of significance rating to noise. This gave a more accurate idea of overall significance. The "percentage contribution" column in Table 12 was simply the percentage contribution of each factor calculated from the F-Ratios.

4.2.4 EXAMPLE CALCULATION USING THE TAGUCHI METHOD

To help explain of the use of the Taguchi method, a sample procedure is given below for the case of factor B - abrasive size.

"Significance rating"

With reference to Table 11. The first two trials were at level 1, i.e. #320 grit size, the third and fourth trials were at level 2, i.e. #120 grit size, the fifth and sixth trials were at level 1 and the seventh and eighth trials at level 2. All material removal rate values obtained at level 1 (trials 1, 2, 5 and 6) were summed, and a value of 0.36 mm^3/sec obtained. Similarly, all material removal rate values at level 2 (trials 3, 4, 7 and 8) were summed, and a value of 1.538 mm3/sec was obtained. The *average* difference between these values indicates the magnitude of the effect of factor B on the process i.e. the significance rating :

$$((1.538 - 0.360)^2)/8 = \mathbf{0.174}$$

If there had been no difference between the material removal rates at level 1 and level 2, then changing from level 1 to level 2 would have had effectively no influence on the material removal rate. The orthogonal array is constructed in such a way that however the trials are arranged, all factors which are not being considered are cancelled out by having equal numbers of trials at level 1 and level 2. Since there *was* a difference between the values, then changing the level must have had some effect. By repeating the calculation for all factors and comparing the values obtained, the relative significance of each factor could be obtained.

"F - Ratio"

Since factor G had no assigned properties, it became a control level, representing experimental noise. As expected, the difference between high and low levels of factor G

was small (0.022). In the case of an ideal experiment, the value would have been zero. The significance rating of a factor was then divided by the significance rating of noise, and an indication of the true importance of a factor obtained. This figure became the F-Ratio. In the case of Factor B :

0.174 / 0.022 = **8.030**

"Percentage contribution"

These figures indicate the overall percentage contribution of a factor, and were calculated from the significance ratings, e.g. for Factor B :

$$\text{Percentage contribution} = \frac{\text{(significance rating for factor B)}}{\text{(sum of all significance ratings)}} \times 100$$

$$\text{Percentage contribution} = \frac{0.174}{0.449} \times 100$$

$$= \mathbf{38.623\ \%}$$

4.2.5 ORTHOGONAL ARRAY AND DATA FOR SLOT MILLING

The data shown in Table 14 was obtained in a similar way to that of hole drilling, with the exception of the F-ratio. Since the orthogonal array for slot milling was "fully saturated", there was no "Noise" factor. In this case, the three factors with the lowest

significance were averaged, and this value taken as equivalent to the significance rating of experimental noise. A summary of the Taguchi analysis results for slot milling is shown in Table 14.

4.2.6 TAGUCHI RESULTS SUMMARY : HOLE DRILLING

Figure 9 is a graphical representation of the results of the Taguchi experiment for hole drilling, and was drawn using the data from Table 12. It was apparent from the data that a clear distinction between the most significant and the least significant factors could be made : factors A (power setting), C (abrasive concentration), D (tool tip diameter) and G (experimental noise) *were not* significant, while factors B (abrasive size), E (tool rotation speed) and F (static tool load) *were* significant.

4.2.7 TAGUCHI RESULTS SUMMARY : SLOT MILLING

Figure 10 is a graphical representation of the results of the Taguchi experiment for hole drilling, and was drawn using the data from Table 14. For slot milling, the least significant factors were : A (power setting), D (tip diameter) and G (traverse speed). The most significant factors were B (abrasive concentration), C (abrasive concentration), E (tool rotation speed) and F (static load).

4.2.8 TAGUCHI RESULTS VERIFICATION

The significant factors obtained were verified in the following manner : By referring to the orthogonal arrays and results, each of the relevant functions were set at the level which yielded the highest material removal rate. Since none of the standard trials incorporated all the factors at their optimum material removal rate level for hole drilling, in theory the material removal rate when all factors were optimised should have yielded a material removal rate which is higher than any in the standard experiment.

The factors and levels which should yield the highest material removal rate for hole drilling are shown in Table 15. The closest trial to this was trial 4 (which yielded the highest material removal rate of 0.725 mm^3/sec.). When the factors and levels were set exactly as in Table 13, the material removal rate (obtained experimentally) was 0.750mm^3/sec.

The corresponding table for slot milling is shown in Table 16. For slot milling, trial 4 corresponded exactly to the optimum conditions, and as expected this yielded the best material removal rate.

4.2.9 SUMMARY OF TAGUCHI EXPERIMENT RESULTS

In summary, the significant factors for ultrasonic hole drilling were :

ABRASIVE SIZE

ROTATION SPEED

STATIC LOAD

The significant factors for slot milling were :

ABRASIVE SIZE

ABRASIVE CONCENTRATION

ROTATION SPEED

STATIC LOAD

With the Taguchi analysis carried out successfully , It was possible to plan the remainder of the experimental programme with confidence.

4.3 FULL FACTORIAL EXPERIMENT RESULTS

4.3.1 RESULTS FOR HOLE DRILLING OF SiC / Al_2O_3 COMPOSITE

The following descriptions are of the graphs represented in Figures 11, 12 and 13. The graphs represent the results obtained for the ultrasonic hole drilling of SiC / Al_2O_3 composite. The raw data used to produce the graphs is included in Tables 17, 18 & 19.

4.3.2 GRIT SIZE vs. MATERIAL REMOVAL RATE

With reference to Figure 11 and Table 17. As average grit particle size reduced (i.e. mesh number increased), material removal rates reduced in proportion. The difference in material removal rates when utilising different tool materials appeared to be more significant for large grit sizes than for smaller ones. The mild steel tool yielded more than double (2.15 times) the material removal rate of stainless steel when using #120 mesh size (a range of 0.304 mm^3/sec.). The significance of tool material appeared to reduce gradually with decreasing grit size, until at #600 mesh, the three tool materials yielded a material removal rate range of only 0.019 mm^3/sec.

4.3.3 TOOL ROTATION SPEED vs. MATERIAL REMOVAL RATE

With reference to Figure 12 and Table 18. Initially, material removal rates increased linearly with increasing tool rotation speed. An optimum value was then reached, before material removal rates began to reduce. In this case the optimum tool rotation speed was

around 600 r.p.m. This value applied to all tool material types tested. The effect of tool material type was significant, with mild steel yielding the highest material removal rates, and Nimonic 80A yielding the lowest rates. The minimum material removal rate range between the three tool materials was 0.251 mm^3/sec. (at 200 r.p.m.), and the maximum range was 0.835 mm^3/sec. (at 800 r.p.m.). The material removal rates obtained with stainless steel and Nimonic 80A tools were similar, with stainless steel marginally higher at specific rotation speeds up to 200 r.p.m., but with progressively higher material removal rates than Nimonic 80A up to the experimental limit of 800 r.p.m. The mild steel tool yielded significantly higher material removal rates at all speeds. All three trend lines were similar in appearance.

4.3.4 STATIC LOAD vs. MATERIAL REMOVAL RATE

With reference to Figure 13 and Table 19. Material removal rates increased in proportion with increasing static load, before reaching an optimum value and subsequently decreasing. In this case the optimum value appeared to be around 2 kg. Tool material was a significant factor in this case, with mild steel yielding the highest overall material removal rates and stainless steel yielding the lowest material removal rates, with Nimonic 80A lying in-between. The inconsistency in the curve relating to Nimonic 80A is most likely to be due to experimental error rather than any significant effect of a 2 kg load when using Nimonic 80A.

4.3.5 DATA PROCESSING FOR HOLE DRILLING OF SiC / Al_2O_3

Figures 14, 15 and 16 were drawn from the raw data included in Tables 17, 18 and 19. In all three cases, the material removal rates for the three tool materials were averaged, and the trend lines plotted using the new data. The equation of each line is shown on the graphs, and may be used as a representation of the empirical expression of the behaviour of the relevant factor.

4.3.6 RESULTS FOR SLOT MILLING OF SiC / Al_2O_3 COMPOSITE

The following descriptions are of the graphs represented in Figures 17, 18, 19 and 20. The graphs represent the results obtained for the ultrasonic slot milling of SiC/Al_2O_3 composite. The raw data used to produce the graphs is included in Tables 20, 21, 22 and 23.

4.3.7 GRIT SIZE vs. MATERIAL REMOVAL RATE

Figure 17 shows that overall, material removal rates decrease as the abrasive size is reduced. Tool material did have some effect on the results, with, on average, mild steel tools yielding the highest, and Nimonic 80A tools yielding the lowest, material removal rates. Material removal rates obtained when using stainless steel tool tips appeared to lie between those of mild steel and Nimonic 80A, except at the extremes of the grit size range : at #120 mesh, the stainless steel tools yielded the lowest material removal rates, and at #600 mesh, the highest. However, the inconsistent data obtained for stainless steel

at #120 grit size is almost certainly due to experimental error. The data used to plot this graph is included in Table 20.

4.3.8 TOOL ROTATION SPEED vs. MATERIAL REMOVAL RATE

Figure 18 shows that the overall, material removal rates increased gradually with increasing tool rotation speed. The effect of tool material on material removal rates was significant, with mild steel proving the most, and Nimonic 80A the least effective. However, stainless steel tool tips yielded the lowest material removal rate at 0 r.p.m., and the highest at 800 r.p.m. The data used to plot this graph is included in Table 21.

4.3.9 STATIC LOAD vs. MATERIAL REMOVAL RATE

Material removal rates increased with increasing static load (Figure 19, Table 22). Once again, mild steel tools yielded on average the highest material removal rates. Stainless steel tool tips yielded the lowest average material removal rates. The results from the use of Nimonic 80A were intermediate between these two extremes. If the overall trends were considered, the mild steel tool appeared to give a low material removal rate at 1kg static load, and Nimonic 80A gave a slightly low value at 3kg. These inconsistent figures may be due to experimental error.

4.3.10 ABRASIVE CONCENTRATION vs. MATERIAL REMOVAL RATE

Figure 20 shows that variations in abrasive concentration when slot milling the SiC/Al_2O_3 composite gave the most complex results of the experimental programme. Tool material had a significant effect on material removal rates, although overall, there appeared to be no obvious tool material which would yield the highest material removal rates at all grit concentrations. For example, at a concentration of 10% grit by volume, material removal rates were all around 0.6 mm^3/sec, (with a spread of 0.105mm^3/sec.). At a concentration of 20% grit by volume, material removal rates varied between 0.784mm^3/sec. (for the mild steel tool) to 1.301mm^3/sec. (for the stainless steel tool), a range of 0.517mm^3/sec. At a concentration of 30% grit by volume, the relative effectiveness of the tool materials was reversed, with stainless steel yielding the lowest material removal rate, and mild steel the highest. The range in this case was 0.365mm^3/sec. At the highest concentration of grit examined, 40% by volume, the trend was reversed once again, with stainless steel yielding the highest material removal rate, and mild steel the lowest. In this case the range was 0.574mm^3/sec. Nimonic 80A tool tips gave the intermediate material removal rates at all concentrations, with the exception of 10% by volume. In this case Nimonic 80A yielded the lowest amount, although by the marginal amount of 0.024mm^3/sec. below mild steel. The data used to plot the graph is shown in Table 23.

4.3.11 DATA PROCESSING FOR SLOT MILLING OF SiC / Al_2O_3

Figures 21, 22, 23 and 24 were drawn from the raw data included in Tables 20, 21, 22 and 23. As in the case of hole drilling, the material removal rates for the three tool materials were averaged, and the trend lines plotted using the new data. The equation of each line is shown on the graphs, and may be used as a representation of the empirical expression of the behaviour of the relevant factor.

4.3.12 SURFACE ROUGHNESS RESULTS OBTAINED AFTER SLOT MILLING SiC/Al_2O_3

Figures 25, 26, 27 and 28 show the surface roughness results obtained as a consequence of the slot milling of SiC/Al_2O_3 composite. To summarise the parameters used when making surface roughness measurements :

Traverse length : 10mm

Evaluation length : 7.5mm

Sample length : 3 x 2.5mm

Filter : Gaussian

Least squares line.

The Ra figures obtained indicate the *increase* in surface roughness (in μm) as outlined in Section 3.10.2 .The data used to plot the graphs is included in Tables 24, 25, 26 and 27.

4.3.13 GRIT SIZE vs. SURFACE ROUGHNESS

Figure 25 shows that in general, a decrease in average grit diameter reduced the surface roughness values. The reduction of surface roughness was most apparent when changing from #120 mesh size to #220 mesh size. When machining with progressively reducing mesh sizes in the range #220 to #600, a more gradual reduction in surface roughness was observed. Tool material did appear to be significant, particularly at mesh sizes from #220 to #600, when Nimonic 80A tools gave the lowest roughness values, and stainless steel the highest. The data used to plot the graph is included in Table 24.

4.3.14 ROTATION SPEED vs. SURFACE ROUGHNESS

Figure 26 indicates that at any speed above 200 r.p.m., rotation speed had little apparent effect on the surface roughness produced. Tool material choice did appear to have some effect, with mild steel tools yielding the higher Ra values at all the rotational speeds used above zero r.p.m. The data used to plot the graph is included in Table 25.

4.3.15 STATIC LOAD vs. SURFACE ROUGHNESS

Figure 27 suggests that an optimum static load of 1kg produces a minimum surface roughness value. There appeared to be no obvious effect of tool material performance, although Nimonic 80A produced the lowest Ra value recorded. The data used to plot the graph is included in Table 26.

4.3.16 ABRASIVE CONCENTRATION vs. SURFACE ROUGHNESS

With reference to Figure 28. At abrasive concentrations below 20%, stainless steel tools yielded the lowest Ra values, and Nimonic 80A the highest. At concentrations of 20% or above, mild steel tools gave the lowest roughness figures, with Nimonic 80A the highest. An exception being at concentrations of around 40%, when the stainless steel tools gave the highest Ra values. The data used to plot the graph is included in Table 27.

4.3.17 RESULTS FOR HOLE DRILLING OF PLATE GLASS

The following graphs (shown in Figures 29, 30 and 31) represent the results obtained for the ultrasonic hole drilling of Plate Glass. The raw data used to draw the graphs is included in Tables 28, 29 and 30.

4.3.18 GRIT SIZE vs. MATERIAL REMOVAL RATE

Figure 29 shows that the overall material removal rates decreased with decreasing abrasive size. The shape of the curves showing the relationships between material removal rate and grit size was characteristic, with minimum slope at intermediate grit sizes, and greater slopes at the higher and lower values of this parameter. This trend applied irrespective of tool tip material. Tool material did appear to be significant, with mild steel yielding the highest material removal rates, and stainless steel the lowest, with Nimonic 80A lying between the two. The average difference in material removal rates between mild steel and stainless steel tools was around 0.5 mm^3/sec., this remained

constant for all static loads tested. The data used to plot this graph is included in Table 28.

4.3.19 ROTATION SPEED vs. MATERIAL REMOVAL RATE

As shown in Figure 30 and Table 29, tool rotation speed appeared to have little effect on material removal rates when using mild steel or mild steel tool tips. The material removal rates were approximately 1mm^3/sec. in all cases. However, when using stainless steel tool tips, material removal rates increased to a maximum at 200r.p.m. before gradually declining again to values similar to those obtained from the other two tool materials at 800 r.p.m.

4.3.20 STATIC LOAD vs. MATERIAL REMOVAL RATE

Figure 31 (plotted from data in Table 30) shows that material removal rates increased with increasing static load, reaching a maximum at a value of 2kg, before reducing again as the load increased to 3kg. This trend applied irrespective of tool material type. Mild steel tools yielded the highest overall material removal rates, closely followed by Nimonic 80A (around 0.1mm^3/sec. less at any given load). Stainless steel tools produced on average 0.4mm^3/sec. less than produced by the Nimonic 80A tool tips when the load applied over the lower part of the range. However, this discrepancy was at about 0.2mm^3/sec. when the load lay in the upper part of the range used.

4.3.21 DATA PROCESSING FOR HOLE DRILLING OF PLATE GLASS

Figures 32, 33 and 34 were drawn from the raw data included in Tables 28, 29 and 30. In all three cases, the material removal rates for the three tool materials were averaged, and the trend lines plotted using the new data. The equation of each line is shown on the graphs, and may be used as a representation of the empirical expression of the behaviour of the relevant factor.

4.3.22 RESULTS FOR SLOT MILLING OF PLATE GLASS

Figures 35, 36, 37 and 38 represent the results obtained as a consequence of the ultrasonic slot milling of plate glass. The raw data used to produce these graphs is included in Tables 31, 32, 33 and 34.

4.3.23 GRIT SIZE vs. MATERIAL REMOVAL RATE

Figure 35 shows that, on average, material removal rates reduce as the grit size reduces. Tool material is significant, especially at the larger grit sizes of #120 and #220. At lower grit sizes, tool material appears to be less significant. Tool material performance was difficult to judge due to the inconsistencies in the material removal rates obtained. For example, mild steel tools yielded both the highest material removal rates (at #120 mesh size) and the lowest material removal rates (at #600 mesh size). Table 31 shows the data used to plot Figure 35.

4.3.24 TOOL ROTATION SPEED vs. MATERIAL REMOVAL RATE

Neither tool rotation speed nor tool material appeared to have a significant effect on material removal rates, with most combinations yielding around 0.7mm^3/sec. (Figure 36, Table 32). The exception was the result obtained with the stainless steel tool at 0r.p.m., which yielded a material removal rate of around 2mm^3/sec. This value may well be the result of experimental error.

4.3.25 STATIC LOAD vs. MATERIAL REMOVAL RATE

Figure 37 suggests that variations in static load do not appear to produce any definite effect on the material removal rate, since the results are scattered from 0.6mm^3/sec. to 1.4mm^3/sec. in a random manner. There was no apparent optimum tool material that maximised material removal rates, although stainless steel yielded the highest value of 1.4mm^3/sec. achieved at a static load of 2kg. The data used to plot Figure 37 is included in Table 33.

4.3.26 ABRASIVE CONCENTRATION vs. MATERIAL REMOVAL RATE

With reference to Figure 38 and Table 34. Abrasive concentration appeared to have only a small effect on material removal rates, showing a slight increase in material removal rate with increasing concentration for all tool materials tested. On average, Nimonic 80A tools yielded the lowest material removal rates, with stainless steel and mild steel tools slightly higher.

4.3.27 DATA PROCESSING FOR SLOT MILLING OF PLATE GLASS

Figures 39, 40, 41 and 42 were drawn from the raw data included in Tables 31, 32, 33 and 34. As in the case of hole drilling, the material removal rates for the three tool materials were averaged, and the trend lines plotted using the new data. The equation of each line is shown on the graphs, and may be used as a representation of the empirical expression of the behaviour of the relevant factor.

4.3.28 SURFACE ROUGHNESS RESULTS OBTAINED AFTER SLOT MILLING PLATE GLASS

Figures 43, 44, 45 and 46 illustrate the surface roughness results obtained from the ultrasonic slot milling of Plate Glass. To summarise the parameters used when making the surface roughness measurements :

Traverse length : 10mm

Evaluation length : 7.5mm

Sample length : 3 x 2.5mm

Filter : Gaussian

Analysis method : Least squares line.

As in the case of slot milling the composite, the Ra figures obtained indicate the *increase* in surface roughness (in μm) as outlined in Section 3.10.2 .The data used to plot the graphs is included in Tables 35, 36, 37 and 38.

4.3.29 GRIT SIZE vs. SURFACE ROUGHNESS

All tool materials showed a reduction in surface roughness as the grit size was reduced (Figure 43, Table 35). The highest surface roughness of 7.8microns was recorded when using #120 mesh size in conjunction with a stainless steel tool. The lowest surface roughness value recorded was produced when using a #600 mesh grit. In this case, both Nimonic 80A and stainless steel tools recorded similar values of around 1.1microns (+/- 0.02microns). On average, the mild steel tool gave the lowest surface roughness values over the whole range of grit sizes examined.

4.3.30 ROTATION SPEED vs. SURFACE ROUGHNESS

Rotation speed appeared to have no significant influence on material removal rates (Figure 44, Table 36). All combinations of tool material and rotation speed yielded surface roughness values of around 0.7microns (+/- 1micron). The greatest variations from this trend were observed at a zero tool rotation speed, with both mild steel and Nimonic 80A tools yielding 5.7microns, and the stainless steel tool yielding 7.8microns.

4.3.31 STATIC LOAD vs. SURFACE ROUGHNESS

Figure 45 (plotted from the data in Table 37) suggests that varying static load appeared to have little effect on surface roughness values irrespective of tool material used. Most values were around 0.6 microns, the exception being obtained with the stainless steel tool when used under a static load of 2kg : this combination yielded a surface roughness

value of 7.7microns, the highest value recorded. The lowest value recorded was 5.6 microns, and was achieved at a static load of 2 kg with a mild steel tool.

4.3.32 ABRASIVE CONCENTRATION vs. SURFACE ROUGHNESS

Results obtained when varying abrasive concentration did not appear to follow any specific pattern, with the results being scattered around the 7micron value (Figure 46). There was no apparent optimum tool material for minimised surface roughness, although stainless steel yielded the lowest value of 5 microns achieved at an abrasive concentration of 40 % by volume. The data used to plot Figure 46 is included in Table 38).

4.4 MICROGRAPHIC RESULTS

4.4.1 USE OF MICROSCOPY IN THE EXPERIMENTAL PROGRAMME

Microscopy was used extensively to determine the effect of ultrasonic machining on the composite material. Both optical and scanning electron microscopes were utilised, depending on the amount of magnification, resolution and depth of focus required (the scanning electron microscope providing much greater magnifications and depth of focus than would have been obtainable with optical microscopy). The initial machining experiments were made in order to ascertain whether the material was capable of withstanding the stresses imposed during the ultrasonic machining process without either delaminating or disintegrating completely by large scale cracking. Had the material shown any significant detrimental effects under the microscope, then a full scale experimental project would have been difficult to justify.

As part of the experimental programme, samples of the SiC / Al_2O_3 were subjected to bending loads and impact loads, and the scanning electron microscope was then used in order to ascertain the nature of fracture of the composite under these conditions. A comparison of fracture damage could then be made with the ultrasonically machined samples, and any similarities noted.

The following descriptions refer to micrographs illustrated in Figures 47 - 63 and Figures 66 - 74.

4.4.2 UNMACHINED COMPOSITE

Figure 47 shows a sectioned and polished sample of SiC/Al_2O_3 composite. The circular dark grey regions are the Silicon carbide (Nicalon®) base fibres. The black circular line around the base fibres is the boron nitride interface material coated on the base fibres by the process of chemical vapour infiltration (C.V.I.). Surrounding the boron nitride is a further layer of silicon carbide, again coated by C.V.I. It is apparent that the silicon carbide of the base fibres appears darker than the silicon carbide of the coating, this is due to the dissimilar crystalline composition of the fibre and coating. The dark grey and black speckled region surrounding the fibres is the alumina matrix of the composite.

4.4.3 INITIAL MACHINING EXPERIMENTS

In the earliest trials, optical microscopy was used to observe the overall surface integrity and dimensional accuracy of holes and slots produced in the SiC / Al_2O_3 composite. Magnifications up to 50x provided adequate views of the holes and slots, and provided enough evidence to suggest that the material was suitable for the process, and that no large scale cracking or delimitation occurred under the machining conditions used.

Figure 48 shows a test hole drilled in SiC/Al_2O_3 composite. The tool diameter for this experiment was 4mm, the hole depth was 1.5mm, and an aqueous solution of #320 SiC grit (40% grit by volume) was used. The machining time was kept at 3 minutes, but in the absence of any machining parameter data, the static load was varied manually during machining in order to obtain the optimum penetration rates. Had the optimum static load been applied throughout the run, machining time could have been shorter. The

micrograph shows a clean, well defined hole with no evidence of delimitation or degradation of the surrounding material.

Figure 49 shows the end of a test slot milled in SiC/Al_2O_3 composite. The tool diameter in this experiment was 4mm, the hole depth was 0.5mm, and an aqueous solution of #320 SiC grit (40% grit by volume) was used. The workpiece was traversed manually, using mechanical end stops in order to govern the slot length. Again, static tool load was adjusted continuously in order to give an acceptable penetration rate. The machining time was 30 seconds. The micrograph shows well defined geometry, as with the test hole shown in Figure 48, again with no evidence of delimitation or degradation of the surrounding material. Since the slot is very shallow, the base of the slot is visible, and the variations in the lay of the fibres with depth may be observed.

Figure 50 shows a test hole drilled in SiC/Al_2O_3 composite. The tool diameter for this trial was 1 mm, the hole depth was 1 mm, and an aqueous solution of #320 SiC grit (40% grit by volume) was used. Due to the absence of any machining data, static tool load was adjusted during the run in order to find the optimum penetration rate. The machining time was 30 seconds.

The geometry of this hole does not appear to be exactly circular in plan view, the hole being slightly ovoid : this may have been due to the tool entering the material at a slight angle rather than in a perpendicular direction. The appearance of the edge of the hole is similar to those in Figures 48 & 49, but the higher magnification in this case reveals a less well defined top edge, and the presence of a small amount of machining debris

around the circumference of the hole. Once again there is no evidence of de-lamination or degradation of the surrounding material.

Figure 51 shows a test hole drilled in SiC/Al_2O_3 composite. The tool diameter for this trial was 1.5 mm, the hole depth was 1.5 mm, and an aqueous solution of #320 SiC grit (40% grit by volume) was used. Once again, due to the absence of any machining data, static tool load was adjusted during the run in order to find the optimum penetration rate. The machining time was 30 seconds. Unlike the previous three trials, this hole was drilled in the edge of the material sample, perpendicular to the layered fibre stack. The fibres may be easily observed running across the sample. The micrograph reveals a well defined circular hole, with a clean edge, but with some evidence of post machining debris just below the top circumference of the hole. Once again, there appears to be no de-lamination or degradation of the surrounding material.

4.4.4 S.E.M. MICROGRAPHS OF SURFACES PRODUCED DURING THE FULL FACTORIAL EXPERIMENTAL PROGRAMME.

The micrographs described in this section (illustrated in Figures 52 - 59) were obtained with the Scanning Electron Microscope (S.E.M.) at the Materials Research Institute at Sheffield Hallam University. The main purpose of this series of micrographs was to obtain a greater understanding of the material removal mechanism by observing fracture surfaces after machining.

All the samples described here were machined with #220 grit, and are typical examples of the results of ultrasonic machining; observations of regions machined with other grit sizes revealed similar characteristics.

Figure 52 shows a plan view of fibres in the base of a slot. Fibres to the right of the viewed area appear to have survived largely intact, although the interface material and outer SiC shell of the uppermost fibres have sustained some damage. Fibres in the top left central region of the image appear to have been sheared under the action of grit particles, with numerous cleanly cut fibres visible. The remains of the alumina matrix can also be seen clinging to the fibres in the less exposed regions between fibres. In the top right region of the image, voids are apparent in some regions parallel to the fibre lay up.

Figure 53 is similar to Figure 52 showing fibres in the base of a slot, but is shown at a higher magnification. Regions of matrix which initially contained fibres (before machining) are clearly visible in the upper and lower thirds of the micrograph. Damage to fibres is readily apparent : the fibre at the bottom of the image has been fractured at the left side, and its' debris removed. To the left of the same fibre, the surface appears to be crushed. The region of alumina matrix over the middle of the fibre appears to be holding this fibre in place. The fibre in the top third of the image is cleanly fractured in two places, and appears to have been displaced slightly, the section of this fibre to the right of the viewed area shows considerable impact damage. Two further fibres have been partly exposed in the central region of the image, and do not appear to have suffered any damage, apart from the removal of their shells and interface coatings - the lower fibre of the two has traces of interface material still attached on the left side of the visible surface.

Figure 54 shows the fracture surface of a fibre shown in Figure 53 under greater magnification. The damaged fibre in question is visible above the right side of the scale bar in Figure 53. The fibre appears to have suffered impact damage, showing the lateral cracks characteristic of indentation fracture of a brittle solid. A significant volume of the fibre has been lost. Deep fractures appear to propagate through the fibre on the top region. This cracking is on a very fine scale, is confined within a single fibre and does not appear to propagate into the alumina matrix. The porous nature of the alumina matrix is also readily observed.

Figure 55 shows fibres at the bottom edge of a slot which have been sheared under the action of grit particles. Part of the interface shell of one fibre is clearly visible in the top left of the image. The alumina matrix is also clearly visible as the porous mass of material in the top right of the image. Fracture surfaces of the fibres do not appear to be clean. There are clear signs of lateral cracks, and in addition, either secondary impacts or the propagation of central cracks transverse to the fibres' axes have caused complete failure with the subsequent loss of the left side of the fibres.

Figure 56 shows a fractured fibre at the base of a slot. The fracture surface of the fibre appears very rough. The interface material appears as a thin, dark coating on the top edge of the fibre, and the SiC shell somewhat thicker. Where the left side of the fibre has been removed, the SiC shell is clearly visible, with what appears to be remains of the interface material present in patches.

Figure 57 shows the side of a slot. Here, a single fibre appears to have been cleanly fractured at the left side. A crack is present to the right of the visible fibre surface, and appears to have propagated through he fibre to an extent which has allowed the left side of the fibre to displace outwards slightly. Most of the interface material and shell has been removed. The alumina matrix material on the right side of the image contains several small cracks, the depth of which are difficult to judge. Some alumina debris particles are present on the top surface of the fibre.

Figure 58 shows part of the end of a fractured fibre in the base of a slot. The uppermost surface of the fracture exhibits "tide marks" (a phenomenon discussed in detail by Lawn [62] and Michalsk [76]) and resembles a glassy, brittle fracture surface, but is quite clean in comparison with the lower region (visible behind the text). The top left of the image shows a section of partially removed interface material coating the surface of a fibre shell.

Figure 59 shows the top edge of a slot. The defocussed region in the top right of the image is the base of the slot, the remaining area of the image is the top surface of the sample. A fibre shell is visible in the centre of the image : this shell contains two fractures, one of which appears to extend laterally through the alumina matrix. The fibre fracture surfaces visible to the top right of the image appear to be clean. A large region of alumina appears to have been removed from above the undamaged fibres to the top left of the image, and the remaining alumina contains a crack running from top to bottom.

4.4.5 S.E.M. MICROGRAPHS OF POST MACHINING DEBRIS

In an attempt to observe the nature of material removal when ultrasonically machining the SiC/Al_2O_3 composite, samples of used abrasive slurry were examined by S.E.M. The used slurry, containing both silicon carbide particles and fragments of the composite, was then examined under the scanning electron microscope.

Figure 60 shows #120 mesh size grit, dried and gold coated after machining the SiC/Al_2O_3 composite. The large dark particle appears to be coated with a granular white deposit, some of which also appears to be dispersed around the image.

Figure 61 was obtained from a sample of #220 mesh silicon carbide, and shows the only identifiable image of an intact fibre section obtained from any of the post machining debris/grit samples examined. The fibre appears to have lost its interface coating, and shows a clean fracture at the right end, and a slightly less well defined surface at the left end. The surface of the fibre appears to have a highly dissipated deposition of small, lightly shaded grains. Examples of the larger dark and light particles are also present in the regions around the fibre.

Figure 62 shows used #320 grit slurry after drying and gold coating. As in Figure 60, this image shows two distinct physical features : large, dark grey, angular masses with smaller, lighter shaded particles dispersed around and congealed between them. Figure 63 shows the surface of one of the darker masses under higher magnification. Two points "A" and "B" were identified on Figure 62. Point "A" is labelled just above the main text

bar of the image, towards the middle, and point "B" is labelled on the smaller of the two white particles on the centre right edge of the image. The chemical composition of points "A" and "B" was investigated using the x-ray analysis facility of the S.E.M. The dark grey regions (represented by point "A") were found to consist mainly of silicon. Given the composition and dimensions of these particles, they may be silicon carbide abrasive particles. The smaller, light grey granules (represented by point "B") were found to contain a high proportion of aluminium. These particles are likely therefore to be the remains of the alumina matrix of the composite. The x-ray analysis plots for areas "A" and "B" are shown in Figures 64 & 65.

Figure 66 shows post machining debris after using #600 mesh size grit. The appearance of the two distinct types of material is once again apparent, with no evidence of complete fibres.

4.4.6 MICROGRAPHS OF BENDING AND IMPACT DAMAGE

As part of the experimental programme, samples of the SiC/Al_2O_3 were subjected to bending loads and impact loads in order to ascertain the nature of fracture of the composite under these conditions. A comparison of fracture damage could then be made with the ultrasonically machined samples, and any similarities and discrepancies noted.

4.4.7 FRACTURE SURFACES OBTAINED FROM BENDING TESTS

Figure 67 shows the fracture surface of a sample of SiC/Al_2O_3 composite which has been subject to a three point bending test. The fracture surface depicted was located beneath the central load point, opposite the contact face, and the fibres shown were orientated perpendicular to the loading axis (shown diagramatically in Figure 68). The exposed fibres show very clean fractures. There are several regions which have obviously been subject to fibre pull-out, with clean holes left where the fibres were located. In many of these regions, the fibre shell remains intact, and appears as a tubular prominence. The alumina matrix appears to remain in good condition, and regions of alumina are easily identifiable as porous areas, especially noticeable to the bottom right of the viewed area. The micrograph illustrates the perpendicular weave of the fibres, with two distinct fibre orientations evident, those to the bottom left of the viewed area, and those in the remainder of the image.

Figure 69 shows the same sample as Figure 67, but under a higher magnification. Again, fibre fracture surfaces appear to be clean, transverse to fibre axis, and regions of fibre pull-out are obvious. Some fibre shells remain intact. The fibre shell to the bottom of the image shows a significant amount of cracking. The alumina matrix appears to remain in good condition, with a limited amount of cracking around fibres, the most obvious example being adjacent to the fibre shell in the centre of the image.

4.4.8 FRACTURE SURFACES OBTAINED FROM IMPACT TESTS

Figure 70 shows a sample of SiC/Al_2O_3 composite which has been subject to multiple impact damage by a spherical indenter of 60 microns diameter (roughly equivalent to #220 mesh size grit). The fracture surfaces of the fibres appear to be rough, with some evidence of chipping around the edges. There is little evidence of fibre pull-out, with no obvious tubular protrusions present. One fibre, in the centre of the image appears to be loose, since it does not lie in the same orientation as its neighbours. There appear to be the remains of fibre shells in the bottom right of the image, and possibly the remains of others among the right side of the image, but this is difficult to ascertain due to the large amount of debris present. The alumina matrix appears to be highly granulated and loose, with particles spread over the entire area of the image.

Figure 71 shows the same sample as depicted in Figure 70, but under a higher magnification. The fibre fracture surfaces show definite signs of chipping. The shell of the fibre in the middle left of the image shows a large axial fracture, and other fibre shells visible show obvious signs of severe cracking : many of the fragmented shells appear to be loose. The alumina matrix is badly damaged, and matrix debris appears to cover much of the surface of the sample.

4.4.9 MICROGRAPHS OF TOOL TIPS

Figures 72 - 74 were obtained from tool tips used during the experimental programme. Similar wear characteristics were observed for all tool materials, and tool life was similar in all cases, although redressing was more frequently required on mild steel than for the other two materials.

Figure 72 shows an unused Nimonic 80A tool tip. Concentric machining marks are visible on the tip and flank, and the small tip radius is visible on the edge circumference.

Figure 73 shows a Nimonic 80A tool tip after drilling 24 holes to a depth of approximately 1mm. The tool shows the characteristic depression in the centre of the tip. Another characteristic of the used tool is the recessed region around the circumference of the tip, which extends to approximately 1mm up the flank. All worn regions have a pitted, burnished surface appearance.

Figure 74 shows a Nimonic 80A tool tip after milling 24 slots approximately 1mm deep x 30mm long. The tip wear pattern has different characteristics from the hole drilling tip : The edge of the tool has become radiussed in the direction of the traverse of the slot, flank wear is still evident, as is the pitted surface appearance of the tool.

4.5 FINITE ELEMENT ANALYSIS

4.5.1 CONTOUR PLOTS

The finite element results included Figures 75 - 77, these show stress contours in the workpiece below the spherical indenter. The three contour plots represent the three principal stresses present in the workpiece.

4.5.2 VECTOR PLOTS

Figures 78 - 80 are vector plots, and represent the directions of the three principal stresses. The stress and direction plots obtained closely resemble the theoretical stress distributions obtained from [71] and [72] and previous studies by Khadem & O'Connor [77] and Pharr *et al* [78], with maximum compressive stress just below the indenter, and a rapidly diminishing stress field in the remaining material.

4.5.3 VON MISES STRESS PLOT

Figure 81, shows the Von-Mises stresses for the same model.

5. DISCUSSION

5.1 INTRODUCTION

This chapter outlines a basic model of the ultrasonic machining process. Throughout the chapter, the model is used as a reference to explain the variations in the experimental results. In some areas, modifications are suggested or ideas expanded in order to offer possible explanations for other observations made when examining micrographs and analysing the machining results. A systematic analysis of the results of the Taguchi experiment is included, followed by a discussion of the results obtained from the main experimental programme. A comparison of the ultrasonic machining characteristics of glass and the composite material is made, followed by an analysis of the micrographs obtained in the experimental programme. Proposed fracture mechanisms are discussed in conjunction with the finite element stress analyses performed. A theoretical model of the material removal method is then proposed in the light of the experimental and theoretical data discussed.

5.2 ULTRASONIC MACHINING PROCESS MODEL

In order to simplify the discussion of the experimental results obtained from this study, the following simple qualitative summary of the ultrasonic machining process (based on the established literature) is included.

5.2.1 THE MECHANISM OF ULTRASONIC MACHINING

There have been many experimental investigations into the nature of material removal in ultrasonic machining including those by Rozenberg [10], Miller [37], Kainth *et al* [39] and Nair & Ghosh [44], all of which were concerned with the ultrasonic machining

process itself rather than its application to any specific material. The proposed mechanisms by which material is removed appear to have widespread support :

The gap between the tool and workpiece varies as the former vibrates ultrasonically. There is therefore a variation during the vibration cycle in the size of particle that could pass between the sonotrode and work and be pushed into the workpiece surface. Thus there is a maximum particle radius (r_{max}) and minimum particle radius (r_{min}) between which machining by peening is possible (refer to Figure 82). Furthermore, as the sonotrode position varies during the cycle, the amount of time available for a particle to enter the gap varies with particle radius. With reference to Figure 83, *at any particular instant*, particles of radii up to a maximum radius of r_1 can enter the gap when the tool end is in the position represented by the shaded part of the diagram. As the tool moves downward, particles of radius greater than r_1 are excluded. Therefore the number of particles present may increase as r_1 decreases. However, the depth of penetration into the workpiece is reduced as r_1 gets smaller, reaching 0 at r_{min}. If there is no resistance to penetration then a particle of radius r_1 ($> r_{min}$) will penetrate to a depth d. In practice, resistance to penetration will produce a smaller value d_1, and both d and d_1 will be a function of r_1 (see Figure 84). Since the material removal depends on both the penetration and the number of particles involved, there will be an intermediate value of r where the rate of material removal is a maximum (see Figure 84). The material removal mechanism just described is known as "Direct Impact", and is responsible for the majority of material removal. This model is over simplified, since it does not consider the effect of particle radius on the stress generated in the material.

5.2.2 ADDITIONAL MATERIAL REMOVAL MECHANISMS

There are however several other mechanisms which may contribute to the overall machining process in varying degrees, these are :

i) Indirect impact (Figure 85 *A*) As the tool tip descends, a grit particle is contacted. This particle in turn contacts a second grit particle causing it to impact the workpiece and causes fracture in a similar way to the previously explained "direct impact" mechanism.

ii) Projection (Figure 85 *B*) As the tool tip moves downward, a grit particle is contacted and an impulse is created. the particle separates from the tool tip and moves downwards through the slurry until the workpiece is contacted. The kinetic energy of the moving particle is transferred to the workpiece surface causing damage to the workpiece and/or grit particle as previously explained in "direct impact".

iii) Cavitation (Figure 85 *C*) This mechanism utilises the slurry rather than the grit particles themselves. The liquid used in the slurry throughout this experimental programme was un-distilled water. As the tool moves upward from the workpiece, air trapped in microscopic pores within the workpiece surface is subjected momentarily to low pressure, causing expansion of the air and the formation of a bubble containing a partial vacuum. As the tool recedes further from the workpiece surface, the low pressure region is replaced by liquid at ambient pressure, and the bubble containing the partial vacuum becomes unstable and implodes, causing a pulse of energy to be released. If the bubble remained on or under the surface of the material, then a sufficient amount of energy to cause fracture may be released. It should also be noted that as well as allowing erosion by cavitation, the liquid base of the slurry may have an effect upon the behaviour of the work-piece material in terms of the environment in which cracks initiate and develop. These environmental considerations are discussed by Likhtman *et al* [79]. This aspect of ultrasonic machining has not been fully investigated, and may prove to be significant when producing material removal rate models.

iv) Fatigue : In this case, workpiece material is removed by repeated impacts of less force than would be required to fracture the material in one impact. This form of damage could be caused by either particle impacts or cavitation. Fatigue is of course a complex

and specialised subject, and has been the subject of many books and papers. The work by Suresh [80] provides much useful information.

Three other methods of possible material removal have been identified, but are not widely quoted as being significant, these are :

i) Debris impact : Material is removed by previously generated workpiece debris which impact on the workpiece either directly or indirectly. The relative extent of cracking of the workpiece and impacting particle would therefore depend entirely on the geometry of the debris.

ii) Tool impact : In this situation, the working gap is devoid of any grit particles, but the gap size is such that the tool is allowed to impact directly on the workpiece at some point in the vibration cycle. This situation could arise due to poor re-circulation of abrasive. The nature of fracture would now depend on the surface roughness of the tool tip, since a perfectly smooth tip would cause mainly peripheral cracking, whereas a rough tip would give multiple impact points within the area of the tool tip face.

iii) Elastic wave propagation : In this case, cracking could conceivably be produced without any contact of grit particles or the tool on the workpiece. A tool vibrating at a high frequency produces pulses of energy which could propagate through the slurry liquid, or in the absence of liquid, through air. Since the tool tip is usually within 20 microns of the workpiece surface, a significant amount of energy could be transferred. As these waves move throughout the workpiece, they are reflected from any boundaries (fibre interfaces, pores or inclusions), generating a complex multitude of compressions and rarefactions which would be of sufficient energy to produce fracture directly, or by fatigue. The concept of elastic wave propagation is noted by Lawn [62] and Michalsk [76], and is discussed in some detail by Bedford & Drumheller [81], and Varner [82].

A full investigation of these additional mechanisms is beyond the scope of this thesis, but possible evidence of at least one of these additional mechanisms (elastic wave propagation) is discussed later.

5.3 TAGUCHI IDENTIFICATION OF SIGNIFICANT FACTORS IN ULTRASONIC MACHINING.

5.3.1 TAGUCHI EXPERIMENT RESULTS OVERVIEW

Ultrasonic machining is a highly complex process with many parameters, some of which play a highly significant part in the material removal process, while others do not. The Taguchi programme performed was aimed at the acquisition of maximum machining rates rather than optimum surface roughness integrity, although some useful information on the factors affecting surface finish was obtained. Had the primary objective been to obtain data on surface roughness and integrity, then the significant parameters obtained from the Taguchi experiment may well have been different. Factors which were fixed e.g. power setting or amplitude may have influenced Ra values to a greater extent than those which *were* varied. The Taguchi experiment was performed in as much depth as possible considering the amount of material available. The identification of significant and insignificant factors obtained from this programme appeared to be very well defined both for slot milling and hole drilling. With reference to Figure 9, Taguchi results for hole drilling, the important factors all have significance ratings in the range of 20% to 40%, whereas the less important factors occupy a range of between 2% and 6% (The sum of all significance ratings is 100%, and the ratings obtained give an indication of the relative importance of a factor, see Section 4.2 for a full explanation). Similarly, with reference to Figure 10, Taguchi results for slot milling, the significant factors have ratings in the range of 7% to 60%, whereas the insignificant factors have ratings in the range of 1% to 1.8%. Again, this shows a definite distinction between significant and insignificant factors. Two other verification techniques were used to validate these initial results : the "noise" factor, and the verification experiments.

5.3.2 VERIFICATION OF THE TAGUCHI EXPERIMENT RESULTS

Firstly, the "noise" factor. The nature of the Taguchi technique means that depending upon the number of significant factors investigated, there could be a number of spare rows in the orthogonal array (Table 3). In the case of slot milling, there were seven variables, and seven columns available so the orthogonal array was said to be "fully saturated". In the case of hole drilling however, there were only six variables which meant that a spare column was available. This column did not therefore represent any defined variable, so all data gathered for this factor may be assigned to experimental noise; in effect a completely random combination of variables which could not possibly have any effect on the results, unless the experiment had either been poorly designed, or none of the variables had a significant effect on the results compared with all the others. In the case of hole drilling, the noise factor gained a significance rating of only 4.8%. Since the significant factors all had ratings of between 20% and 40%, the difference between noise and significant factors was therefore very well defined, furthermore, the insignificant factors were all closely ranged around the 4.8% noise value, so the identification of these factors is on a secure basis. The second verification technique used was a more practical procedure. By analysing the orthogonal arrays and data tables, the level of each factor which yielded the highest material removal rate could be obtained (see Section 4.2). In the case of hole drilling, none of the orthogonal array rows contained a combination of levels which would have yielded the theoretical highest material removal rate. When the factors were set to this optimum combination, the material removal rate should exceed the highest value obtained in the Taguchi experiment. When this procedure was performed, the material removal rate obtained under optimum conditions exceeded the previous maximum by the amount of $0.025mm^3/sec$. This figure may seem insignificant, but it must be noted that the nearest trial to the ideal, trial 4, Table 11, had only one factor - factor A, power setting - which differed from the optimum. The difference would not therefore be expected to be great. In the case of slot milling, the same procedure was applied, but in this case, the optimum

settings coincided with a standard trial, trial 4, Table 13, and as expected this was the trial which yielded the highest material removal rate of the experiment.

5.3.3 TAGUCHI EXPERIMENT SUMMARY

In terms of procedure and verification, the Taguchi experiment proved to be a valuable statistical tool, and the results gained enabled the significant factors to be examined in more detail with as much confidence as possible without the use of an excessive amount of material. The factors are now examined in turn :

Factor A : Power Setting : Power setting gained a significance rating of 2% for hole drilling and 1.8% for slot milling, and was therefore considered insignificant. Since power setting is directly related to the force applied to the sonotrode, the amplitude of vibration and thus to the size of abrasive particle which may be admitted to the working gap, the apparent insignificance of this may seem surprising (see the previously outlined process model, Section 5.2.1). The explanation for this may lie in the control method of machine control used. As outlined in Section 3.2.1, the power setting had three positions : Low, Medium and High, there being no indication of the actual amplitude being used. As part of the commissioning process on the machine (Section 3.2.2), amplitudes of vibration were obtained using a transducer fitted to the sonotrode. It was found that the amplitude represented by the low setting was 13.6 microns, and the high setting represented 22.7 microns, a difference of only 9.1 microns. If this slight variation is taken into consideration, then it is not so surprising that power setting was not considered significant, since the difference in amplitude represented may not have been great enough to cause any significant change in machining rate. Indeed, the difference of 9.1 microns does not approach the difference in average grit size when changing between two abrasive grades (see Table 2).

Factor B : Abrasive Size : Abrasive size gained significance ratings of 38% for hole drilling, and 60% for slot milling, and was considered to be significant in both cases. This is not surprising if it is assumed that larger particles remove more material per impact than smaller ones, as discussed in the process model earlier in this chapter (Section 5.2).

Factor C : Abrasive Concentration : Abrasive concentration gained a significance rating of 2.5% for hole drilling and was not considered important. This is surprising, since the concentration of abrasive particles under the tool should be directly related to the amount of material removed per tool impact (see the explanation in the process model earlier in this chapter). When abrasive concentration was varied for slot milling however, a value of 14% was obtained, and the factor *was* considered to be significant. A possible explanation for this is that the method of abrasive delivery to the tool tip during hole drilling was not efficient, and that the actual abrasive concentration under the tool tip was not representative of the abrasive in the reservoir. When slot milling however, the tool is constantly moving over the workpiece, allowing fresh abrasive to flow unimpeded to the working gap, thereby giving a more accurate indication of the true significance of abrasive concentration. With this potential problem in mind, an abrasive concentration test was performed after the Taguchi experiment (Section 3.7.8). Although this showed that the concentration delivered from the nozzle was representative of the concentration in the reservoir, the actual concentration in the working gap when slot milling remains extremely difficult to obtain.

Factor D : Tool Tip Diameter : Tool tip diameter gained a significance rating of 5.8% for hole drilling and 1% for slot milling, and was not therefore considered important in either case. This came as no surprise, since although a smaller tool will contact fewer particles than a larger one, the force per particle will be higher, leading to an increased volume of material removed per particle. A larger tool will contact more particles, each of which will remove a lesser amount of material compared with the smaller tip case.

Factor E : Tool Rotation Speed : Tool rotation speed gained a significance rating of 20% for hole drilling, and 14% for slot milling, and was considered relevant for both cases. Again, this was expected due to the findings of previous experimental programmes such as those conducted by Kazantsev & Rozenberg [21] and Komaraiah & Reddy [26]. It has been established that, up to a certain limit, rotating the tool tip increases abrasive flow into the working gap, making material removal more efficient since fresh, sharp abrasive grains are able to replace the used, blunted grains more quickly.

Factor F : Static Load : The static load placed upon the tool during machining is another factor which directly affects the force upon abrasive particles within the working gap between the tool and workpiece. Increasing static load correspondingly increases the total force available for material removal, resulting in higher material removal rates. If there were no static load on the tool, then machining would only take place for a few seconds until a region of workpiece had been eroded from directly under the tool tip, the depth of which would correspond approximately to the maximum abrasive diameter present under the tool tip, this in turn would be closely related to the amplitude of vibration of the tool (see Section 5.2.1). The significance rating of static load was 26% for hole drilling, and 7% for slot milling, so in both cases, static load was considered important.

Factor G : Tool Traverse Speed (slot milling) / Noise (hole drilling) : Factor G represented tool traverse speed in the slot milling experiment, and gained a low significance rating of 1%. This was not surprising since a high traverse speed affects a greater length of workpiece per unit time, but does not yield as high an overall depth of penetration as would be the case with a slower traverse speed. A slower traverse speed allows abrasive grains to remove material from a smaller area in a given time, therefore increasing the depth of erosion. A higher traverse speed, affects a greater workpiece area in a given time, but to a lesser extent in terms of erosion. There would appear to be little

to be gained in terms of material removal rate by varying traverse speed. The effect on surface finish is considered later.

In the case of hole drilling, factor G was a spare entity, representing no physical factor (see Section 4.2.3). It was therefore assigned as experimental noise, giving an indication of the degree of experimental error present in the Taguchi programme. Noise gained a significance rating of 4.8% in hole drilling. As expected this was one of the lowest values, and was not considered important.

5.4 EFFECT OF INDIVIDUAL VARIATION OF SIGNIFICANT PARAMETERS ON THE MACHINING PROCESS (FULL FACTORIAL EXPERIMENTAL PROGRAMME)

The data obtained from the full experimental programme, which involved the variation of the most significant parameters one at a time, gave much useful information. The graphs obtained from the experiments showed similar general characteristics to those obtained from previous studies of ultrasonic machining of various materials including ceramics, notably those by Komaraiah & Reddy [26], Koval'chenco *et al* [27] and Dam *et al* [29]. The following observations and theories are based upon the results of the full experimental programme, and refer to specific graphs (described in Section 4.3) which are of the most interest.

5.4.1 ULTRASONIC HOLE DRILLING OF SiC / Al_2O_3

5.4.2 VARIABLE : GRIT SIZE

With reference to the results (Section 4), and the process model (Section 5.2). The effect of varying grit size (Figure 11), showed that as average grit particle size was reduced, material removal rates also reduced. This effect may be explained by the fact that large grit particles remove more material per impact than smaller ones. As the tool moves downwards, large particles are contacted at a much earlier stage in the sinusoidal cycle than smaller ones. The depth of penetration when using larger particles is therefore much higher than with smaller ones, leading to higher machining rates. When smaller average grit diameters are used with the same amplitude of vibration, the depth of penetration into the workpiece is obviously much smaller, notwithstanding the greater stress concentrations caused by the smaller particles. The physical depth of penetration when large particles are mechanically pressed into the workpiece is always greater than the

effective penetration caused by the multiple small cracks caused by smaller grit diameters (see the process model, Section 5.2).

The difference between tool material types is more significant for large grit sizes than for smaller ones. This may be explained by considering tool hardness values. A relatively soft tool material such as mild steel is able to withstand a significant amount of impact damage from grit particles. This is not the case with harder tool materials such as stainless steel or Nimonic 80A. In the case of these materials, grit particle impacts are not "absorbed" as easily as compared with mild steel, and so the impact energy is transferred to the grit particles, sometimes causing fracture of the grit particles rather than the workpiece (since the abrasive used is silicon carbide, and has similar bulk properties to the workpiece). The material removal rates are therefore reduced. In the case of smaller mesh sizes such as #600, this effect is not as pronounced because of the much lower forces of each impact - the forces are distributed over a much larger number of particles, lowering the force per particle.

5.4.3 VARIABLE : TOOL ROTATION SPEED

Figure 12 shows the effect of varying tool rotation speed on material removal rate. Initially, material removal rate increases in proportion with rotation. This is because the circulation of abrasive beneath the tool tip becomes more efficient as the rate of rotation increases a phenomenon discussed by Komariah & Reddy [25], [26]. However, at higher speeds, the effect is negated as the abrasive slurry feed is deflected away from the working gap by the effect of rotation before it can penetrate beneath the tool. An optimum value is therefor reached, which in this case is around 600 r.p.m. This value applies to all tool material types tested. The effect of tool material type is significant, for similar reasons previously discussed.

5.4.4 VARIABLE : STATIC TOOL LOAD

Figure 13 shows the effect of varying static tool load on the material removal rate. The trends observed may be described as follows : material removal rates increase in proportion to increasing static load, before reaching an optimum value and subsequently decreasing. In this case, the optimum value appears to be around 2kg. The effect of static load may be explained by once again considering the circulation of slurry beneath the tool tip. Under relatively low static load conditions (e.g. 0.5 - 2 kg), grit particles move through the working zone freely, enabling fresh particles to be constantly exposed to the workpiece surface. As static load increases between these limits, so the average force imparted to each particle increases (the power and amplitude of the sonotrode remaining constant), and more material per impact is removed. When static loads in excess of 2 kg. are applied, the machining head moves downwards at a rate which significantly reduces the effective working gap between the tool and workpiece. During the upward phase of the tool tip's displacement (opening the workpiece gap), the entire machining head is moving *downwards,* thereby counteracting the movement of the tool tip. This effectively reduces the working gap and thus restricts the slurry flow to the working gap, resulting in greatly reduced process efficiency and lower material removal rates. Tool material also plays an important role in this case for similar reasons as previously explained in the notes of "grit size vs. material removal rate". The inconsistency in the curve relating to Nimonic 80A is most likely due to experimental error rather than any significant effect of a 2kg. load when using Nimonic 80A.

5.4.5 ULTRASONIC SLOT MILLING OF SiC / Al_2O_3

5.4.6 VARIABLE : GRIT SIZE

With reference to Section 4.3.6 : the results for slot milling of the composite material. Figure 17 shows the effect of varying grit size on material removal rates. As average grit particle size reduces, material removal rates also reduce. This trend may be explained in a similar way to the hole drilling experiment, i.e. larger grit particles removing more material per impact than small grit particles. The tool material effect is also valid in this situation, with the mild steel tool being the most effective on average. It may be noted that the material removal rates for slot milling are around 0.2 mm^3/sec higher than those for hole drilling when grit size is varied between #120 and #600. This can be explained by the additional material removal mechanism present in the case of slot milling i.e. the grazing effect of the traversing tool when grit particles are trapped between the tool and workpiece. Evidence of this effect is present in micrograph 25, a Nimonic 80A tool tip after milling 24 slots. The flank wear pattern suggests that as grit particles are forced under the tool when traversing, the tool becomes worn at these edges, so creating a rounded edge at two diametrically opposite points in the direction of traverse (since the tool moves in opposing directions).

5.4.7 VARIABLE : TOOL ROTATION SPEED

With reference to Figure 18 which shows the effect of tool rotation speed when slot milling the composite. There appears to be an overall increase in material removal rate throughout the range 200 r.p.m. - 600 r.p.m. In the case of mild steel tools and Nimonic 80A tools, an optimum rotation speed value of around 600 r.p.m. is reached before a subsequent decline in material removal rate. In the case of stainless steel tools, there is an overall increase in material removal rate, although the stainless steel tool does not appear to follow the same trends as the other two tool materials. This is probably due to

experimental error. Again, on average, mild steel produces the most effective material removal rates. It may be noted that the mild steel trend line is very similar in appearance to that obtained for the composite hole drilling experiment. The magnitude of values that the line represents is also similar. This suggests that the grazing effect discussed previously is largely negated due to the additional rotation of the tool.

5.4.8 SURFACE ROUGHNESS VALUES

Evidence of the relative magnitude of impact damage when using differing grit sizes is reinforced when considering the surface roughness results after the slot milling of composite. As discussed previously, the assumption was that as grit size increased, so the impact craters generated would increase in proportion. This assumption is backed up by referring to Figure 25 : as grit size increases, so surface roughness increases. If it is assumed that each grit particle removes an approximately hemispherical volume of material, and that the radius of each hemisphere reduces in proportion to grit particle size, then the depth of each "crater" also reduces in proportion resulting in progressively lower Ra values. the effect of increasing static load was also discussed, and assumed that as static load increased, so the average force on each particle increased resulting in a greater amount of material being removed. This theory is also supported by referring to surface roughness values when varying static load (Figure 27). This trend can be explained by the assumption that a larger amount of material is removed by each grit particle when overall load is increased, thus resulting in deeper impressions being made by each particle, thereby increasing Ra values.

5.5 COMPARISON OF THE MATERIAL REMOVAL RATE RESULTS FOR THE ULTRASONIC HOLE DRILLING OF SiC / Al_2O_3 COMPOSITE COMPARED WITH THOSE OF PLATE GLASS.

A parallel experimental programme was carried out in order to ascertain the machining properties of a well known homogeneous brittle material (plate glass) so that these characteristics can be compared with those of the composite material under investigation. Firstly, a comparison of hole drilling characteristics with reference to Figures 11 - 13 (for the composite), and Figures 29 - 31 (for plate glass). When grit size was varied, the material removal rate curves obtained were very similar in both cases. The tool material types also yielded similar relationships between grit size and material removal rate, with mild steel being the most effective, stainless steel the least effective and Nimonic 80A in-between. Perhaps the most significant feature of the results is the difference between the magnitude of results obtained between the two materials. A summary of the average material removal rates for each variable is given in Table 39

The *average* material removal rate for all experimental runs involving the hole drilling of the composite was 0.436 mm^3/sec, compared with 0.790 mm^3/sec for plate glass. The ratio of average material removal rates of glass to composite is 1.81 : 1. It is clear from Table 39 that glass yields the higher material removal rates, and is therefore easier to machine than the composite. This is not altogether surprising, sine the additional toughening mechanism of the fibre reinforcement of the composite should make machining more difficult. If however, the relative magnitudes of fracture toughness values are considered (Table 40), it becomes apparent that a much greater difference in these values might be expected.

5.5.1 SIGNIFICANCE OF FRACTURE TOUGHNESS ON THE RESULTS

Fracture toughness is a key property in the determination of the effectiveness of ultrasonic machining on a material as discussed by Komaraiah & Reddy [26], Nandy *et al* [28], Dam *et al* [29], Haas [30] and Grathwohl *et al* [31]. The tensile strength of a material has also been found to have a significant bearing on the machining rates. If the relative values of fracture toughness and tensile strength of the composite material and plate glass are examined, it is evident that the fracture toughness of the composite is four times that of plate glass, and that the tensile strength of the composite is some four and a half times that of plate glass. These figures indicate that the composite material should be very difficult to machine ultrasonically, and that the machining rate values for glass should be at least four times higher than that of the composite rather than only two times higher.

5.5.2 SIGNIFICANCE OF MATERIAL PROPERTY TEST METHODS

It is clear that the behaviour of the composite under ultrasonic machining conditions is quite different from it's behaviour under the conditions in which the fracture toughness and tensile strength values of the material were obtained, and indeed the conditions under which the material is designed to operate in service. Standard tests for fracture toughness are designed to determine reproducible values for K_{IC} (mode I crack opening). For composites, the single edge-notched bend test piece (SEN) is usually used in the test process. The test piece is prepared with a notch conforming to standard dimensions, and with a crack emanating from the notch. The crack is generally developed from the base of the notch by a fatigue process to a pre-determined size. During a fracture toughness test, the values of applied force required to cause given amounts of crack extension are measured, and the fracture toughness determined from standard equations considered by Partridge [46], Ashbee [47], Hull [48] and Matzke [83]. Clearly, this method of testing

bears little relation to the types of loading sustained by the composite when ultrasonic machining is being performed (i.e. impact loading and indentation).

5.5.3 FRACTURE MECHANISMS IN FIBRE REINFORCED COMPOSITES

The main advantage of a ceramic composite over a homogeneous ceramic is enhanced fracture toughness and hence greater resistance to brittle fracture under both mechanical loading and thermal shock conditions. The two main mechanisms by which these improved properties are achieved are :

1) Fibre pull-out.
2) Crack deflection along fibre-matrix boundaries.

With reference to Figure 86 : Fibre pull-out (described by Partridge [46], Ashbee [47], Hull [48] and Davidge [49]) occurs when the material is stressed axially in the direction of the fibres. As the matrix cracks under direct tension, the different mechanical properties of the fibre and matrix ensure that cracks do not occur in both the fibre and matrix simultaneously. Cracking occurs in the matrix around a fibre, and the matrix begins to separate. The fibre is then held in tension between the two separating matrix faces and is stressed axially, the fibre being held in place by the appropriate interface material. Eventually, the fibre cannot withstand the applied stress, and fractures. Fracture usually occurs at a point within one of the separating matrix blocks, and energy is therefore required to break the interfacial bond.

This sequence of events may be repeated hundreds or thousands of times during a loading cycle depending on the dimensions and lay-up of the composite fibres, and results in a large amount of energy being dissipated in breaking the interfacial bonds rather than propagating straight through the material as would be the case with a single phase material. The properties of the interface material are therefore absolutely critical in

determining the overall strength of the composite. This fibre pull-out mechanism results in composites failing gradually under direct or bending stress, rather than catastrophically, as would be the case without fibre reinforcement.

Crack deflection along and around fibre-matrix boundaries may occur when a crack has initiated, and is propagating through the matrix. When the crack tip reaches the fibre interface, the interface forms a weak point in the material and allows the energy at the crack tip to break the interfacial bond, and in effect deflects the crack around the fibre, leaving it intact. The crack may then continue until it either reaches another fibre interface, or all the crack tip energy is dissipated. Once again, the properties of the interface material is critical, since if the interfacial bonding was too strong, the crack would propagate straight through the fibre without losing a significant amount of energy, in effect negating the addition of the fibre.

5.5.4 EVIDENCE OF THE INEFFECTIVENESS OF FIBRE REINFORCEMENT IN ULTRASONIC MACHINING

Returning to the probable cause of the higher than expected machining rates of the composite. It has been established by previous investigators (see Section 2.3) that material removal during ultrasonic machining is mainly due to multiple impacts of abrasive particles (see the process model, Section 5.2). These particles vary in size depending on the mesh size used in the preparation of the slurry from being of a comparable size to the diameter of a single fibre (around 12 microns for #600 grit) to several times the size of a fibre for #120 grit. The destruction of fibres when ultrasonically machining the composite does not appear to affect the material's resistance to impact damage; evidence of this comes from two observations :

1) When grit size is varied (Figure 11), the graphs generated do not show any significant anomalies at or around the grit sizes which are similar to fibre diameter. If the

fibres were providing any additional strength to the bulk properties of the material, there would be a difference in machining rate between when the fibres were being chipped at by the small impacts of the lower grit sizes, as opposed to when the fibres were being destroyed *en masse* by impacts by the larger grit particles.

2) The material removal rate curves generated when the size of the particles in the slurry is varied (i.e. mesh size) are of similar *shape* (but of different magnitude) when the composite and plate glass are compared, suggesting that the composite behaves as a homogeneous material when subjected to ultrasonic machining.

Reference to the micrographs obtained (Section 4.4) provides clearer evidence of the fracture mechanisms present.

5.6 MICROGRAPHIC OBSERVATION OF MACHINED SURFACES

5.6.1 BENDING AND IMPACT SIMULATIONS

By referring to the micrographs obtained from the bending and impact damage experiments (Figure 67, and Figures 69 - 71), and comparing them with micrographs obtained from the ultrasonic hole drilling and slot milling experimental programmes(Figures 52 - 59), it becomes clear that impact damage is the main mechanism by which material is removed during ultrasonic machining, and *not* a fibre pull out related mechanism (such as bending).

The post-bending test micrographs (Figures 67 and 69) clearly show evidence of fibre pull out. Empty fibre shells are present, and the clean fracture surfaces of the fibres suggest failure under tensile loading, since no chipping around the fracture surfaces (associated with particle impacts) is apparent.

The post-impact test micrographs (Figures 70 and 71) show numerous cracked fibres, some of which have been displaced slightly, but remain attached to their shells. There appear to be no empty fibre shells present in the areas shown. Numerous cracks in the alumina matrix are visible, as is a considerable amount of debris.

Micrographs of the machined samples show some evidence of fibres fractured cleanly (Figures 52, 57 and 58 for example). This suggests that a certain amount of fracture was *not* caused by direct impact of grit particles on a particular fibre. A grit impact on the end of a previously exposed fibre could cause a clean fracture as seen in the previously mentioned micrographs. Impact damage of this nature would cause a certain amount of fibre pull out, as the fibre in question would in effect be a cantilever, loaded at the unsupported end. A restraining force within the matrix or fibre shell must therefore be present, and must either be overcome before pull-out occurs, or would be of sufficient

strength to cause fracture of the fibre at the very edge of the restraining material. Clear evidence of this can be seen in Figure 59.

5.6.2 ELASTIC WAVE PROPAGATION

The concept of elastic wave propagation was briefly mentioned earlier in this chapter, and some evidence of this phenomenon may be observed in the fracture surface micrographs (Figures 57 & 58). The fracture surface of the fibre shown in Figure 57 shows a number of very faint undulations. Similar features can be seen in Figure 58, running perpendicular to the larger "tide marks" on the surface. These lines appear to be "Wallner Lines", described by Lawn [62], Michalsk [76], Varner [82] and Wallner [84]. Wallner lines are undulations caused by transient variations in the applied stress field. The lines represent a 'snapshot' of the crack front shape and position during these transients. Transients are usually caused by two means : viz. the crack front passes an inclusion or pore in the material which alters the local stress field, or mechanical ringing of the sample occurs as stress waves reflect across the interior of the sample during failure. The mechanics of ultrasonic wave propagation could lead to the production of stress waves which may, under certain conditions, cause fracture of the workpiece, leaving Wallner lines behind as evidence. Alternatively, the lines could be produced as the fibre is fractured (by the established action of grit particles). The stress transients which lead to the formation of Wallner lines could be produced by reflections of the fracturing stress wave itself. It is possible that both mechanisms are present to certain degrees, but without further investigation the significance of this mechanism is uncertain.

An example of possible impact damage is visible in Figure 54. The fibre has probably been subject to a direct impact by either a grit particle or a piece of previously removed debris. The absence of the fibre's shell and most of it's interface material suggests the systematic removal of these features by previous impacts. It is interesting

to note that apart from the obvious impact zone, the fibre appears to be undamaged. This suggests that the fibre's shell and interface material behaved in the expected manner : the interface material provided a weakness in the continuum which allowed the shell to break away leaving the fibre intact. Numerous examples of this may be seen in Figures 52, 53, 55 and 59.

5.7 STRESS GENERATION IN MACHINED MATERIAL

5.7.1 FINITE ELEMENT MODEL

The finite element model represented a single spherical grit particle impinging on a horizontal workpiece. Variations in grit geometry would cause some changes to the results, but since there is an infinite number of geometric possibilities, an idealised geometry was considered appropriate at this stage. The grit particle was modelled using un-deformable "rigid surface" elements. This method gave the most consistent results, and minimised possible errors caused by misalignment of elements which would make contact during loading. This was considered to be a greater benefit than the inclusion of the small amount of elastic deformation present in the particle. Since the model used was intended only to give an estimate of the stress levels incurred during indentation of the material, the loss of accuracy caused by not fully meshing the grit particle (and therefore giving some representation of stress relief due to the deformation of the particle) was thought to be acceptable (see Section 3.8).

When the rigid grit particle was displaced according to data obtained experimentally, the maximum principal stresses induced in the workpiece around the contact circle were of the order of 20GPa, considerably more than the 225MPa tensile strength of the composite material. These results indicate that some cracking will be produced during loading of the machined surface, and that this is the primary cause of material removal. However, the finite element calculations referred to above did not include any facility to

introduce geometrical changes as the cracks were initiated during loading. In consequence these results are indicative only, and further progress required the use of other methods (viz. a fracture mechanics approach. Nevertheless these preliminary results do suggest that sub-yield fatigue cracks are not the main cause of material removal in the system studied, since the maximum principal stress will exceed the uni-axial fracture stress.

To obtain a more realistic model, the fracture mechanics of the problem were required (see below). Firstly, the general character of fracture under impact loading is considered.

5.8 FRACTURE MECHANISM OF INDENTATION

Many investigators who have proposed process models used established brittle fracture mechanics mechanisms as a basis for their mathematical models. Since ultrasonic machining is fundamentally an impact process, many of these mathematical process models involve the assumption of multiple impacts by particles upon a flat workpiece material surface. The impacting particles are usually assumed to have either spherical or pointed geometries, both of which have been the subject of much experimental investigation in the past, notably by Evans & Wilshaw [40].

5.8.1 CRACK MECHANISMS INDUCED BY BLUNT INDENTERS

It has been established that indenters of spherical or "blunt" geometry result in the formation of cone cracks, a phenomenon investigated by Hertz [85], resulting in loadings of this type being referred to as "Hertzian contact" loading. In this scenario, as the spherical indenter is pressed into the workpiece, the proceeding system evolves, described by Lawn [62] :

1) Pre-present surface flaws are subjected to tensile stresses outside the contact zone (Figure 87, i)

2) At some point in the loading a favourably located flaw runs around the contact circle to form a surface "ring crack" (Figure 87, ii)

3) On further loading, the embryonic ring crack grows incrementally downward in the rapidly weakening tensile field (Figure 87, iii)

4) At critical load the ring crack becomes unstable and propagates downward into the full frustum of the Hertzian cone, this stage is often referred to as "pop-in" (Figure 87, iv)

5) At still further loading the cone continues in stable growth, unless the contact circle expands beyond the surface ring crack, in which case the cone is engulfed in the compressive contact zone (Figure 87, v)

6) On unloading, the cone crack closes (Figure 87, vi)

The cone cracks described, or cracks resembling cone cracks are likely to be formed during the ultrasonic machining process. The initially irregularly shaped SiC abrasive particles become blunted as machining proceeds, and become spheroidal, as noted experimentally by Koval'chenco *et al* [27]. It is possible that if cone cracking is predominant in a material, material could be removed by means of the intersection of multiple cone cracks as depicted in Figure 88.

5.8.2 CRACK MECHANISMS INDUCED BY SHARP INDENTERS

In the case of pointed or "sharp" indenters, the formation and propagation of cracks is quite different, again described below by Lawn [62] :

1) The sharp point induces inelastic, irreversible deformation (Figure 89, i)

2) At a critical load one or more nascent flaws within the deformation zone become unstable, and pop-in to form subsurface radial cracks on tensile median planes i.e., planes containing the load axis (and, usually, some line of stress concentration, e.g. impression diagonal or cleavage-plane trace in the specimen surface (Figure 89, ii)

3) On increased loading, the crack propagates incrementally downward (Figure 89, iii)

4) On unloading, the median cracks close up *below* the surface, but simultaneously open up in the residual tensile field *at* the surface as the contact recovers its elastic component (Figure 89, iv)

5) Just prior to removal of the indenter the residual field becomes dominant, further expanding the surface radials and initiating a second system of sideways spreading, saucer like lateral cracks near the base of the deformation zone (Figure 89, v)

6) The expansion continues until indenter removal is complete, both crack systems ultimately tending to half pennies centred about the load point (Figure 89, vi)

5.8.3 INDENTATION TYPES GENERATED IN ULTRASONIC MACHINING

Since the SiC particles used in ultrasonic machining are initially of faceted appearance, fracture by sharp indentation is likely if an edge or tip at the intersection of the facets is pressed into the work surface. Although the abrasive particles become blunted, fracture of the abrasive particles can occur, resulting in newly formed sharp particles. As in the case of cone cracking, material removal by sharp indention is also possible as shown in Figure 90

It is more likely that material during ultrasonic machining is removed by a combination of the two mechanisms, and indeed, after inspection of the plate glass samples which were subjected to ultrasonic machining (one of which is shown in Figure 91), evidence of both types of crack was observed, suggesting that the overall fracture mechanics assumptions of previous investigators were valid. It should be borne in mind that the preceding mechanisms were proposed in relation to brittle homogeneous solids, and much of the experimental work, both for the investigations into crack types and propagation *and* the investigations into ultrasonic machining were conducted using glass specimens.

5.9 SUMMARY OF THE FINDINGS OF THE EXPERIMENTAL INVESTIGATION

The present work involves a more complex material than the homogeneous materials considered previously. Although indentation is obviously involved, the results obtained show significant variations from classical theory of a single phase structure. There was no visible conclusive evidence of either crack type when the SiC/Al_2O_3 composite was examined. The structure of the composite, with SiC tows and the porous Al_2O_3 matrix makes accurate visual identification of either crack type difficult, and the formation of either of the fully developed cracks of the types discussed would be impaired by the same discontinuities of the material which make visual identification difficult. However, *some*

evidence of surface cracking should be found if one or both of the classical mechanisms described above are in operation. Absence of these crack types may suggest an alternative mechanism is present in the case of SiC/Al_2O_3 composite.

The micrographs of the machined surface of the composite material show very small particles of debris with no large scale cracks. This would suggest the creation of a large number of very fine cracks that overlap, but do not penetrate far below the surface. To investigate this possibility further, a related project was carried out by Woon [75] as part of an M.Sc. project. This investigation involved the use of a finite element model using the same loading, penetration and geometry as the existing finite element model (Section 3.8.1), but cracks of various lengths were introduced at the positions where cone cracks would be expected to form (i.e. just outside the contact circle, see Section 5.8.1). A full description of the modelling technique used is included in Section 3.8 . The finite element analysis results were used to obtain the corresponding J-Integral values, from which the associated K values were determined. From the published toughness values T for the materials involved, it was possible to obtain K/T ratios as a function of load and crack length. In all the calculations involving the composite, K/T was less than unity, but this was *not* the case in those relating to glass. This would support the suggestion that sub-critical cracks initiated in glass would grow spontaneously and cause large scale fracture, but the surface cracks in the composite would remain sub-critical. This would be consistent with the observations of large scale cracking in the glass specimen, and its absence in the composite. However, the rate of indention is extremely large (around 20 KHz.) so an extremely large number of sub-critical cracks on the machined surface is possible. These could lead to the removal of surface material in the form of very fine debris rather than as large chips, as in the case of glass. This is consistent with the micrographic evidence (Figures 60, 61, 62, 63 and 66).

There is at the present time no quantitative model based on such a mechanism, and the problems involved in its creation are great. In the first instance, the theory of sub-critical

surface cracks is much less developed than is the case with post-critical fracture. Surface condition and the environment is also significant where very small cracks are involved. Much more experimental data will be required to support the development of such a model (see Section 7).

Some caution is required with respect to the use of T values in the case of indention loadings produced in ultrasonic machining, since T values are obtained with a completely different stress system (load transverse to the crack direction). The type of fracture produced in the composite by these two loading conditions are dissimilar, so the T values may not be equally applicable in both cases. Even so, the analysis carried out by Woon [75] is valuable with the present state of knowledge, and is consistent with the experimental observation of the machined surface.

6. CONCLUSIONS

As a result of this investigation into the ultrasonic machining characteristics of SiC fibre reinforced Al_2O_3, the following conclusions may be drawn :

1) Ultrasonic machining can be successfully used for both hole drilling and slot milling of SiC fibre reinforced Al_2O_3.

2) The significant experimental factors for ultrasonic hole drilling were found to be abrasive size, abrasive concentration, tool rotation speed and static load. The corresponding significant factors for ultrasonic slot milling were abrasive size, tool rotation speed and static load. In both cases, amplitude of vibration (or power setting) may also be significant, but this cannot be verified without further experimentation. Empirical equations have been developed to relate these variables to the rate of machining.

3) During ultrasonic machining of the composite, material is not removed from the composite by established brittle fracture mechanisms, i.e. cone cracks or radial/median cracks. It is suggested that material is removed by fine scale chipping or erosion of the material. This process involves the creation of very small cracks that overlap and eventually create the small chips. Additional material removal mechanisms such as cavitation or elastic wave propagation may also be in operation.

4) Because of the effect noted in (3), the crack deflection and crack stopping mechanisms which give fibre reinforced composites enhanced toughness values do not appear to apply during the ultrasonic machining of SiC fibre reinforced Al_2O_3, giving rise to higher material removal rates than would be expected from the toughness values of the composite.

5) The magnitude of the stresses set up during ultrasonic machining are sufficient to exceed the fracture strength of the material. Low stress fatigue cracks are unlikely to be significant in these circumstances.

6) Unlike the ceramic composite, glass specimens subjected to the same machining conditions show evidence of classical indentation fracture. This is associated with lower toughness in the case of the glass.

7) The results of this work agree qualitatively with published relationships between machining rate and the relevant process parameters. However, comparison with the associated mathematical relationships has not been possible since these equations contain empirical constants which are material specific, and which cannot be evaluated in the present case.

8) The results obtained here suggest a complex mechanism that relates to very small sub-critical crack formation. The theory of such mechanisms is not well understood, so a comprehensive model of the process is not yet possible. However, the present work is a good basis on which further programmes can be built.

7. RECOMMENDATIONS FOR FUTURE WORK

1) To perform a full factorial experiment, and to use a more extensive range of values between high and low values of each factor. This would give a more accurate indication of the trends obtained in this study.

2) To investigate alternative fracture mechanisms to those proposed in previously presented process models, i.e. surface erosion or chipping.

3) To construct a three dimensional finite element model of the process using a realistic fibre - matrix for the workpiece, fully meshed grit particles (to allow for stress relief), and a range of grit particle geometries. This would give more accurate stress patterns within the workpiece and grit.

4) The development of a mathematical model incorporating data obtained from items 1, 2 and 3 above.

[1] T. E. Schmid.
"Ceramic composites for advanced gas turbine engines".
Superalloys 1992.
Champion, Pennsylvania, 20 - 24 Sept. 1992, pp 401 - 407.

[2] J. B. Kohls.
"Ultrasonic manufacturing processes : ultrasonic machining (USM) and ultrasonic impact grinding (USIG)".
The Carbide and Tool Journal.
Sept / Oct. 1984, pp 12 - 15.

[3] D. Moore.
"Ultrasonic impact grinding".
Nontraditional Machining (pp 137 - 139)
1986, American Society for Metals.

[4] M. A. Moreland.
"Ultrasonic machining"
'Engineered materials handbook Vol. 4' (pp 359 - 362)
ASM Int., 1991.

[5] W. A. J. Chapman.
"Workshop technology - part III".
(pp 207 - 213).
Arnold.

[6] J. Kaczmarek.
"Principles of machining by cutting, abrasion and erosion".
(Chapter 21).
Peter Peregrinus Ltd.

[7] A. Davidson.
"Handbook of precision engineering".
(pp 53 - 60).
Philips Technical Library.

[8] H. Kamoun.
"Mechanisms of ultrasonic machining"
Thesis, 1994.
E.N.S.A.M., Paris.

[9] A. I. Markov.
"Ultrasonic machining of intractable materials".
London Iliffe Books Ltd. 1966.

[10] L. D. Rozenberg.
"Ultrasonic cutting".
Consultants Bureau, New York, 1964.

[11] R. Komanduri.
"Machining fibre-reinforced composites".
Mechanical Engineering.
April 1993, pp 58 - 64.

[12] S. Abrate & D. Walton.
"Machining of composite materials. Part II : Non-traditional methods"
Composites Manufacturing (U.K.)
1992, Vol. 3, 2, pp 85 - 94.

[13] L. M. Sheppard.
"Machining of advanced ceramics".
Advanced Materials and Processes inc. Metal Progress.
December 1987, pp 40 - 48.

[14] D. Kremer & J. Mackie.
"Ultrasonic machining applied to ceramic materials".
L'Industrie Céramique.
No. 830, September 1988, pp 632 - 637.

[15] C. Watkins.
"Outsmarting ceramic machining problems".
Manufacturing Systems.
1991, Vol. 9, 11, pp 42 - 44.

[16] P. Black.
"An ultrasonic impact grinding technique for electrode - forming and redressing".
Nontraditional Machining (American society for metals)
1986, pp 129 - 136.

[17] S. M. Trendler.
"ECM and Ultrasonic machining for faster die finishing".
Die Casting Engineer.
Jan. / Feb. 1985, pp 66 - 67.

[18] M. Waplington, L. Blunt, A. D. Walmsley & P. J. Lumley.
"Dental hard tissue cutting characteristics of an ultrasonic drill".
Int. J. Mach Tools Manufact.
Vol. 35 (1995), No. 2, pp 339 - 343.

[19] K.Suzuki, T. Tochinai, T. Uematsu & S. Mishiro.
"A new grinding method for ceramics using a biaxially vibrated nonrotational ultrasonic tool".
Annals of the CIRP.
Vol. 42, 1, 1993.

[20] X. Li.
"The effect of tool vibration on tool wear in ultrasonic vibration cutting".
A.S.T.M. Special technical publication.
May 1995, Vol. 1247, pp 62 - 73.

[21] V. F. Kazantsev & L. D. Rosenberg.
"The mechanism of ultrasonic cutting".
Ultrasonics.
October - December 1965. pp 166 - 174.

[22] V. Soundararajan & V. Radhakrishnan.
"An experimental investigation on the basic mechanisms involved in ultrasonic machining".
Int. J. Mach. Tool Des. & Res.
1985, Vol. 26, (3), pp 307 - 321.

[23] W. König & M. Hilleke.
"Technology of ultrasonic machining of advanced ceramics".
cfi/Ber. DKG
1995, Vol. 72, (4), pp 175 - 179.

[24] M. Komaraiah.
"Experimental studies on ultrasonic machining".
Production Engineer.
December 1984, pp 40 - 41.

[25] M. Komaraiah & P. Narasimha Reddy.
"Relative performance of tool materials in ultrasonic machining".
Wear.
1993, Vol. 161, (1-2), pp1 - pp10.

[26] M. Komaraiah & P. Narasimha Reddy.
"A study on the influence of workpiece properties in ultrasonic materials".
Int. J. Mach. Tools & Manuf.
1993, Vol. 33, (3), pp 495 - 505.

[27] Koval'chenko, A. V. Paustovskii & V. A. Perevyazco.
"Influence of properties of abrasive materials on the effectiveness of ultrasonic machining of ceramics".
Soviet Powder Metallurgy and Metal Ceramics.
1986, Vol. 25, (7), pp 560 -562.

[28] G. Nandi, S. K. Mukherjee, J. Saha, P.K. Mishra & A. Bhattacharyya.
"Tool wear in ultrasonic trepanning of glass - ceramics".
Procs. of the 5th. Int. Conf. on Prod. Eng.
9 - 11 July 1984, Tokyo, Japan. pp 283 - 287.

[29] H. Dam, P. Quist & M. P. Schreiber.
"Productivity, surface quality and tolerances in ultrasonic machining of ceramics".
Journal of Materials Processing Technology.
1995, 51, pp 358 - 368.

[30] R. Haas.
"Ultrasonic erosion under investigation" *(translated paper)*
Industrielle Anzeiger
1989, (99), pp 26 - 29.

[31] Grathwohl, H. Iwanekog & F. Thümmler.
"Ultrasonic machining of hard ceramics" *(translated paper)*
Mat. -wiss. u. werkstofftechn.
1988, Vol. 19, (19), pp 81 - 86.

[32] M. Komaraiah, M. A. Manan, P. Narasimha Reddy & S. Victor.
"Investigation of surface roughness and accuracy in ultrasonic machining".
Precision Engineering.
1988, Vol.10, (2), pp 59 - 65.

[33] J. Zhixin & A. Xing.
"Influence of constant machining parameters on material removal rate in ultrasonic machining".
Modelling, measurement and control B: solid and fluid mechanics and thermics, mechanical systems.
1995, Vol. 57, (4), pp 9 - 24.

[34] G. Ghosal, A. R. Choudhury, D. C. Roy & P. K. Mishra.
"Behaviour of glass in machining by ultrasonics".
12th. AIMTDR Conference, IIT Delhi.
1986, Tata McGraw-Hill Pub. Co. Ltd., New Delhi.

[35] H. Hocheng & C. C. Hsu.
"Preliminary study of ultrasonic drilling of fibre - reinforced plastics".
Journal of Materials Processing Technology.
1995, 48, pp 255 - 266.

[36] M. T. Sykes, R. O. Scattergood & J. L. Routbort.
"Erosion of SiC - reinforced alumina ceramic composites".
Composites.
April 1987, Vol. 18, No. 2, pp 153 - 163.

[37] G. E. Miller.
"Special theory of ultrasonic machining".
Journal of Applied Physics.
1957, (28), pp 149.

[38] M. C. Shaw.
"Ultrasonic grinding".
Microtechnic.
1956, (10), pp 257.

[39] G. S. Kainth, A. Nandy & K. Singh.
"On the mechanics of material removal in ultrasonic machining".
Int. J. Mach. Tool Des. & Res.
1979, Vol. 19, pp 33 - 41.

[40] A. G. Evans & T. R. Wilshaw.
"Quasi - static solid particle damage in brittle solids - I. Observations, analysis and implications".
Acta Metallurgica.
1976, Vol. 24, pp 939 - 956.

[41] B. R. Lawn & M. V. Swain.
"Microfracture beneath point indentations in brittle solids".
Journal of Materials Science.
1975, (10), pp 113 - 122.

[42] B. Lawn & R. Wilshaw.
"Review - indentation fracture: principles and applications".
Journal of Materials Science.
1975, Vol. 10, pp 1049 - 1081.

[43] R. F. Cook & G. M. Pharr.
"Direct observation and analysis of indentation cracking in glasses and ceramics".
J. Am. Ceram. Soc.
1990, Vol. 73, (4), pp 787 - 817.

[44] E. V. Nair & A. Ghosh.
"A fundamental approach to the study of the mechanics of ultrasonic machining".
Int. J. Prod. Res.
1985, Vol. 23, (4), pp 731 - 753.

[45] S. W. Dharmadhikari & C. S. Sharma.
"Optimisation of abrasive life in ultrasonic machining".
Journal of Engineering for Industry.
November 1985, Vol. 107, pp 361 - 364.

[46] I. K. Partridge.
"Advanced composites".
Elsevier Applied Science 1989.

[47] K. Ashbee.
"Fundamental principles of fibre reinforced composites".
Technomic (Second Edition). 1993.

[48] D. Hull.
"An introduction to composite materials".
Cambridge University Press. 1993.

[49] R. W. Davidge.
"Fibre - reinforced ceramics".
Composites.
April 1987, Vol. 18, (2), pp 92 - 97.

[50] C. Newey & G. Weaver.
"Materials principles and practice".
Butterworth - Heinemann 1990.

[51] H. Frei & G. Grathwohl.
"Microstructure and strength of advanced ceramics after machining".
Ceramics International.
1993, Vol. 19, pp 93 - 104.

[52] A. G. Evans.
"Strength degradation by projectile impacts".
Journal of the American ceramic society.
Aug. 1973, Vol. 56, No. 8.

[53] K. J. Wynne & R. W. Price.
"Ceramics via. polymer pyrolysis".
Ann. Rev. Mat. Sci.
1984, Vol. 14, pp 279 - 334.

[54] S. Yajima, H. Kayamo, K. Okamura, M. Omori, J. Hayashi, T. Matsuzama & K. Akutsu.
"Elevated temperature strength of continuous SiC fibres".
Am. Cer. Soc. Bull.
1976, Vol. 55 (12), pp 1065 - 1066.

[55] **"New product information".**
Dow Corning Corporation.
1983.

[56] K. R. Stull & A. Parvizi - Majidi.
"Fracture toughness of fibre-reinforced glass ceramic and ceramic matrix composites".
Ceram. Eng. Sci. Proc.
1991 Vol. 12, (7 - 8), pp 1452 - 1461.

[57] V. K. Sarin & M. Ruhle.
"Microstructural studies of ceramic-matrix composites".
Composites.
April 1987, Vol. 18, No.2.

[58] M. Hunt.
"Metal and ceramic composites come down to earth".
Materials Engineering.
July 1992, pp 11 - 14.

[59] P.Barron - Antolin, G. H. Schiroky & C. A. Andersson.
"Properties of fibre - reinforced alumina matrix composites".
Ceramic Engineering and Science Proceedings.
July - Aug. 1988, Vol. 9, pp 759 - 766. (ISSN 0196-6219).

[60] A. W. Urquhart.
"Engineered materials handbook Vol. 4"
'Directed Metal Oxidation' (pp 232 - 235)
ASM Int., 1991.

[61] B. R. Lawn & T. R. Wilshaw.
"Fracture of brittle solids".
Cambridge 1975.

[62] B. R. Lawn.
"Fracture of brittle solids - second edition"
Cambridge, 1993.

[63] B. R. Lawn, T. P. Dabbs & C. J. Fairbanks.
"Kinetics of shear-activated indentation crack initiation in soda-lime glass".
Journal of Materials Science.
1983, Vol. 18, pp 2785 - 2797.

[64] J. T. Hagan & M. V. Swain.
"The origin of median and lateral cracks around plastic indents in brittle materials".
J. Phys. D : Appl. Phys.
1978, Vol. 11, pp 2091 - 2102.

[65] D. Tabor.
"Wear - a critical synoptic view".
Journal of Lubrication Technology.
Oct. 1977, Vol. 99, No. 4, pp 387 - 395.

[66] B. R. Lawn, A. G. Evans & D. B. Marshall.
"Elastic / plastic indentation damage in ceramics: the median / radial crack system".
Journal of the American Ceramic Society.
Sept. - Oct. 1980, Vol. 63, (9 - 10).

[67] K. Zeng, A. E. Giannakopoulos & D. J. Rowcliffe.
"Vickers indentations in glass - II. Comparison of finite element analysis and experiments".
Acta Metall. Mater.
1995, Vol. 43, No. 5, pp 1945 - 1954.

[68] J. S. Lyons.
"Finite element prediction of the fracture mechanisms of short fibre-reinforced ceramic matrix composites".
Ceram. Eng. Sci. Proc.
1991, Vol. 12, 7 - 8, pp 1359 - 1374.

[69] M-C. Jeng, J-L. Doong & W-C. Liu.
"Finite element analysis of crack growth life prediction under complex load history".
Engineering Fracture Mechanics.
1993, Vol. 46, No. 4, pp 607 - 616.

[70] H. Hamlili, L. Thery, J. Von Stebut & M. Gueury.
"Finite element analysis of damage and brittle fracture of an orthotropic material using a simple personal computer".
Mechanics and mechanisms of damage in composites and multi-materials.
Nov. 1989, Nov. Saint Etienne, France.
Published MEP 1991.

[71] **"The Hertz contact problem"**
ABAQUS / Standard, Example Problems Manual.
Hibbitt, Karlsson & Sorensen, Inc. 1994.
Volume I, pp 1.2.3-1 to 1.2.3-22.

[72] **"Conical crack in a half-space with and without submodelling"**
ABAQUS / Standard, Example Problems Manual.
Hibbitt, Karlsson & Sorensen, Inc. 1994.
Volume II, pp7.1.3-1 to 7.1.3-31.

[73] P. J. Ross.
"Taguchi techniques for quality engineering".
McGraw - Hill. 1988.

[74] Bhattacharya & W. D. Nix.
"Finite element analysis of cone indentation".
Int. J. Solids Structures.
1991,Vol. 27, (8), pp 1047 - 1058.

[75] R. Woon.
"Finite element crack growth analysis of ultrasonic machining"
M.Sc. project report.
Sheffield Hallam University, 1996.

[76] T.A. Michalsk.
"Quantitative fracture surface analysis"
'Engineered materials handbook Vol. 4' (pp 652 - 662)
ASM Int., 1991.

[77] R. Khadem & J. J. O'Connor.
"Axial compression of an elastic circular cylinder in contact with two identical elastic half spaces".
Int. J. Engng. Sci.
1969, Vol. 7, pp 785 - 800.

[78] G. M. Pharr, W. C. Oliver & F. R. Brotzen.
"On the generality of the relationship among stiffness, contact area, and elastic modulus during indentation".
J. Mater. Res.
Mar. 1992, Vol. 7, No. 3, pp 613 - 617.

[79] V. I. Likhtman, P. A. Rebinder & G. V. Karpenko.
"Effect of a surface-active medium on the deformation of metals"
Department of Scientific and Industrial Research (Translation).
Her Majestys Stationary Office, London, 1958.

[80] S. Suresh.
"Fatigue of materials"
Cambridge University Press, 1994.

[81] A. Bedford & D. S. Drumheller.
"Introduction to elastic wave propagation"
Wiley, 1994.

[82] J. R. Varner.
"Descriptive fractography"
'Engineered materials handbook Vol. 4, (pp 635 - 644)
ASM Int., 1991.

[83] H. Matzke.
"Indentation techniques for evaluation of mechanical properties of ceramics and glasses".
Key Engineering Materials.
1991, Vols. 56 - 57, pp 365 - 392.

[84] V. H. Wallner.
"Linienstrukturen an bruchflachen "
Phys.,Vol. 114, 1939 (pp 368 - 378)

[85] H. Hertz.
"Verhandlungen des Vereins zur Beförederung des Gewerbe Fleisses"
J. Reine Angew. Math.
Vol. 92, 1881, pp 156 *et seq.*
Reprinted in English in **"Hertz's miscelleneous papers"**
Macmillan, London, 1896, Chapters 5 & 6.

Table 1

Sections 3.5.2 & 3.5.4

Factors & levels used in the Taguchi experiment

FACTOR	MEANING	LEVEL 1	LEVEL 2
A	Power setting	Low	High
B	Abrasive size	#320	#120
C	Abrasive conc.	40% v/v	20% v/v
D	Tool tip diameter	1mm	6mm
E	Tool rotn. speed	0 r.p.m.	300 r.p.m.
F	Static tool load	1 kg.	5 kg.
G	Tool traverse speed	150 mm/min.	1000 mm/min.

Table 2

Section 3.5.2

Commonly used silicon carbide abrasive mesh sizes

Grit size (#)	Average particle size (microns)
120	142
150	122
220	66
320	32
500	17
600	14
800	9
1000	5

Table 3

Sections 3.5.3, 4.2.1 & 5.3.2

The L8 orthogonal array

		FACTOR						
		A	B	C	D	E	F	G
T	1	1	1	1	1	1	1	1
R	2	1	1	1	2	2	2	2
I	3	1	2	2	1	1	2	2
A	4	1	2	2	2	2	1	1
L	5	2	1	2	1	2	1	2
	6	2	1	2	2	1	2	1
N	7	2	2	1	1	2	2	1
O	8	2	2	1	2	1	1	2

Table 4

Section 3.7.2

Ultrasonic hole drilling variables

Abrasive size	# 120	# 220	# 320	# 600	-
Static tool load	0.5 kg	1 kg	2 kg	3 kg	-
Tool rotn. speed	0 r.p.m.	200 r.p.m.	400 r.p.m.	600 r.p.m.	800 r.p.m.

Table 5

Section 3.7.2

Ultrasonic slot milling variables

Abrasive size	# 120	# 220	# 320	# 600	-
Static tool load	0.5 kg	1 kg	2 kg	3 kg	-
Tool rotn. speed	0 r.p.m.	200 r.p.m.	400 r.p.m.	600 r.p.m.	800 r.p.m.
Abrasive conc.	10 % v/v	20 % v/v	30 % v/v	40 % v/v	-

Table 6

Section 3.7.3

Ultrasonic hole drilling : nominal parameter settings

PARAMETER	NOMINAL SETTING
Abrasive size	#120
Static tool load	2 kg
Tool rotation speed	0 r.p.m.
Abrasive concentration	30 % v/v
Tool tip diameter	3 mm
Power setting	High (20 microns)

Table 7

Section 3.7.3

Ultrasonic slot milling : nominal parameter settings

PARAMETER	NOMINAL SETTING
Abrasive size	#120
Static tool load	2 kg
Tool rotation speed	0 r.p.m.
Abrasive concentration	30 % v/v
Tool tip diameter	3 mm
Power setting	High (20 microns)
Traverse speed	250 mm/min.

Table 8

Section 3.7.8

Abrasive slurry concentration test results

Sample No.	Water Vol. (cm^3)	Grit Vol. (cm^3)	Grit conc. (%)
1	42	26	61.90
2	42	26	61.90
3	38	24	63.16
4	44	28	63.63

Table 9

Section 4.2.1

Raw data obtained from the Taguchi hole drilling experiment

Hole No.	Diameter (mm)	Depth (mm)	Vol. Removed. (cm^3)
1	1.618	0.966	1.986
2	1.481	0.952	1.640
3	1.536	0.773	1.432
4	*	*	*
5	6.244	0.036	1.102
6	6.101	0.033	0.965
7	1.903	0.756	2.150
8	1.870	0.322	0.884
9	1.797	0.648	1.643
10	6.526	2.209	73.889
11	6.512	2.028	67.544
12	6.453	1.661	54.323
13	1.850	2.209	5.937
14	1.850	1.057	2.841
15	1.883	1.748	4.868
16	5.913	0.189	5.190
17	6.810	0.231	8.414
18	6.542	0.184	6.185
19	2.063	1.197	4.001
20	1.869	1.319	3.619
21	1.755	0.654	1.582
22	6.443	0.839	27.354
23	5.546	0.035	0.833
24	6.306	0.999	31.201

* Note

Geometry data from hole number 4 was not included due to the movement of the workpiece during machining. The movement was not detected during the process, but the result was a stepped hole being machined. Any possibility of a repeated error was eliminated by modifying the clamping system used (see Section 3.7.1)

Table 10

Section 4.2.1

Raw data obtained from the Taguchi slot milling experiment

Hole No.	Width (mm)	Length (mm)	Depth (mm)	Vol. Removed. (mm^3)
1	1.500	21.230	0.550	17.249
2	1.400	21.130	0.660	19.247
3	1.500	21.200	0.710	22.235
4	6.200	27.420	0.160	25.881
5	6.200	27.310	0.160	25.772
6	6.500	27.390	0.130	21.966
7	2.100	22.650	0.400	18.647
8	2.300	23.150	0.275	14.330
9	2.000	23.300	0.300	13.722
10	6.100	25.760	0.780	116.338
11	5.500	24.570	0.130	16.724
12	6.200	25.510	0.350	52.469
13	1.650	23.150	0.300	11.284
14	2.000	23.370	0.285	13.076
15	1.850	23.220	0.236	11.105
16	5.750	25.710	0.001	0.140
17	6.000	25.660	0.125	18.279
18	6.050	25.850	0.175	25.994
19	2.350	23.000	0.350	18.503
20	2.250	23.000	0.325	16.466
21	2.300	23.000	0.200	10.353
22	6.250	27.570	0.275	45.081
23	6.100	27.570	0.275	44.053
24	6.100	27.610	0.275	44.120

Table 11

Sections 4.2.2, 4.2.4 & 5.3.2

Orthogonal array and material removal rate data from the Taguchi hole drilling experiment .

		F A C T O R							Machining time	Vol. Removed	Material removal rate.	Average material removal rate
		A	B	C	D	E	F	G	(sec.)	(mm^3)	(mm^3/sec.)	(mm^3/sec.)
TRIAL	1								60	1.986	0.033	0.028
		1	1	1	1	1	1	1	60	1.640	0.027	
									60	1.432	0.024	
	2								*	*	*	0.009
		1	1	1	2	2	2	2	120	1.102	0.009	
									120	0.965	0.008	
	3								30	2.150	0.072	0.052
		1	2	2	1	1	2	2	30	0.884	0.029	
									30	1.643	0.055	
	4								90	73.889	0.821	0.725
		1	2	2	2	2	1	1	90	67.544	0.750	
									90	54.323	0.604	
	5								27	5.937	0.220	0.279
		2	1	2	1	2	1	2	30	2.841	0.095	
									20	4.868	0.243	
	6								150	5.190	0.035	0.044
		2	1	2	2	1	2	1	150	8.414	0.056	
									150	6.185	0.041	
	7								15	4.001	0.267	0.360
		2	2	1	1	2	2	1	8	3.619	0.452	
									25	1.582	0.063	
	8								60	27.354	0.456	0.401
		2	2	1	2	1	1	2	35	0.833	0.024	
									90	31.201	0.347	

* Note :

This data could not be included due to the unavailibility of material removal data from the trial (see note in Table 9)

Table 12

Sections 4.2.3 & 4.2.6

Significance rating analysis for the Taguchi analysis of ultrasonic hole drilling

Factor	Significance rating	F-Ratio	Percentage contribution
A	0.009	0.422	2.030
B	0.174	8.030	38.623
C	0.011	0.529	2.545
D	0.026	1.226	5.898
E	0.090	4.148	19.954
F	0.117	5.435	26.140
G	0.022	n/a	4.810
		Total	100.000

Table 13

Sections 4.2.5 & 5.3.2

Orthogonal array and material removal rate data from the Taguchi slot milling experiment

		F A C T O R							Machining time	Vol. Removed	Material removal rate.	Average material removal rate
		A	B	C	D	E	F	G	(sec.)	(mm^3)	(mm^3/sec.)	(mm^3/sec.)
T R I A L	1								90	17.249	0.192	0.179
		1	1	1	1	1	1	1	120	19.247	0.160	
									120	22.235	0.185	
	2								120	25.881	0.216	0.204
		1	1	1	2	2	2	2	120	25.772	0.215	
									120	21.966	0.183	
	3								30	18.674	0.622	0.519
		1	2	2	1	1	2	2	30	14.330	0.478	
									30	13.722	0.457	
	4								90	116.338	1.293	0.938
		1	2	2	2	2	1	1	*	16.724	*	
									90	52.469	0.583	
	5								30	11.284	0.376	0.394
		2	1	2	1	2	1	2	30	13.076	0.436	
									30	11.105	0.370	
	6								*	0.140	*	0.217
		2	1	2	2	1	2	1	*	18.279	*	
									120	25.994	0.217	
	7								30	18.503	0.617	0.527
		2	2	1	1	2	2	1	30	16.466	0.549	
									25	10.353	0.414	
	8								90	45.081	0.501	0.453
		2	2	1	2	1	1	2	90	44.053	0.489	
									120	44.120	0.368	

* Note

This data could not be included due to errors in the timing of the trial caused by either inadvertant operation of the timing apparatus or by a misjudgement of the point of machining initiation.

Table 14

Sections 4.2.5 & 4.2.7

Significance rating analysis for the Taguchi analysis of ultrasonic slot milling

Factor	Significance rating	F-Ratio	Percentage contribution
A*	0.008	1.283	1.816
B	0.260	42.522	60.202
C	0.062	10.154	14.376
D*	0.005	0.762	1.079
E	0.060	9.900	14.017
F	0.031	5.055	7.157
G*	0.006	0.955	1.353
	Average 0.0061		Total 100.000

* Note

This signifies the factors with the lowest three significance rating values, the average of which was then calculated.

Table 15

Section 4.2.8

Factors and levels which yield the highest theoretical material removal rate value for ultrasonic hole drilling (see Table 1 for full descriptions)

Factor	Level
A	2
B	2
C	2
D	2
E	2
F	1

Table 16

Section 4.2.8

Factors and levels which yield the highest theoretical material removal rate value for ultrasonic slot milling (see Table 1 for full descriptions)

Factor	Level
A	1
B	2
C	2
D	2
E	2
F	1
G	1

Table 17

Sections 4.3.1, 4.3.2 & 4.3.5

Material removal rate data from the ultrasonic hole drilling of SiC/Al_2O_3 composite, main experimental programme, **Variable : Abrasive grit size**

Grit size	Run	Tool material		
		Mild steel	Stainless steel	Nimonic 80A
#120	1 (mm^3/sec)	0.680	0.259	0.413
	2 (mm^3/sec)	0.453	0.267	0.338
	Ave.	**0.567**	**0.263**	**0.376**
#220	1 (mm^3/sec)	0.512	0.237	0.377
	2 (mm^3/sec)	0.364	0.175	0.369
	Ave.	**0.438**	**0.206**	**0.373**
#320	1 (mm^3/sec)	0.196	0.041	0.119
	2 (mm^3/sec)	0.206	0.095	0.098
	Ave.	**0.201**	**0.068**	**0.109**
#600	1 (mm^3/sec)	0.053	0.020	0.039
	2 (mm^3/sec)	0.049	0.043	0.038
	Ave.	**0.051**	**0.032**	**0.039**

Table 18

Sections 4.3.1, 4.3.3 & 4.3.5

Material removal rate data from the ultrasonic hole drilling of SiC/Al_2O_3 composite, main experimental programme, **Variable : Tool rotation speed**

Rotation speed	Run	Tool material		
		Mild steel	Stainless steel	Nimonic 80A
0 r.p.m	1 (mm^3/sec)	0.818	0.390	0.413
	2 (mm^3/sec)	0.534	0.466	0.338
	Ave.	**0.676**	**0.428**	**0.376**
200 r.p.m.	1 (mm^3/sec)	0.966	0.594	0.649
	2 (mm^3/sec)	0.718	0.587	0.427
	Ave.	**0.842**	**0.591**	**0.538**
400 r.p.m.	1 (mm^3/sec)	1.084	0.808	0.630
	2 (mm^3/sec)	1.248	0.727	0.614
	Ave.	**1.166**	**0.768**	**0.622**
600 r.p.m.	1 (mm^3/sec)	1.340	0.905	0.649
	2 (mm^3/sec)	1.453	0.810	0.615
	Ave.	**1.397**	**0.858**	**0.632**
800 r.p.m.	1 (mm^3/sec)	1.123	0.809	0.501
	2 (mm^3/sec)	1.386	0.687	0.339
	Ave.	**1.255**	**0.748**	**0.420**

Table 19

Sections 4.3.1, 4.3.4 & 4.3.5

Material removal rate data from the ultrasonic hole drilling of SiC/Al_2O_3 composite, main experimental programme, **Variable : Static tool load**

Static load	Run	Tool material		
		Mild steel	Stainless steel	Nimonic 80A
0.5 kg	1 (mm^3/sec)	0.419	0.160	0.165
	2 (mm^3/sec)	0.320	0.115	0.242
	Ave.	**0.370**	**0.138**	**0.204**
1 kg	1 (mm^3/sec)	0.486	0.238	0.254
	2 (mm^3/sec)	0.350	0.229	0.230
	Ave.	**0.418**	**0.234**	**0.242**
2 kg	1 (mm^3/sec)	0.680	0.390	0.189
	2 (mm^3/sec)	0.453	0.466	0.189
	Ave.	**0.567**	**0.428**	**0.189**
3 kg	1 (mm^3/sec)	0.471	0.369	0.272
	2 (mm^3/sec)	0.483	0.348	0.461
	Ave.	**0.477**	**0.359**	**0.367**

Table 20

Sections 4.3.6 & 4.3.7

Material removal rate data from the ultrasonic slot milling of SiC/Al_2O_3 composite, main experimental programme, **Variable : Abrasive grit size**

Grit size	Run	Tool material		
		Mild steel	Stainless steel	Nimonic 80A
#120	1 (mm^3/sec)	0.719	0.375	0.605
	2 (mm^3/sec)	0.782	0.397	0.561
	Ave.	**0.751**	**0.386**	**0.583**
#220	1 (mm^3/sec)	0.698	0.577	0.438
	2 (mm^3/sec)	0.600	0.696	0.451
	Ave.	**0.649**	**0.637**	**0.445**
#320	1 (mm^3/sec)	0.469	0.329	0.271
	2 (mm^3/sec)	0.341	0.327	0.260
	Ave.	**0.405**	**0.328**	**0.266**
#600	1 (mm^3/sec)	0.296	0.354	0.147
	2 (mm^3/sec)	0.185	0.286	0.230
	Ave.	**0.241**	**0.320**	**0.189**

Table 21

Sections 4.3.6 & 4.3.8

Material removal rate data from the ultrasonic slot milling of SiC/Al_2O_3 composite, main experimental programme, **Variable : Tool rotation speed**

Rotation speed	Run	Tool material		
		Mild steel	Stainless steel	Nimonic 80A
0 r.p.m	1 (mm^3/sec)	0.719	0.375	0.605
	2 (mm^3/sec)	0.782	0.397	0.561
	Ave.	**0.751**	**0.386**	**0.583**
200 r.p.m.	1 (mm^3/sec)	0.599	0.603	0.459
	2 (mm^3/sec)	0.830	0.606	0.467
	Ave.	**0.715**	**0.605**	**0.463**
400 r.p.m.	1 (mm^3/sec)	1.208	0.556	0.490
	2 (mm^3/sec)	1.032	0.469	0.559
	Ave.	**1.120**	**0.512**	**0.525**
600 r.p.m.	1 (mm^3/sec)	1.513	1.047	0.641
	2 (mm^3/sec)	1.144	1.025	0.635
	Ave.	**1.329**	**1.036**	**0.638**
800 r.p.m.	1 (mm^3/sec)	1.387	1.574	0.664
	2 (mm^3/sec)	1.060	1.296	0.560
	Ave.	**1.224**	**1.435**	**0.612**

Table 22

Sections 4.3.6 & 4.3.9

Material removal rate data from the ultrasonic slot milling of SiC/Al_2O_3 composite, main experimental programme, **Variable : Static tool load**

Static load	Run	Tool material		
		Mild steel	Stainless steel	Nimonic 80A
0.5 kg	1 (mm^3/sec)	0.596	0.278	0.347
	2 (mm^3/sec)	0.366	0.441	0.351
	Ave.	**0.481**	**0.360**	**0.349**
1 kg	1 (mm^3/sec)	0.426	0.318	0.429
	2 (mm^3/sec)	0.375	0.325	0.580
	Ave.	**0.401**	**0.322**	**0.505**
2 kg	1 (mm^3/sec)	0.719	0.375	0.605
	2 (mm^3/sec)	0.782	0.397	0.561
	Ave.	**0.751**	**0.386**	**0.583**
3 kg	1 (mm^3/sec)	0.960	0.392	0.371
	2 (mm^3/sec)	1.000	0.477	0.465
	Ave.	**0.980**	**0.435**	**0.418**

Table 23

Sections 4.3.6 & 4.3.10

Material removal rate data from the ultrasonic slot milling of SiC/Al_2O_3 composite, main experimental programme, **Variable : Abrasive concentration**

Abrasive conc.	Run	Tool material		
		Mild steel	Stainless steel	Nimonic 80A
10% v/v	1 (mm^3/sec)	0.522	0.624	0.544
	2 (mm^3/sec)	0.591	0.652	0.521
	Ave.	**0.557**	**0.638**	**0.533**
20% v/v	1 (mm^3/sec)	0.811	1.515	1.214
	2 (mm^3/sec)	0.756	1.087	1.040
	Ave.	**0.784**	**1.301**	**1.127**
30% v/v	1 (mm^3/sec)	0.719	0.375	0.605
	2 (mm^3/sec)	0.782	0.397	0.561
	Ave.	**0.751**	**0.386**	**0.583**
40% v/v	1 (mm^3/sec)	0.881	1.815	1.238
	2 (mm^3/sec)	0.833	1.046	1.238
	Ave.	**0.857**	**1.431**	**1.238**

Table 24

Sections 4.3.12 & 4.3.13

Surface roughness data from the ultrasonic slot milling of SiC/Al_2O_3 composite, main experimental programme, **Variable : Abrasive grit size**

Grit size	Run	Tool material		
		Mild steel	Stainless steel	Nimonic 80A
#120	1 (Δ Ra/μm)	4.070	2.875	4.648
	2 (Δ Ra/μm)	3.705	4.648	4.637
	Ave.	**3.888**	**3.762**	**4.642**
#220	1 (Δ Ra/μm)	3.679	3.135	0.725
	2 (Δ Ra/μm)	3.683	2.034	0.653
	Ave.	**3.681**	**2.584**	**0.689**
#320	1 (Δ Ra/μm)	0.819	2.248	0.955
	2 (Δ Ra/μm)	1.659	2.248	-0.203
	Ave.	**1.239**	**2.248**	**0.376**
#600	1 (Δ Ra/μm)	1.233	1.646	-1.134
	2 (Δ Ra/μm)	0.798	3.151	1.688
	Ave.	**1.016**	**2.398**	**0.277**

Table 25

Sections 4.3.12 & 4.3.14

Surface roughness data from the ultrasonic slot milling of SiC/Al_2O_3 composite, main experimental programme, **Variable : Tool rotation speed**

Rotation speed	Run	Tool material		
		Mild steel	Stainless steel	Nimonic 80A
0 r.p.m	1 (Δ Ra/μm)	4.070	2.875	3.809
	2 (Δ Ra/μm)	3.705	4.648	4.535
	Ave.	**3.888**	**3.762**	**4.172**
200 r.p.m.	1 (Δ Ra/μm)	7.774	2.354	5.023
	2 (Δ Ra/μm)	5.395	3.998	5.630
	Ave.	**6.584**	**3.176**	**5.327**
400 r.p.m.	1 (Δ Ra/μm)	4.881	5.239	2.466
	2 (Δ Ra/μm)	7.209	2.377	3.766
	Ave.	**6.045**	**3.808**	**3.116**
600 r.p.m.	1 (Δ Ra/μm)	4.663	2.226	3.424
	2 (Δ Ra/μm)	6.958	4.062	4.064
	Ave.	**5.811**	**3.144**	**3.744**
800 r.p.m.	1 (Δ Ra/μm)	5.373	4.286	3.558
	2 (Δ Ra/μm)	6.668	4.455	3.620
	Ave.	**6.020**	**4.370**	**3.589**

Table 26

Sections 4.3.12 & 4.3.15

Surface roughness data from the ultrasonic slot milling of SiC/Al_2O_3 composite, main experimental programme, **Variable : Static tool load**

Static load	Run	Tool material		
		Mild steel	Stainless steel	Nimonic 80A
0.5 kg	1 (Δ Ra/μm)	5.372	3.527	3.618
	2 (Δ Ra/μm)	4.577	2.424	4.139
	Ave.	**4.974**	**2.975**	**3.878**
1 kg	1 (Δ Ra/μm)	1.936	2.304	2.059
	2 (Δ Ra/μm)	4.784	3.694	2.639
	Ave.	**3.360**	**2.999**	**2.349**
2 kg	1 (Δ Ra/μm)	1.965	2.875	3.809
	2 (Δ Ra/μm)	4.959	4.648	4.535
	Ave.	**3.462**	**3.762**	**4.172**
3 kg	1 (Δ Ra/μm)	5.272	3.726	4.387
	2 (Δ Ra/μm)	3.285	4.739	4.006
	Ave.	**4.278**	**4.232**	**4.196**

Table 27

Sections 4.3.12 & 4.3.16

Surface roughness data from the ultrasonic slot milling of SiC/Al_2O_3 composite, main experimental programme, **Variable : Abrasive concentration**

Abrasive conc.	Run	Tool material		
		Mild steel	Stainless steel	Nimonic 80A
10% v/v	1 (Δ Ra/μm)	7.360	4.740	7.313
	2 (Δ Ra/μm)	3.436	2.541	7.426
	Ave.	**5.398**	**3.641**	**7.369**
20% v/v	1 (Δ Ra/μm)	3.888	4.381	5.218
	2 (Δ Ra/μm)	4.751	4.731	8.162
	Ave.	**4.320**	**5.446**	**6.690**
30% v/v	1 (Δ Ra/μm)	4.070	2.875	4.648
	2 (Δ Ra/μm)	3.705	4.648	4.637
	Ave.	**3.888**	**3.762**	**4.642**
40% v/v	1 (Δ Ra/μm)	2.672	4.907	5.230
	2 (Δ Ra/μm)	4.447	9.915	6.521
	Ave.	**3.560**	**7.411**	**5.876**

Table 28

Sections 4.3.17 & 4.3.18

Material removal rate data from the ultrasonic hole drilling of plate glass, main experimental programme, **Variable : Abrasive grit size**

Grit size	Run	Tool material		
		Mild steel	Stainless steel	Nimonic 80A
#120	1 (mm^3/sec)	1.024	0.285	0.833
	2 (mm^3/sec)	0.919	0.833	0.844
	Ave.	**0.972**	**0.559**	**0.859**
#220	1 (mm^3/sec)	0.706	0.339	0.525
	2 (mm^3/sec)	0.791	0.466	0.547
	Ave.	**0.749**	**0.403**	**0.536**
#320	1 (mm^3/sec)	0.730	0.403	0.491
	2 (mm^3/sec)	0.655	0.398	0.491
	Ave.	**0.693**	**0.401**	**0.491**
#600	1 (mm^3/sec)	0.426	0.096	0.143
	2 (mm^3/sec)	0.390	0.116	0.150
	Ave.	**0.408**	**0.106**	**0.147**

Table 29

Sections 4.3.17 & 4.3.19

Material removal rate data from the ultrasonic hole drilling of plate glass, main experimental programme, **Variable : Tool rotation speed**

Rotation speed	Run	Tool material		
		Mild steel	Stainless steel	Nimonic 80A
0 r.p.m	1 (mm^3/sec)	0.732	0.754	0.833
	2 (mm^3/sec)	0.919	1.581	0.972
	Ave.	**0.826**	**1.168**	**0.903**
200 r.p.m.	1 (mm^3/sec)	0.830	2.188	1.228
	2 (mm^3/sec)	0.805	2.154	1.196
	Ave.	**0.181**	**2.171**	**1.212**
400 r.p.m.	1 (mm^3/sec)	0.950	1.702	0.885
	2 (mm^3/sec)	0.864	1.812	1.052
	Ave.	**0.907**	**1.757**	**0.969**
600 r.p.m.	1 (mm^3/sec)	0.989	1.591	0.989
	2 (mm^3/sec)	1.222	1.429	1.222
	Ave.	**1.106**	**1.510**	**1.106**
800 r.p.m.	1 (mm^3/sec)	0.944	1.206	0.949
	2 (mm^3/sec)	1.092	1.383	0.946
	Ave.	**1.018**	**1.295**	**0.948**

Table 30

Sections 4.3.17 & 4.3.20

Material removal rate data from the ultrasonic hole drilling of plate glass, main experimental programme, **Variable : Static tool load**

Static load	Run	Tool material		
		Mild steel	Stainless steel	Nimonic 80A
0.5 kg	1 (mm^3/sec)	0.674	0.204	0.636
	2 (mm^3/sec)	0.737	0.180	0.612
	Ave.	**0.706**	**0.192**	**0.624**
1 kg	1 (mm^3/sec)	0.819	0.191	0.817
	2 (mm^3/sec)	0.861	0.164	0.760
	Ave.	**0.840**	**0.178**	**0.789**
2 kg	1 (mm^3/sec)	1.024	0.356	0.833
	2 (mm^3/sec)	0.919	0.833	0.972
	Ave.	**0.972**	**0.595**	**0.903**
3 kg	1 (mm^3/sec)	0.880	0.668	0.761
	2 (mm^3/sec)	0.737	0.558	0.749
	Ave.	**0.809**	**0.613**	**0.755**

Table 31

Sections 4.3.22 & 4.3.23

Material removal rate data from the ultrasonic slot milling of plate glass, main experimental programme, **Variable : Abrasive grit size**

Grit size	Run	Tool material		
		Mild steel	Stainless steel	Nimonic 80A
#120	1 (mm^3/sec)	0.722	2.457	0.681
	2 (mm^3/sec)	0.838	1.499	0.717
	Ave.	**0.780**	**1.978**	**0.699**
#220	1 (mm^3/sec)	0.978	0.545	0.380
	2 (mm^3/sec)	0.929	0.582	0.355
	Ave.	**0.954**	**0.564**	**0.368**
#320	1 (mm^3/sec)	0.583	0.487	0.417
	2 (mm^3/sec)	0.593	0.440	0.444
	Ave.	**0.588**	**0.464**	**0.431**
#600	1 (mm^3/sec)	0.206	0.165	0.318
	2 (mm^3/sec)	0.167	0.151	0.324
	Ave.	**0.187**	**0.158**	**0.321**

Table 32

Sections 4.3.22 & 4.3.24

Material removal rate data from the ultrasonic slot milling of plate glass, main experimental programme, **Variable : Tool rotation speed**

Rotation speed	Run	Tool material		
		Mild steel	Stainless steel	Nimonic 80A
0 r.p.m	1 (mm^3/sec)	0.722	2.457	0.681
	2 (mm^3/sec)	0.838	1.499	0.717
	Ave.	**0.780**	**1.978**	**0.699**
200 r.p.m.	1 (mm^3/sec)	0.676	0.947	0.902
	2 (mm^3/sec)	0.697	0.900	0.941
	Ave.	**0.687**	**0.924**	**0.922**
400 r.p.m.	1 (mm^3/sec)	0.993	0.951	0.772
	2 (mm^3/sec)	0.747	0.577	0.761
	Ave.	**0.870**	**0.764**	**0.767**
600 r.p.m.	1 (mm^3/sec)	0.822	0.596	0.700
	2 (mm^3/sec)	0.775	0.834	0.768
	Ave.	**0.799**	**0.715**	**0.734**
800 r.p.m.	1 (mm^3/sec)	0.829	0.746	0.916
	2 (mm^3/sec)	0.939	0.737	0.754
	Ave.	**0.884**	**0.742**	**0.835**

Table 33

Sections 4.3.22 & 4.3.25

Material removal rate data from the ultrasonic slot milling of plate glass, main experimental programme, **Variable : Static tool load**

Static load	Run	Tool material		
		Mild steel	Stainless steel	Nimonic 80A
0.5 kg	1 (mm^3/sec)	0.374	0.836	1.076
	2 (mm^3/sec)	0.803	0.650	0.955
	Ave.	**0.589**	**0.743**	**1.016**
1 kg	1 (mm^3/sec)	0.810	1.177	0.950
	2 (mm^3/sec)	0.608	1.058	0.708
	Ave.	**0.709**	**1.118**	**0.829**
2 kg	1 (mm^3/sec)	0.722	1.327	0.681
	2 (mm^3/sec)	0.838	1.499	0.717
	Ave.	**0.780**	**1.413**	**0.699**
3 kg	1 (mm^3/sec)	1.128	0.725	1.074
	2 (mm^3/sec)	0.942	0.787	0.901
	Ave.	**1.035**	**0.756**	**0.988**

Table 34

Sections 4.3.22 & 4.3.26

Material removal rate data from the ultrasonic slot milling of plate glass, main experimental programme, **Variable : Abrasive concentration**

Abrasive conc.	Run	Tool material		
		Mild steel	Stainless steel	Nimonic 80A
10% v/v	1 (mm^3/sec)	1.205	1.069	0.793
	2 (mm^3/sec)	1.062	0.749	0.948
	Ave.	**1.134**	**0.909**	**0.871**
20% v/v	1 (mm^3/sec)	1.419	1.534	1.090
	2 (mm^3/sec)	1.295	1.371	1.001
	Ave.	**1.357**	**1.453**	**1.046**
30% v/v	1 (mm^3/sec)	2.457	0.722	0.681
	2 (mm^3/sec)	1.499	0.838	0.717
	Ave.	**1.978**	**0.780**	**0.699**
40% v/v	1 (mm^3/sec)	1.230	1.084	1.565
	2 (mm^3/sec)	1.295	1.576	1.213
	Ave.	**1.236**	**1.330**	**1.389**

Table 35

Sections 4.3.28 & 4.3.29

Surface roughness data from the ultrasonic slot milling of plate glass, main experimental programme, **Variable : Abrasive grit size**

Grit size	Run	Tool material		
		Mild steel	Stainless steel	Nimonic 80A
#120	1 (Δ Ra/μm)	6.084	7.699	5.667
	2 (Δ Ra/μm)	5.232	7.857	5.797
	Ave.	**5.658**	**7.778**	**5.732**
#220	1 (Δ Ra/μm)	5.072	4.434	5.575
	2 (Δ Ra/μm)	5.018	4.648	5.656
	Ave.	**5.045**	**4.541**	**5.615**
#320	1 (Δ Ra/μm)	1.899	3.030	3.132
	2 (Δ Ra/μm)	3.139	3.628	3.048
	Ave.	**2.519**	**3.329**	**3.090**
#600	1 (Δ Ra/μm)	1.160	1.092	1.885
	2 (Δ Ra/μm)	1.160	1.270	6.234
	Ave.	**1.160**	**1.181**	**4.059**

Table 36

Sections 4.3.28 & 4.3.30

Surface roughness data from the ultrasonic slot milling of plate glass, main experimental programme, **Variable : Tool rotation speed**

Rotation speed	Run	Tool material		
		Mild steel	Stainless steel	Nimonic 80A
0 r.p.m	1 (Δ Ra/μm)	6.084	7.699	5.667
	2 (Δ Ra/μm)	5.232	7.857	5.797
	Ave.	**5.658**	**7.778**	**5.732**
200 r.p.m.	1 (Δ Ra/μm)	6.832	6.814	7.777
	2 (Δ Ra/μm)	6.759	6.497	5.442
	Ave.	**6.796**	**6.656**	**6.609**
400 r.p.m.	1 (Δ Ra/μm)	6.549	6.663	6.473
	2 (Δ Ra/μm)	6.119	6.719	5.907
	Ave.	**6.334**	**6.691**	**6.190**
600 r.p.m.	1 (Δ Ra/μm)	6.598	5.946	5.605
	2 (Δ Ra/μm)	6.455	6.438	5.466
	Ave.	**6.526**	**6.192**	**5.536**
800 r.p.m.	1 (Δ Ra/μm)	5.695	5.933	5.844
	2 (Δ Ra/μm)	5.470	5.933	7.698
	Ave.	**5.583**	**5.933**	**6.771**

Table 37

Sections 4.3.28 & 4.3.31

Surface roughness data from the ultrasonic slot milling of plate glass, main experimental programme, **Variable : Static tool load.**

Static load	Run	Tool material		
		Mild steel	Stainless steel	Nimonic 80A
0.5 kg	1 (Δ Ra/μm)	5.757	6.017	7.493
	2 (Δ Ra/μm)	6.593	5.453	5.710
	Ave.	**6.175**	**5.735**	**6.601**
1 kg	1 (Δ Ra/μm)	6.234	6.069	5.809
	2 (Δ Ra/μm)	6.222	7.756	7.383
	Ave.	**6.228**	**6.912**	**6.596**
2 kg	1 (Δ Ra/μm)	6.084	7.699	5.667
	2 (Δ Ra/μm)	5.232	7.857	5.797
	Ave.	**5.658**	**7.778**	**5.732**
3 kg	1 (Δ Ra/μm)	6.362	6.083	5.835
	2 (Δ Ra/μm)	6.362	6.117	5.920
	Ave.	**6.362**	**6.100**	**5.878**

Table 38

Sections 4.3.28 & 4.3.32

Surface roughness data from the ultrasonic slot milling of plate glass, main experimental programme, **Variable : Abrasive concentration**

Abrasive conc.	Run	Tool material		
		Mild steel	Stainless steel	Nimonic 80A
10% v/v	1 (Δ Ra/μm)	6.812	7.899	6.456
	2 (Δ Ra/μm)	5.394	6.901	6.666
	Ave.	**6.103**	**7.400**	**6.561**
20% v/v	1 (Δ Ra/μm)	6.282	5.546	8.238
	2 (Δ Ra/μm)	6.436	6.299	6.612
	Ave.	**6.359**	**5.922**	**7.425**
30% v/v	1 (Δ Ra/μm)	7.699	6.084	5.667
	2 (Δ Ra/μm)	7.857	5.232	5.797
	Ave.	**7.778**	**5.658**	**5.732**
40% v/v	1 (Δ Ra/μm)	6.743	5.471	7.136
	2 (Δ Ra/μm)	6.436	4.705	8.234
	Ave.	**6.589**	**5.088**	**7.685**

Table 39

Section 5.5.1

Comparison of average material removal rates for the ultrasonic hole drilling of plate glass and SiC/Al_2O_3 composite

		Material removal rate (mm^3/sec)		
		SiC/Al_2O_3	Plate glass	Ratio of m.r.r.'s
Variable	Abrasive size	0.227	0.527	2.32 : 1
	Static tool load	0.332	0.664	2 : 1
	Tool rotation speed	0.750	1.181	1.57 : 1
		Average 0.436	Average 0.790	Average 1.81 : 1

Table 40

Section 5.5

Comparison of material properties of plate glass and SiC/Al_2O_3 composite.

	SiC/Al_2O_3	Plate glass
Young's modulus (GPa)	1,2 125 1,3 190	69
Poisson's ratio	1,2 0.22 1,3 0.19	-
Fracture toughness (MPa$\sqrt{m}$)	2.8	0.7
Tensile strength (MPa)	225	50

Figure 1
Diagram of standard ultrasonic machine
Section 3.2.1

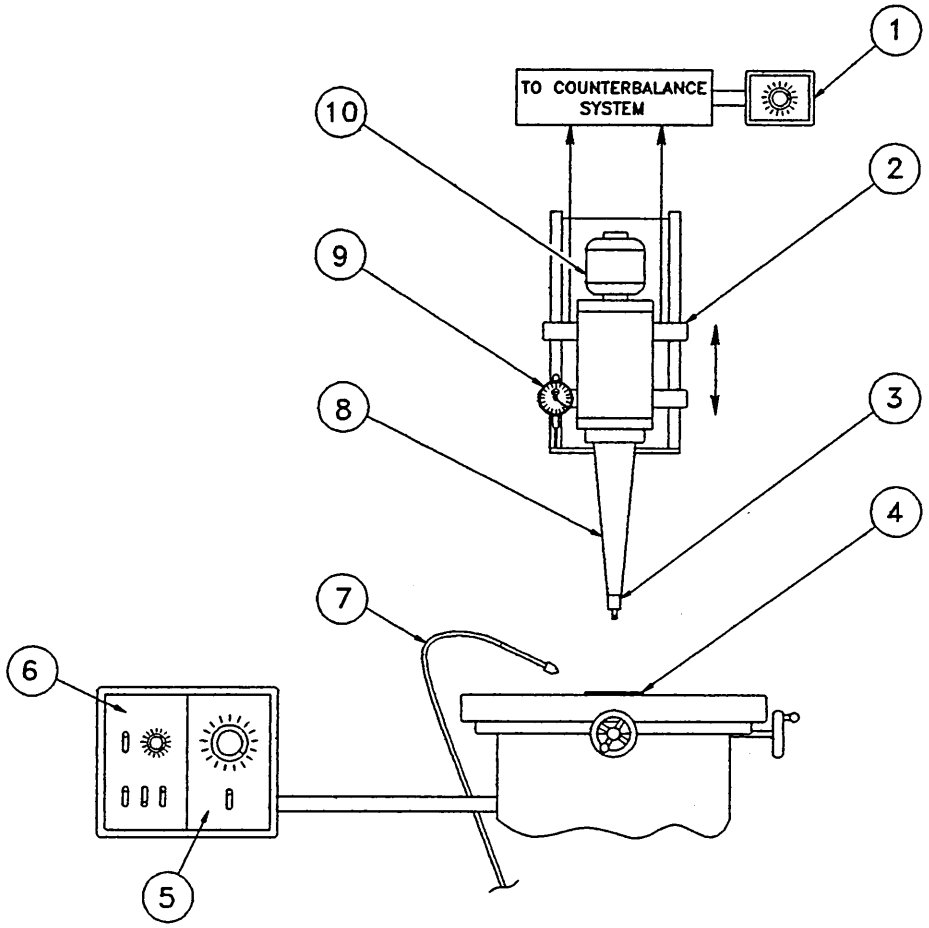

COMPONENTS			
1	STATIC LOAD VALVE	6	ACOUSTIC SYSTEM CONTROLLER
2	LINEAR BEARINGS	7	COOLANT JET
3	DIAMOND ENCRUSTED TOOL	8	SONOTRODE
4	WORKPIECE	9	DIAL TEST INDICATOR
5	ROTATION SPEED CONTROLLER	10	TOOL ROTATION MOTOR

Figure 2
Diagram of modified ultrasonic machine
. Sections 3.2.2 & 3.7.1

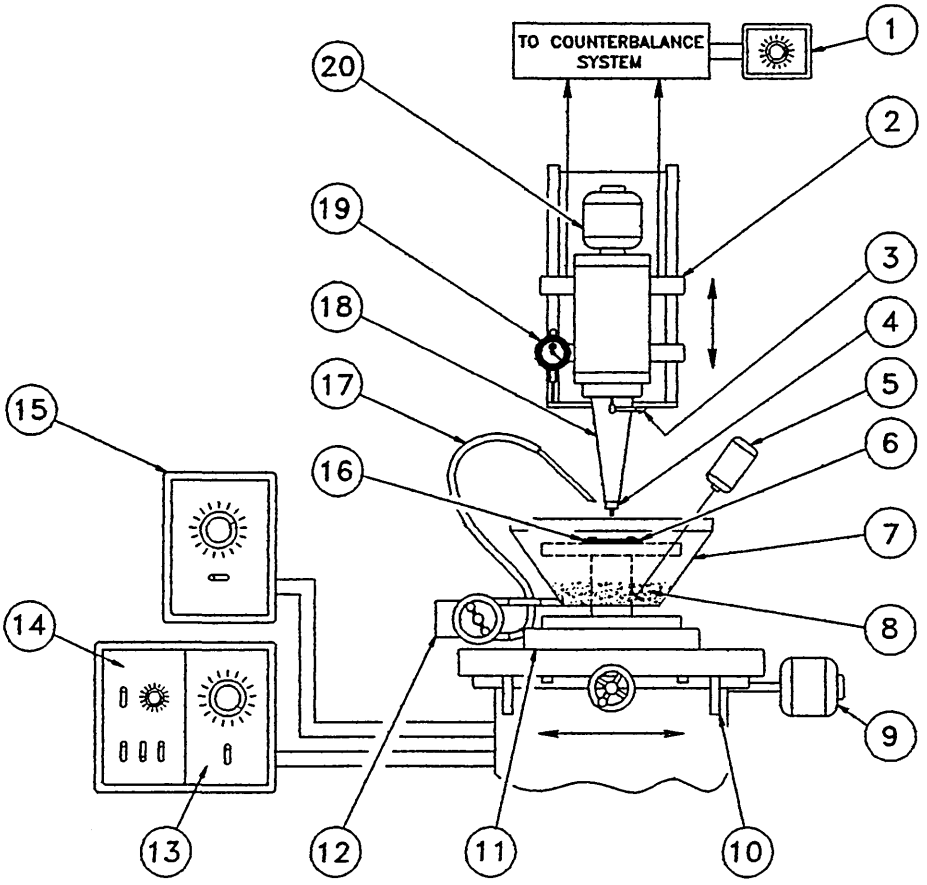

COMPONENTS			
1	STATIC LOAD VALVE	11	LOAD CELL
2	LINEAR BEARINGS	12	PERISTALTIC PUMP
3	AMPLITUDE TRANSDUCER	13	ROTATION SPEED CONTROLLER
4	TOOL TIP	14	ACOUSTIC SYSTEM CONTROLLER
5	SLURRY STIRRER	15	TRAVERSE SPEED CONTROLLER
6	WORKPIECE CLAMPS	16	WORKPIECE
7	SLURRY HOPPER	17	SLURRY DELIVERY TUBE
8	ABRASIVE SLURRY	18	SONOTRODE
9	TRAVERSE MOTOR	19	DIAL TEST INDICATOR
10	LIMIT SWITCHES	20	TOOL ROTATION MOTOR

Figure 3
Drawings of replacement sonotrode & tool tips
Sections 3.2.2 & 3.7.4

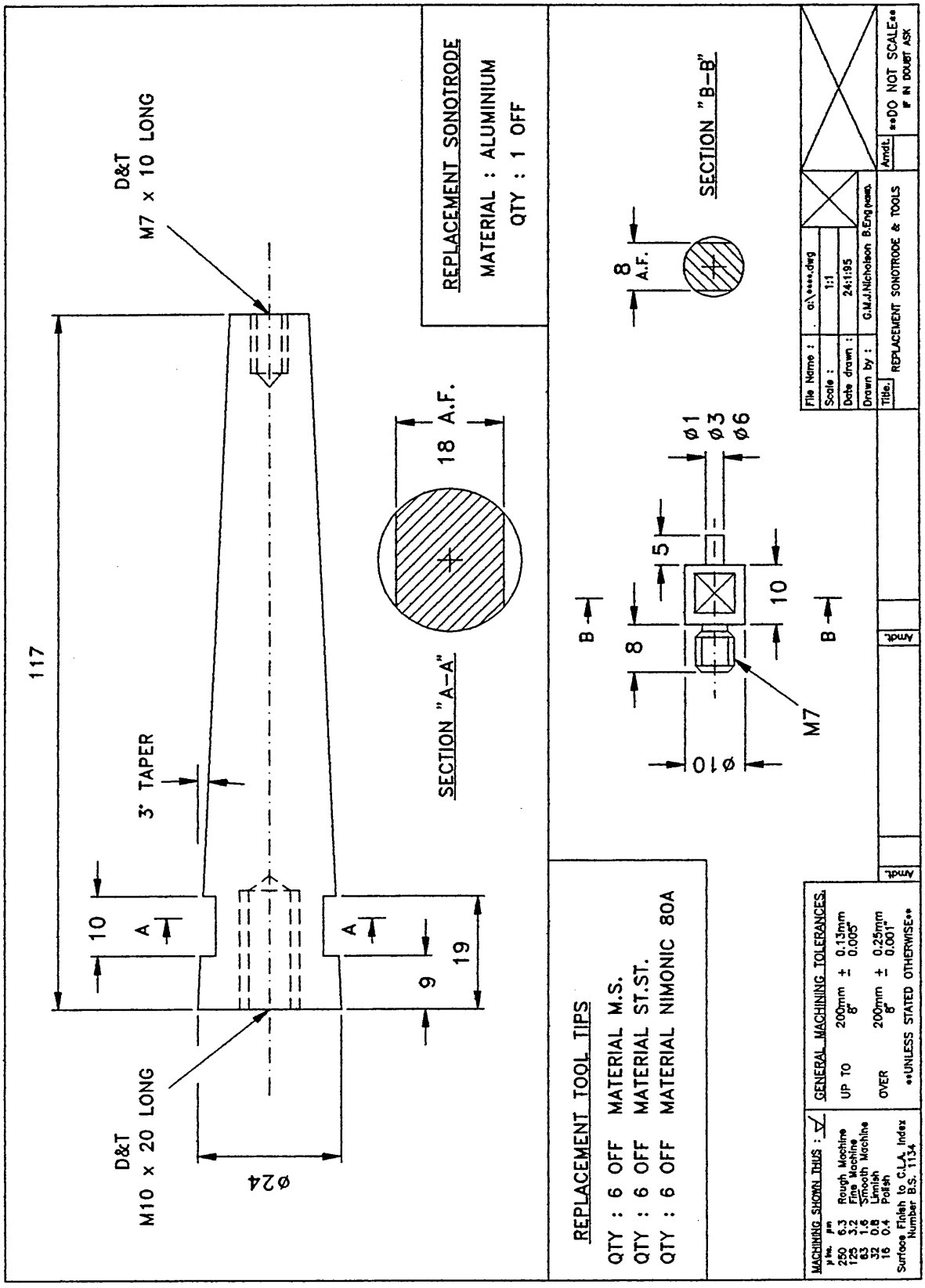

Figure 4
Drawing of slurry hopper
Section 3.2.2

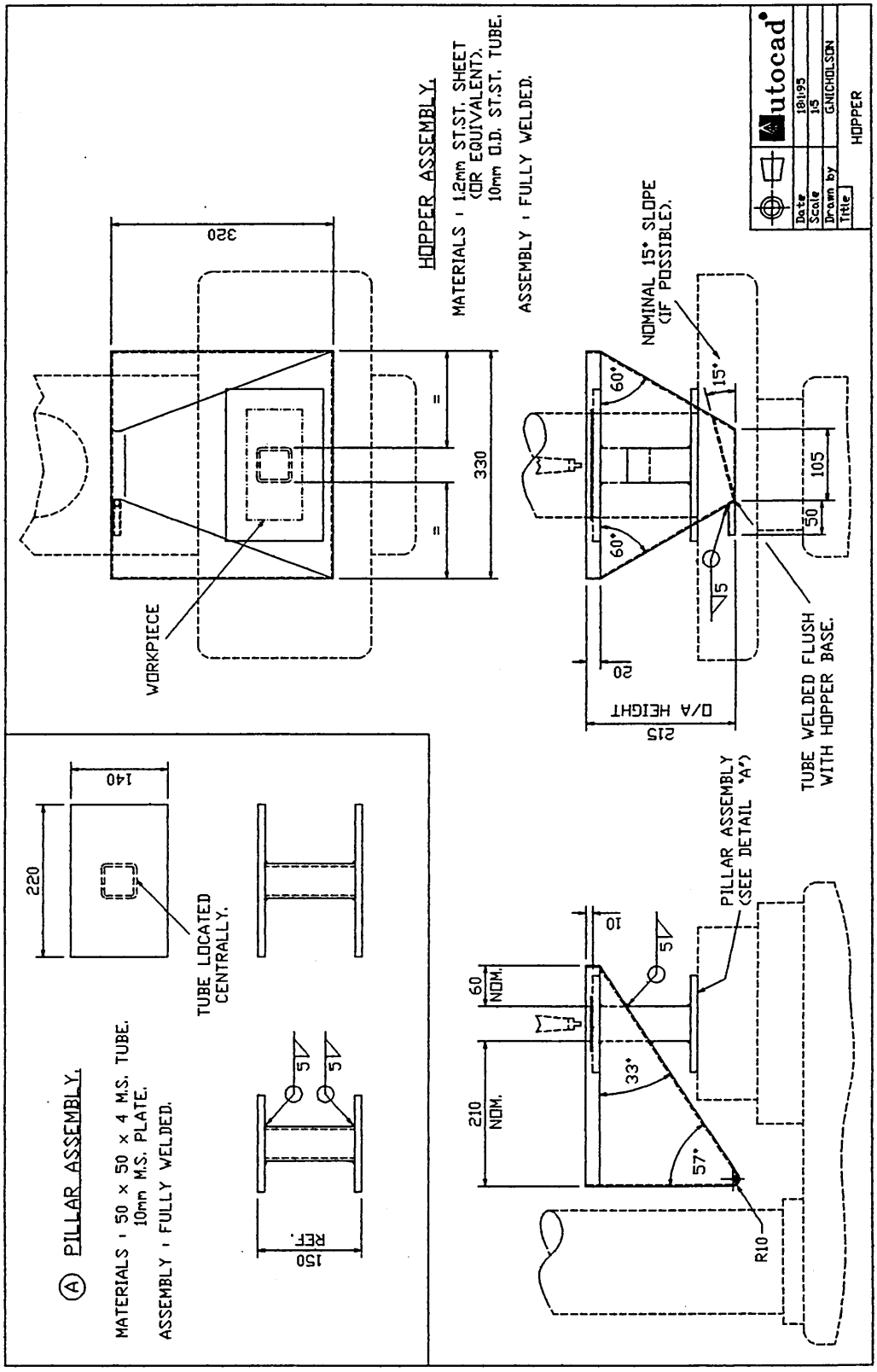

Figure 5
Calibration chart for static tool load valve
Section 3.2.2

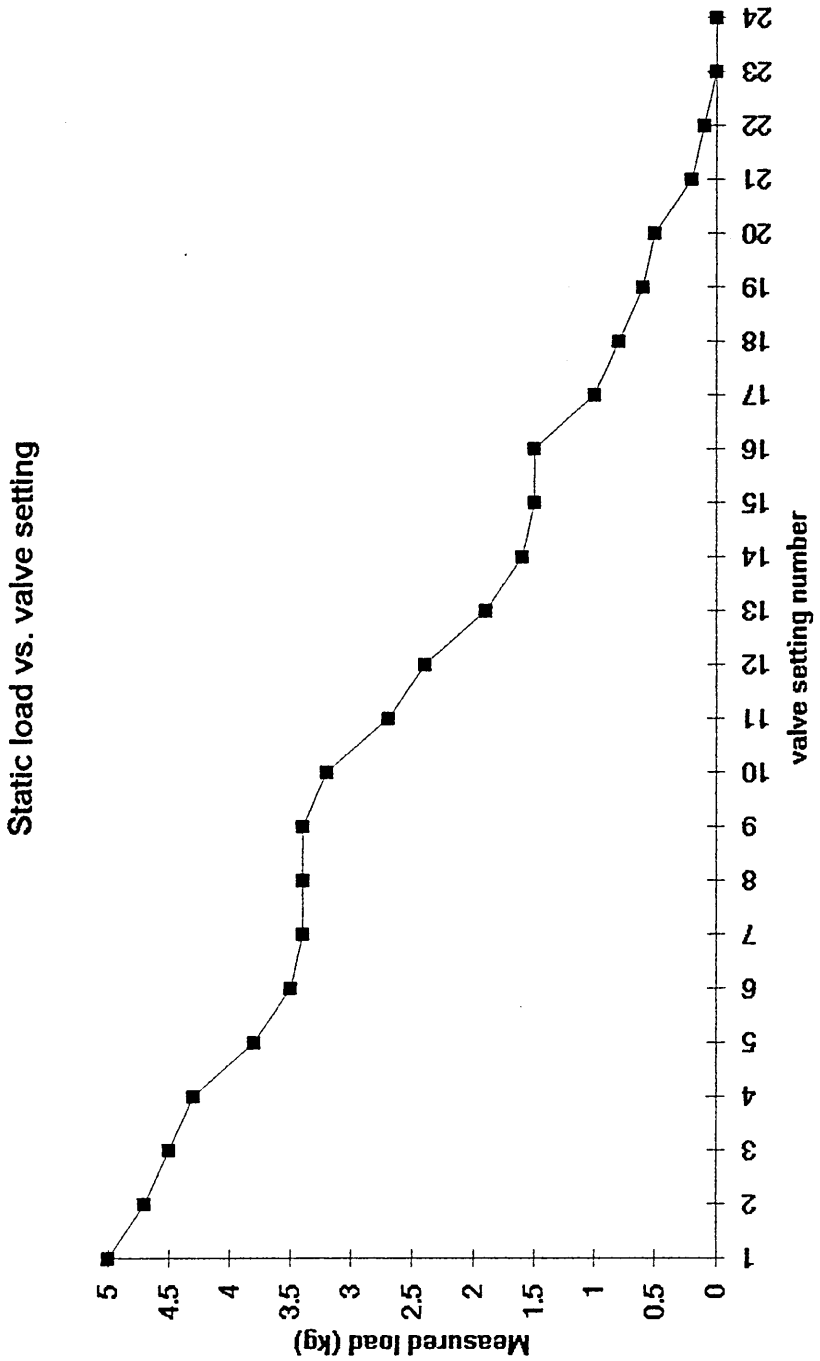

Figure 6
Calibration chart for amplitude transducer (slope ≡ 2.14 mV/micron)
Sections 3.2.2 & 3.7.9

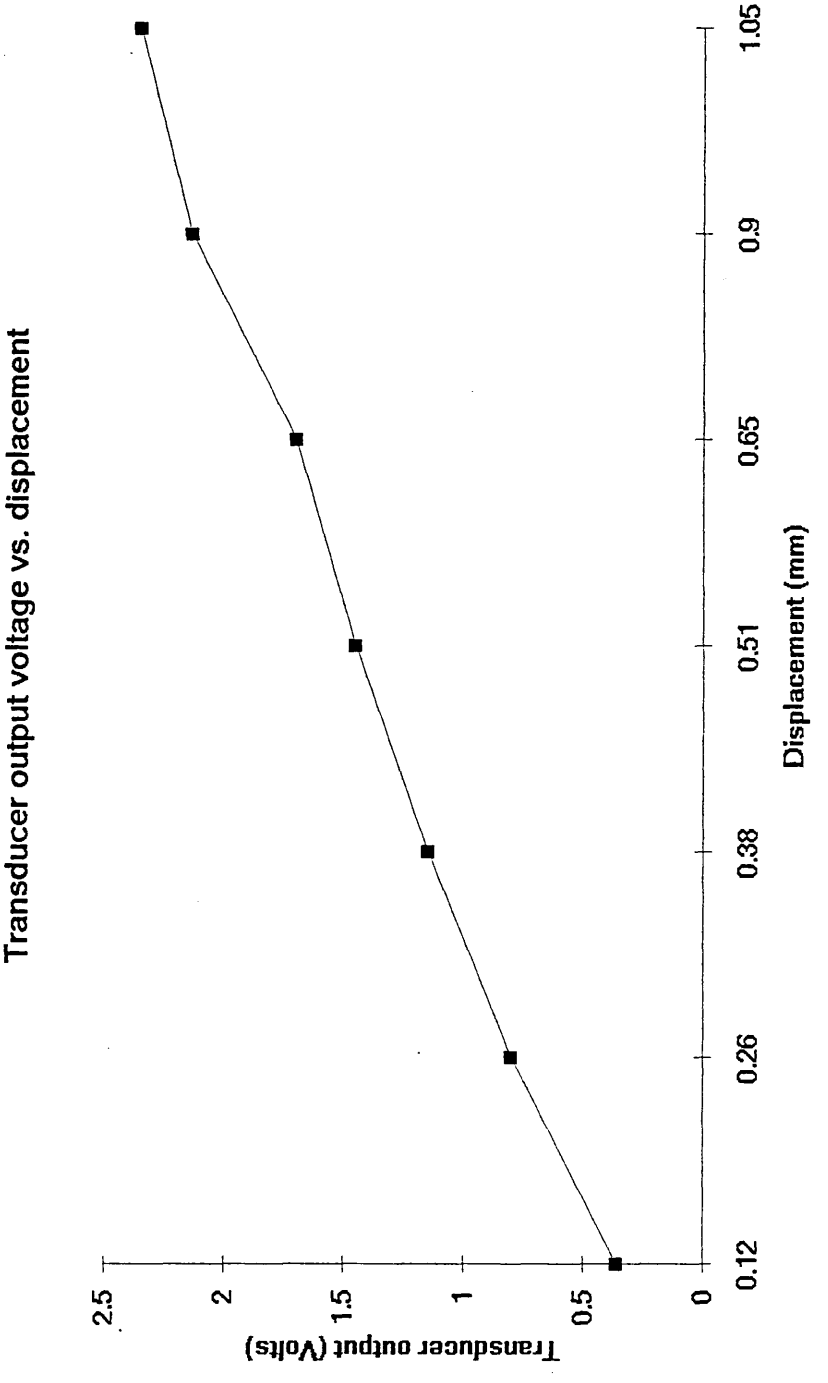

Figure 7
Calibration chart for traverse speed controller
Section 3.2.2

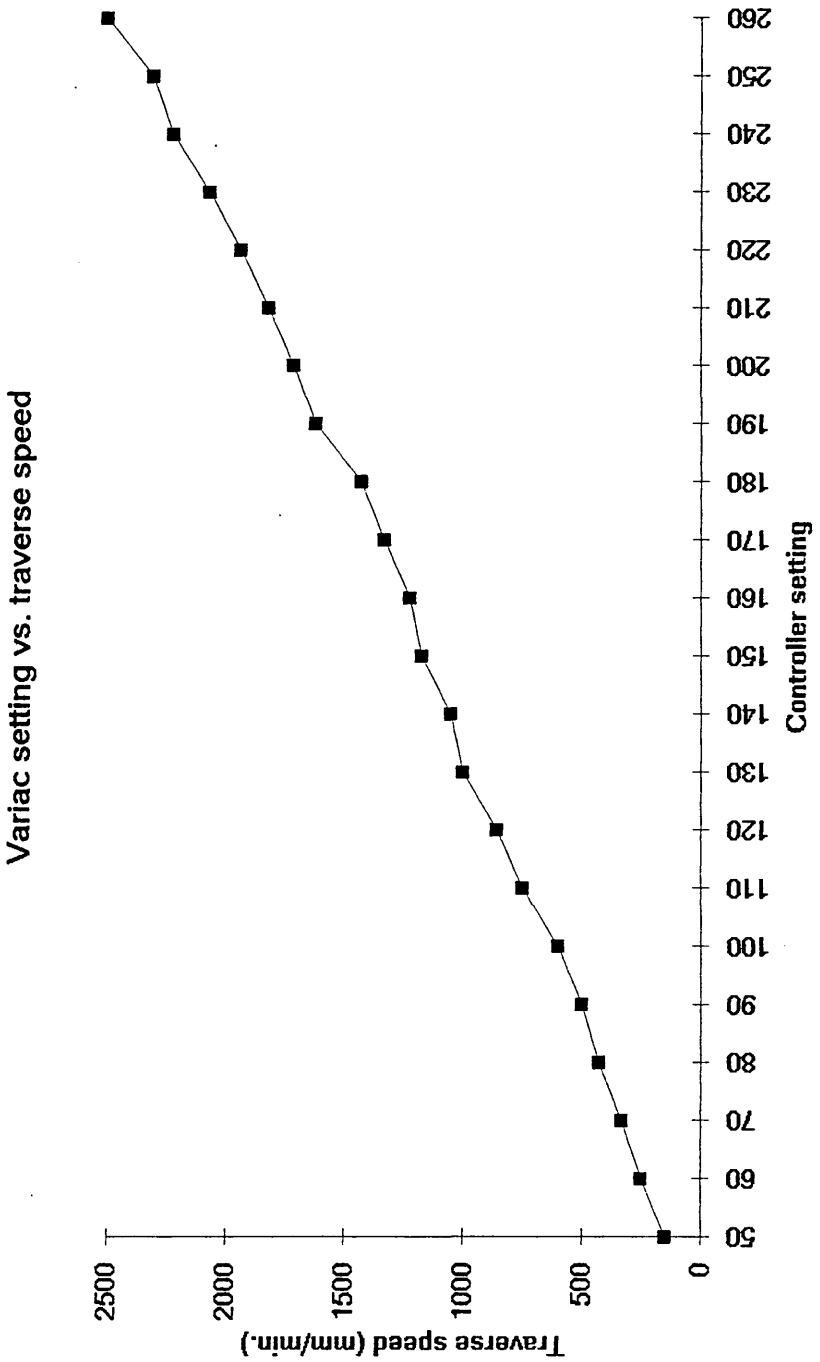

Figure 8
Calibration chart for tool rotation speed controller
Section 3.2.2

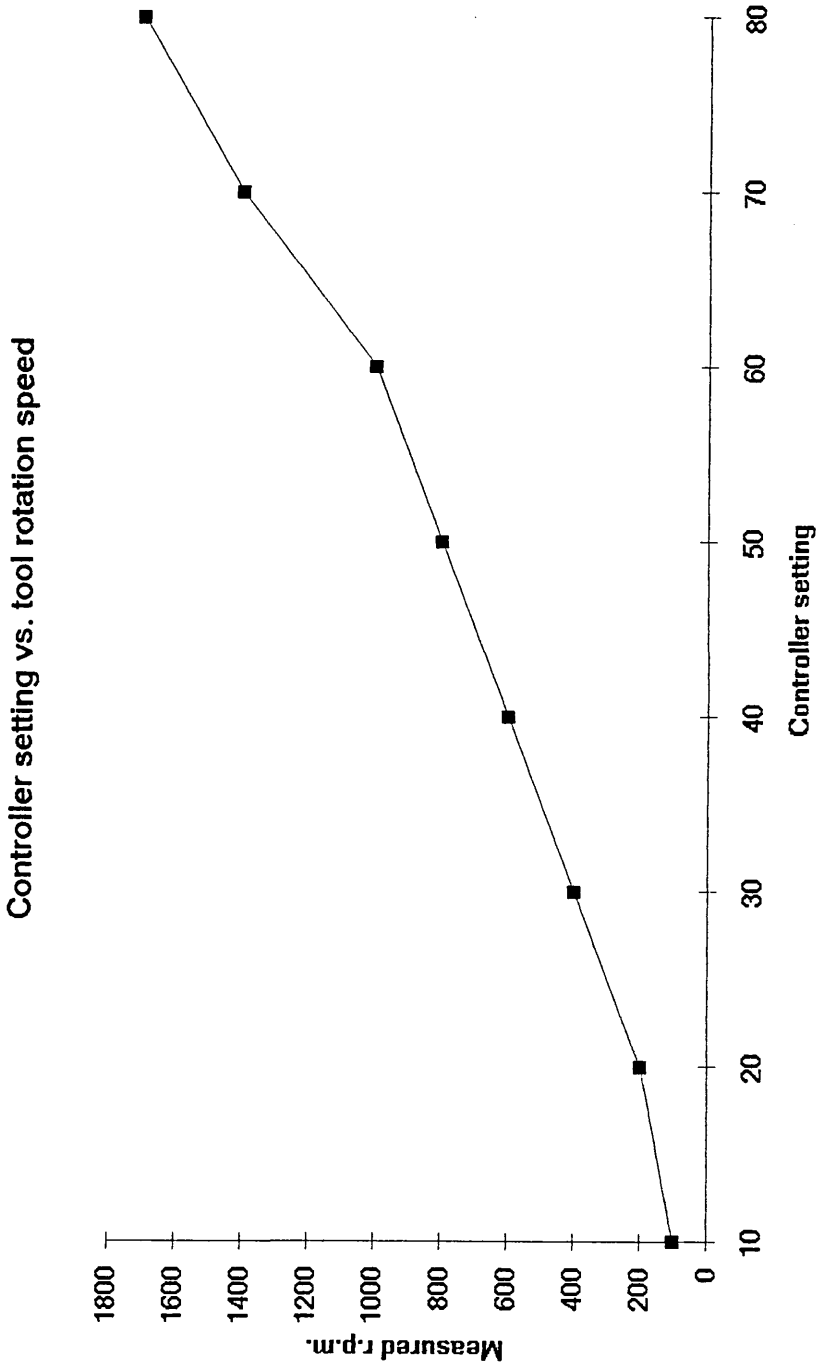

Figure 9
Summary of Taguchi results for composite hole drilling
Sections 4.2.6 & 5.3.1

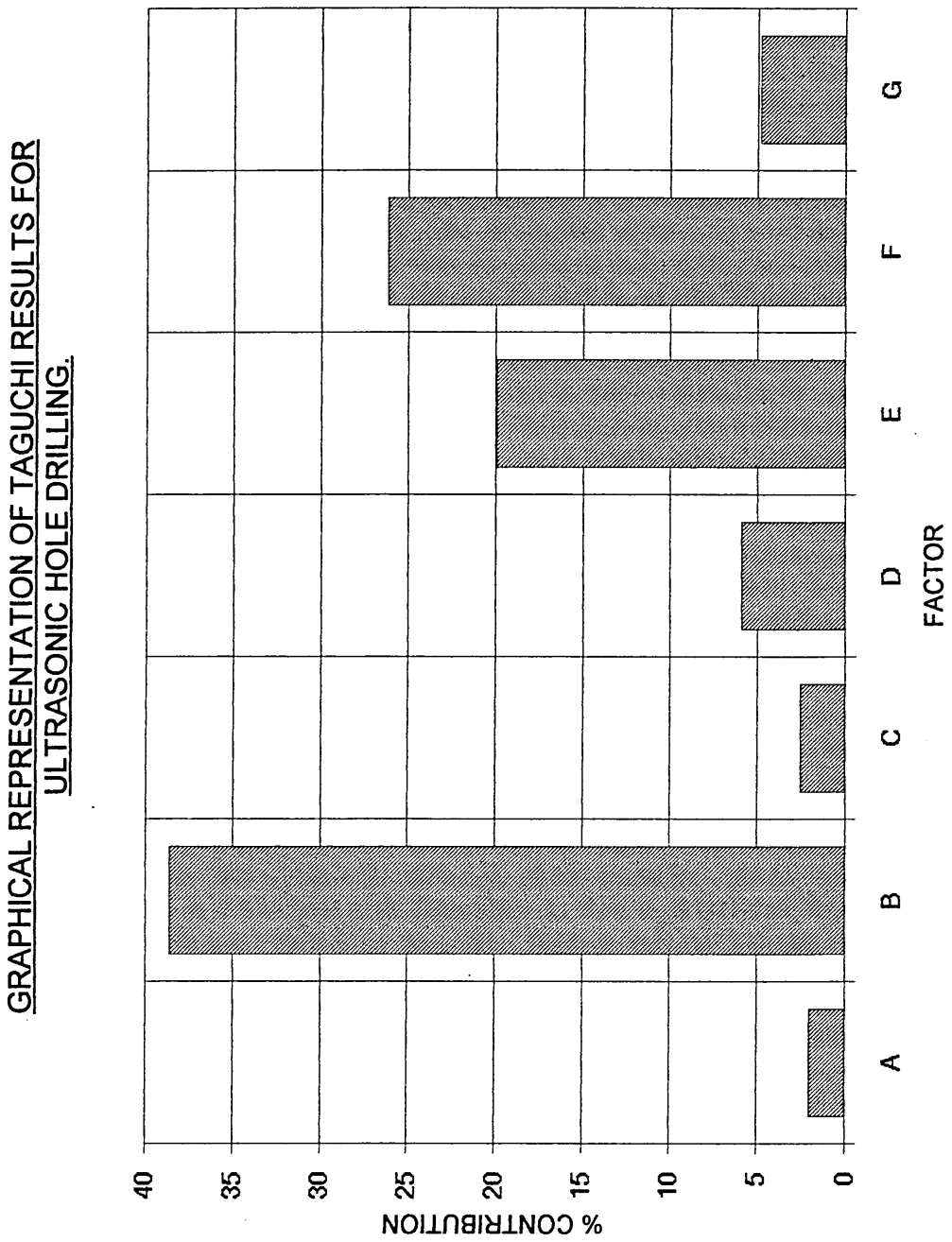

Figure 10
Summary of Taguchi results for composite slot milling
Sections 4.2.7 & 5.3.1

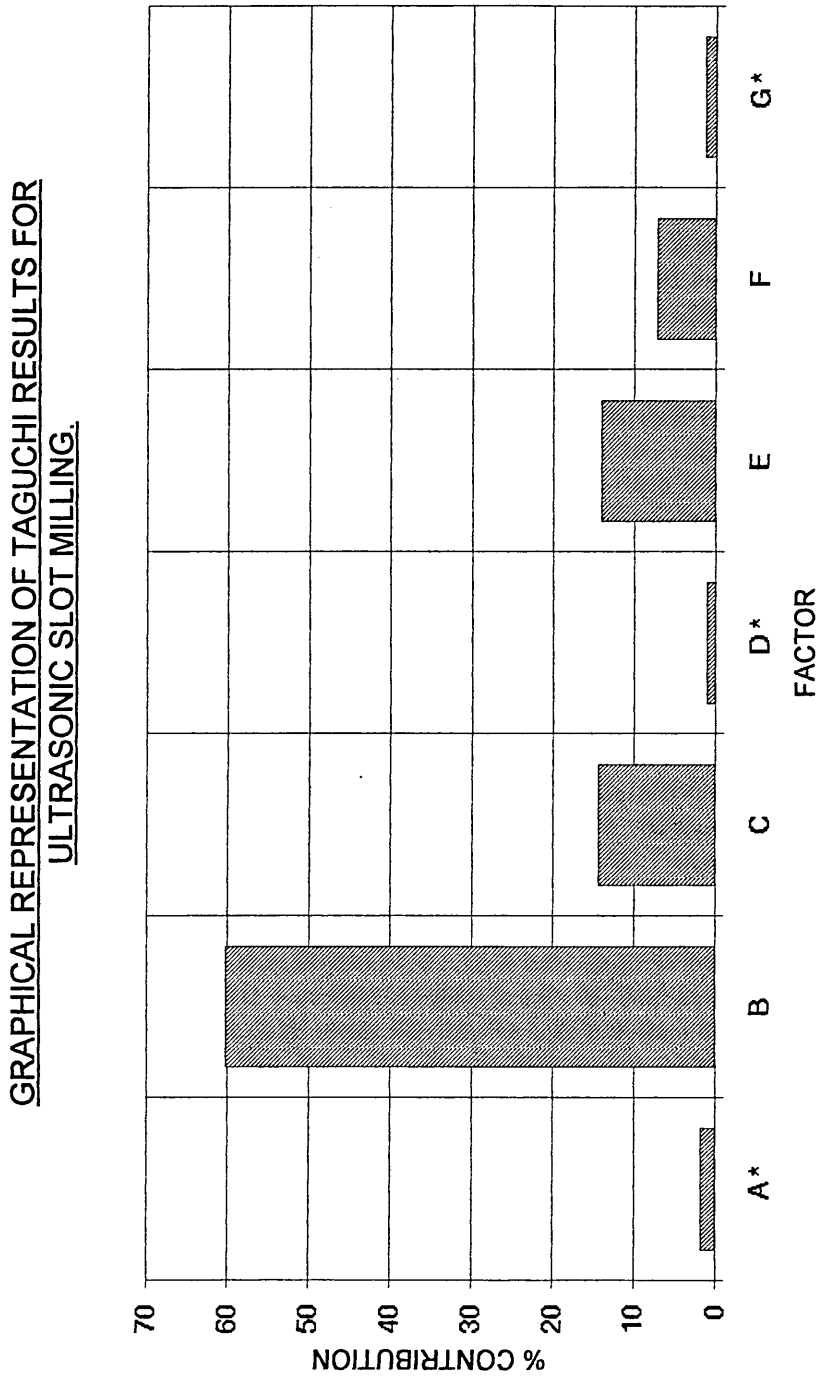

Figure 11
Sections 4.3.1 & 4.3.2

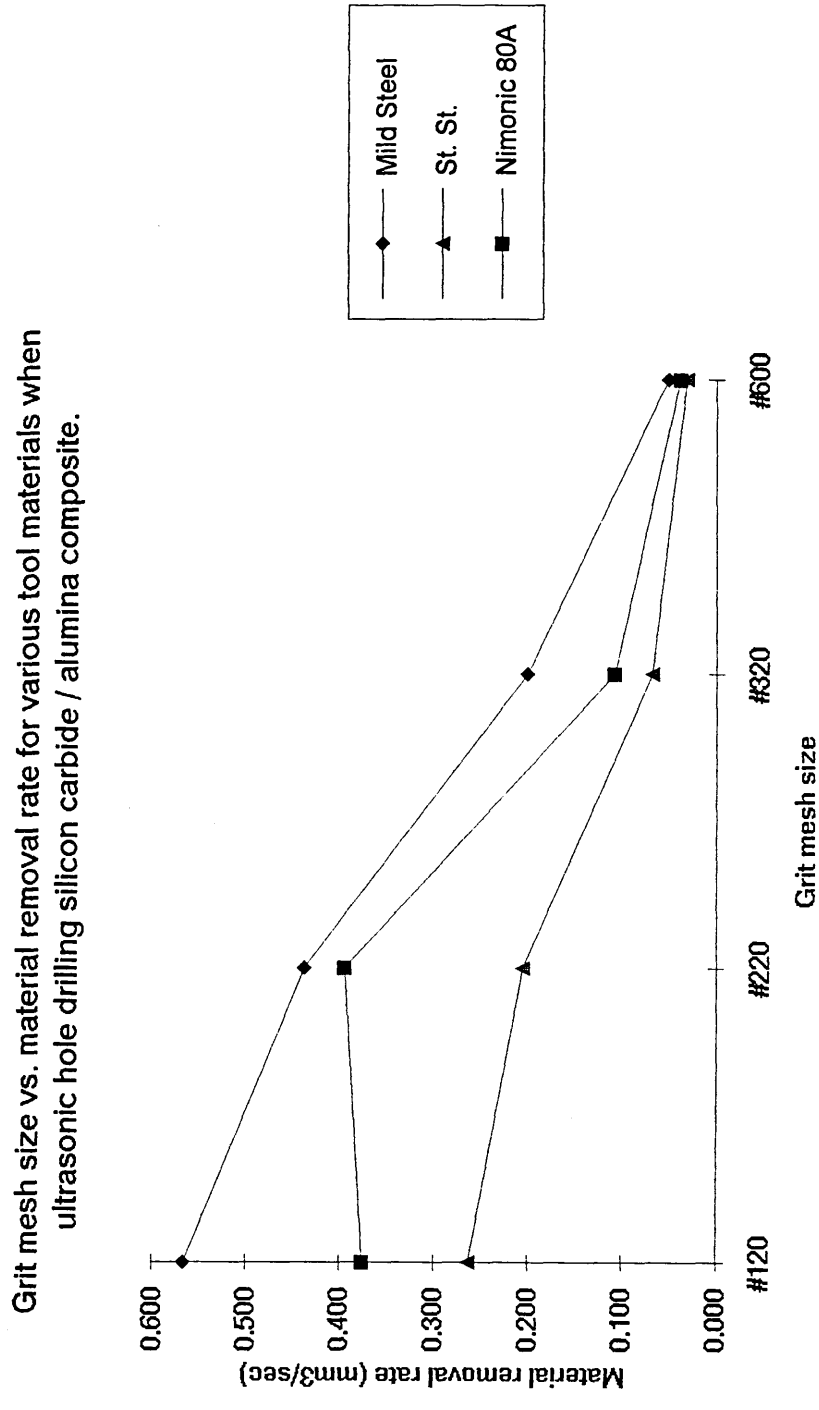

Figure 12
Sections 4.3.1 & 4.3.3

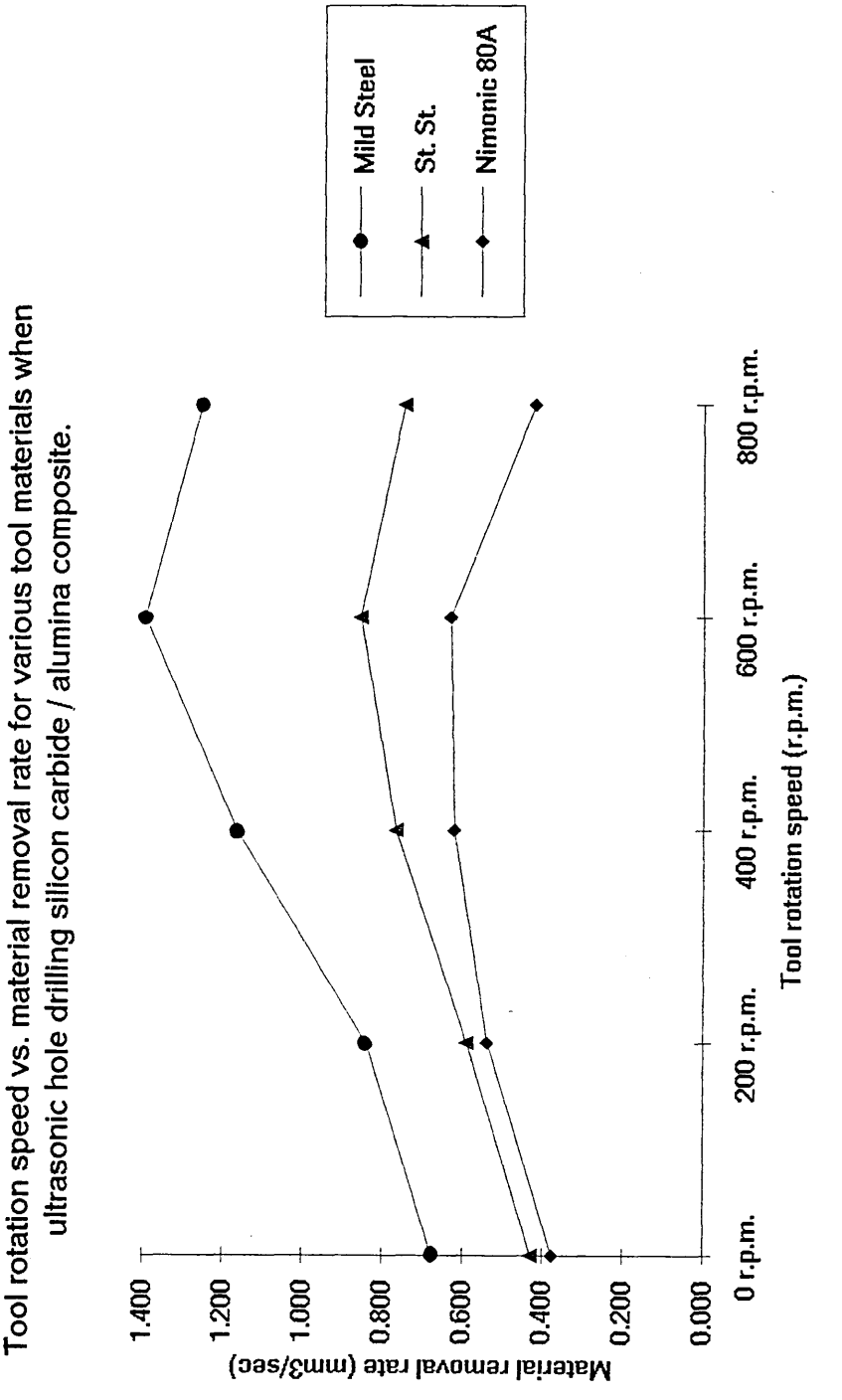

Figure 13
Sections 4.3.1 & 4.3.4

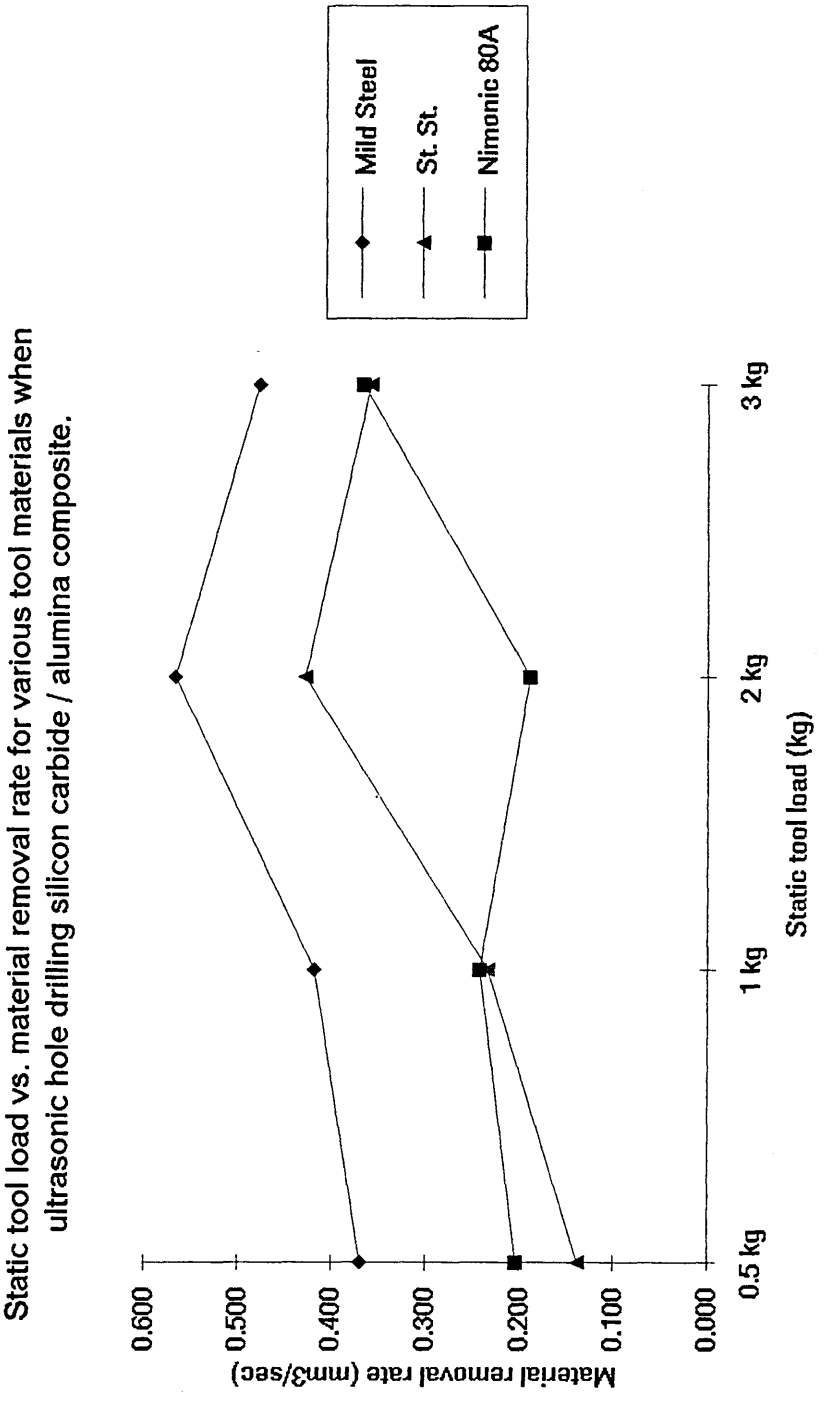

Figure 14
Sections 4.3.5

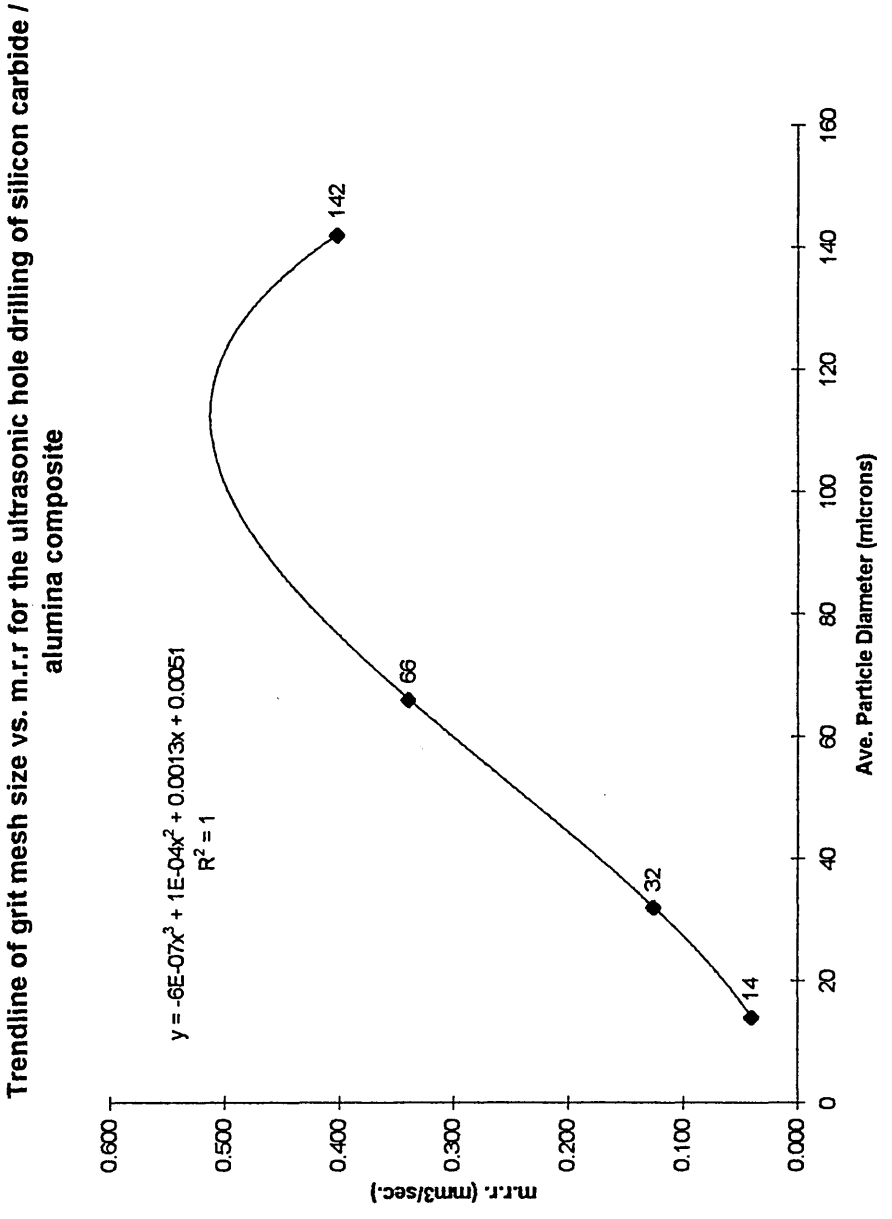

Figure 15
Sections 4.3.5

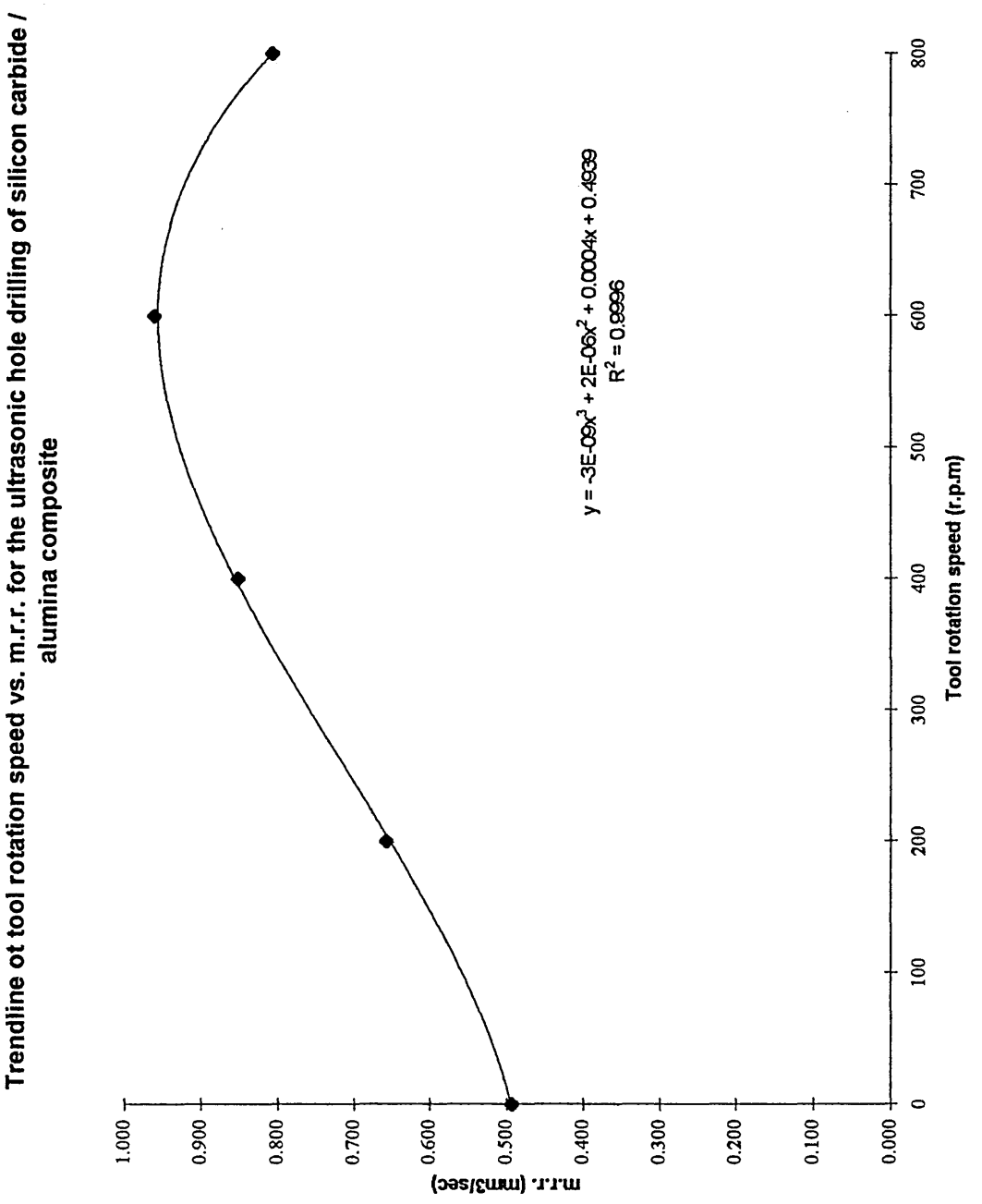

Figure 16
Sections 4.3.5

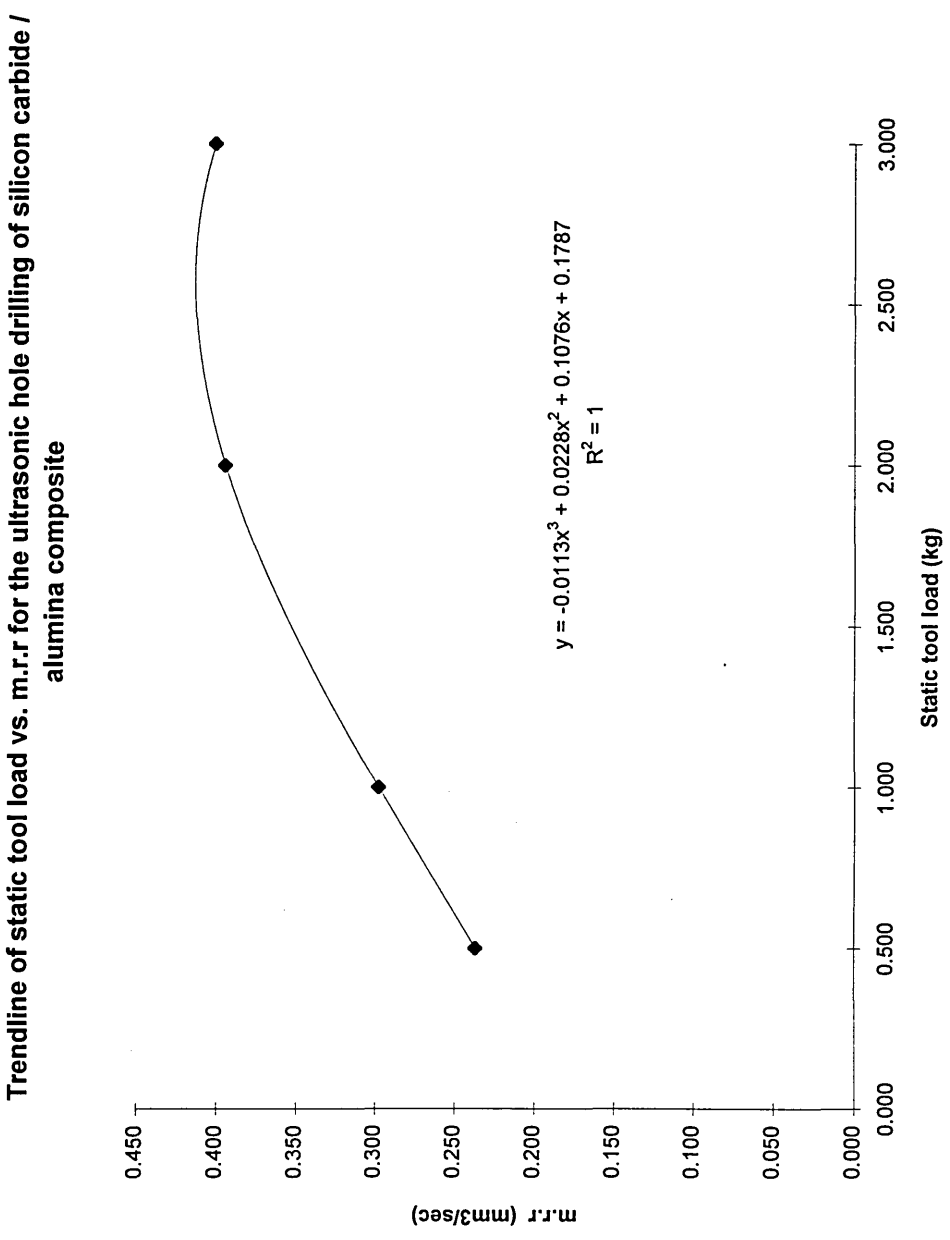

Figure 17
Sections 4.3.6 & 4.3.7

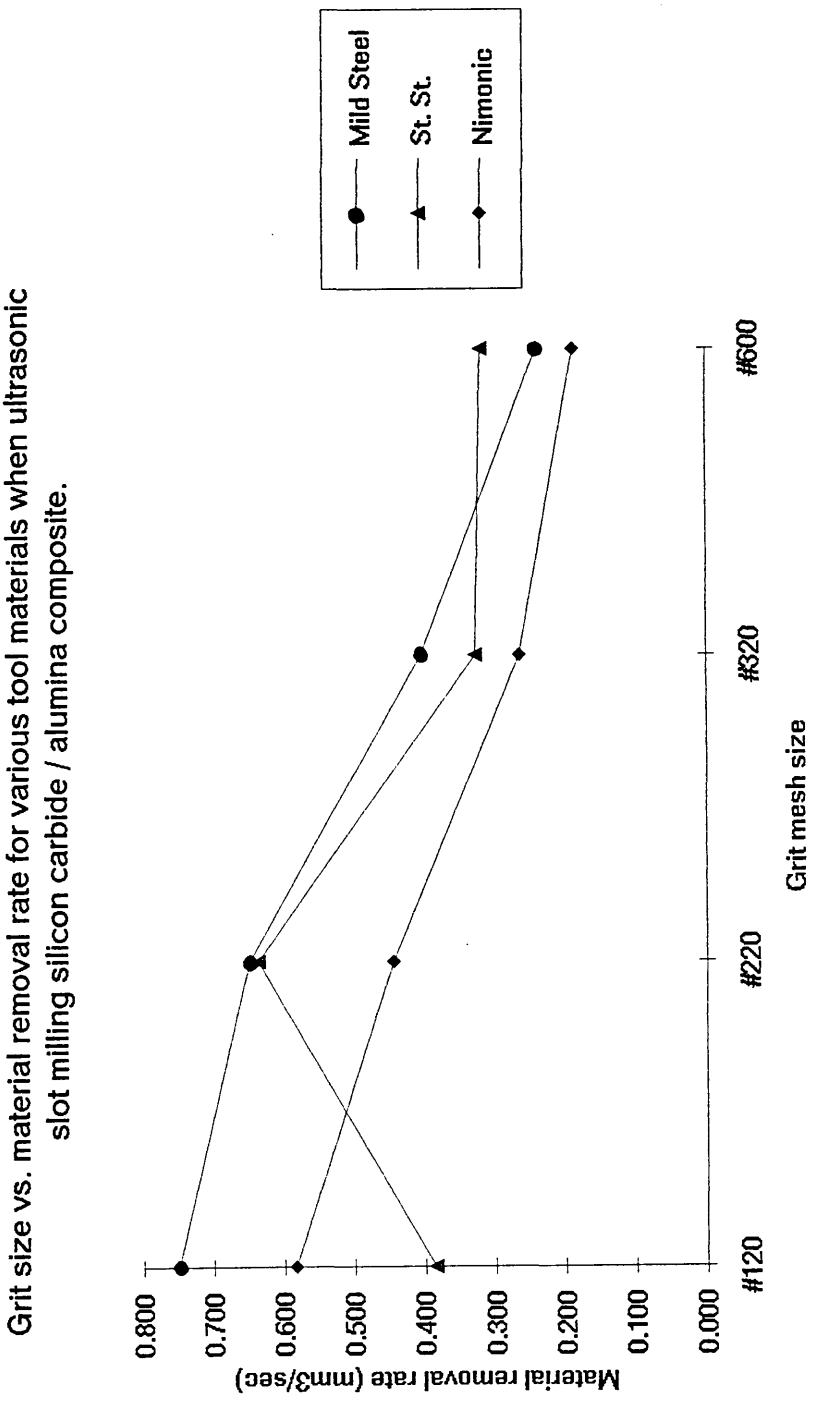

Figure 18
Sections 4.3.6 & 4.3.8

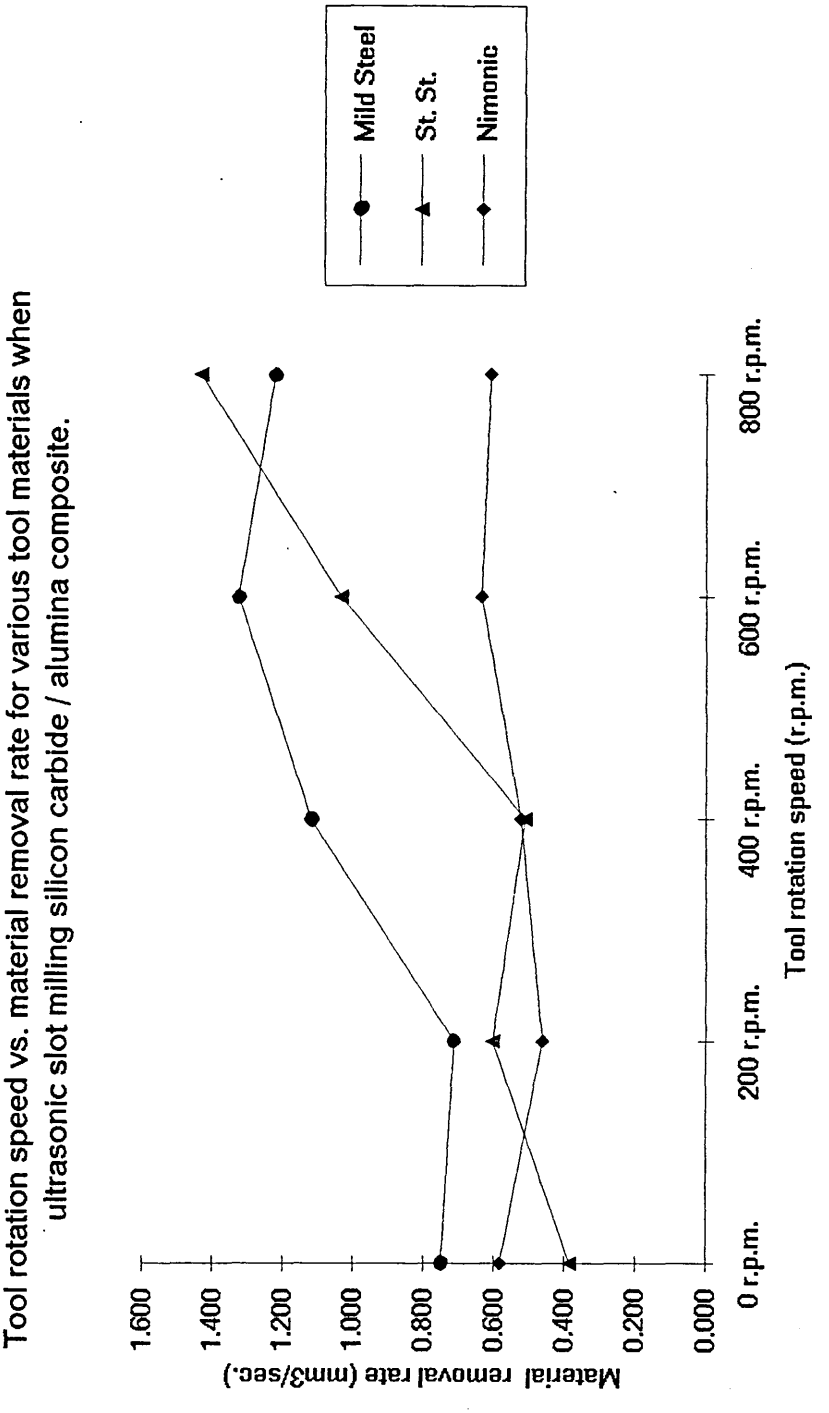

Figure 19
Sections 4.3.6 & 4.3.9

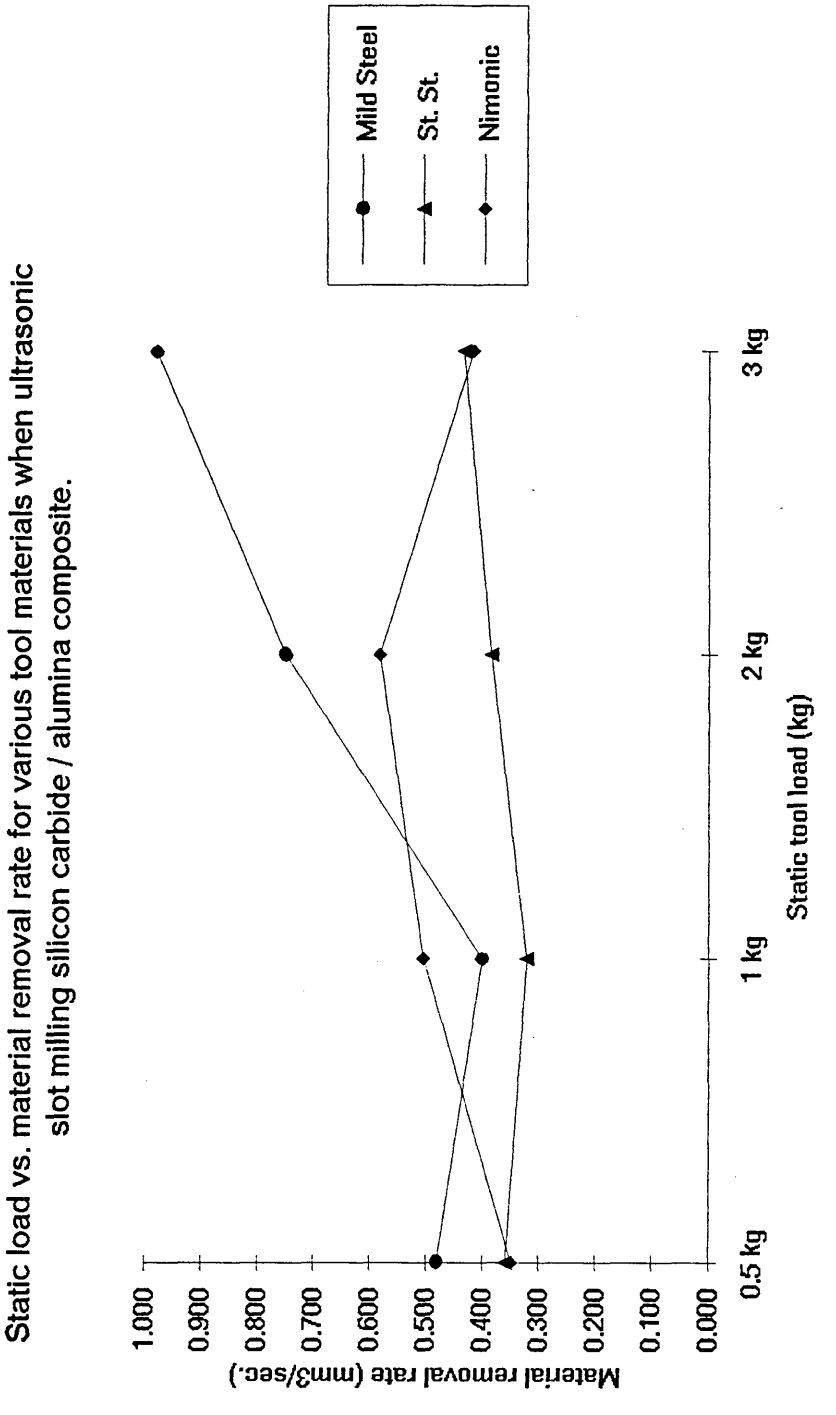

Figure 20
Sections 4.3.6 & 4.3.10

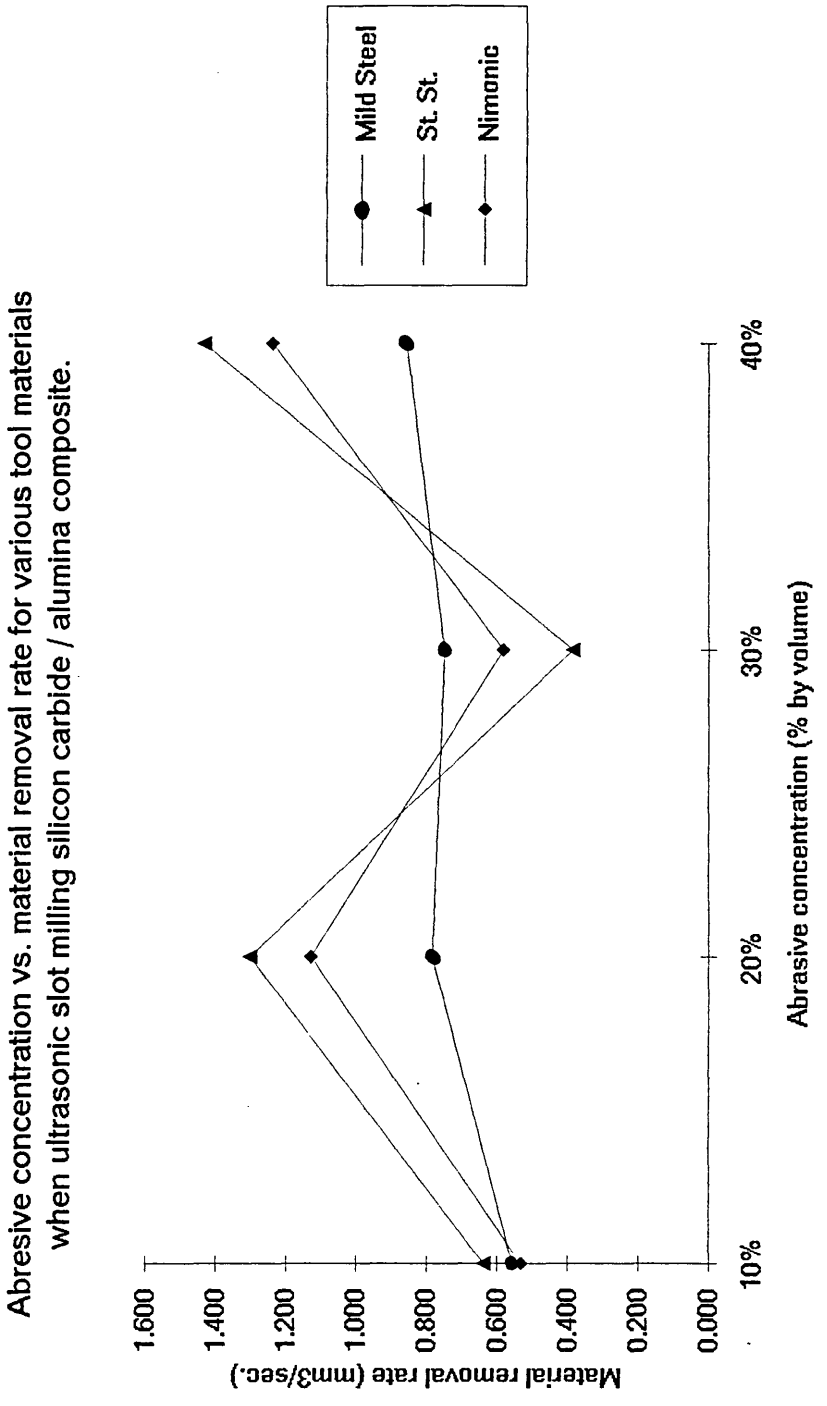

Figure 21
Sections 4.3.11

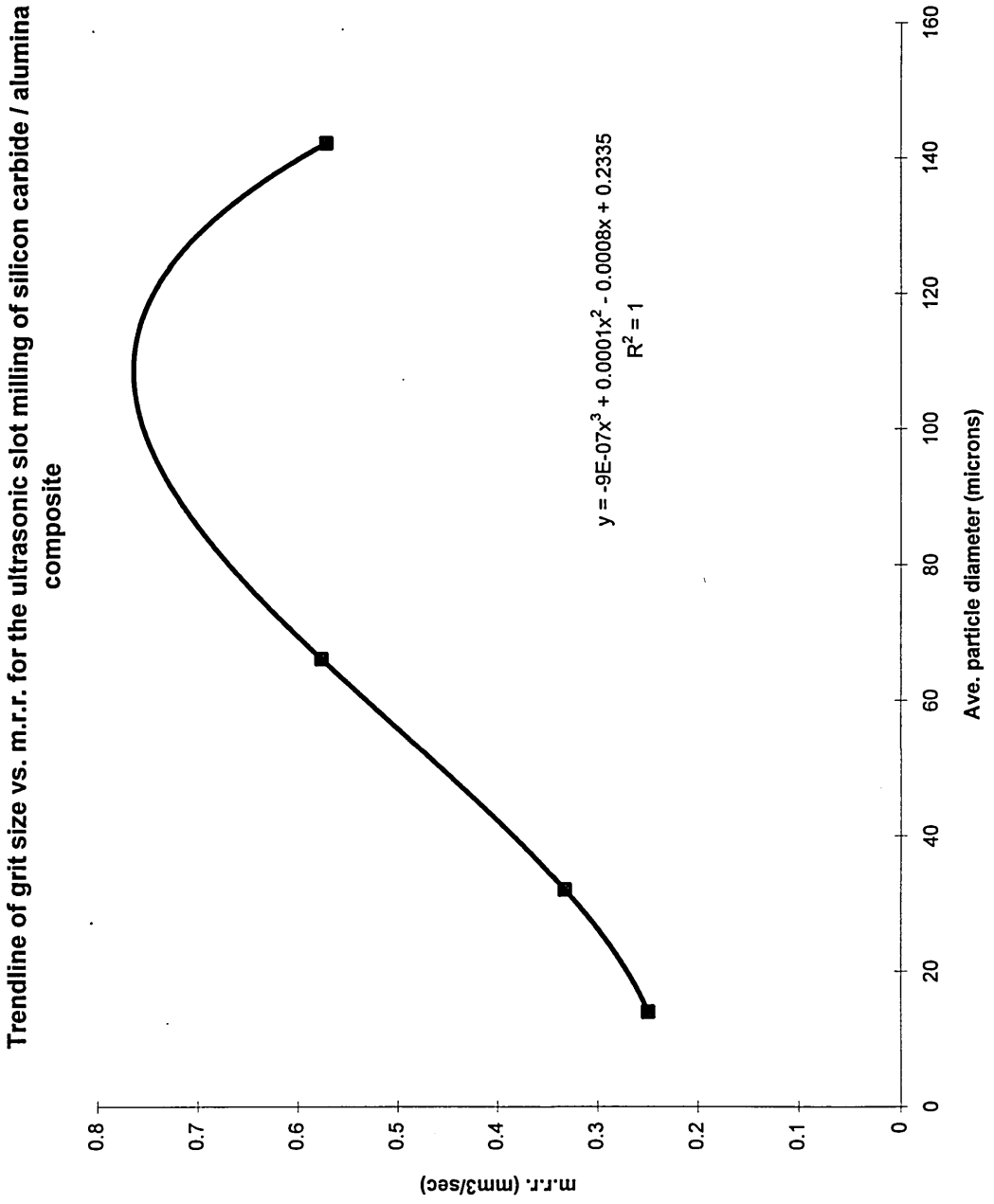

Figure 22
Sections 4.3.11

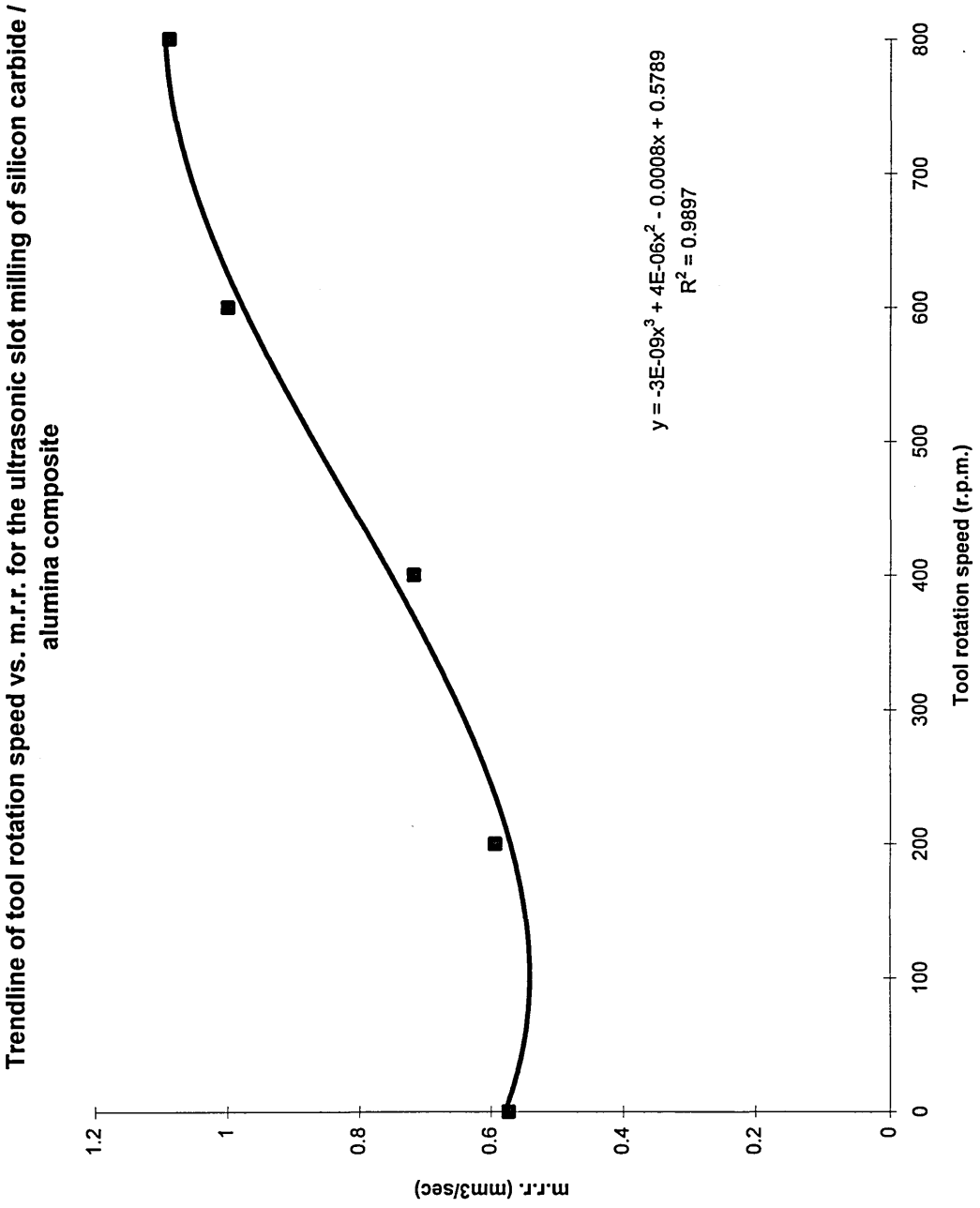

Figure 23
Sections 4.3.11

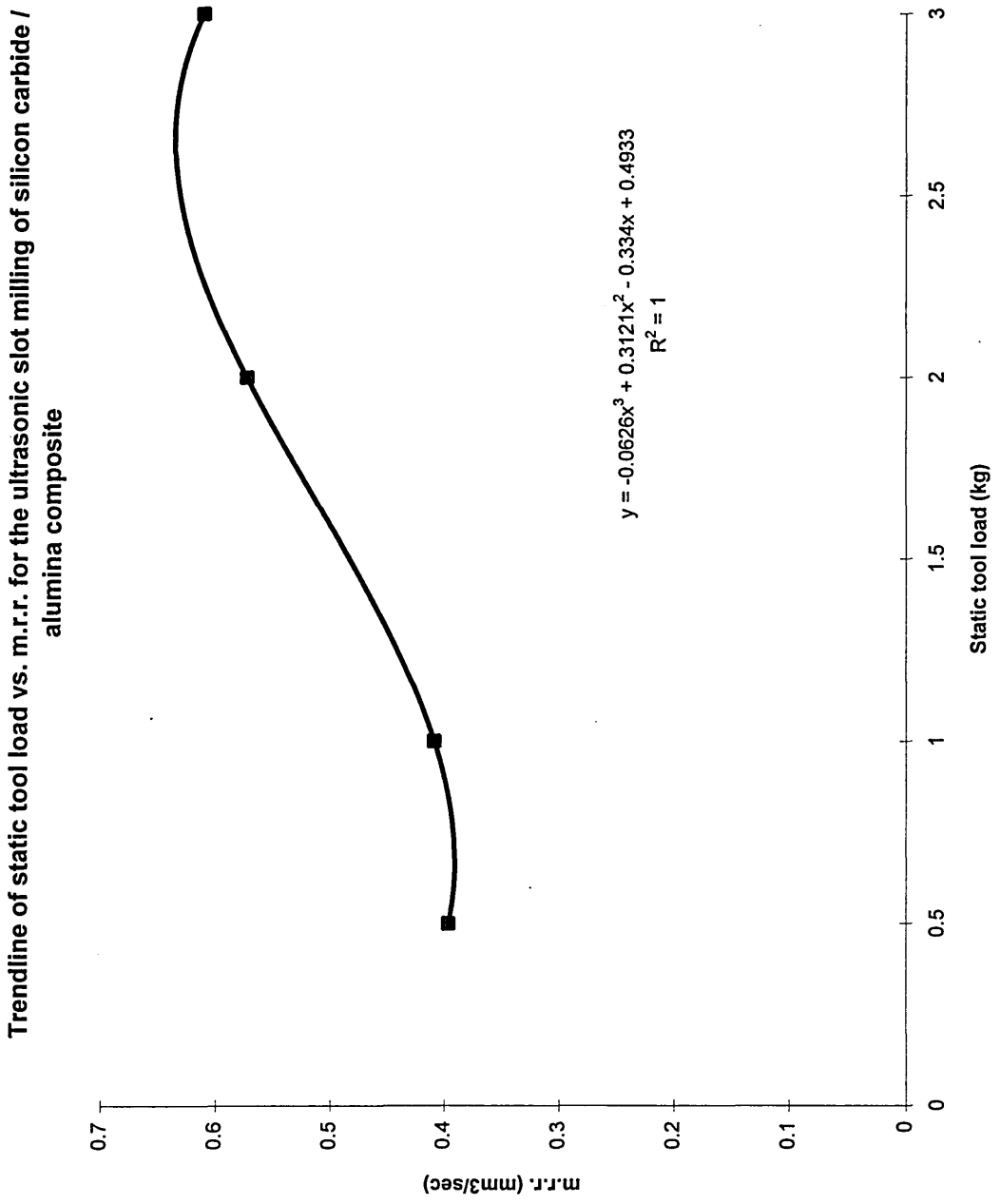

Figure 24
Sections 4.3.11

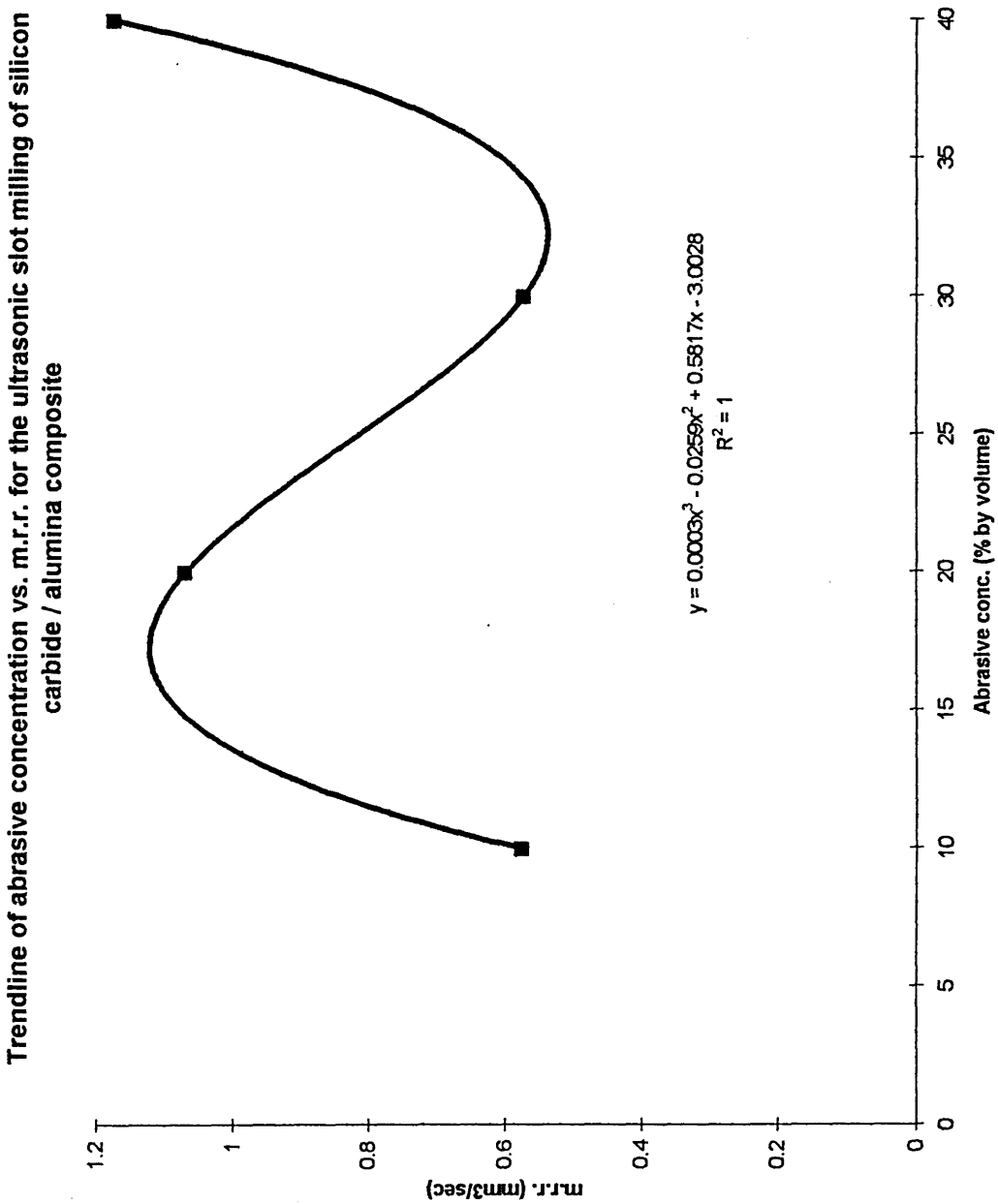

Figure 25
Sections 4.3.12 & 4.3.13

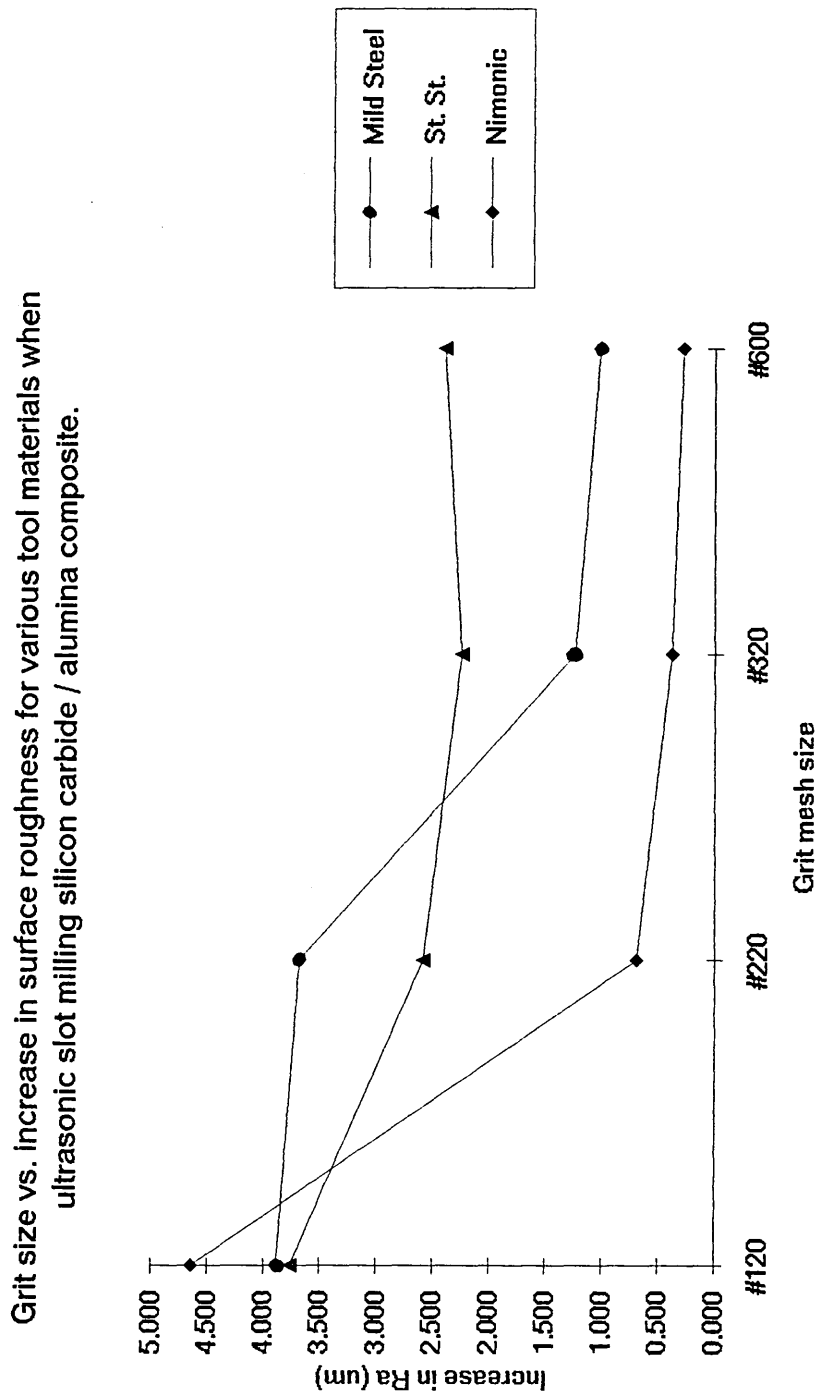

Figure 26
Sections 4.3.12 & 4.3.14

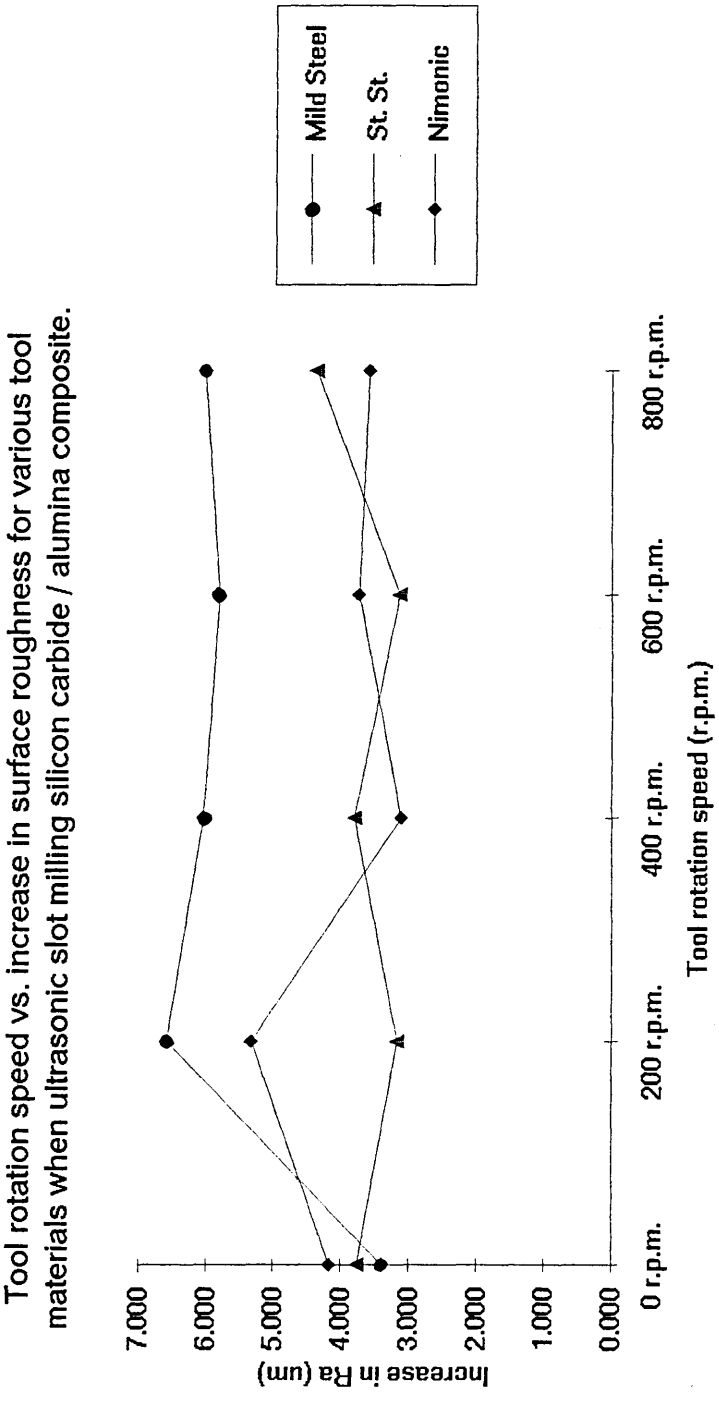

Figure 27
Sections 4.3.12 & 4.3.15

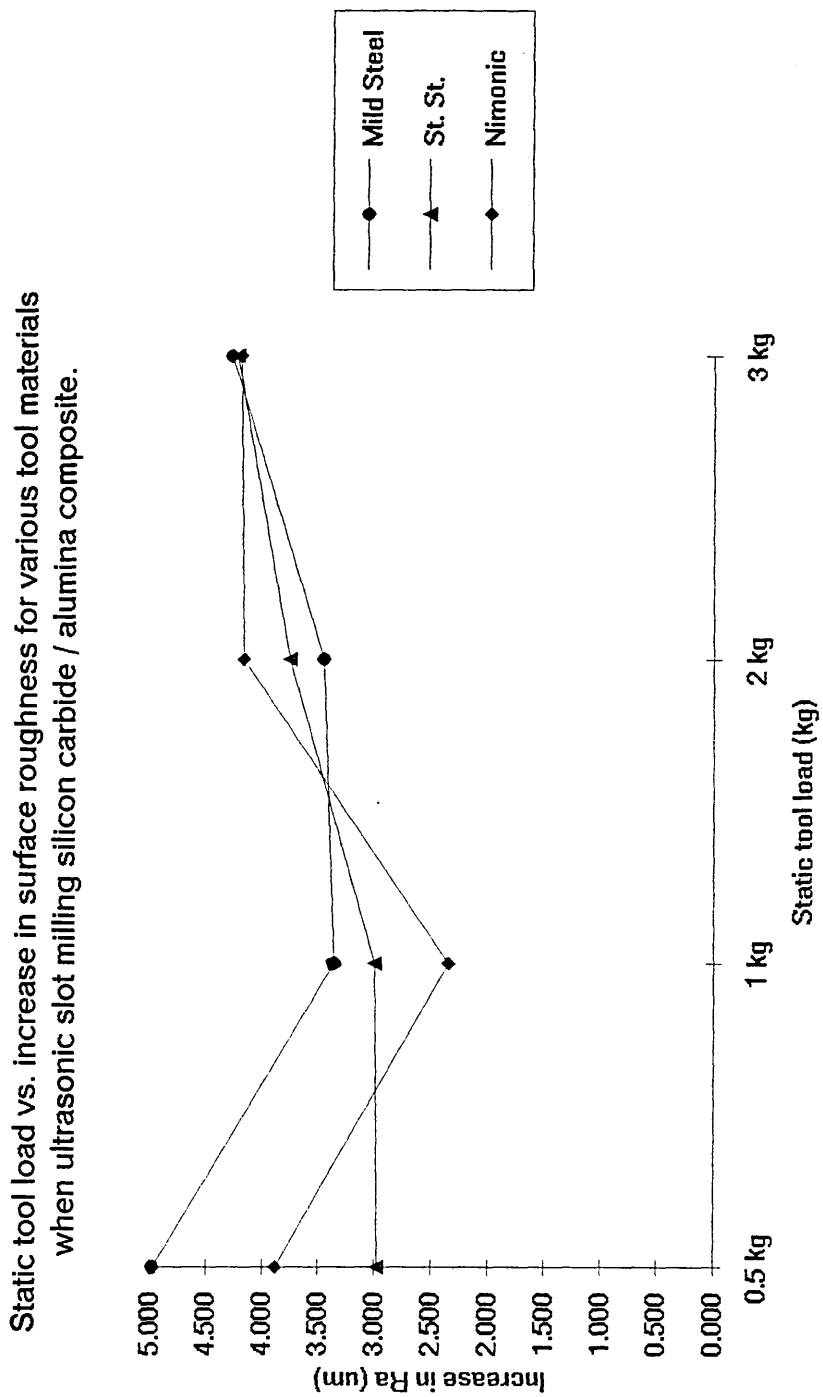

Figure 28
Sections 4.3.12 & 4.3.16

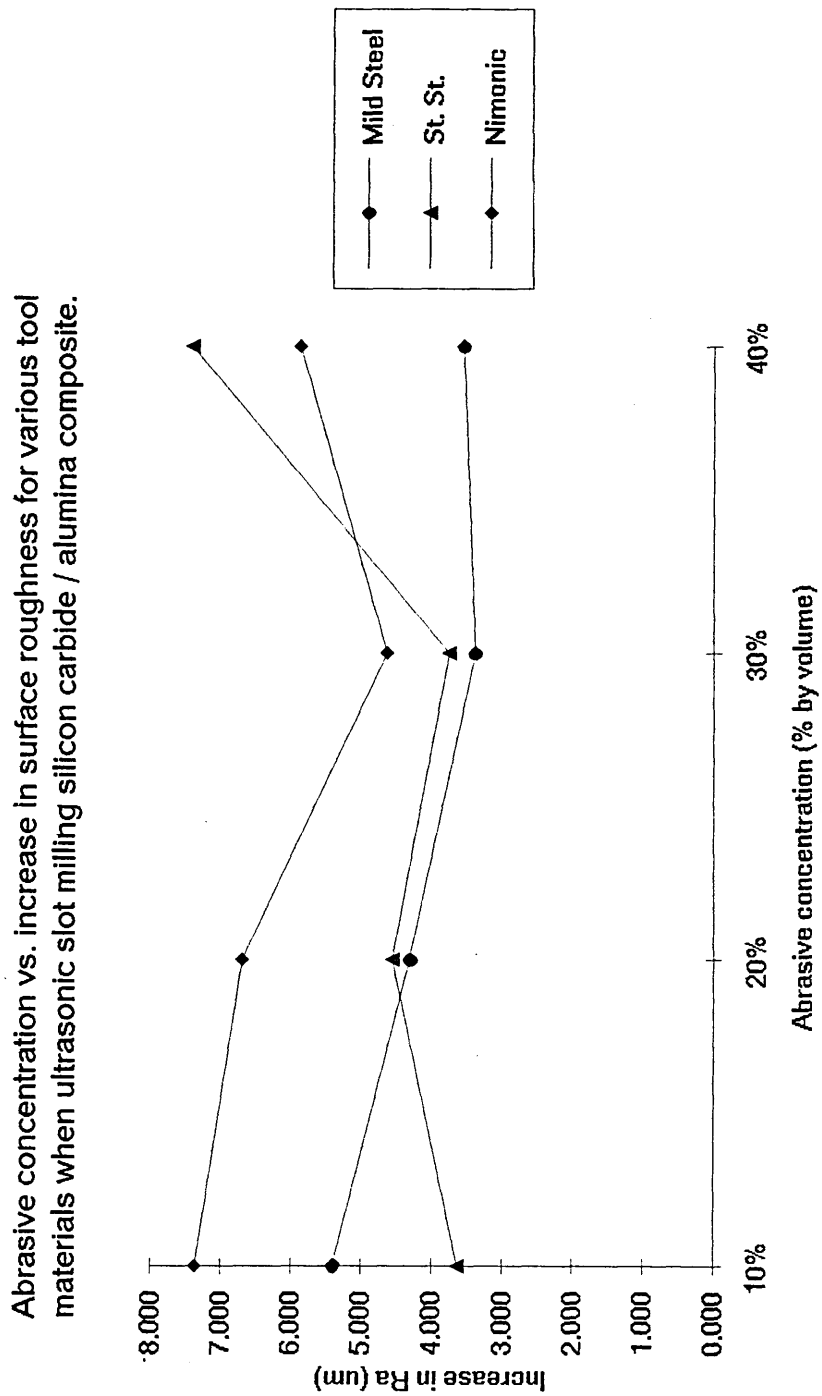

Figure 29
Sections 4.3.17 & 4.3.18

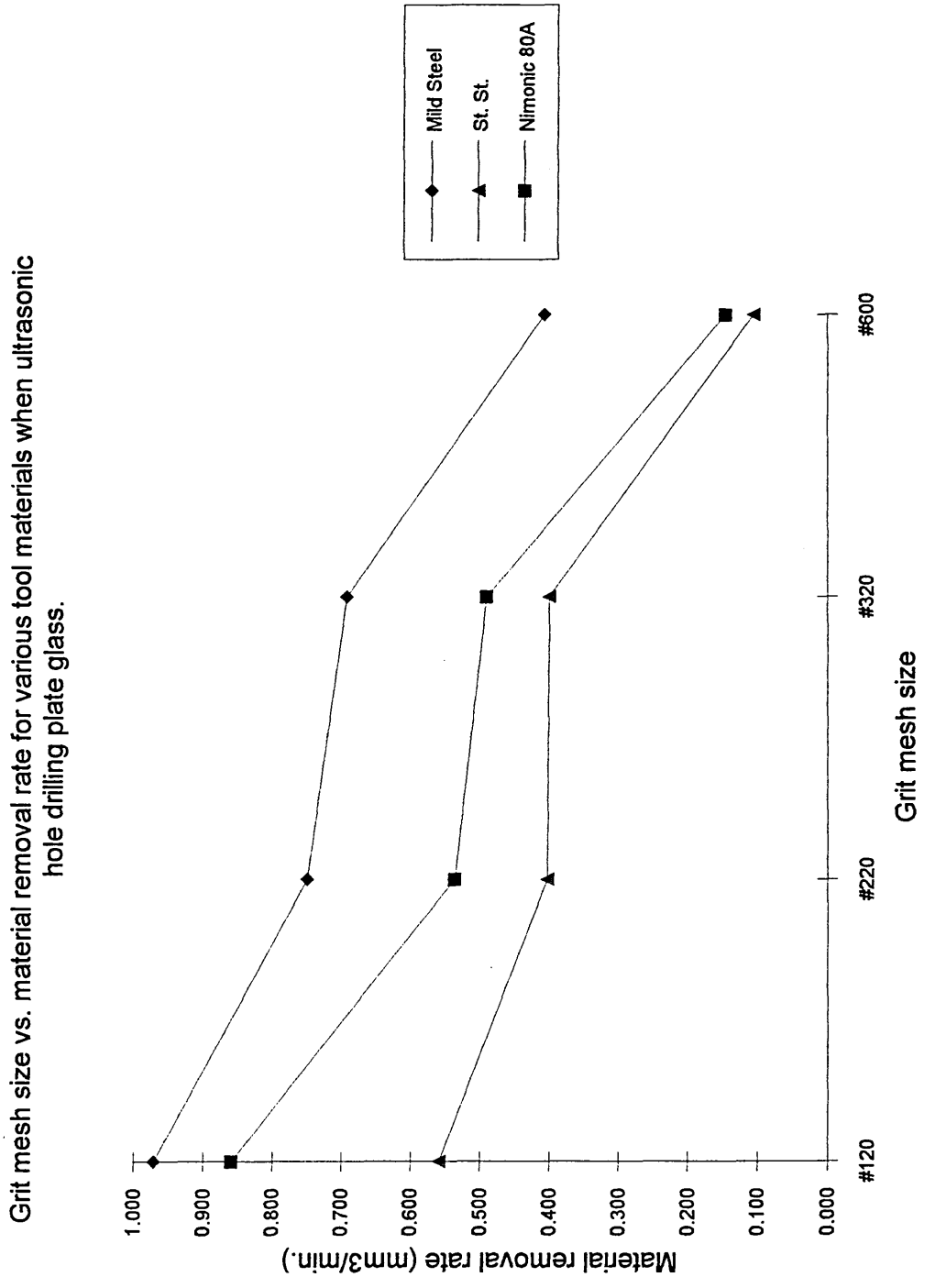

Figure 30
Sections 4.3.17 & 4.3.19

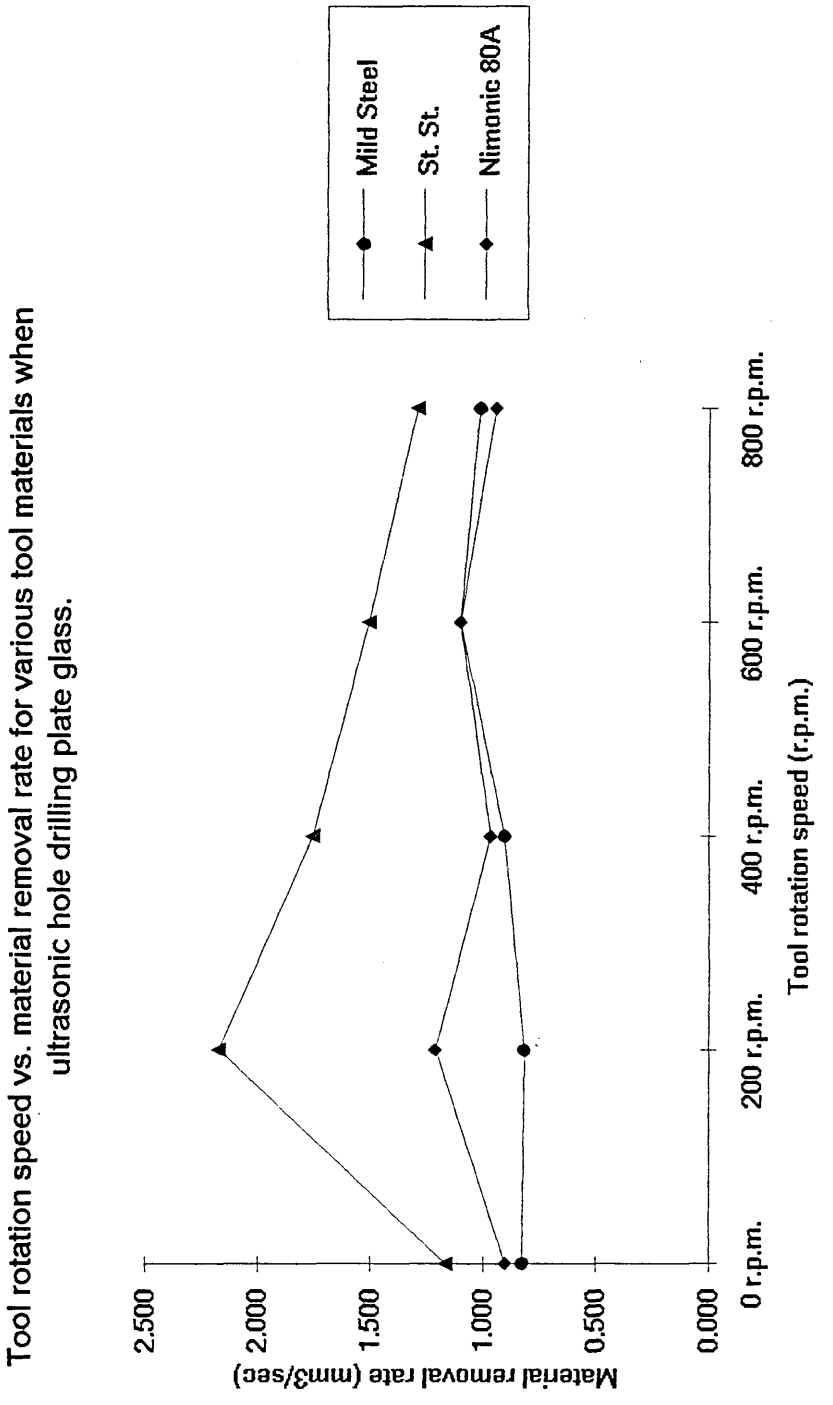

Figure 31
Sections 4.3.17 & 4.3.20

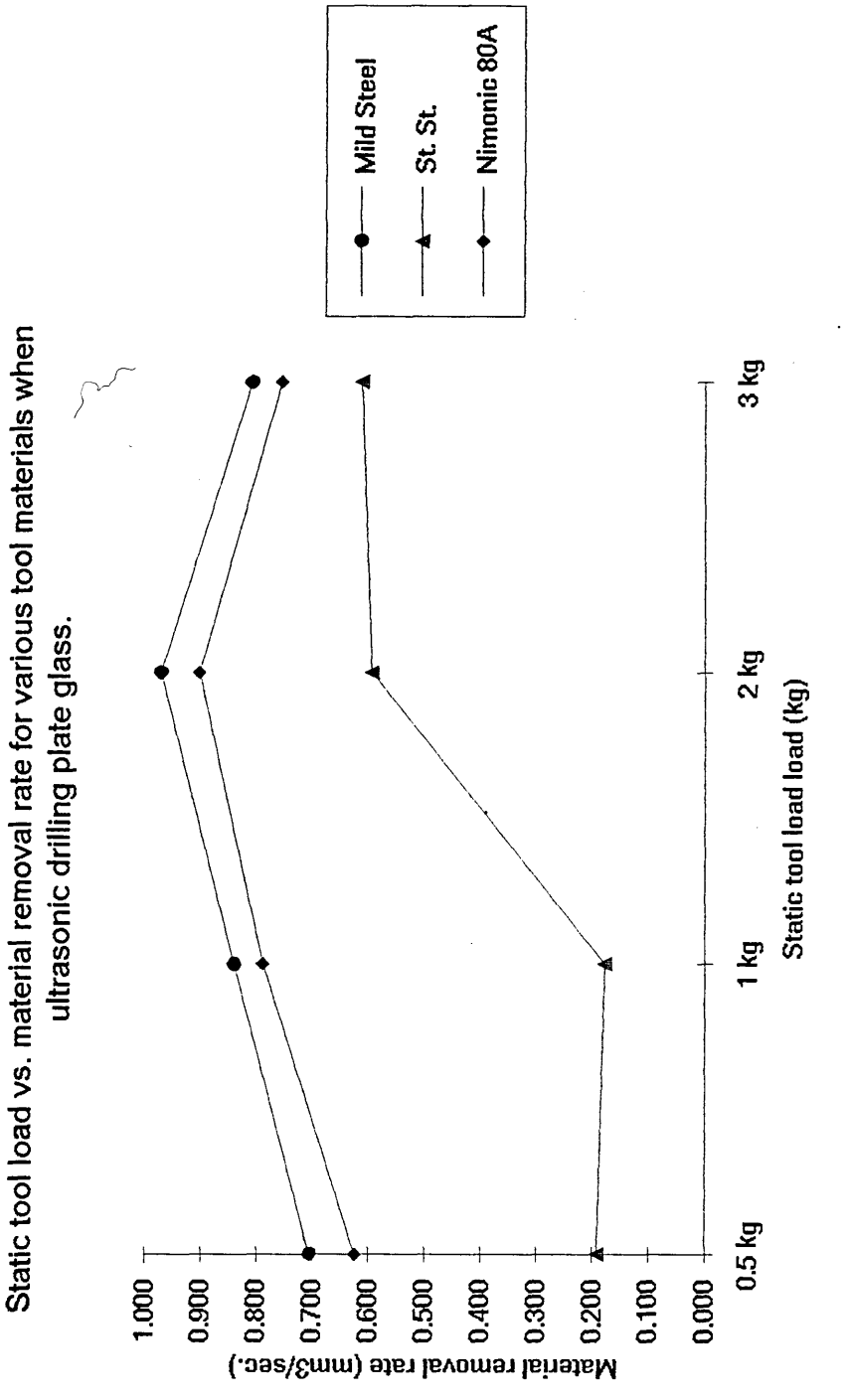

Figure 32
Sections 4.3.21

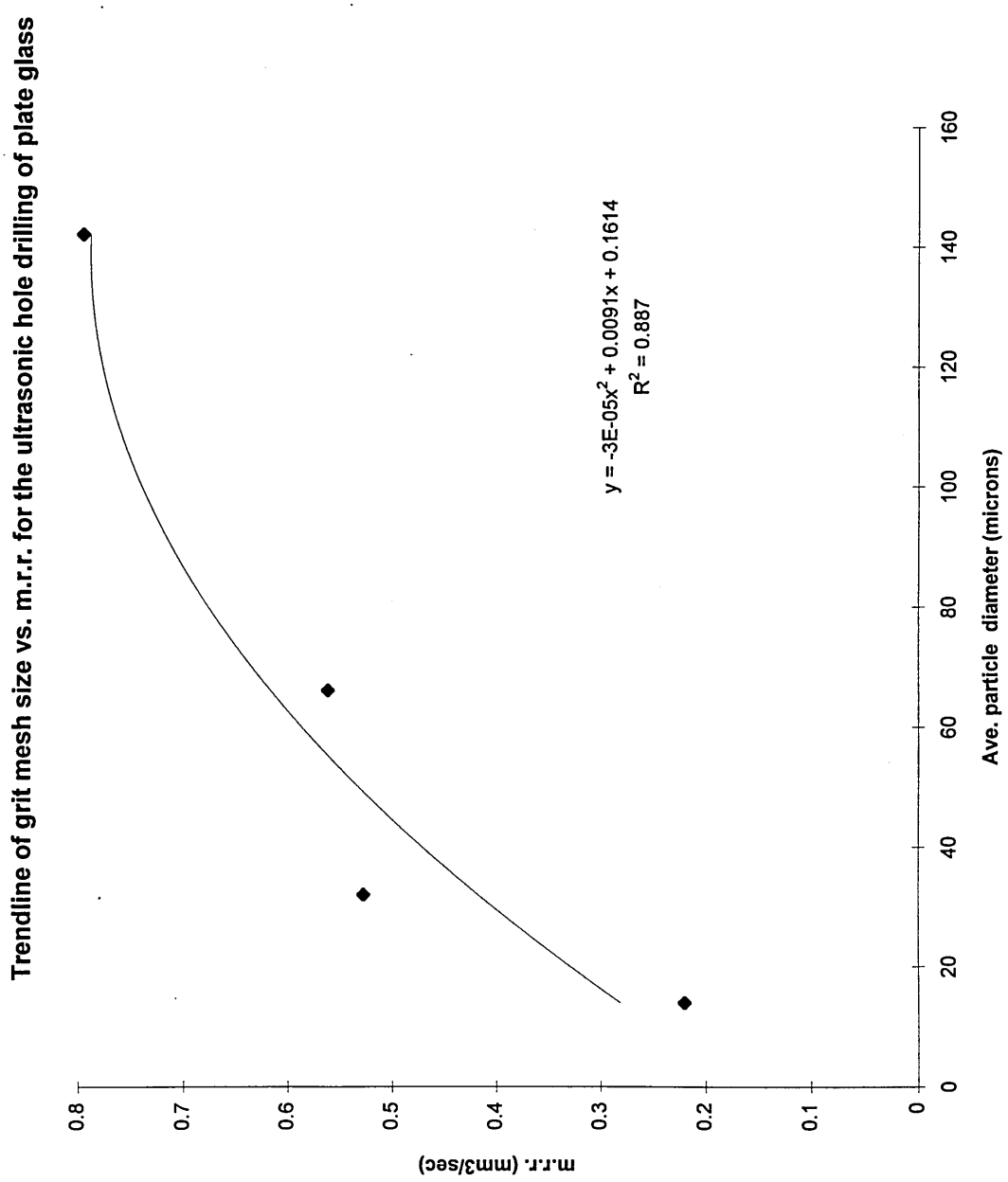

Figure 33
Sections 4.3.21

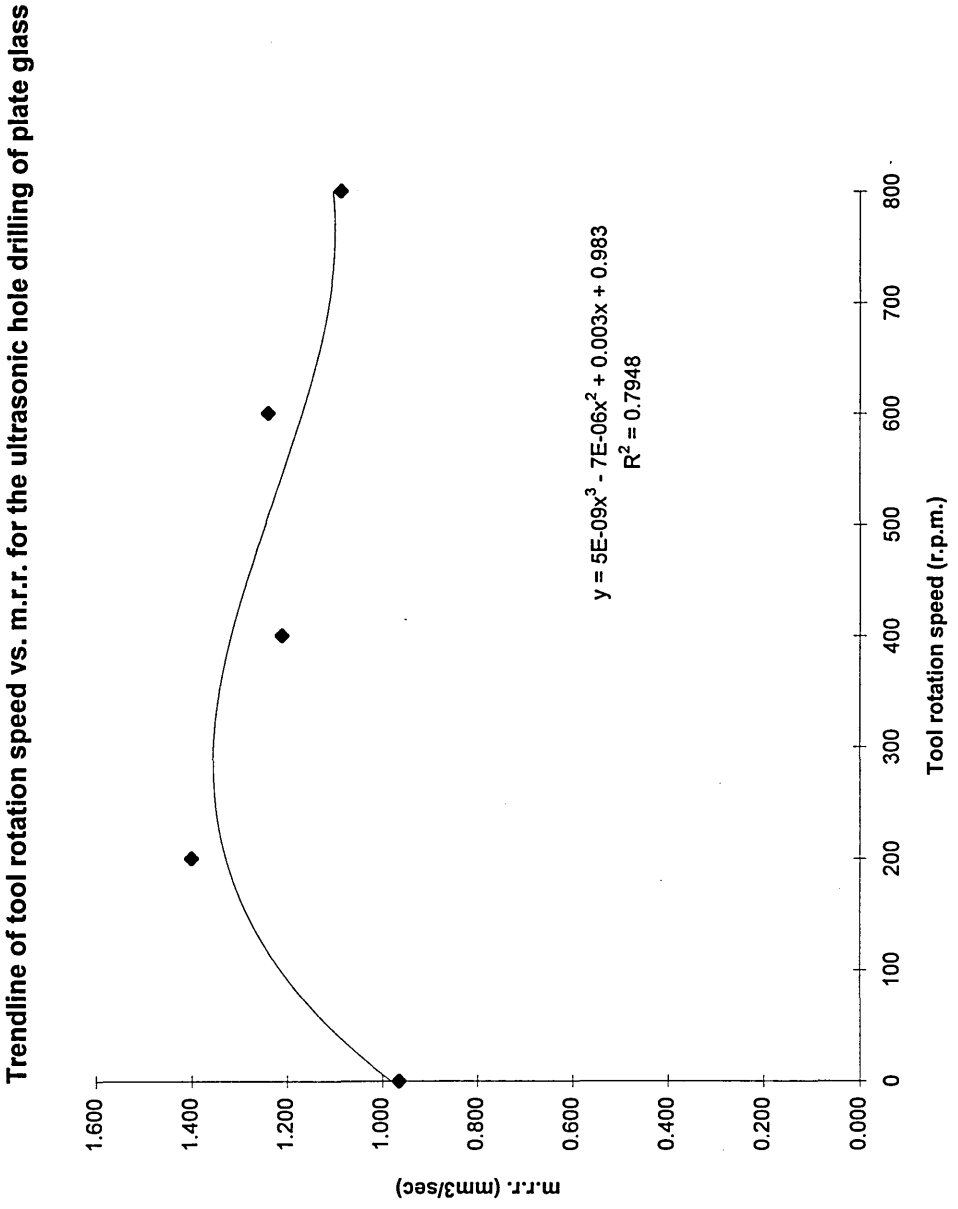

Figure 34
Sections 4.3.21

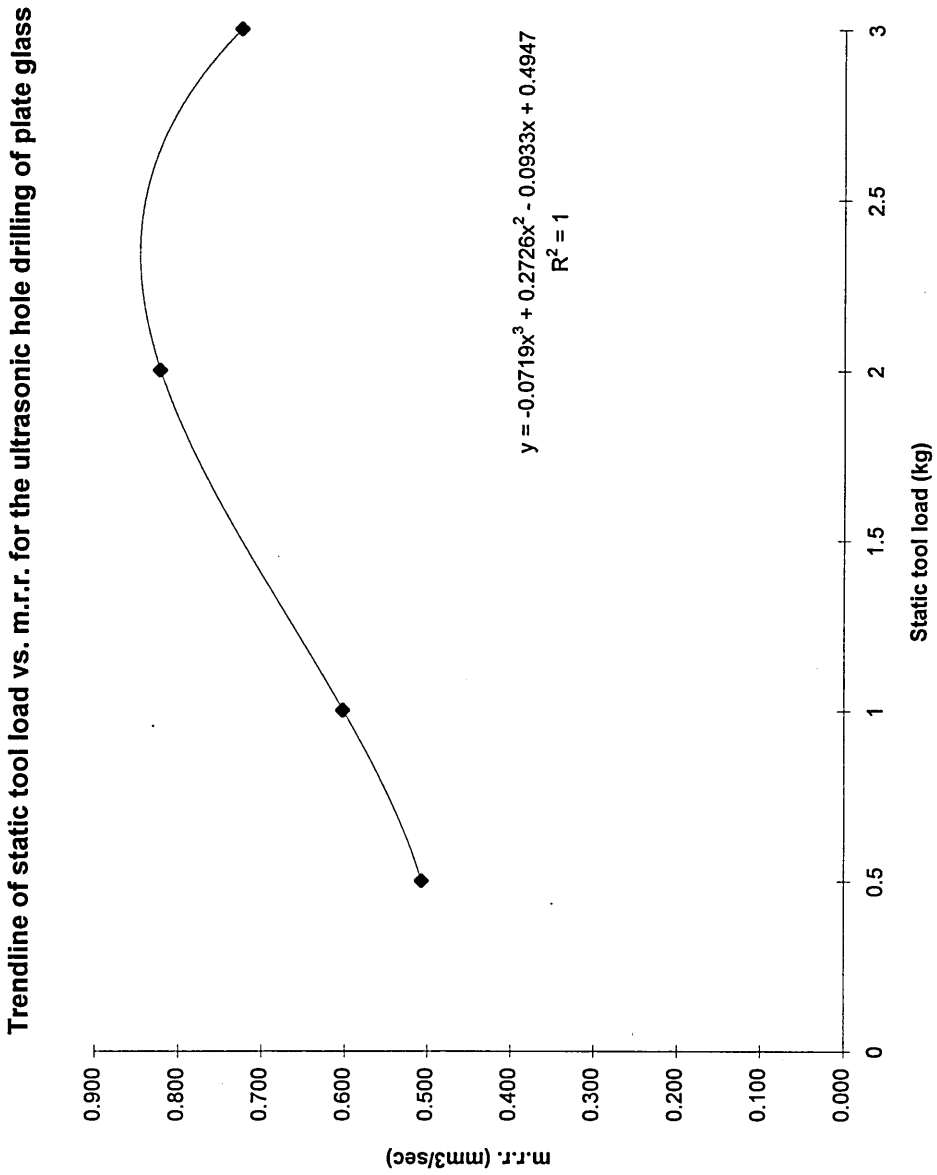

Figure 35
Sections 4.3.22 & 4.3.23

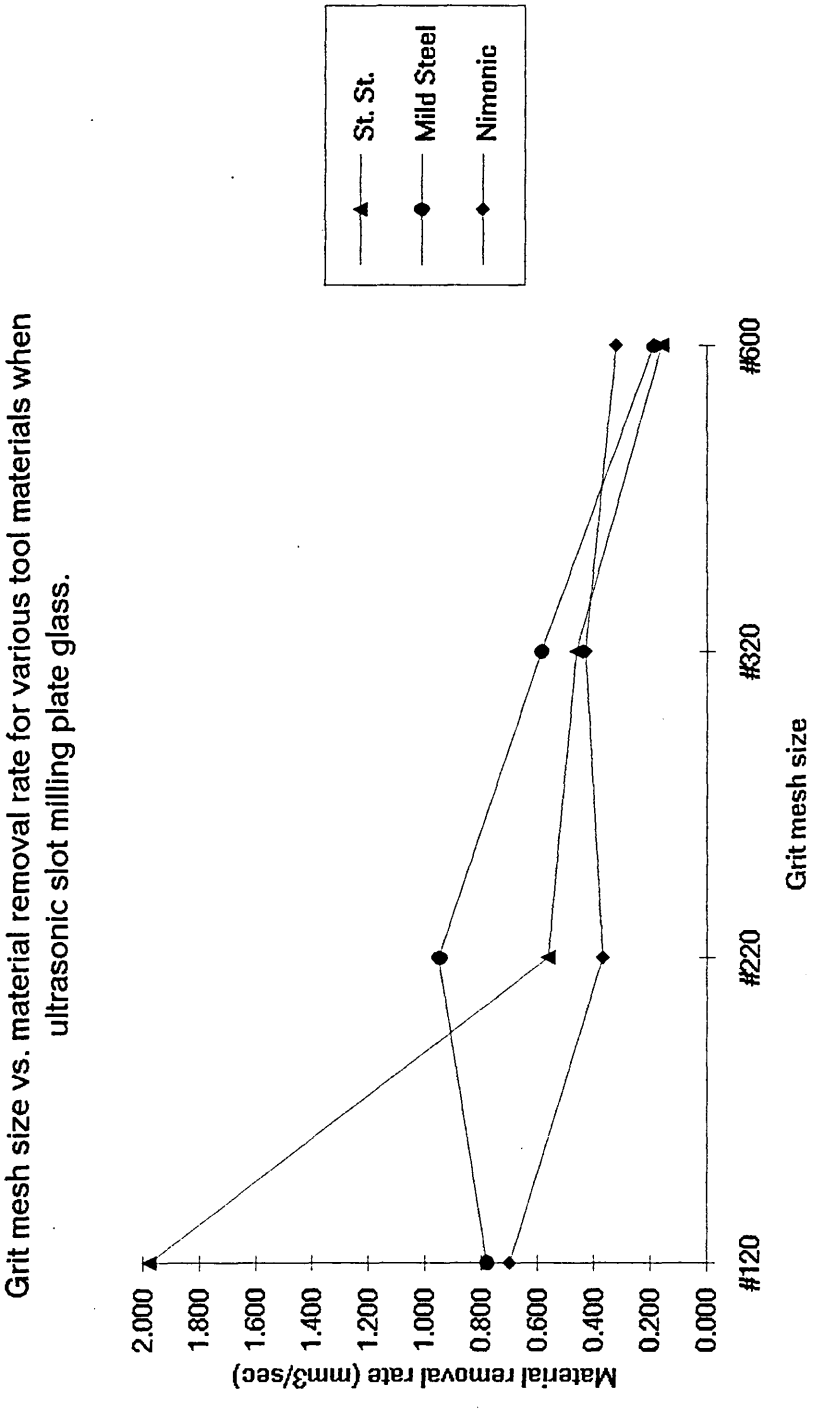

Figure 36
Sections 4.3.22 & 4.3.24

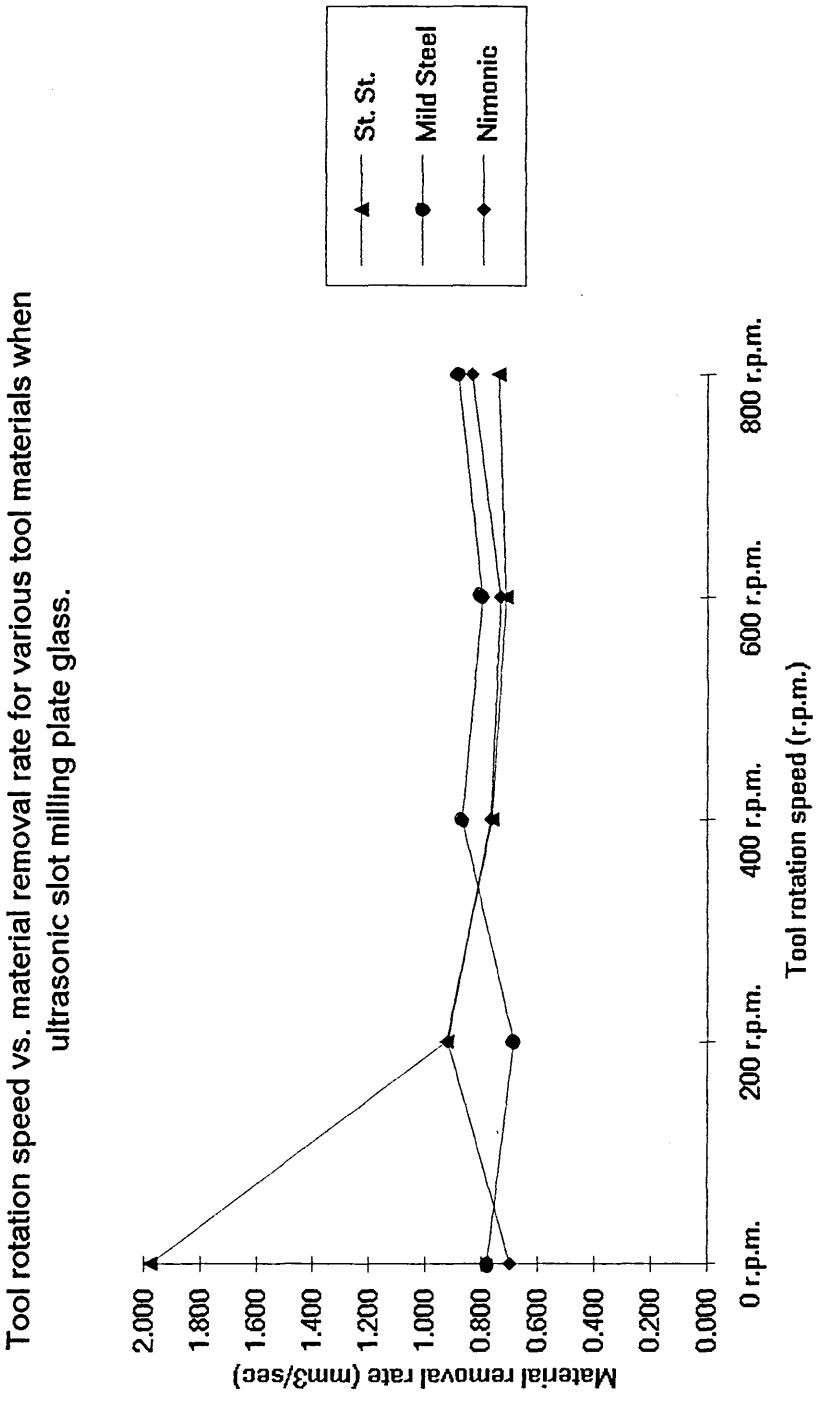

Figure 37
Sections 4.3.22 & 4.3.25

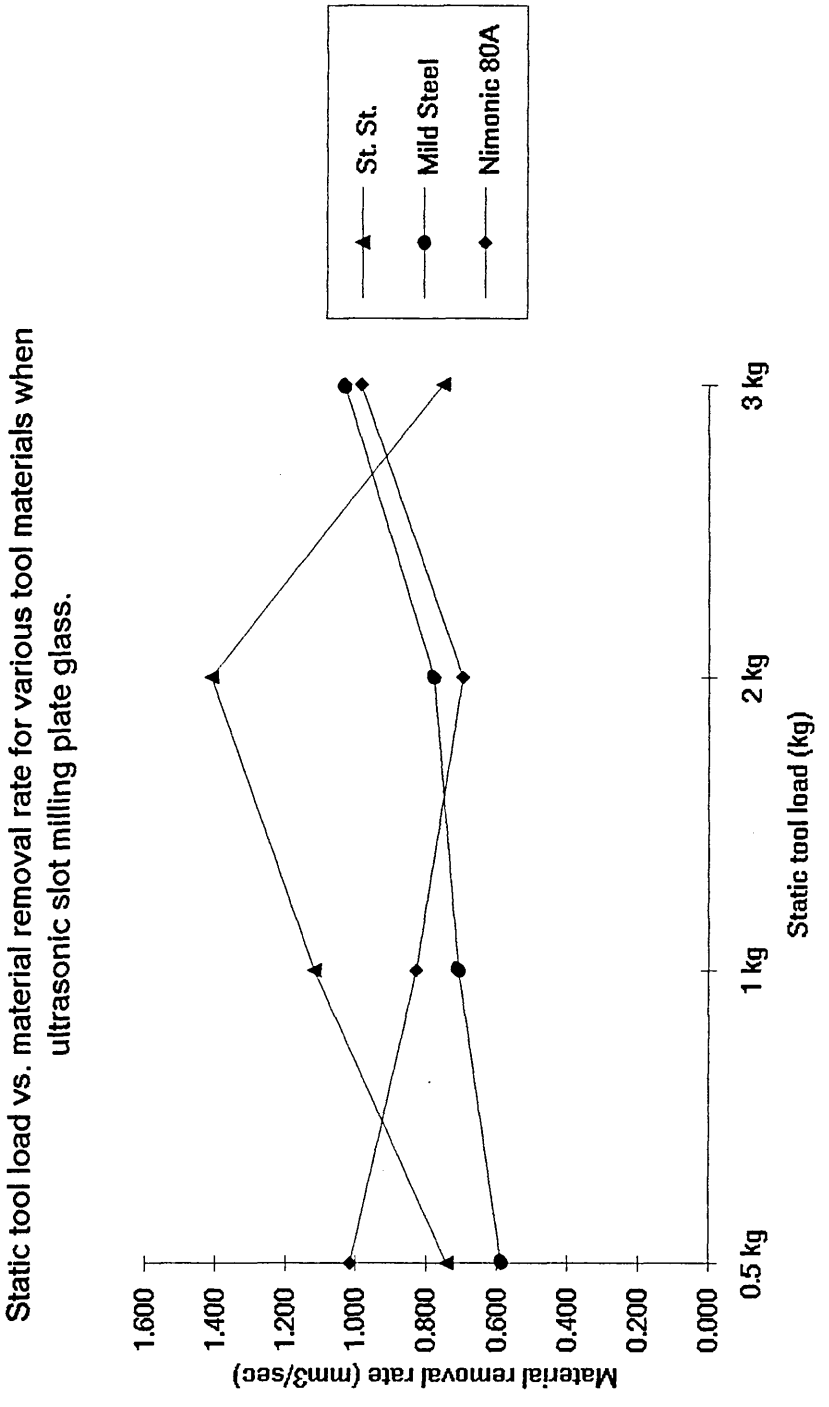

Figure 38
Sections 4.3.22 & 4.3.26

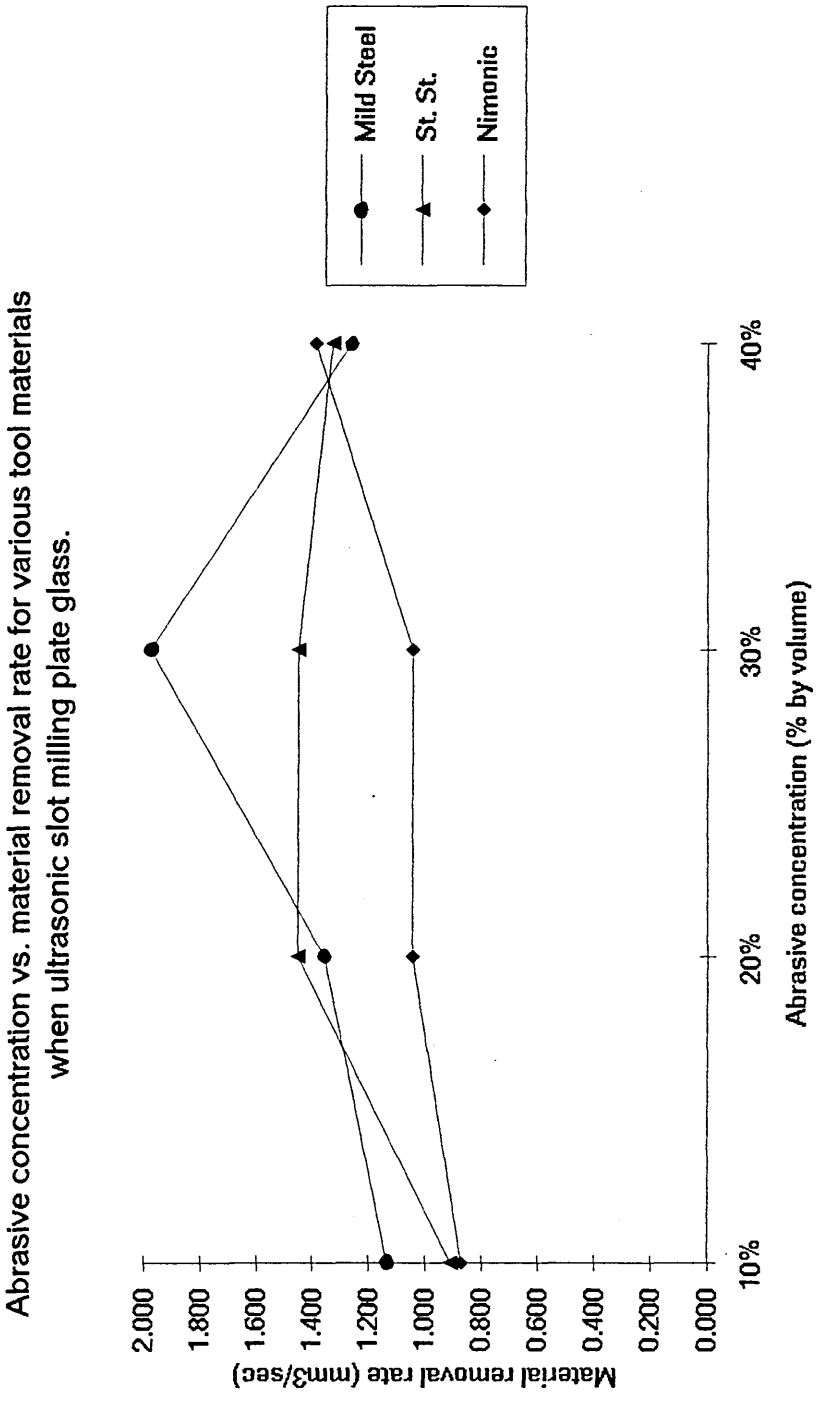

Figure 39
Sections 4.3.27

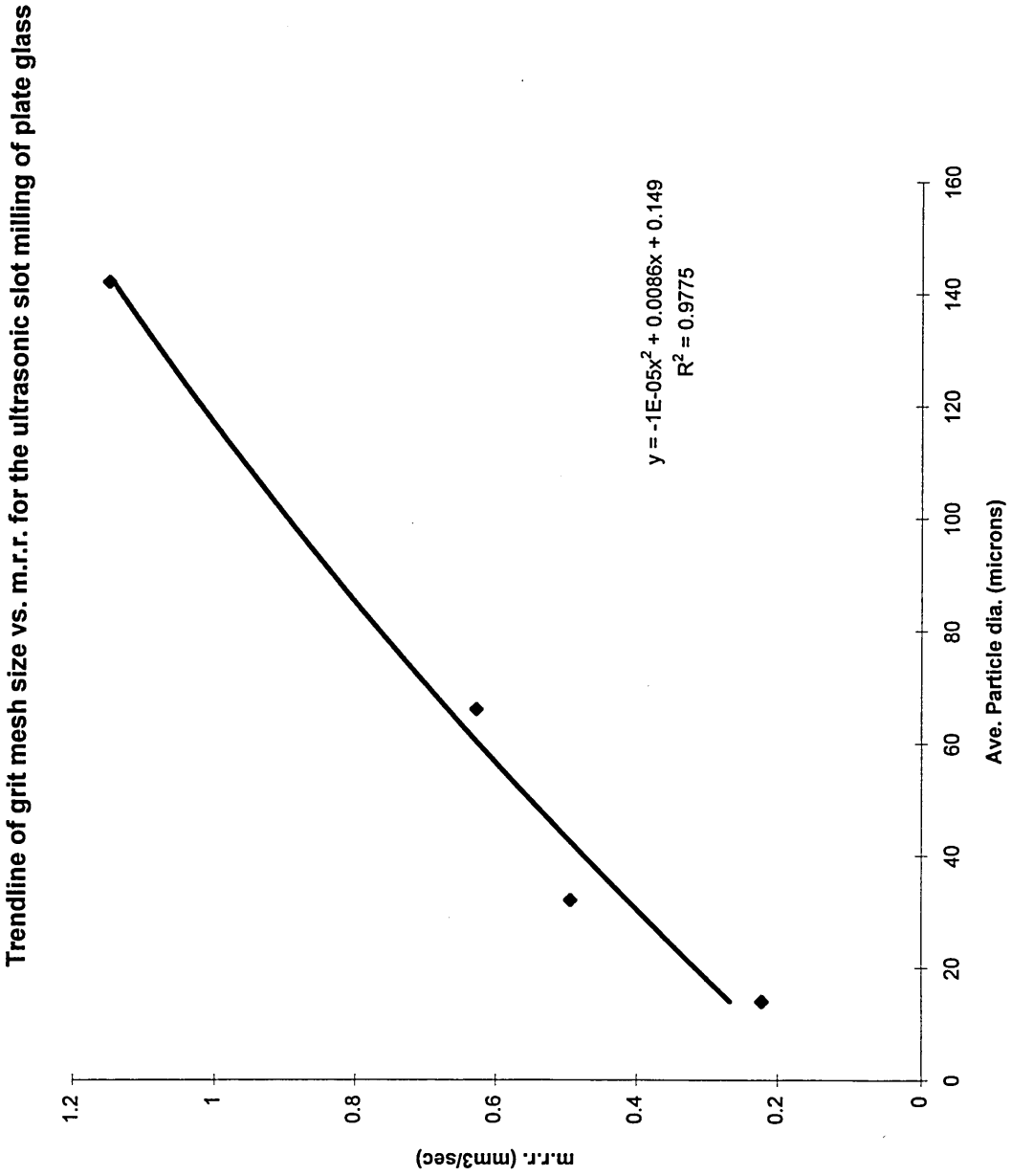

Figure 40
Sections 4.3.27

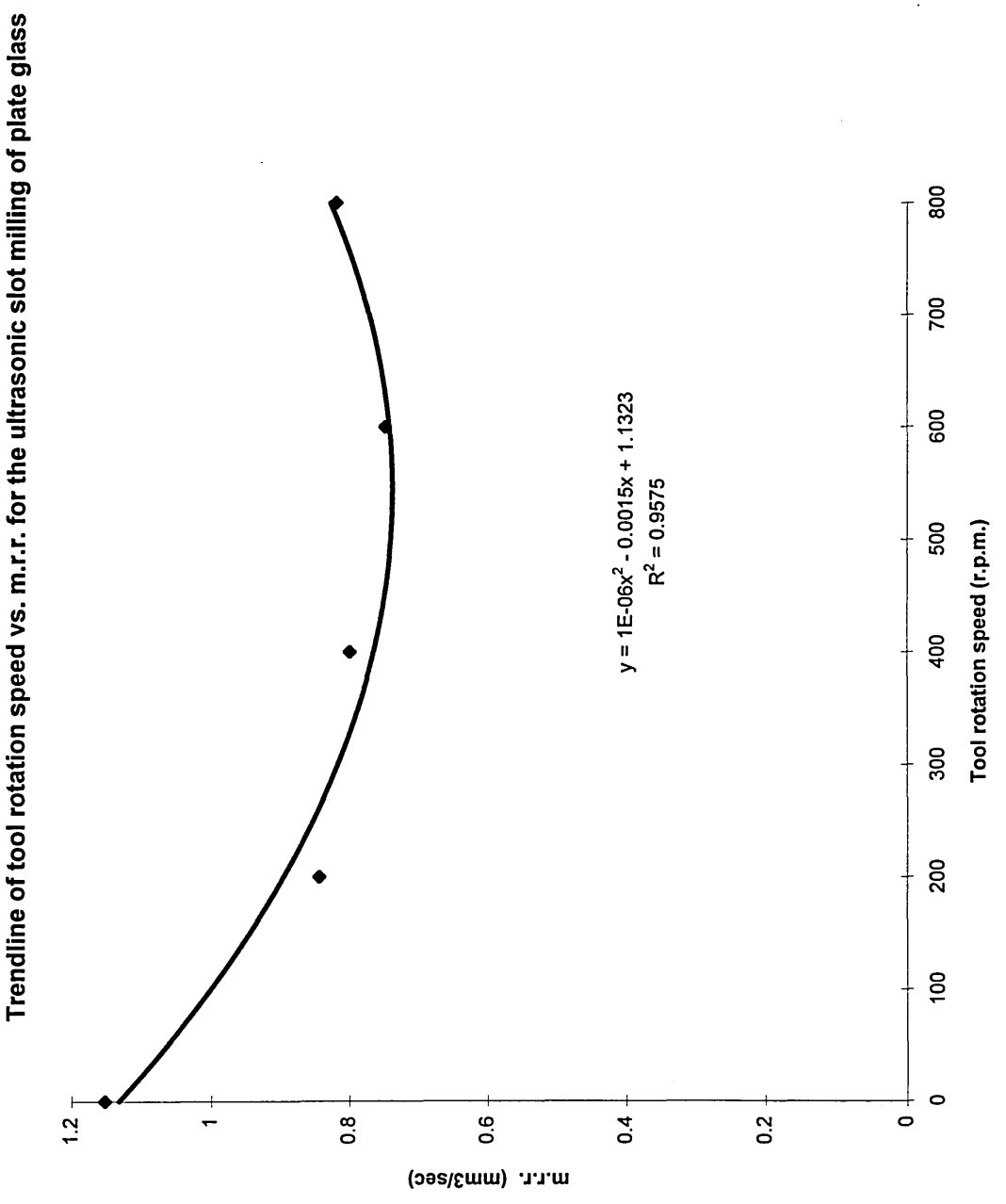

Figure 41
Sections 4.3.27

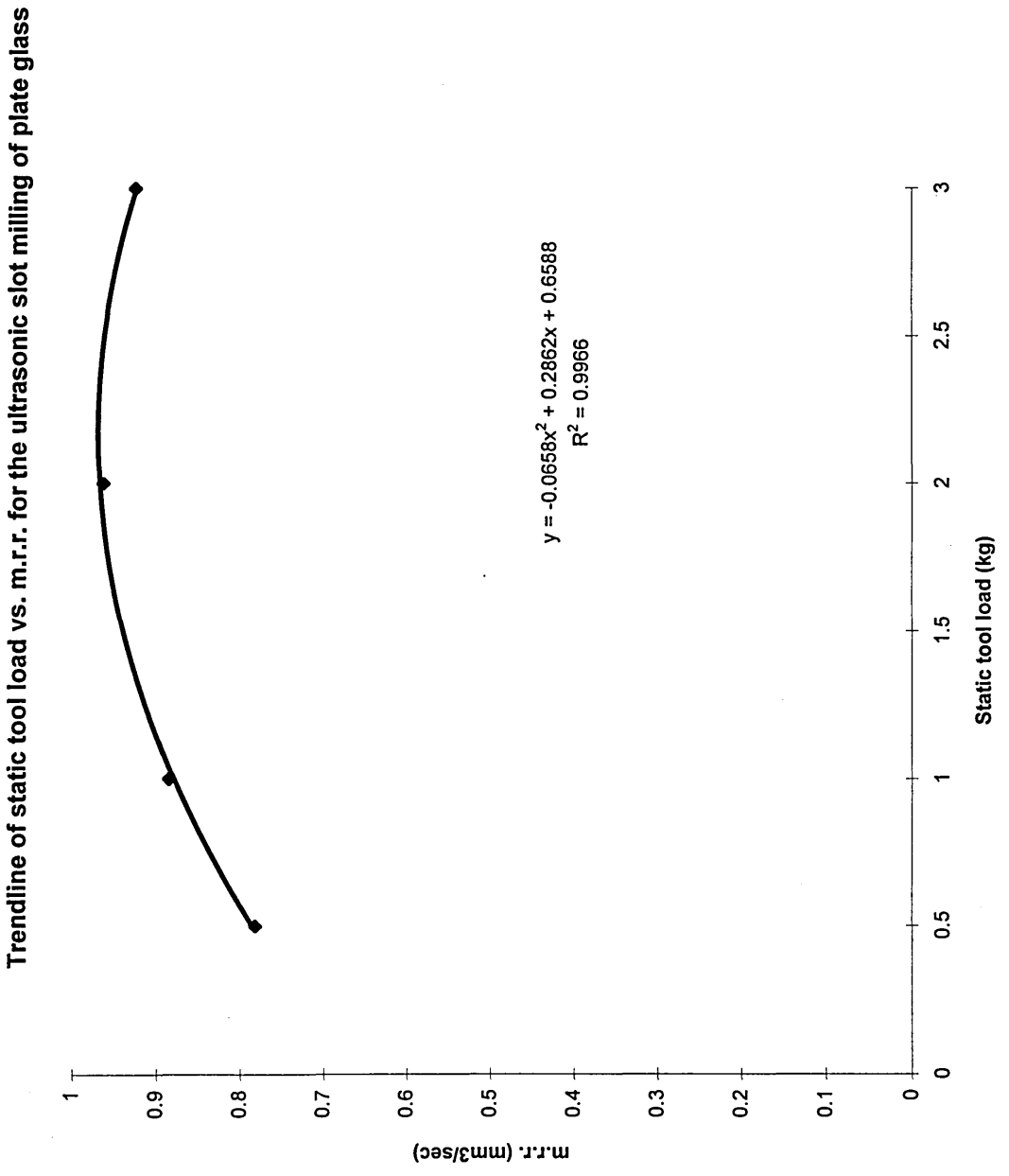

Figure 42
Sections 4.3.27

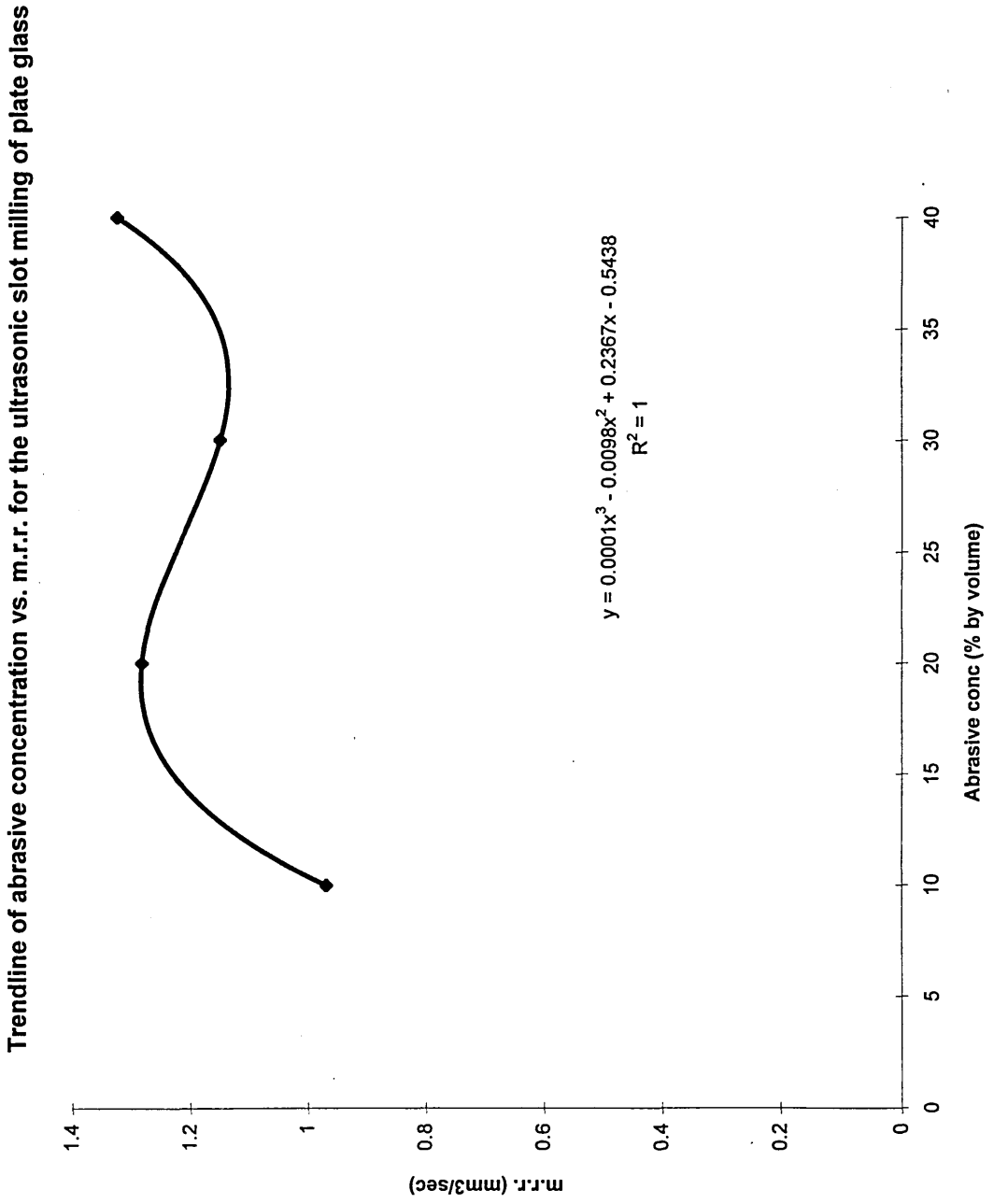

Figure 43
Sections 4.3.28 & 4.3.29

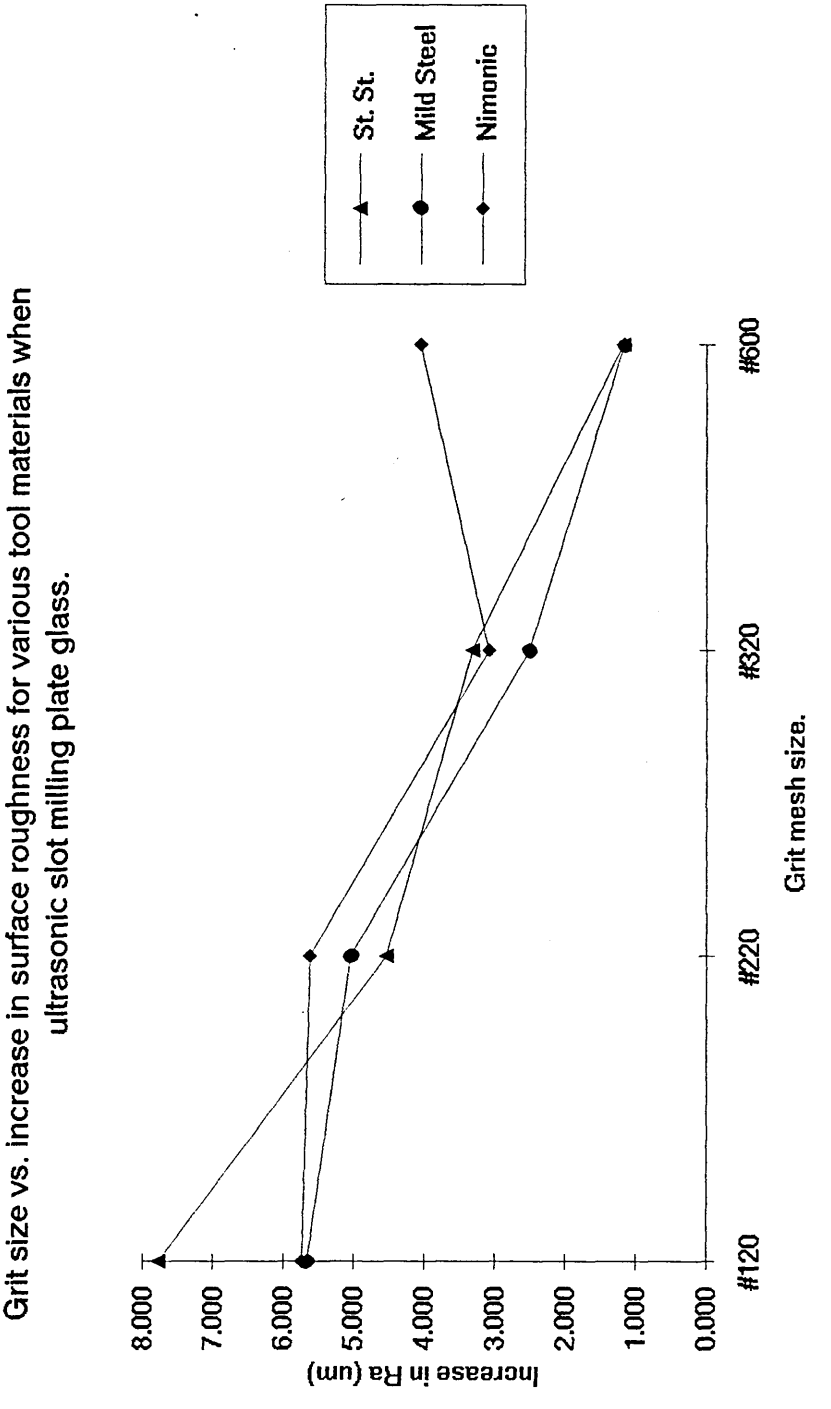

Figure 44
Sections 4.3.28 & 4.3.30

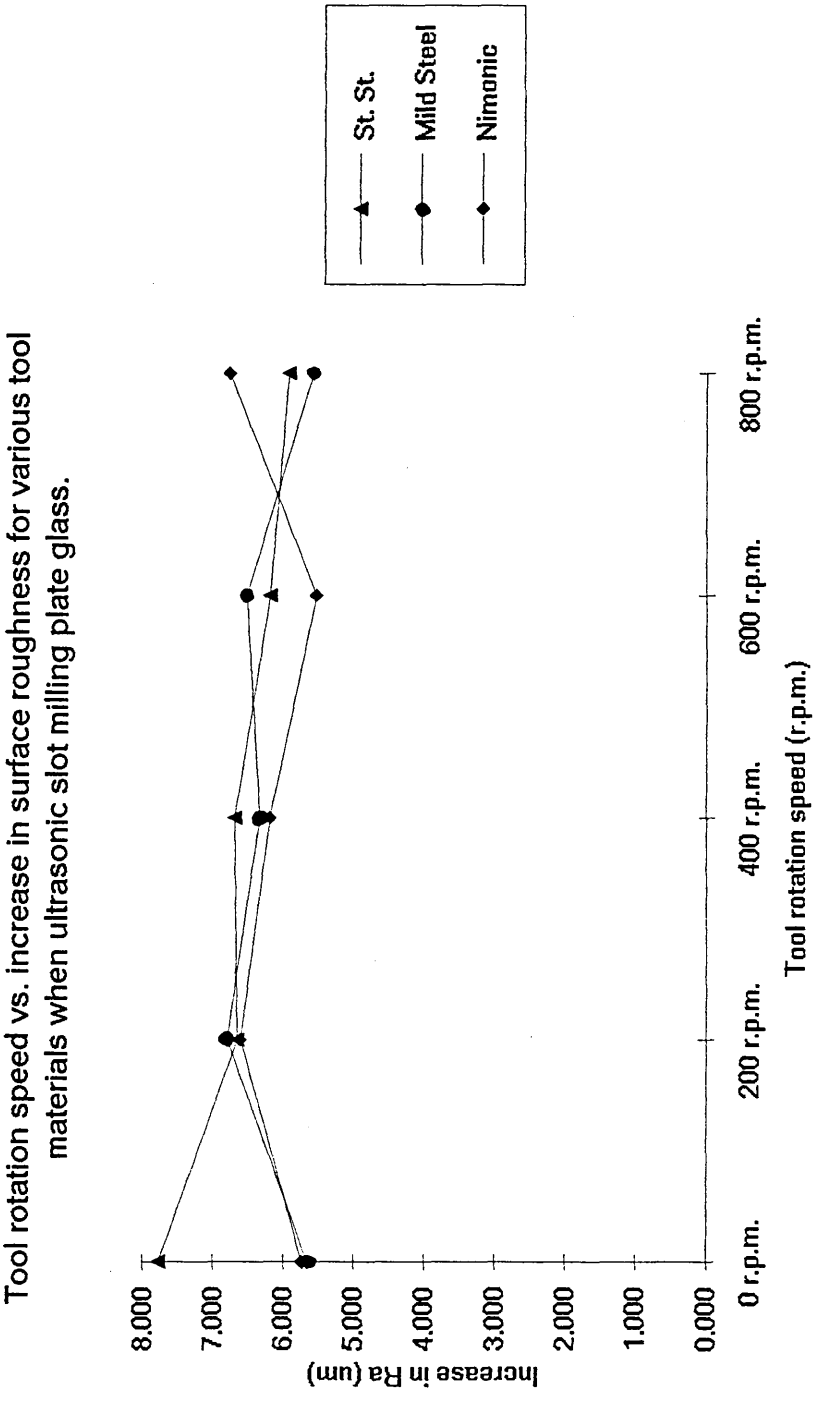

Figure 45
Sections 4.3.28 & 4.3.31

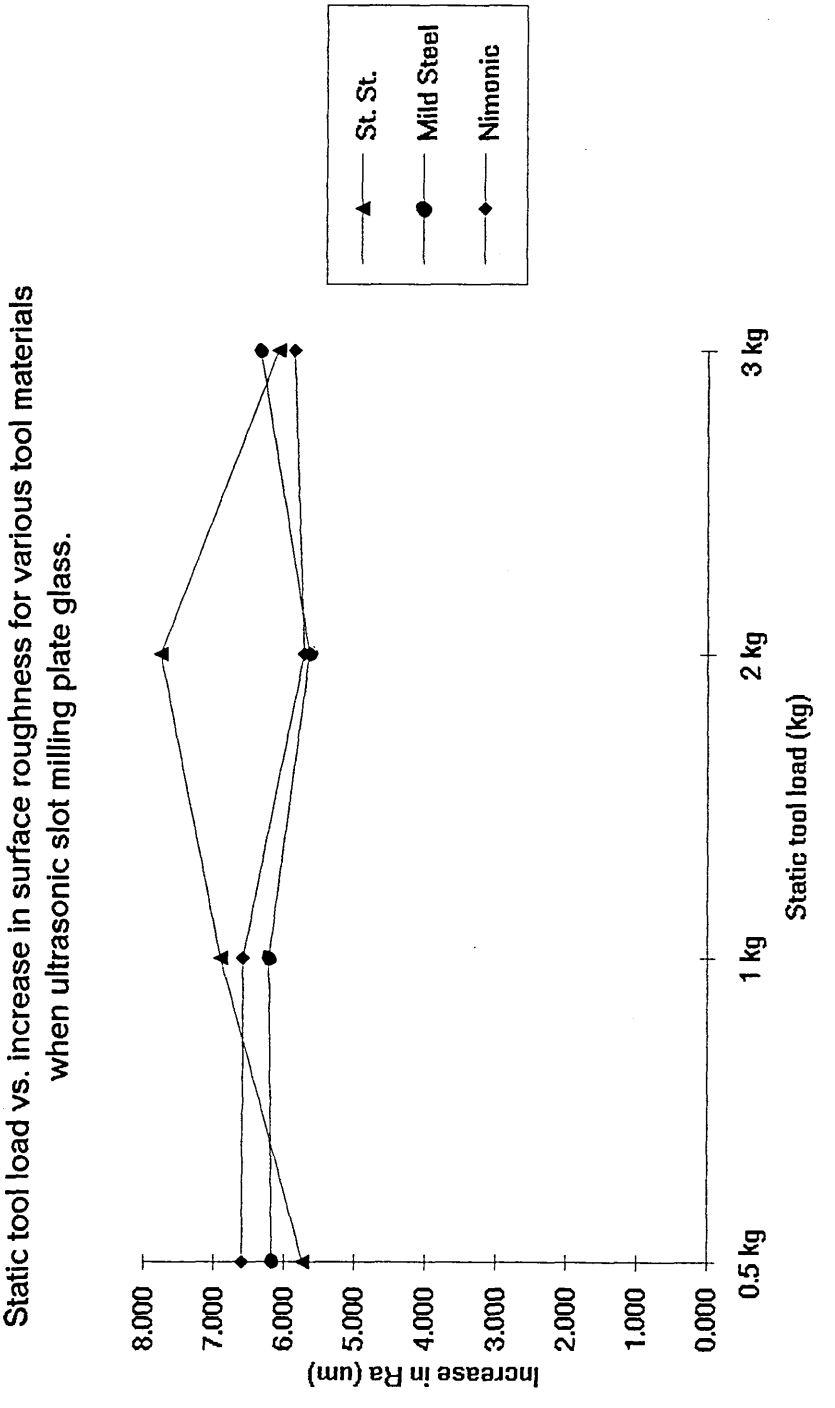

Figure 46
Sections 4.3.28 & 4.3.32

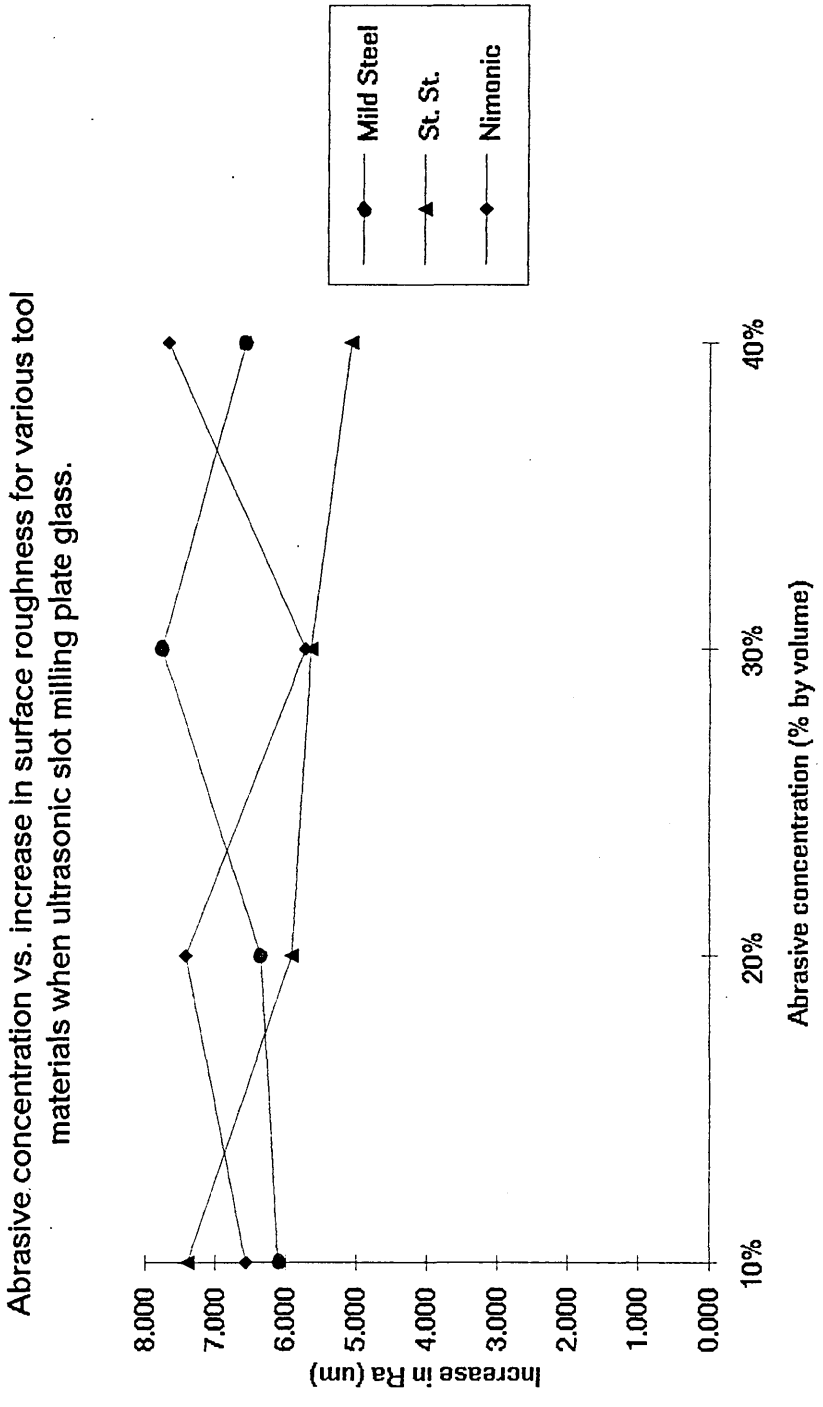

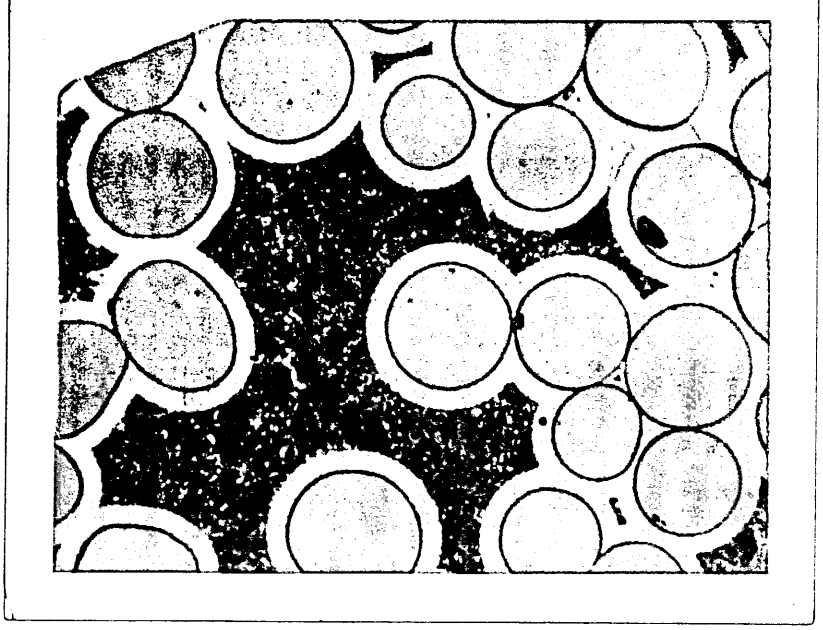

Figure 47
Sectioned & polished sample of SiC/Al_2O_3 composite
Mag. 1000x (Optical)
Section 4.4.2

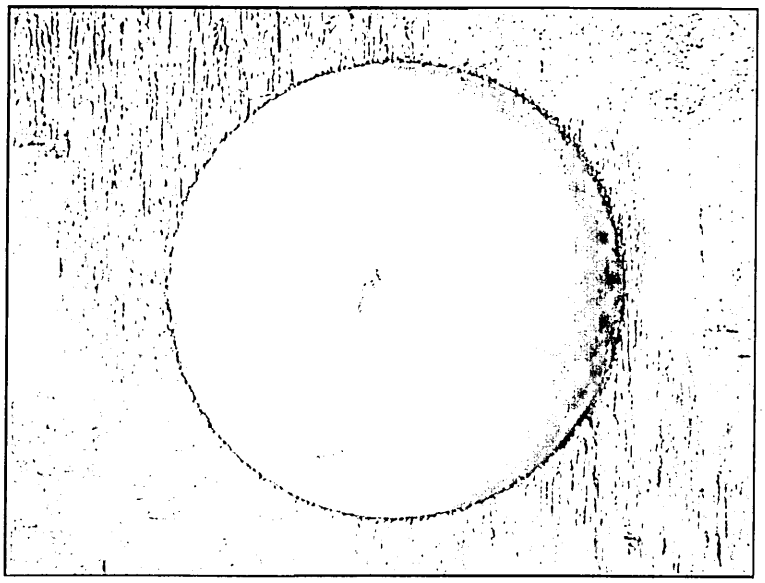

Figure 48
Test hole ultrasonically drilled in SiC/Al_2O_3 composite
Mag. 16.5x (Optical)
Section 4.4.3

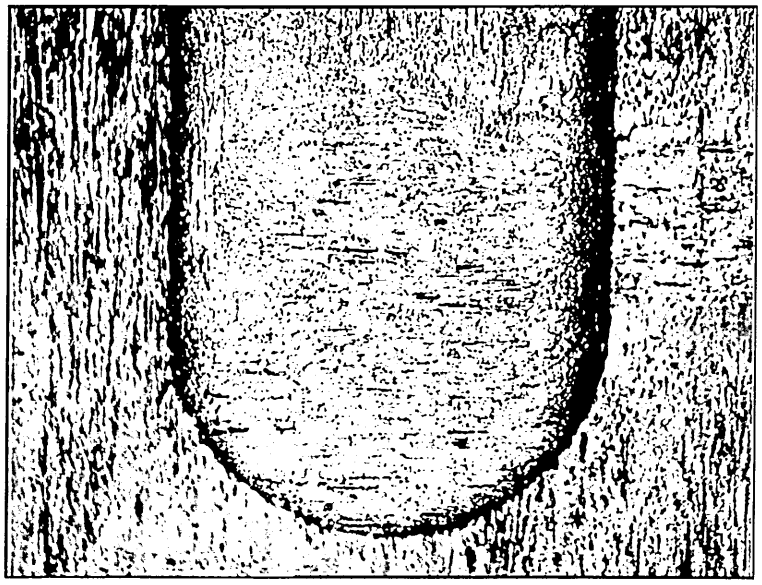

Figure 49
Test slot ultrasonically milled in SiC/Al_2O_3 composite
Mag. 16.5x (Optical)
Section 4.4.3

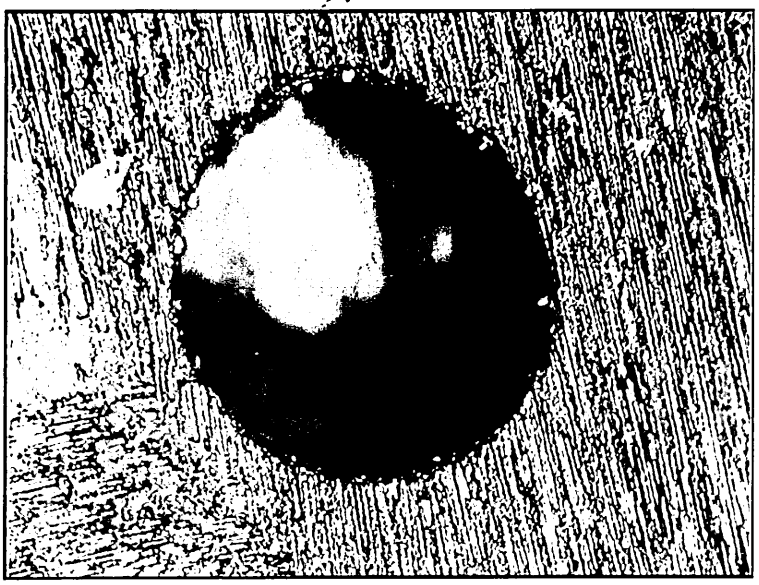

Figure 50
Test hole ultrasonically drilled in SiC/Al_2O_3 composite
Mag. 50x (Optical)
Section 4.4.3

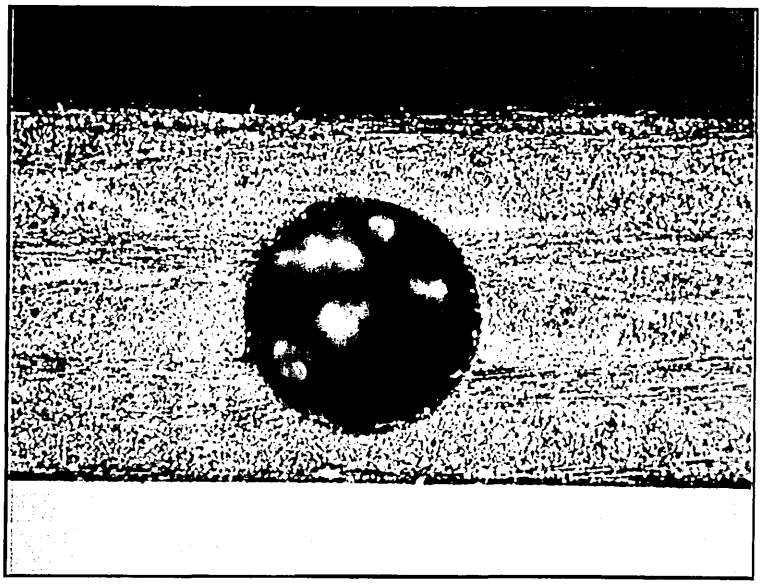

Figure 51
Test hole ultrasonically drilled in SiC/Al_2O_3 composite
Mag. 16.5x (Optical)
Sections 4.4.3 & 5.6.1

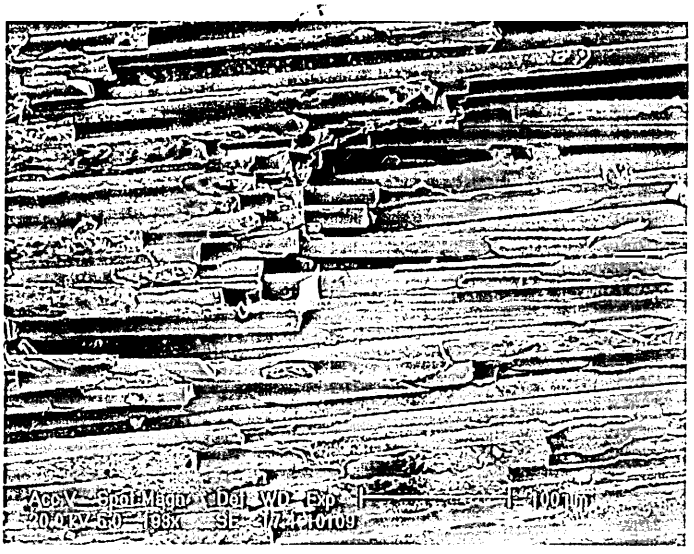

Figure 52
Fibres in the base of an ultrasonically milled slot in SiC/Al_2O_3 composite
Mag. 193x (S.E.M.)
Sections 4.4.4, 5.6.1 & 5.6.2

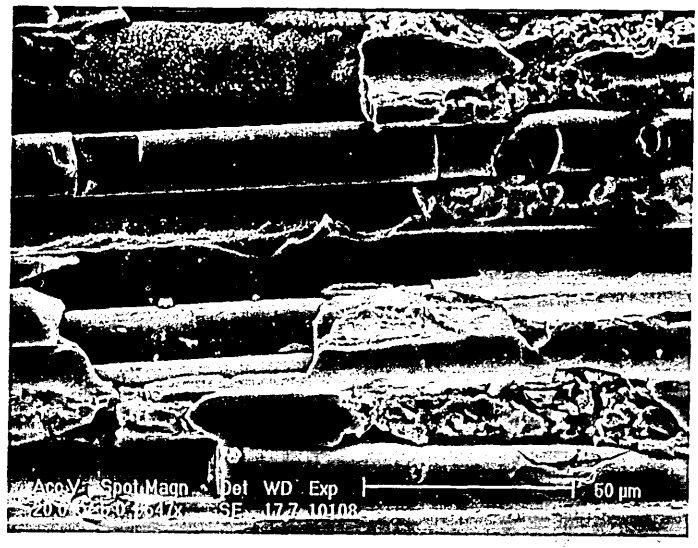

Figure 53
Fibres in the base of an ultrasonically milled slot in SiC/Al_2O_3 composite
Mag. 547x (S.E.M.)
Sections 4.4.4, 5.6.1 & 5.6.2

Figure 54
Fractured SiC fibre after ultrasonic milling of SiC/Al_2O_3 composite
Mag. 2188x (S.E.M.)
Sections 4.4.4 & 5.6.1

Figure 55
Fibres at the bottom edge of an ultrasonically milled slot in SiC/Al_2O_3 composite
Mag. 1280x (S.E.M.)
Sections 4.4.4, 5.6.1 & 5.6.2

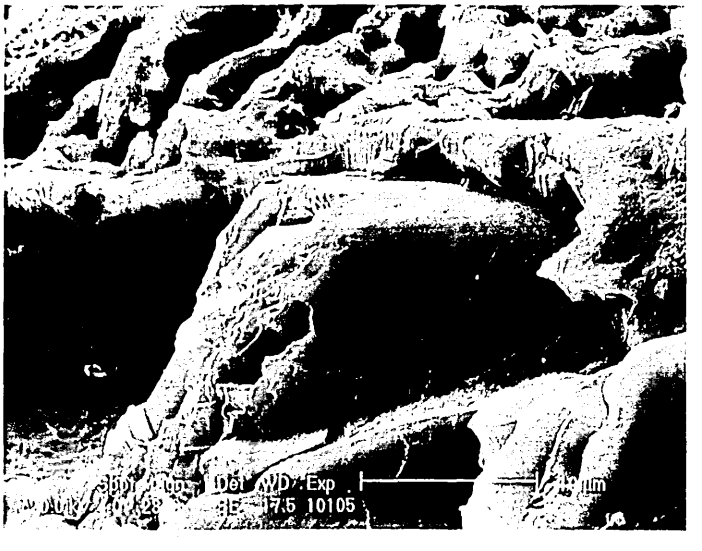

Figure 56
Fractured SiC fibre in the base of an ultrasonically milled slot in SiC/Al_2O_3 composite
Mag. 2319x (S.E.M.)
Sections 4.4.4 & 5.6.1

Figure 57
Fractured SiC fibre after ultrasonic machining of SiC/Al_2O_3 composite
Mag. 3092x (S.E.M.)
Sections 4.4.4, 5.6.1 & 5.6.2

Figure 58
Fractured SiC fibre after ultrasonic milling of SiC/Al_2O_3 composite
Mag. 6184x (S.E.M.)
Sections 4.4.4, 5.6.1 & 5.6.2

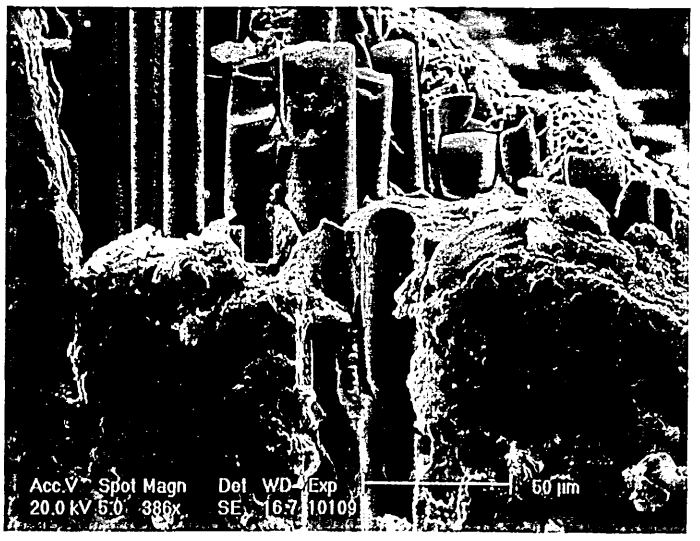

Figure 59
Top edge of an ultrasonically machined slot in SiC/Al_2O_3 composite
Mag. 386x (S.E.M.)
Sections 4.4.4, 5.6.1 & 5.6.2

Figure 60
#120 mesh size SiC abrasive particle after machining of SiC/Al_2O_3 composite
Mag. 567x (S.E.M.)
Sections 4.4.5 & 5.9

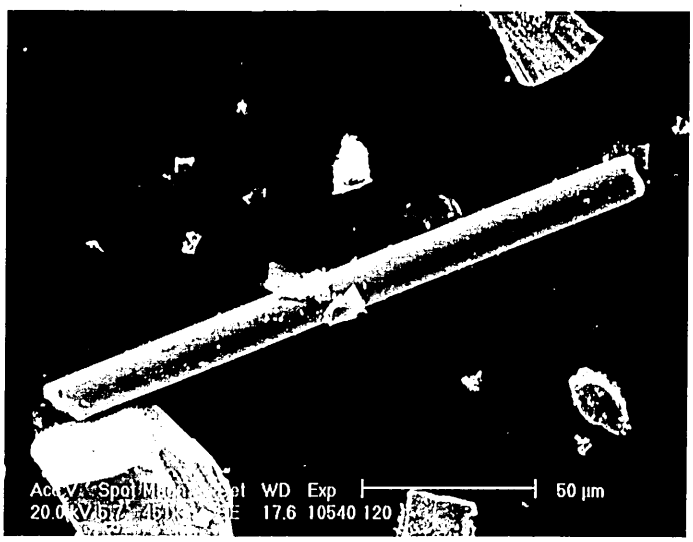

Figure 61
SiC fibre within abrasive slurry after the ultrasonic machining of SiC/Al_2O_3 composite
Mag. 451x (S.E.M.)
Sections 4.4.5 & 5.9

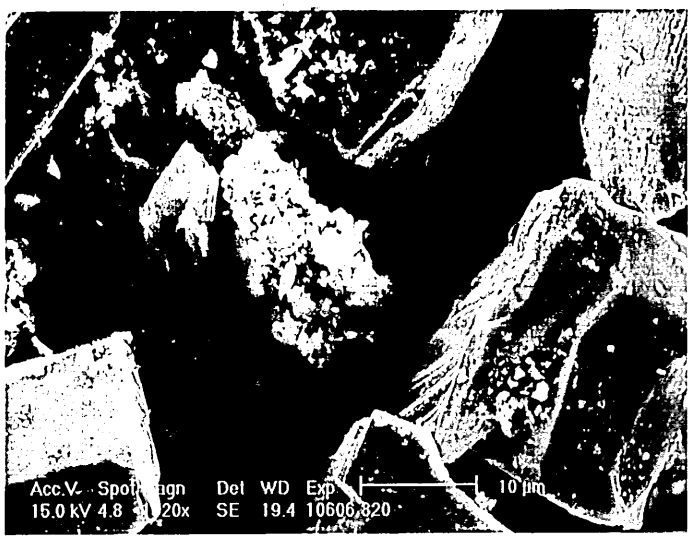

Figure 62
#120 mesh size SiC abrasive particle after machining of SiC/Al_2O_3 composite
Mag. 1520x (S.E.M.)
Sections 4.4.5 & 5.9

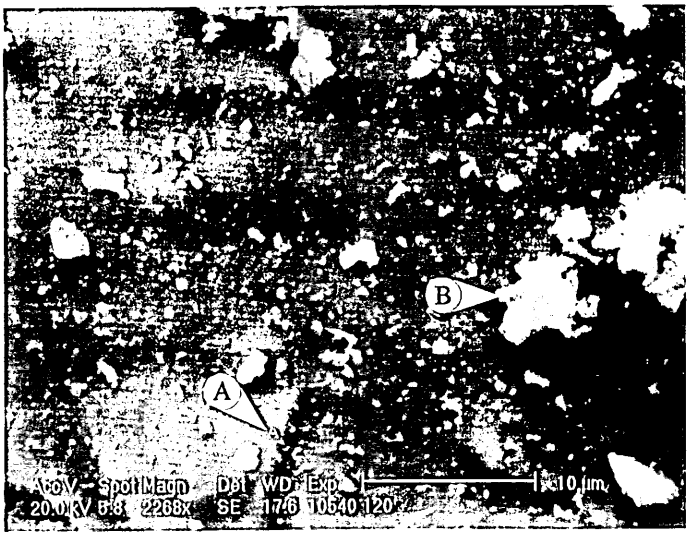

Figure 63
Enlarged region of abrasive particle in Figure 62
A & B indicate regions investigated by x-ray analysis (see Figures 64 & 65)
Mag. 2286x (S.E.M.)
Sections 4.4.5 & 5.9

Figure 64
X-ray analysis of area "A" in Figure 63
Section 4.4.5

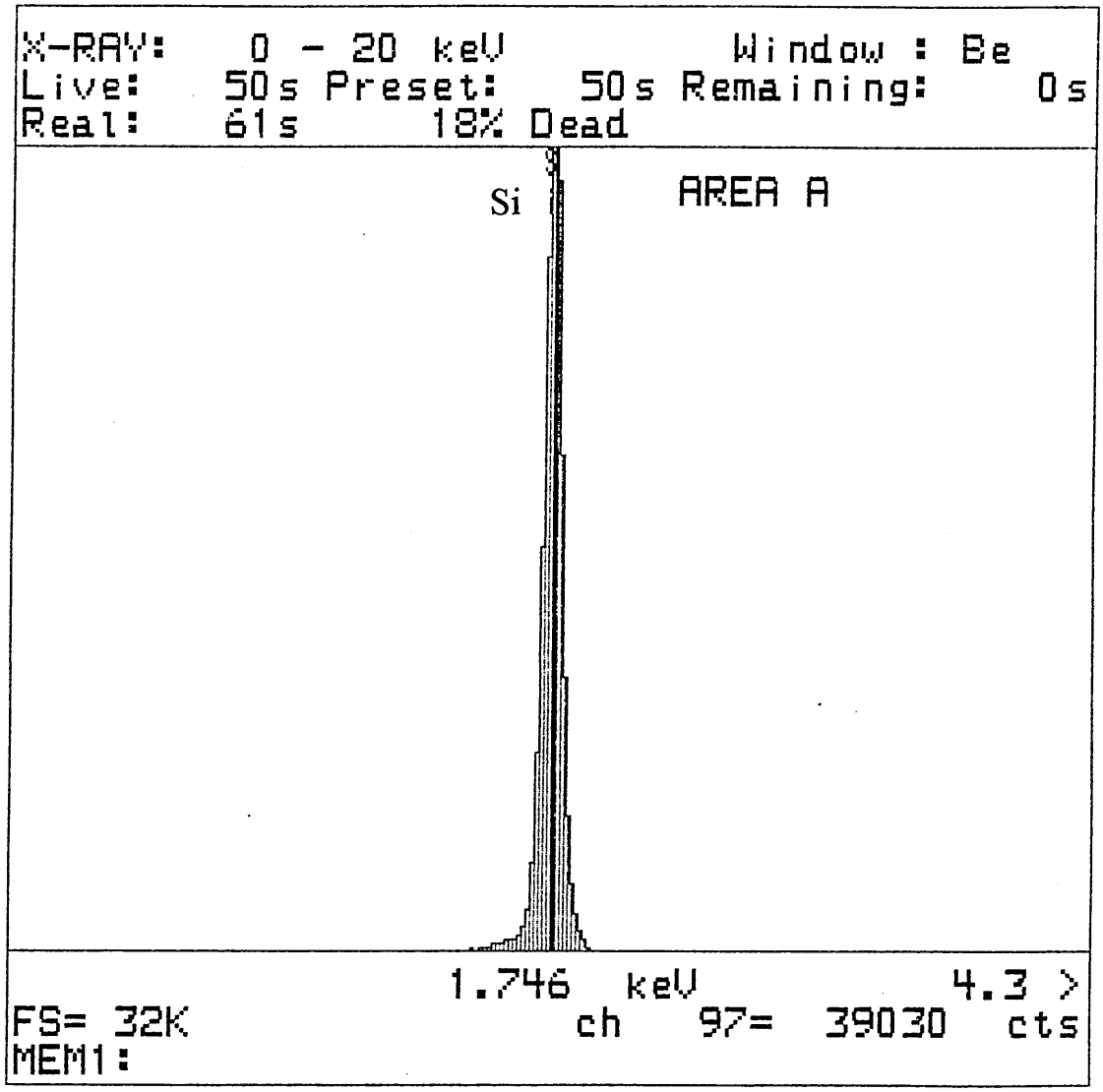

Figure 65
X-ray analysis of area "B" in Figure 63
Section 4.4.5

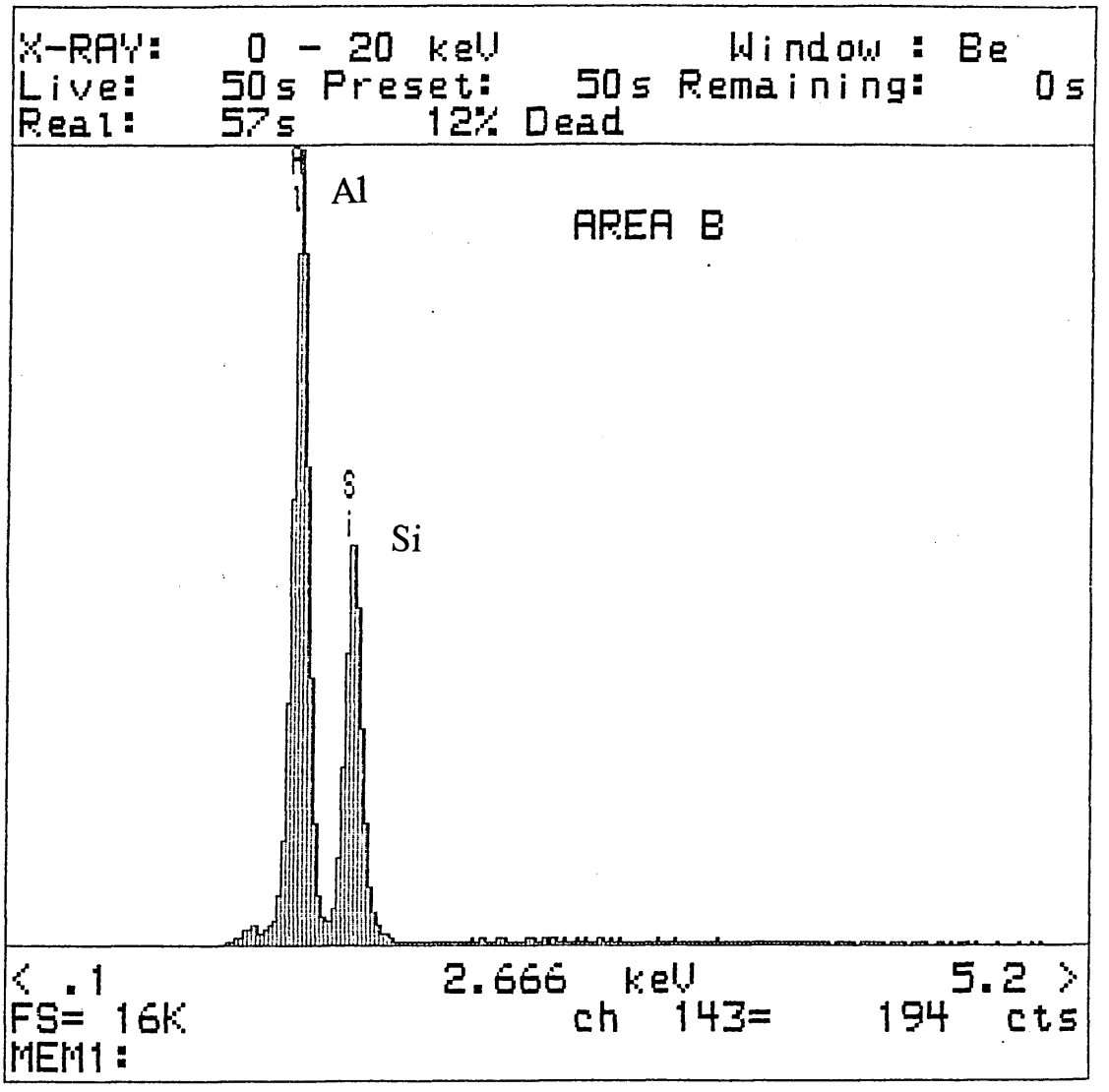

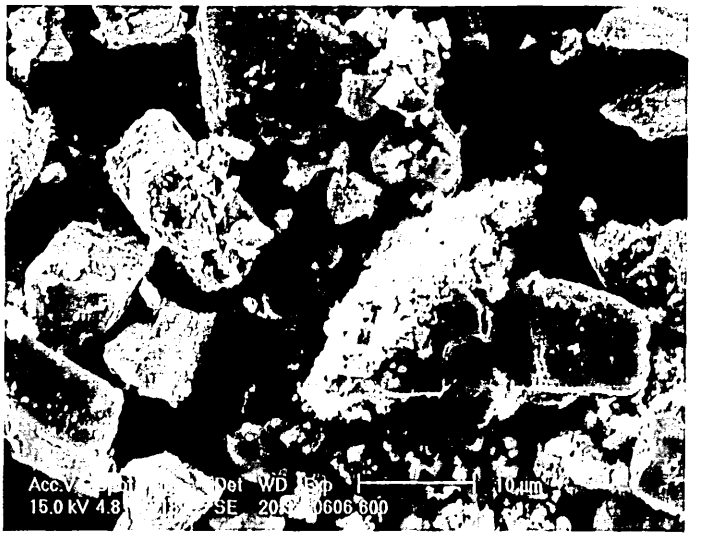

Figure 66
#600 mesh size SiC abrasive after the ultrasonic machining of SiC/Al_2O_3 composite
Mag. 1518x (S.E.M.)
Sections 4.4.5 & 5.9

Figure 67
Fracture surface of SiC/Al_2O_3 composite after being subjected to a bending test
Mag. 211x (S.E.M.)
Sections 4.4.7 & 5.6.1

Figure 68
Diagram of bending test and fracture plane
Section 4.4.7

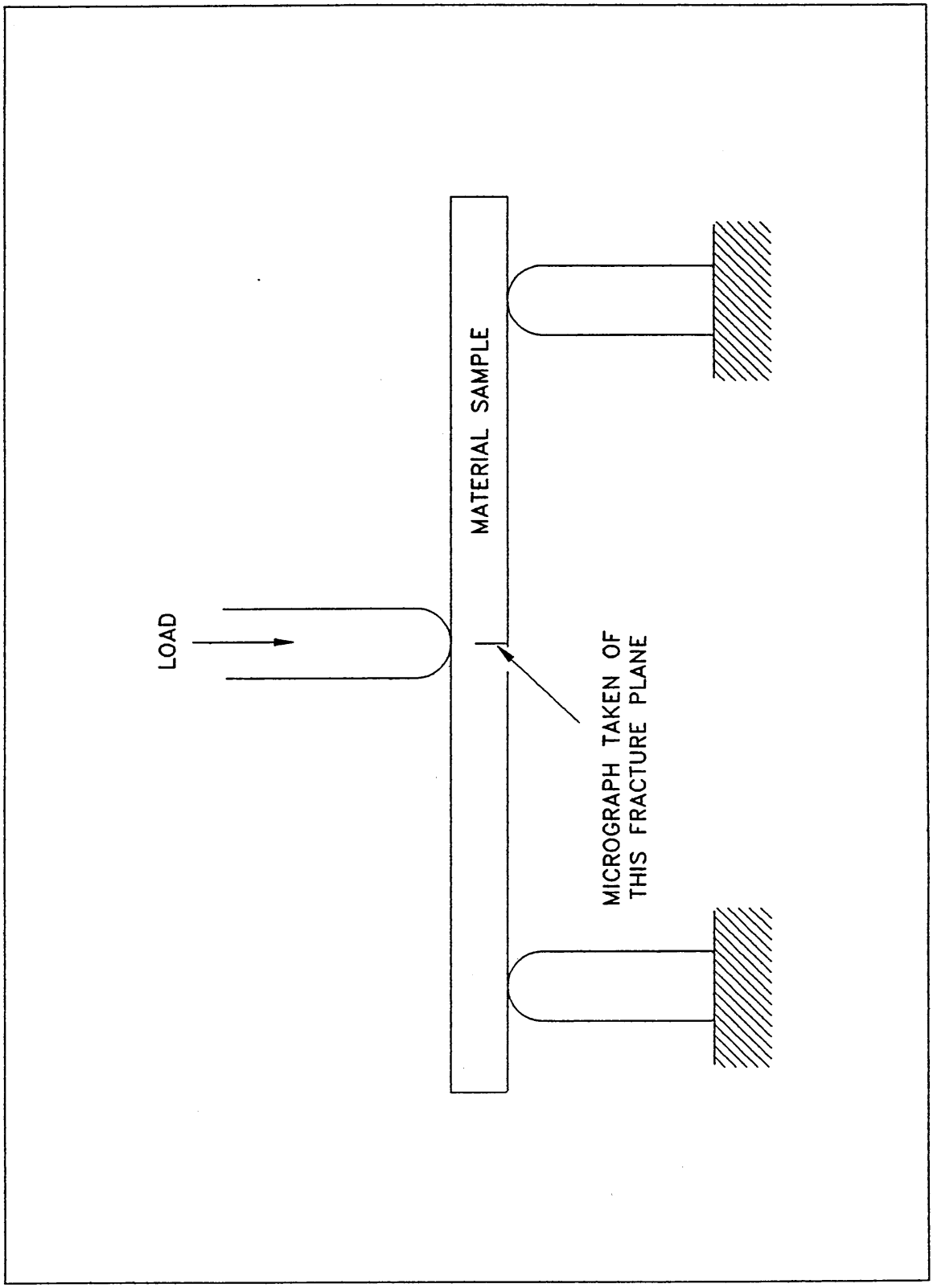

Figure 69
Region of Figure 68 under higher magnification
Mag. 422x (S.E.M.)
Sections 4.4.7 & 5.6.1

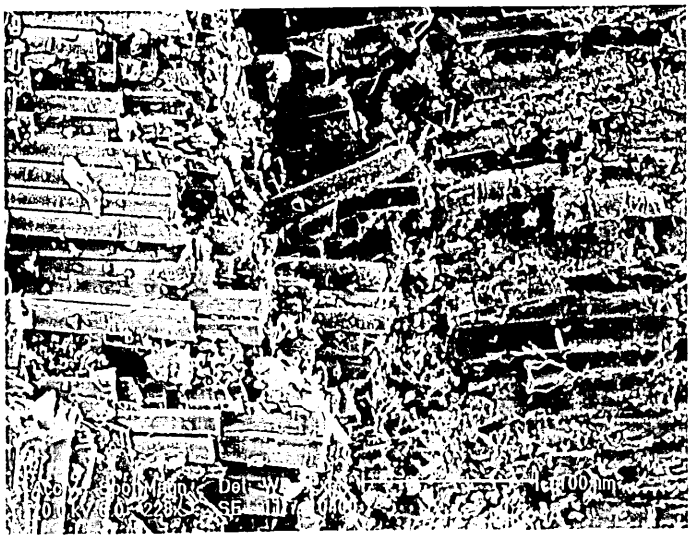

Figure 70
SiC/Al_2O_3 composite after being subjected to an impact test
Mag. 228x (S.E.M.)
Sections 4.4.8 & 5.6.1

Figure 71
Region of Figure 70 under higher magnification
Mag. 457x (S.E.M.)
Sections 4.4.8 & 5.6.1

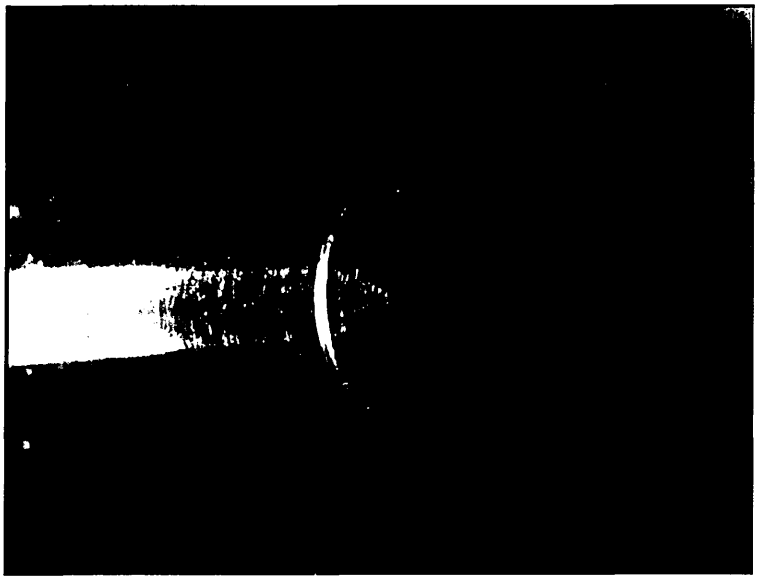

Figure 72
Unused Nimonic 80A tool tip
Mag. 12x (Optical)
Section 4.4.9

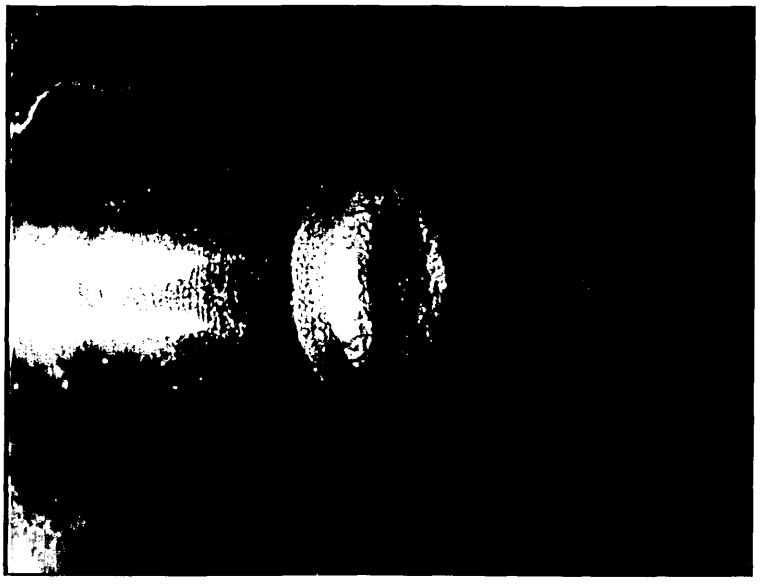

Figure 73
Nimonic 80A tool tip after ultrasonically drilling 24 holes in SiC/Al_2O_3 composite
Mag. 12x (Optical)
Section 4.4.9

Figure 74
Nimonic 80A tool tip after ultrasonically milling 24 slots in SiC/Al_2O_3 composite.
Mag. 12x (Optical)
Section 4.4.9

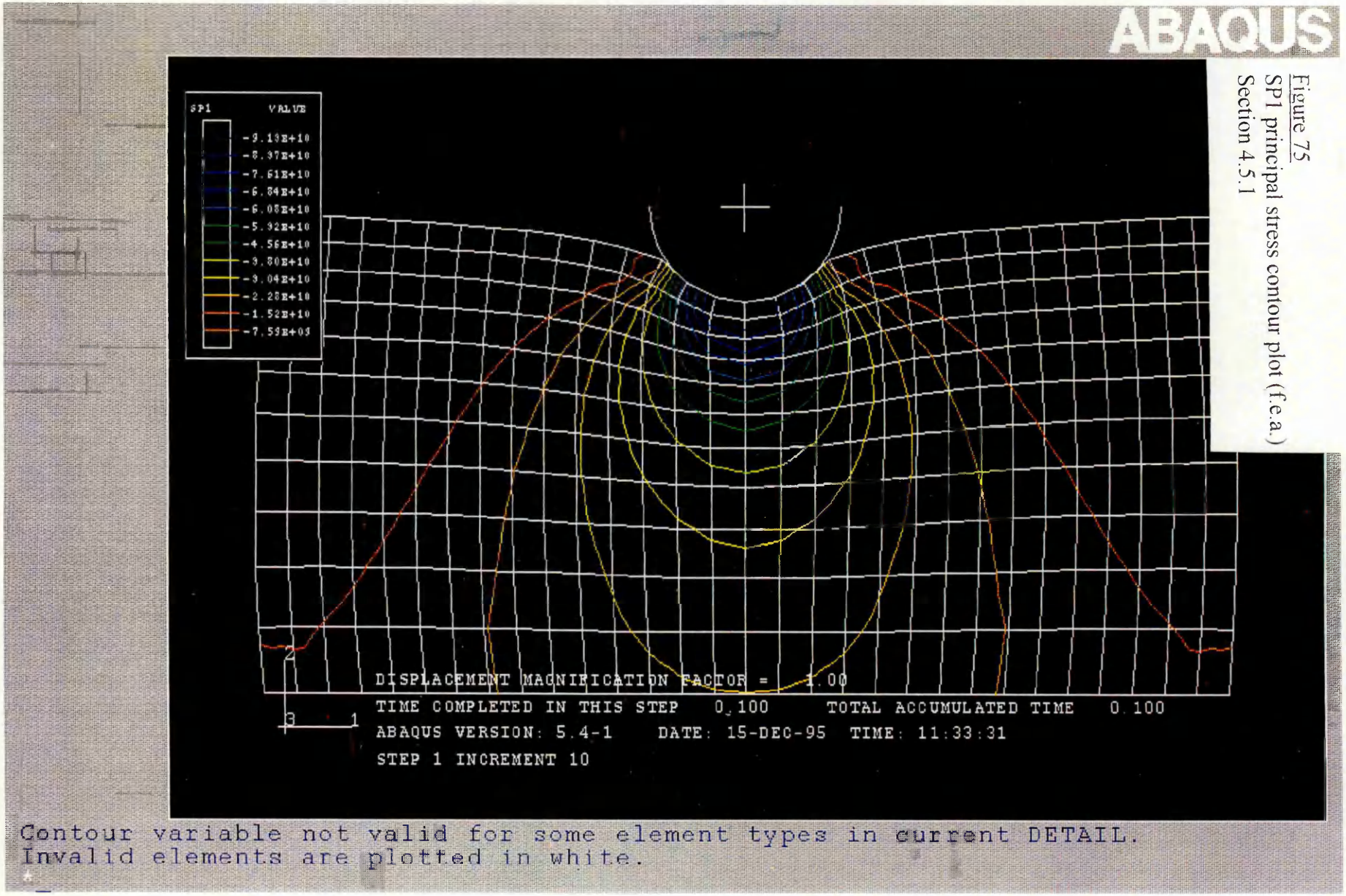

Figure 75
SP1 principal stress contour plot (f.e.a.)
Section 4.5.1

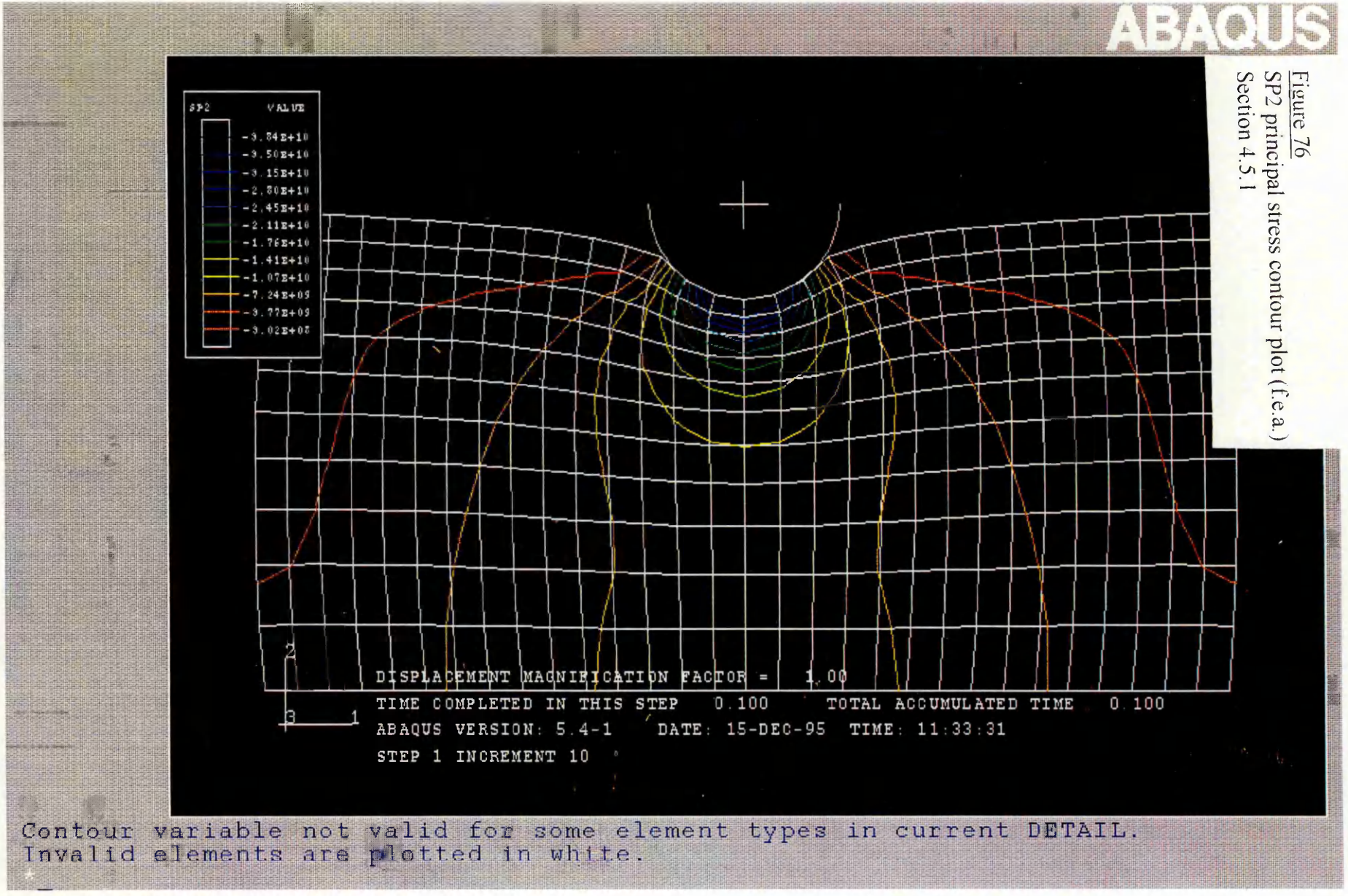

Figure 76
SP2 principal stress contour plot (f.e.a.)
Section 4.5.1

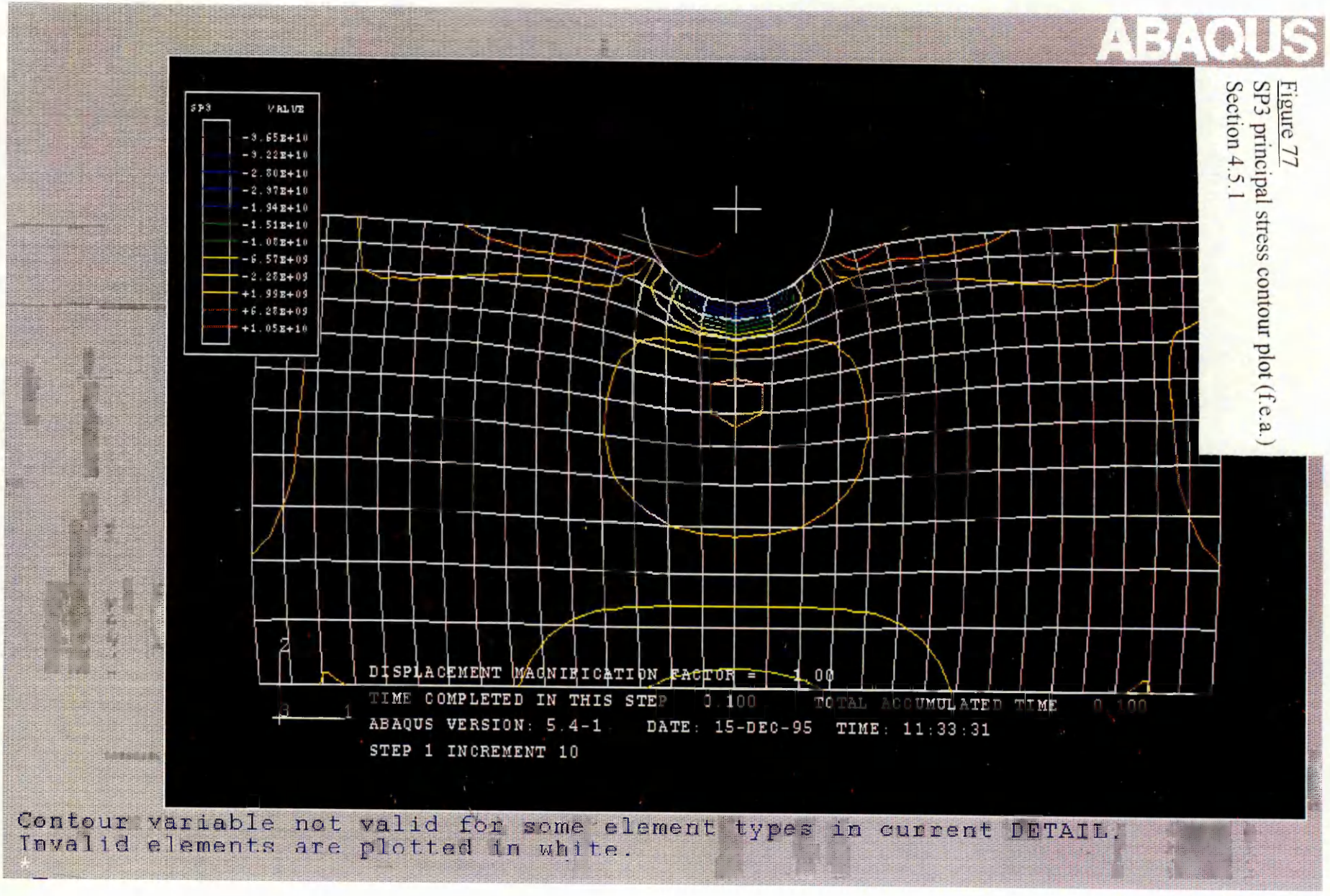

Figure 77
SP3 principal stress contour plot (f.e.a.)
Section 4.5.1

Figure 78
SP1 principal stress vector plot (f.e.a.)
Section 4.5.2

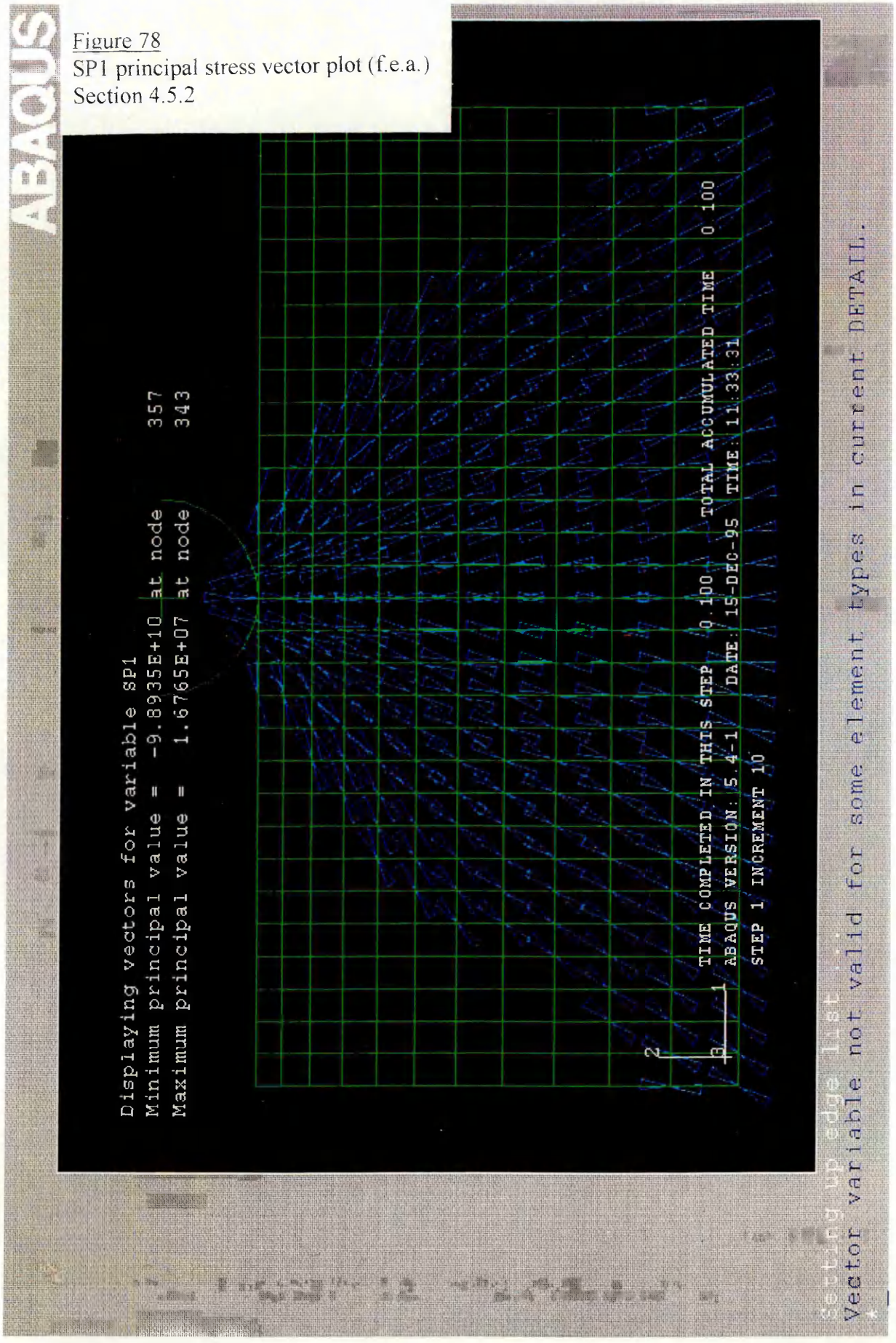

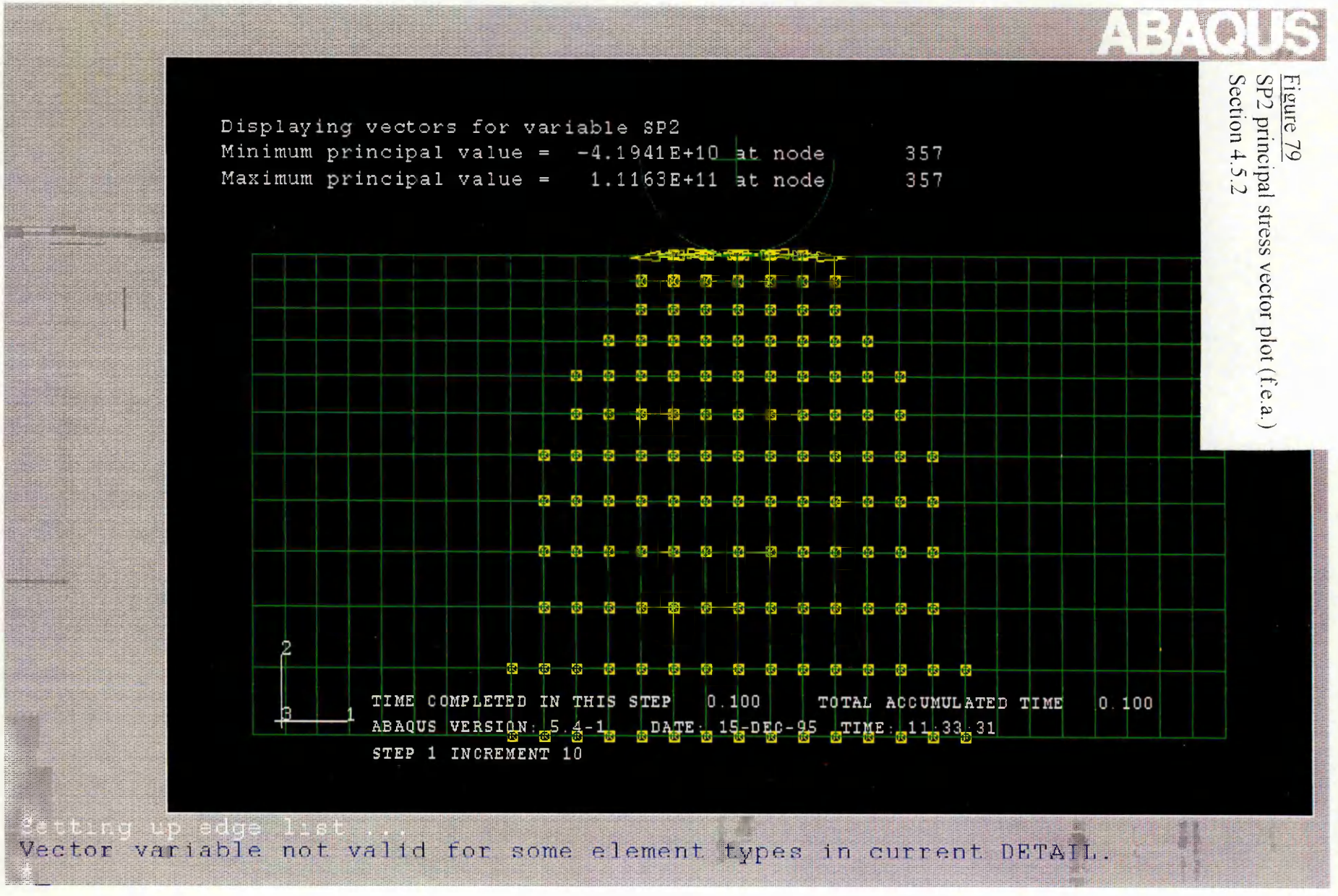

Figure 79
SP2 principal stress vector plot (f.e.a.)
Section 4.5.2

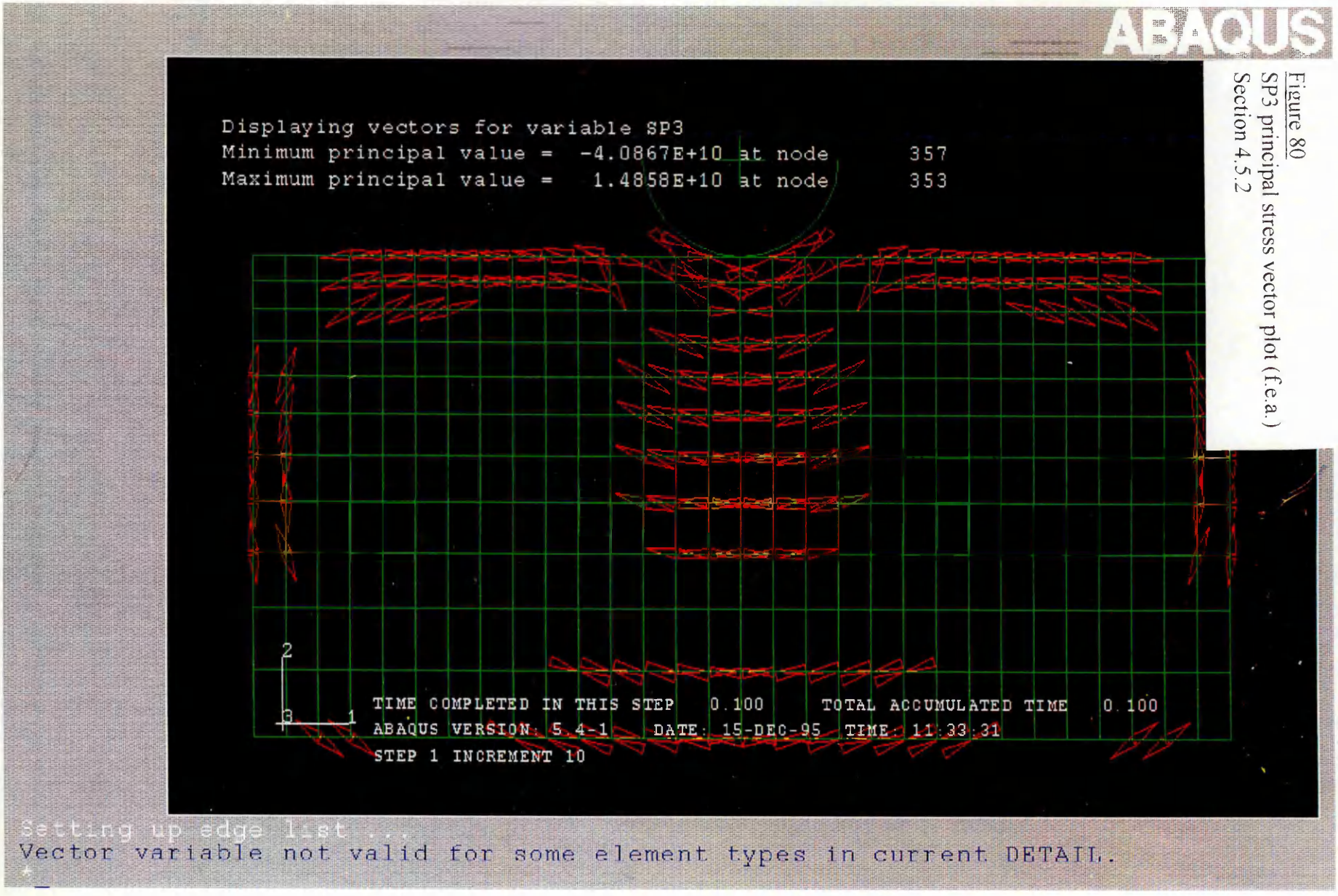

Figure 80
SP3 principal stress vector plot (f.e.a.)
Section 4.5.2

Figure 81
Von Mises stress contour plot (f.e.a.)
Section 4.5.3

Figure 82
Section 5.2.1

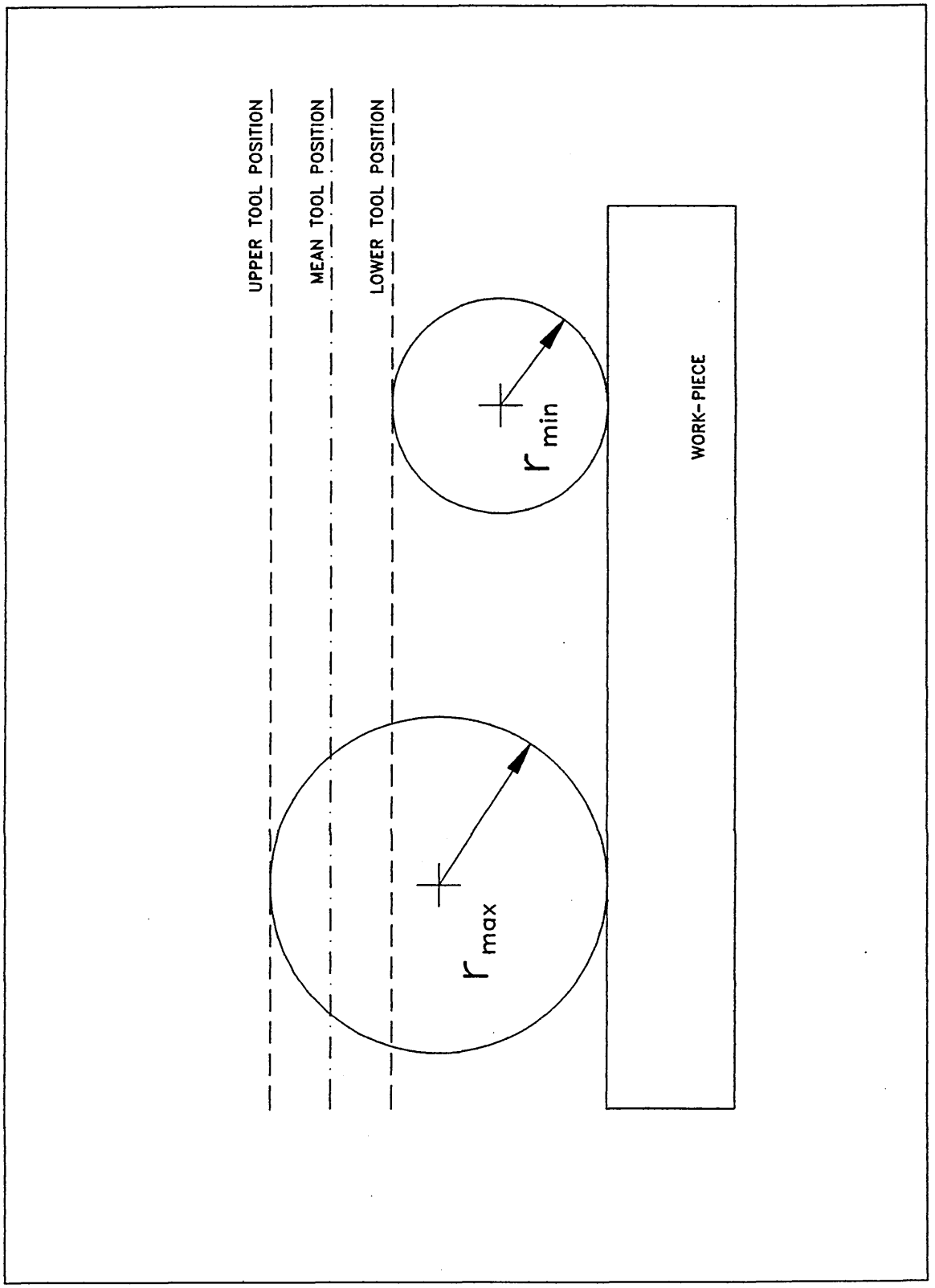

Figure 83
Section 5.2.1

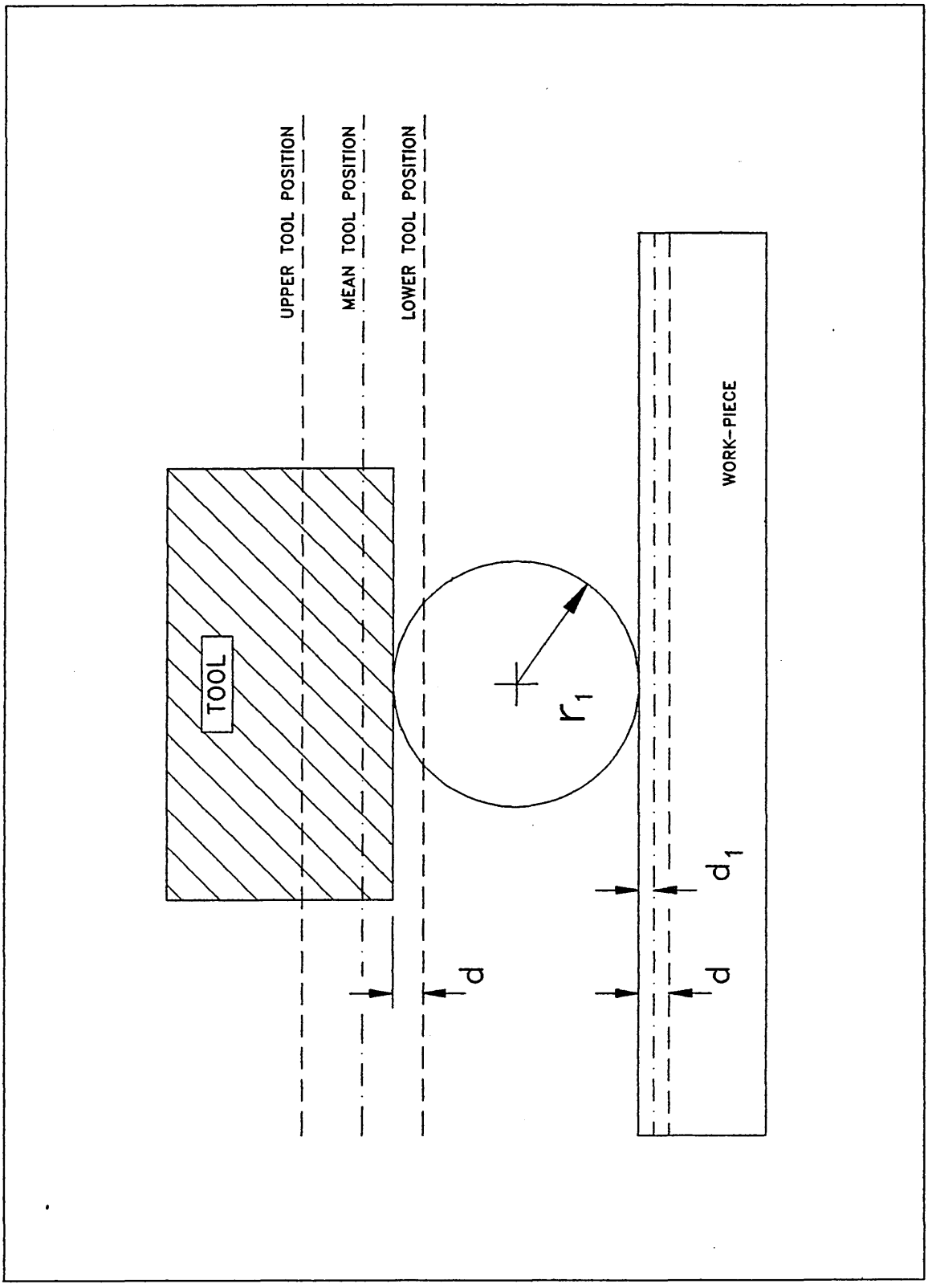

Figure 84
Section 5.2.1

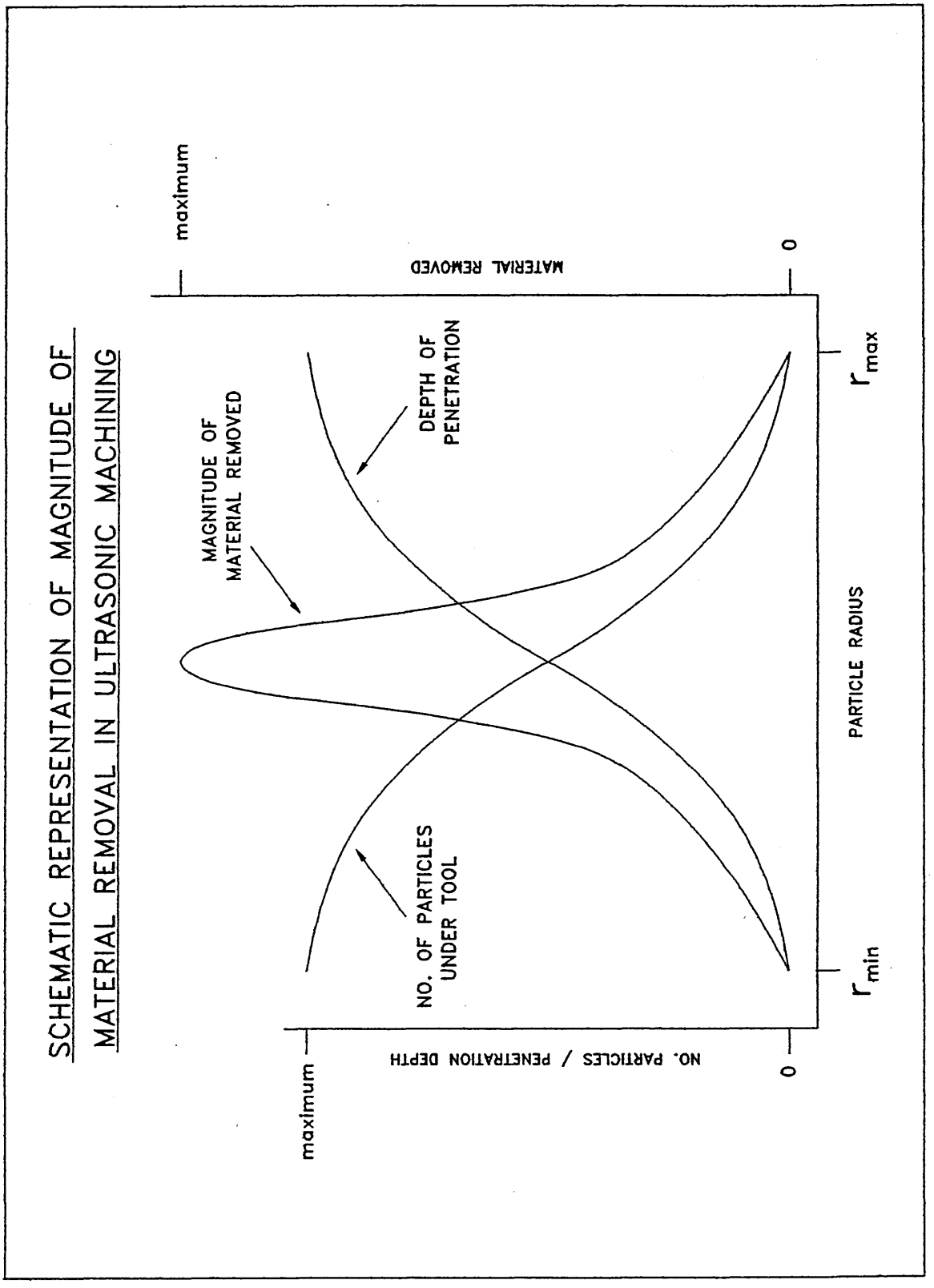

Figure 85
Diagram of material removal mechanisms in ultrasonic machining
Section 5.2.2

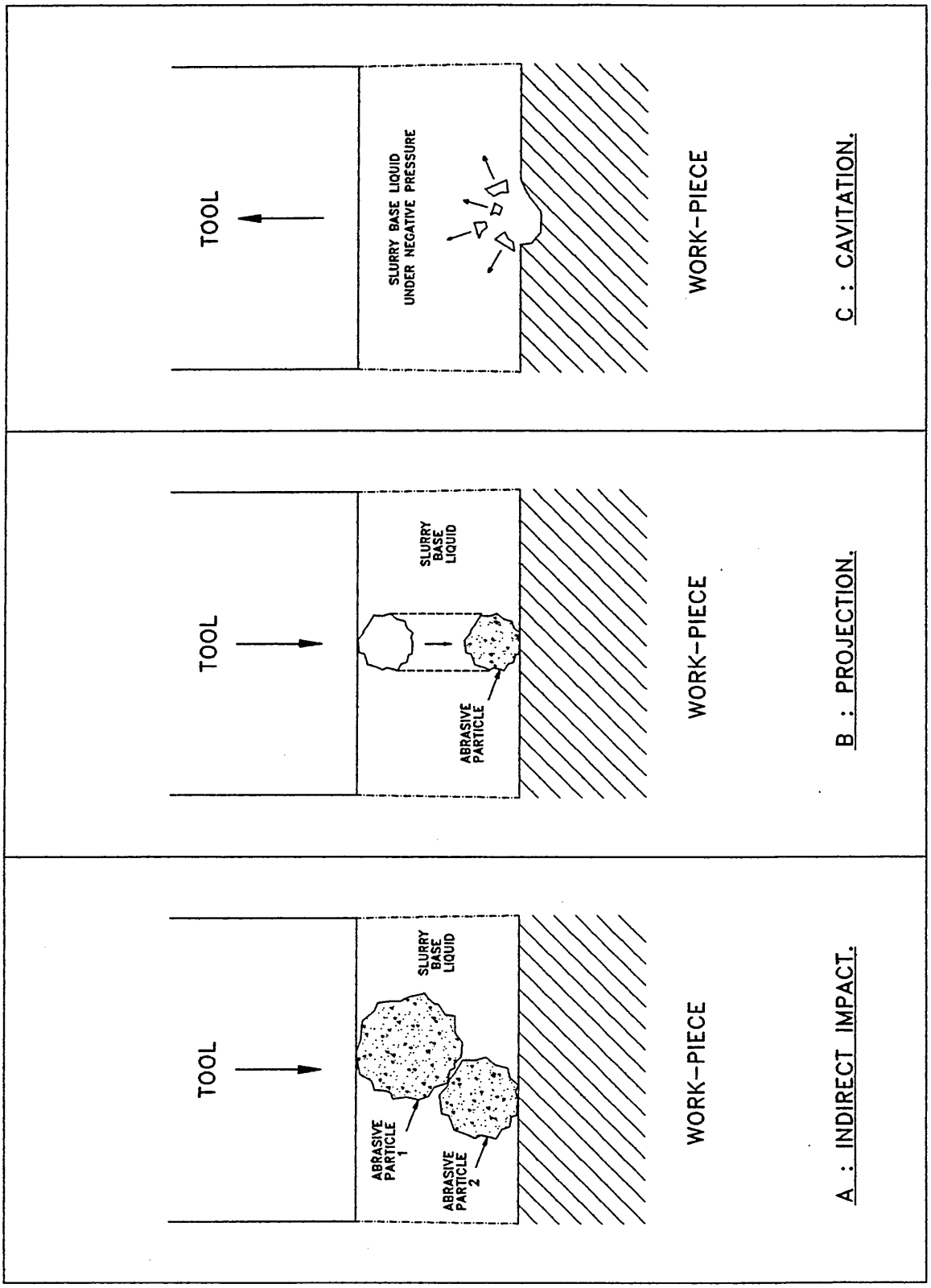

Figure 86
Diagram of fibre pull-out
Section 5.5.3

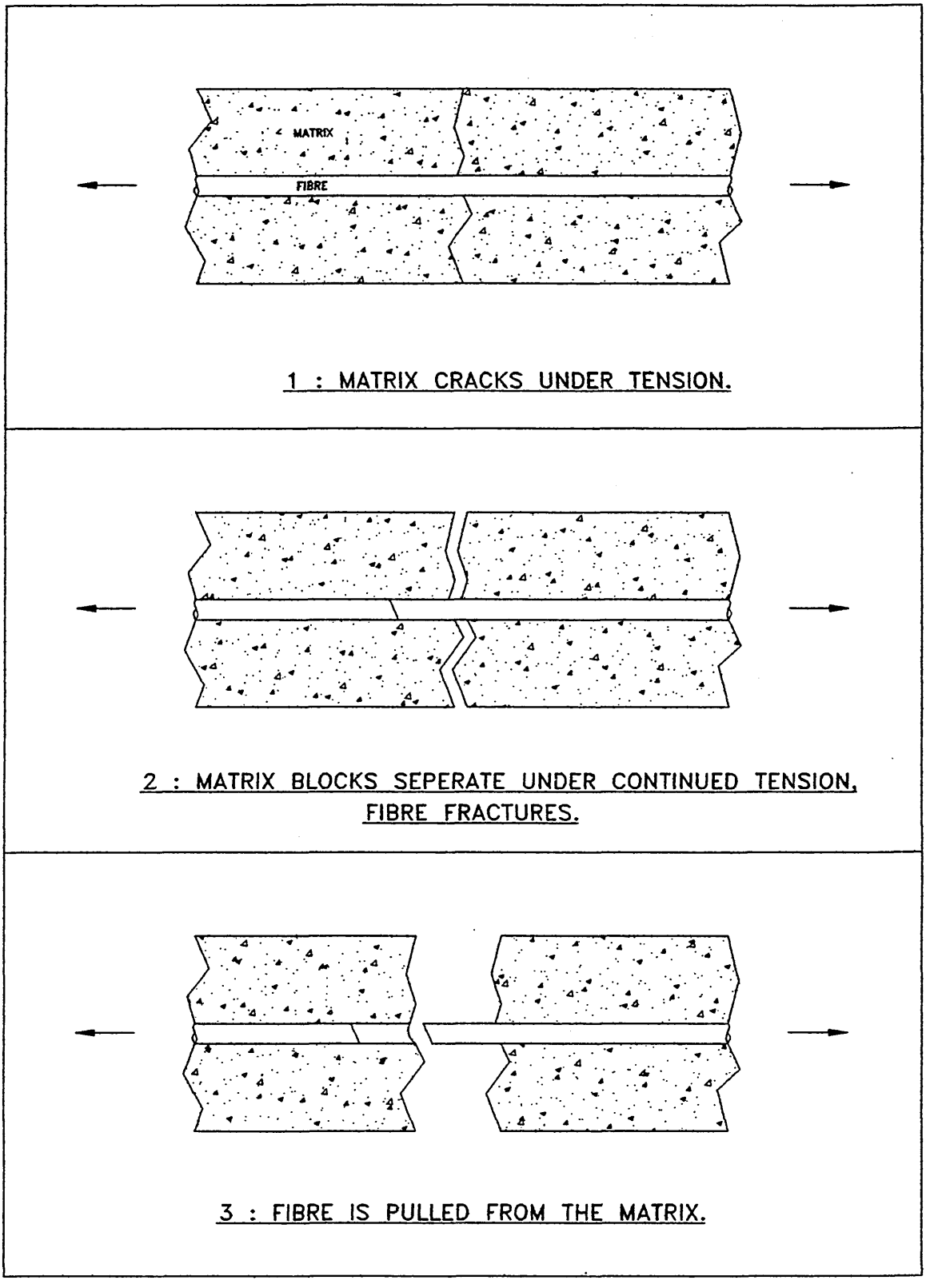

Figure 87
Fracture mechanism when using a blunt indenter
Section 5.8.1

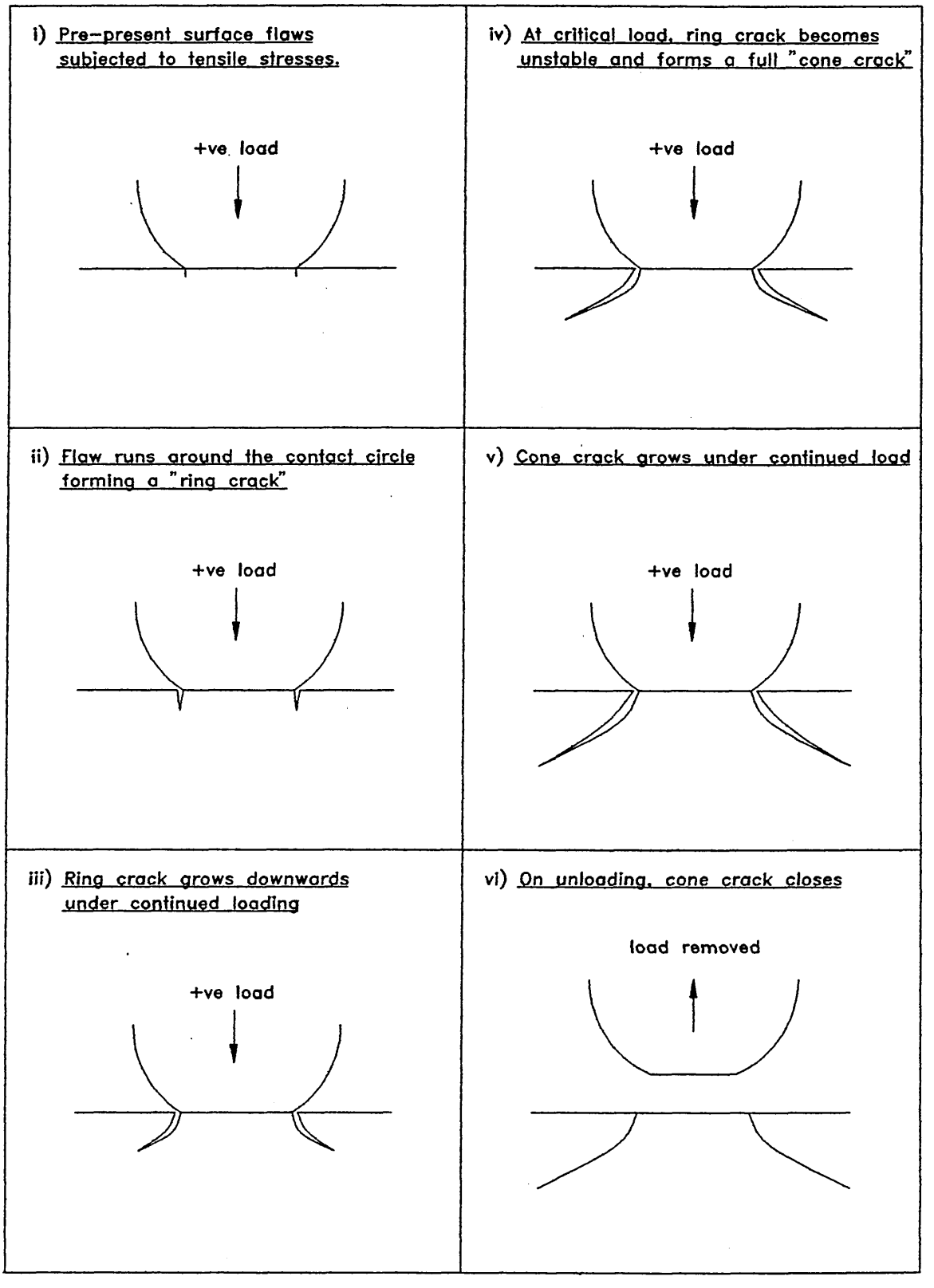

Figure 88
Possible material removal mechanism when using multiple blunt indenters
Section 5.8.1

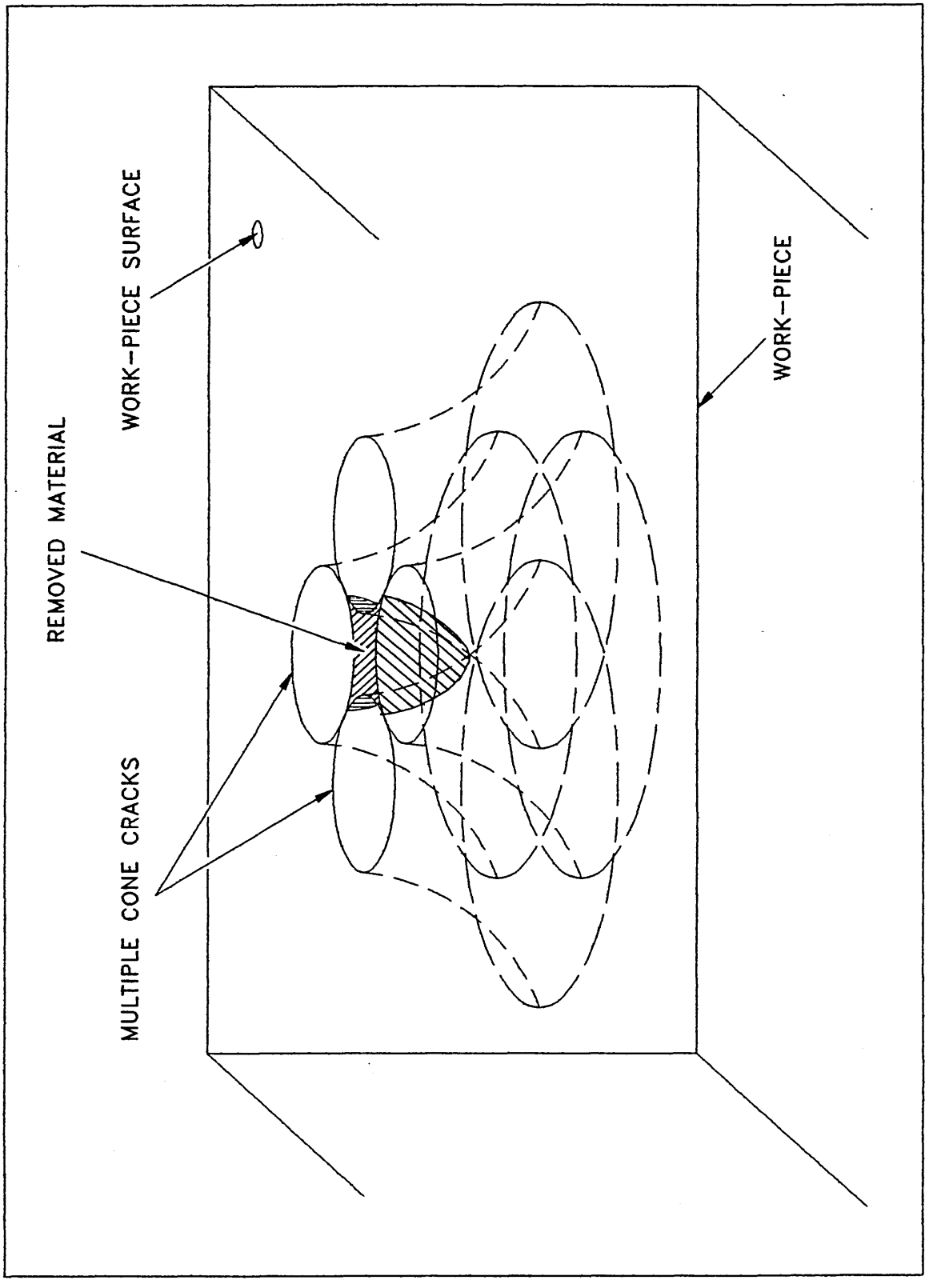

Figure 89
Fracture mechanism when using a sharp indenter
Section 5.8.2

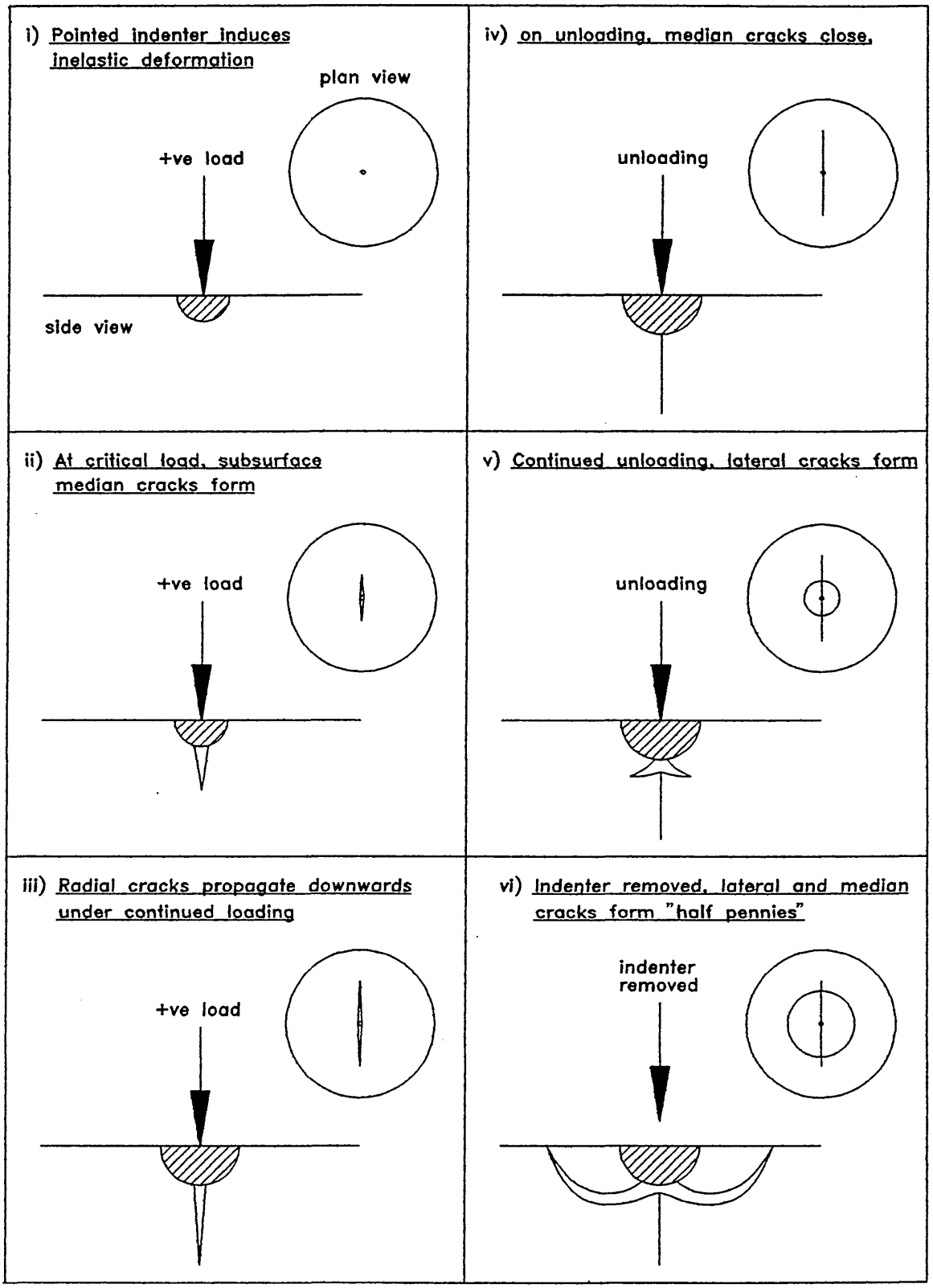

Figure 90
Possible material removal mechanism when using multiple sharp indenters
Section 5.8.3